Assessment of the energy performance, economics and environmental footprint of silicon heterojunction photovoltaic technology

Assessment of the energy performance, economics and environmental footprint of silicon heterojunction photovoltaic technology

This work was carried out within the programme Fundamentals and Application of Silicon Heterojunction technology (FLASH) under the Perspectief programme (project number 12172), supported by the Stichting Technische Wetenschappen, which is part of the Netherlands Organisation for Scientific Research (NWO) and partly funded by the Ministry of Economic Affairs.

ISBN: 978-90-8672-075-0
Print: Ridderprint B.V. | www.ridderprint.nl

Assessment of the energy performance, economics and environmental footprint of silicon heterojunction photovoltaic technology

Beoordeling van de energie prestaties, economie and milieu-voetafdruk van silicium heterojunctie fotovoltaïsche technologie

(met een samenvatting in het Nederlands)

Proefschrift

ter verkrijging van de graad van doctor aan de Universiteit Utrecht op gezag van de rector magnificus, prof. dr. G.J. van der Zwaan, ingevolge het besluit van het college voor promoties in het openbaar te verdedigen op vrijdag 20 januari 2017 des middags te 2.30 uur

door

Atse Louwen

geboren op 16 april 1986 te Bodegraven

Promotoren:	Prof. dr. R.E.I. Schropp
	Prof. dr. A.P.C. Faaij
Copromotor:	Dr. W.G.J.H.M. van Sark

Summary

To make the transition towards a more sustainable energy supply, it is necessary that we drastically increase the share of renewable electricity generation. Solar photovoltaic energy is regarded as one of the prime options to reduce the greenhouse gas intensity of our electricity supply, and many different types of photovoltaics are being investigated to develop ever cheaper and more efficient photovoltaic devices. Silicon heterojunction technology combines the experience in both crystalline and thin film silicon photovoltaics, and offers highly efficient solar cells, although its market penetration is still very limited. As main patents describing this technology have expired, many research groups are presently investigating a variety of silicon heterojunction cell designs.

In this thesis, a comprehensive assessment of silicon heterojunction technology is performed, taking into account the environmental footprint and economics of different silicon heterojunction solar cell designs and complete photovoltaic systems based on them, as well as an analysis of the performance of commercial solar modules, including silicon heterojunction modules, is given. Furthermore, the development of the complete photovoltaic industry is analysed to establish the net contribution of solar energy in terms of energy generation and reduction of greenhouse gas emissions.

A life cycle inventory was built, that details all the material and energy flows in and out of the production chains of the silicon heterojunction designs (Chapters 2 and 3). The results indicate that current silicon heterojunction technology has lower environmental impact compared to crystalline silicon, but similar or higher costs. Prospective silicon heterojunction designs are able to significantly decrease environmental impact and production cost, relatively more than the prospective crystalline silicon reference design that is investigated here.

In order for silicon heterojunction technology to compete with alternative photovoltaic technologies, the outdoor performance should be comparable with or better than these alternatives. Under practical operating conditions, silicon heterojunction photovoltaic modules show very similar performance compared to both mono- and polycrystalline PV modules, both in detailed measurements conducted at a single North-Western European location (Chapter 4) as well as based on performance modelling for a broad geographical range (Chapter 5). The smaller effect of temperature on the performance of silicon heterojunction can benefit this technology compared to crystalline silicon, although other parameters also significantly affect module performance (Chapters 4 and 5). Because of the significant variation of performance of photovoltaics, the environmental impact and costs as-

sociated with photovoltaic electricity show strong variation over large geographical ranges (Chapter 5).

The continued and fast growth of the photovoltaic industry has raised concerns that it could result in the creation of an energy sink or a net greenhouse gas emission instead of a positive energy balance and net reduction of greenhouse gas emissions. Chapter 6 shows that there has been a strong decrease over time of the environmental impact of photovoltaics, and as a result, it is likely that a break even has already occurred between the cumulative energy investments made and cumulative greenhouse gas emissions released to manufacture photovoltaics, and the cumulative energy production and greenhouse gas emission reductions (Chapter 6).

Contents

1
Introduction

1.1 Context

Earth, the planet we call our home, is unique. As far as we know, it is the only place in the universe where we can live. It might even be unique among 70^{20} different Earth-like planets [1]. It has been our home for millions of years and has spawned many societies, our current one being the most advanced. The composition of our planet's atmosphere offers nearly ideal conditions for us to live on, to raise our children, to produce our food, and enjoy our ever longer lives. It has a perfect balance of oxygen, to breathe and enable the metabolism of almost all living things, nitrogen, which is part of the building blocks of life: DNA, RNA, amino acids and proteins, and carbon dioxide (CO_2), which regulates the temperature of the surface and lower atmosphere of our planet to levels that are suitable for life, by absorbing long wavelength radiation from the Earth's surface.

The continued development of our society has profoundly changed the way we live and has been concurrent with a dramatic population growth. This has distorted the balance between our activities, and our planet's ability to cope with them. Our ecological footprint currently exceeds the biocapacity of the planet by 50% [2], e.g. we would need 1.5 Earths to sustain our current society. Especially our consumption of large amounts of fossil fuel for generation of electricity and heat, and for agriculture, industry and transport has resulted in the emission of large amounts of carbon dioxide (CO_2), but also methane (CH_4) and many other greenhouse gasses (GHGs). These gasses have always been part of and emitted to the Earth's atmosphere, however, by our doing, the concentrations of these gasses in the atmosphere are increasing much faster than our planet is able to balance them by moving them to a non-atmospheric reservoir (e.g. oceans, biosphere, lithosphere and fossil fuels). As a result, atmospheric CO_2 levels are at a level higher than ever observed in millions of years, and as a result, the climate of our planet is being affected significantly. Anthropogenic climate change has been linked to increased land and ocean surface temperatures [3], more extreme weather events including hurricanes and droughts [4, 5], loss of biodiversity [6], shrinking polar icecaps and polar and alpine glaciers [3] and even armed conflicts [7, 8]. While Earth itself will survive, mankind and plant and animal life will not necessarily in its present forms continue to exist.

In order to try to limit global climate change, there is a strong need for *decarbonisation* of our energy supply: we should find a way to keep providing energy to our society, whilst drastically lowering the amount of CO_2 and other GHGs we emit. We can achieve a large part of this by being more efficient with the energy we use, however, there is also a strong need for renewable forms of energy supply. Within much less than a century, we need to decrease the share of fossil fuels in our energy supply from roughly two-thirds now, to almost zero, and shift to sources of energy that are (on a net emission basis) much less CO_2 intensive. We need renewable energy technologies to supply our energy needs, technologies like bioenergy, hydro-, wind and solar energy.

The focus of this thesis is the assessment of a specific variety of one of these renewable energy technologies, namely solar photovoltaic energy, or in short: PV. In the context of what is described above, there are large R&D efforts being made to develop and improve many different varieties of PV. One of these PV varieties is the silicon heterojunction (SHJ) technology, which combines wafer based and thin-film silicon technologies. In this thesis, we analyse SHJ technology from different perspectives, and try to assess whether it meets the criteria for a future energy technology. In the rest of this chapter we introduce the technology and history of PV, describe SHJ technology, and discuss our approach for this thesis.

1.2 Photovoltaic Technology

Photovoltaic energy, the conversion of solar irradiation into electricity, saw its first implementation well over a century ago, although the first practical solar cell (with an efficiency of 6%) was developed in 1954 by Bell Laboratories [9]. Solar cells operate because of the photovoltaic effect: the generation of a voltage and, as a result of that, electrical current in a material upon its exposure to light. An incoming photon is absorbed by the material, resulting in an electron being separated from its atom, leaving behind a positively charged hole, which is like the electron not bound to an atom and thus mobile (although less mobile compared to the free electrons). In a solar cell the generated holes and electrons are separated on opposite sides of the cell, leading to the build up of a voltage over the material. Connecting the opposite sides of the cell with a conductor results in a current through this conductor, which can perform work (power = voltage $\times$ current). From this very basic description of the photovoltaic effect we can see that four characteristics are vital for the solar cell's operation: absorption of photons, generation of free electrons and holes, charge separation and charge collection. During normal operation, the voltage over the cells is regulated by a maximum powerpoint (MPP) tracker, which optimises the voltage to achieve maximum power out of the cell given its current-

voltage characteristics. For an ideal cell, these current-voltage characteristics are described by the Shockley ideal diode equation:

$$I = I_{\text{ph}} - I_0 \left(\exp\left(\frac{qV}{kT} \right) - 1 \right) \tag{1.1}$$

where I is the current through the cell, I_{ph} the light-generated current, I_0 a leakage current called the diode saturation current, V the voltage over the cell, T the cell temperature and q and k constants (elementary charge and Boltzmann constant, respectively). Figure 1.1 illustrates the relations between cell current, voltage, and power.

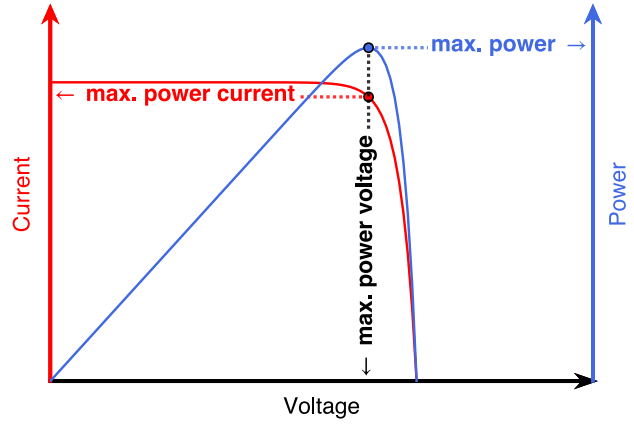

Figure 1.1 · Example of a solar cell current-voltage curve and a power-voltage curve

Solar PV cells consist of a semiconductor material, in which, through the irradiation by photons from the sun, free electrons and holes are generated, separated, and collected. In principle, every semiconductor material could be used to generate electricity from solar irradiation, but the band gap (E_g), the energy gap between the valence band and the conduction band of the material, is specific to this material [10]. The energy of an incoming photon (E_{ph}) should be sufficient to excite electrons from the valence band to the conduction band, thus crossing this energy gap. However, the photons that reach the earth's surface have a large variation in available energy. When we examine the spectral distribution of the incoming light on our planet (Figure 1.2) we see an uneven distribution of photon wavelengths (λ), and thus a variation in photon energy, as $E_{\text{ph}} = hc/\lambda$, where h is Planck's constant and c is the speed of light. Only those photons with $E_{\text{ph}} \geq E_g$ can excite an electron into the conduction band. This requirement, and the fact that the excess photon energy does not result in more electron-hole pairs being generated, is one of the main reasons of the limited efficiency of (single junction) solar cells. This

requirement also has the consequence that only a limited variety of materials have band-gap energies suitable for PV electricity production using light from the sun[1].

To produce electricity from PV cells, they are aggregated in a PV module, which typically consists of 60 cells connected in series to increase the voltage. In a PV array, multiple PV modules are connected, in series or in parallel, and the combined set of PV modules is connected to an inverter when electricity is to be fed into the electricity grid. The inverter converts the direct current output of the PV array into alternating current at a voltage level suitable for feed-in to the electricity grid.

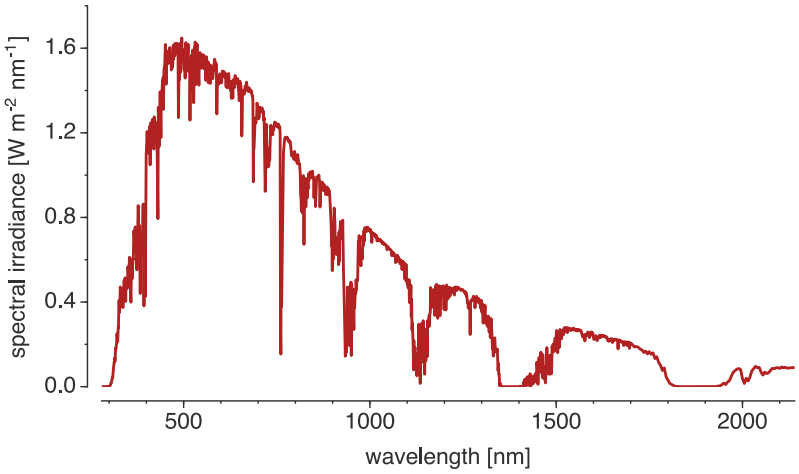

Figure 1.2 · Spectral power density for light traveling through 1.5 air mass. Source: NREL [12]

1.2.1 Main photovoltaic technologies

The crystalline silicon solar cell is currently the most common type of solar cell. Since the first implementation of silicon PV panels, its efficiency has increased from about 6% for the Bell Labs cell, to up to 25% for the current record efficiency cell (under laboratory conditions). This type of solar cell consists of a thin crystalline silicon wafer (either multi- or monocrystalline) in which a *p-n junction* is formed – commonly through diffusion – with dopants like boron or phosphorus. The majority (about 90%) of solar cells sold today are crystalline silicon cells, with a roughly even split between the multi- and monocrystalline cells. Monocrystalline cells are more expensive and energy intensive to produce compared to multicrystalline cells, but also have higher efficiency (25% [13] vs. 21.3% [14] respectively; see Figure 1.3).

[1] In very specific implementations of PV, other materials might be suitable. For instance, in thermophotovoltaics, heat radiation (infrared light) with very long wavelengths and thus very low photon energies is converted to electricity, allowing (or even requiring) the use of low-bandgap materials [11]

Thin-film solar cells account for the largest part of the remaining 10% market share. Generally, they are produced as a thin film of active material, deposited on a substrate like glass, metal or plastic sheet or foil. Compared to the wafer based crystalline silicon cells, much less active material is normally needed, reducing production costs. There are various types of thin-film solar cells, silicon based cells made from amorphous (hydrogenated) silicon (a-Si:H), but also cells made from other semiconductors such as cadmium telluride (CdTe), and copper indium gallium (di)selenide (CIGS). Small area record cell efficiencies (see Figure 1.3) are 13.6% (a-Si[1]), 21.0% (CdTe), and 21.0% (CIGS) [14].

1.2.2 PV as a viable source of electricity

Solar panels have been known for many decades, and for a long part of this period have been surrounded by an "aura" of high-tech and high costs. The application of solar panels was restricted to experiments and in space, for powering satellites and spacecraft. Gradually, the idea started to grow that PV could also contribute to electricity generation on Earth, but the high prices of solar panels remained a barrier to deployment. More recently, solar panels are being seen as a viable option of generating electricity on a large scale in the built environment of our planet, as an alternative to fossil fuel based electricity generation. The main drivers behind this shift are the steady increase in solar cell efficiency and especially the steady decrease in solar cell, module, and system prices over the last decades, which has strongly accelerated the last 5-10 years. The increases in solar cell efficiency are a result of continued research and development in the PV industry, leading to improvements in production processes and solar cell and module materials and layouts. The cost reductions are mainly a result of more efficient material use (especially silicon and silver use reductions) and increased cell efficiency, which results in a decrease of the cost of PV per watt of output power.

Electricity generated with solar panels is often viewed as one of the cleanest forms of electricity, together with wind and hydro-power. A distinct advantage of solar electricity is its renewable character: it does not rely (necessarily) on fossil fuels. Furthermore, because of the modular character of solar panels, PV can be applied from very small (under 1 kW for dedicated PV systems, but even in the mW scale for product integrated applications[2] [15]) to very large (over 100 MW) scales. This results in possible application for instance for consumers in developed countries, but also as a means to achieve off-grid, rural electrification in developing

[1] The record cell efficiency for a-Si shown here refers to a triple-junction cell, in contrast to the other technologies discussed. For a single junction a-Si cell, the record efficiency is 10.2% [14]

[2] For example: solar cells integrated with calculators, battery chargers and other small electronics

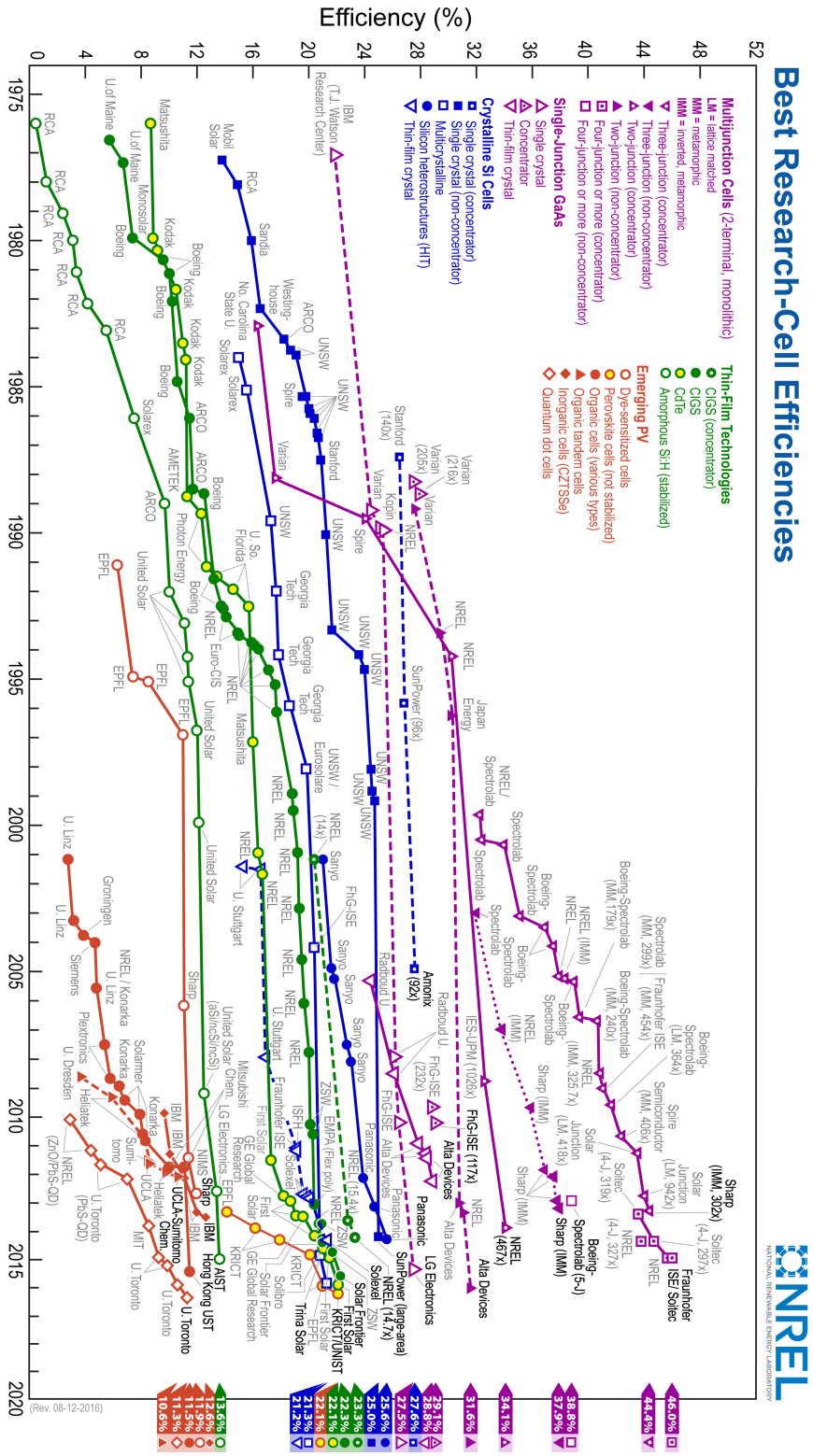

Figure 1.3 · Best research-cell efficiencies of various types of PV cells from 1975 to present. We can see that SHJ cells offer cell efficiencies that are higher than mono-crystalline cells and thin-film technologies under standard test conditions. Source: NREL [12]

countries. The modular character, combined with the fact that PV panels do not involve moving parts, also allows PV to be integrated in buildings and infrastructure objects [16], further increasing the wide range of applications for PV.

1.3 PV in the global energy supply system

Especially the last few years, the cumulative installed PV capacity has increased tremendously. In the last ten years, it has grown from under 5 GW_p by the end of 2005, to over 230 GW_p by the end of 2015. Figure 1.4 shows this trend. Traditionally, Japan was the major PV market, but around the beginning of this century, there were major developments in Germany, where strong government support schemes drastically increased the installed PV capacity. More recently the market has increased dramatically in China, which became the number one PV market in 2015, while growth has somewhat stalled in Germany. In Italy, installed capacity increased dramatically in 2011, but growth stalled soon after. The United States have seen steady growth since 2004, which is expected to increase in the near future.

When we examine the supply side of the PV market, the picture is quite different, especially for the last ten years. The price of solar panels dropped tremendously, as annual production figures increased from 2 GW_p/year in 2005 to almost 50 GW_p/year in 2014. In the same period, demand for solar panels drastically dropped due to the economic crisis. Traditionally, Japan and Europe were the main producers of solar panels, however, since 2007-2008, the market is dominated by Chinese production. Figures 1.5 clearly confirm this very dynamic market of the last ten years. Roughly doubling its production capacity between 2007 and 2011, China has increased its market share as a producer (in terms of cell production) from about 25% in 2007 to around 60% in 2014 [17, 18, 21]. Meanwhile market shares for other major producers, like Germany, Japan and the US have fallen despite (relatively small) production capacity increases [18, 21]. In the rest of the market, Taiwan is a major producer with 16% production share in 2014. In terms of module production, China has an even greater market share at around 64% [18].

The contribution of PV electricity to the global energy supply so far has been limited, when we compare it to traditional electricity sources like fossil fuels (66.7%), hydropower (16.4%) and nuclear (10.6%) plants. As of 2015, PV is estimated to supply over 300 $TWh \cdot y^{-1}$, or about 1.3% of the total world electricity production [18]. This is low compared to other renewables such as wind and biofuels that contribute about 2.9% and 1.9% respectively [23], however, the installed PV capacity and resulting electricity generation is growing faster compared to these other

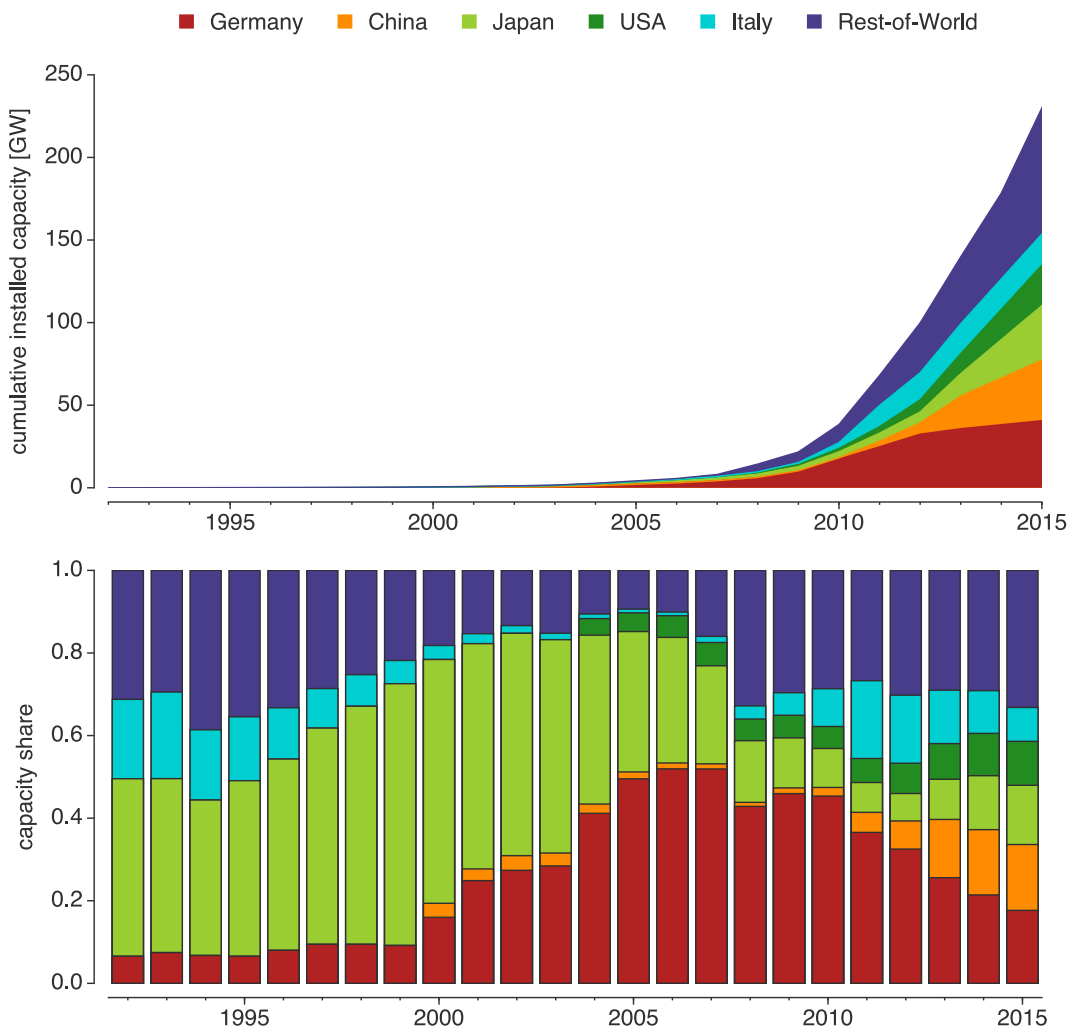

Figure 1.4 · Cumulative installed PV capacity for the countries reporting to the IEA PVPS. A breakdown is shown for the top 5 countries based on 2011 cumulative installed capacity, and the rest of the countries. Source: IEA PVPS [17–20]

renewable technologies. When examining only Europe, the share of PV in the electricity mix is much higher, at 3.5% [17]. Especially in Italy (8%), Greece (7.4%) and Germany (7.1%) the share of PV electricity is substantial. By the end of 2016, there are likely 25 countries where PV accounts for more than 1% of the generated electricity, this includes countries like China, the USA, and India. Furthermore, as is shown above, the cumulative installed PV capacity is growing extremely fast, so its contribution to electricity generation will do the same.

1.3.1 Cost of PV

As dramatically as the cumulative installed PV capacity has grown, the prices of PV modules have decreased over the last decades. While a PV module in 1985 cost

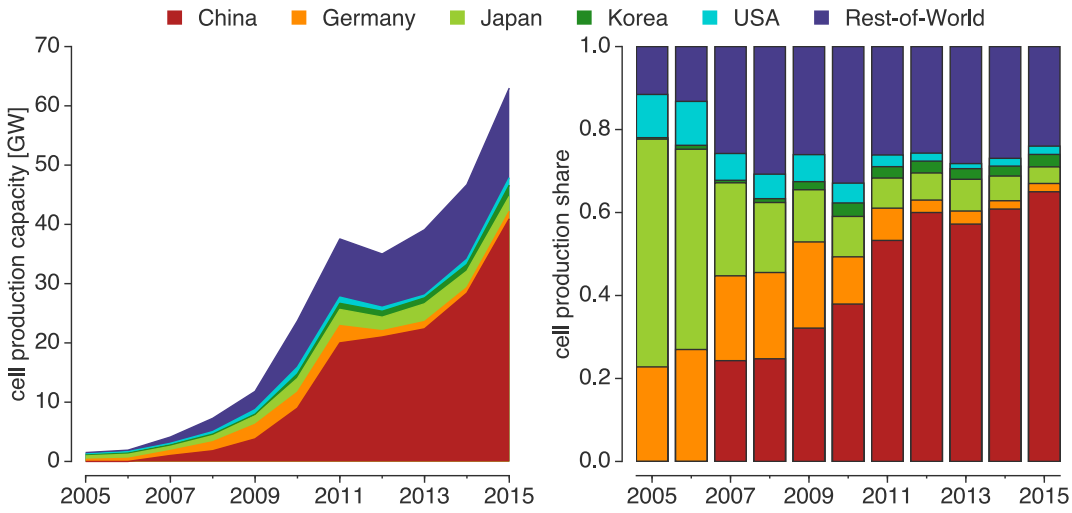

Figure 1.5 · Global PV cell production from 2005-2015 for 5 major producing countries and the rest of the countries reporting to the IEA PVPS. Source: IEA PVPS [17–20, 22]

over 20 EUR/W_p, the current cost of PV modules is around or below 0.5 EUR/W_p, while the cost of PV inverters has decreased from over 1 EUR/W_p in 1990 to around 0.1 EUR/W_p in 2013 [24]. On average, the cost of PV modules and inverters was found to decline by around 20% and around 19%, respectively, for every doubling of cumulative production. As a result, a complete PV system now costs around 1 EUR/W_p, and the LCOE of PV electricity is around 8 EUR/MWh in Central and Southern Europe [24]. In countries with very high solar irradiance, recently power purchase agreements have been signed to deliver electricity at a cost as low as 2.4 USD/MWh (2.2 EUR/MWh) [25], undercutting the cost of local fossil fuel alternatives.

1.3.2 Projections

While the share of PV in the global energy supply system might at the moment still be considered minor, various projections of the development of installed PV capacity attribute a large future role for PV in supplying our electricity. On the short term, the cumulative installed capacity is expected to grow to 490-716 GW_p by 2020 [24, 26, 27], while on the longer term, projections vary even more, from 569-938 GW_p by 2030, and 773-1519 GW_p by 2040 in International Energy Agency (IEA) scenarios [28] or 4295-30749 GW_p in 2050 in much more optimistic scenarios by Fraunhofer ISE [24]. The current growth rate of installed capacity of around 50 GW_p/year would be sufficient to achieve the higher end of the IEA scenarios, while for the lower and higher ends of the Fraunhofer ISE scenarios, the current growth rate would need to increase to 175 and 1583 GW_p/year, respectively, e.g.

an increase of the annual market size with a factor 3.5 and 32, respectively. PV system prices are expected to decline to 0.28-0.61 EUR/W_p in 2050, lowering the LCOE in Central and Southern Europe to 1.8-4.4 EUR/MWh [24].

1.4 Silicon heterojunction solar cells

As described above, there are two main technologies that dominate the PV market: poly- and monocrystalline silicon. These technologies have demonstrated enormous cost reductions over the last 50-60 years, concurrent with improvements in the production process, enhanced material utilisation and increased cell and module efficiencies. However, although electricity production costs of PV are now competitive with those from fossil fuels in some locations with high irradiance, this is not yet the case for large areas that receive less solar irradiance. In order for PV to become a major globally dispersed source of electricity, there is thus the need for further cost reductions and improvements in cell and module efficiency, and a requirement that the produced PV modules are produced with materials that are earth-abundant, durable and stable over long system lifetimes of over 25 years [29].

As a result of these requirements, and despite continued R&D to improve the major crystalline silicon technologies, a wide range of alternative PV technologies is being developed. Examples include the aforementioned thin-film technologies, but also relative newcomers like organic based, and perovskite based PV cells. Especially perovskite PV has shown dramatic improvements in small area cell efficiency over the last years, increasing from around 12% in 2013 to 22.1% recently [12]. Both technologies however have issues with long-term stability [30] and scalability, and most perovskite cells to date currently rely on a lead-based perovskite structure, which is regarded as undesirable due to the toxicity of lead.

One of the technologies that are being investigated that build on the experience with crystalline silicon is the **silicon heterojunction** (SHJ) technology. This technology combines crystalline silicon wafers and thin-film amorphous silicon. Since the 1990's we have seen the gradual development of SHJ solar cells, which accelerated somewhat more recently due to the increase in production development owing to the expiry of core patents for SHJ technology. This type of cell consists of a crystalline silicon layer, on top of which amorphous silicon layers are deposited. The main advantages of this type of solar cells is the potential for high efficiency and the lower temperature processing required to produce this type of PV cell. Also, the production process is said to be simplified in comparison to conventional crystalline silicon PV cells [29]. The c-Si/a-Si SHJ cell was first developed by Sanyo (now Panasonic) some twenty years ago. The core patents of this

technology described the addition of intrinsic (undoped) and hydrogenated a-Si layers in between the doped c-Si layer and the doped a-Si emitter. These patents recently expired, resulting in a strong increase in R&D on SHJ solar cells. Very recently, Kaneka became the world-record holder for SHJ efficiency, with a back-contacted SHJ cell with an efficiency of 26.3% [31]. For SHJ cells, generally the efficiency reaches these high values because of the excellent passivation properties of the intrinsic a-Si:H layers, leading to a very high open-circuit voltage V_{oc} [29, 32]. In other research groups, a variety of SHJ cells based largely on the design by Sanyo/Panasonic is being investigated, with multiple groups reporting cell efficiencies of over 20% [29]. These high efficiencies demonstrate this technology's ability to approach the efficiency of conventional crystalline silicon PV panels while offering advantages in the production process. An additional advantage is the low temperature coefficient which might lead to higher energy yield. Current SHJ cells require comparatively large amounts of silver for contact formation [33], and are usually made with indium-tin-oxide (ITO) transparent conductive oxide (TCO) on the front and back to improve lateral conductivity. Because of the high price of these materials, and because of some parasitic absorption of light in the ITO layers, metallisation and TCO are main research areas for improving the efficiency and cost of SHJ solar cells. R&D in this context focuses on silver consumption reduction by alternative metallisation schemes, substitution of silver with copper, predominantly using copper electroplating, and substitution of indium with alternative TCO materials.

One of the R&D projects working on SHJ cells was the project *"Heterojunction Solar Cells based on a-Si/c-Si"* (HETSI) project [34]. This project was supported by the European Commission under their *Seventh Framework Programme*, and was a cooperation between various European research institutes. The project resulted in an SHJ cell with a European record efficiency of 20.7%. As a Dutch national follow-up, the project *"Fundamentals and Application of Silicon Heterojunction solar cells"* (FLASH) was started in 2011, aiming to continue R&D on SHJ cells. The FLASH programme is an STW *Perspectief* programme and is comprised of in total 9 projects spread over 4 *Work Packages* focussing on fundamentals (WP1), application (WP2), scaling up (WP3), and environmental and economic assessment (WP4) of SHJ technology. The work performed in WP4 is presented in this thesis, its outline and aim are detailed in the sections below.

1.5 Environmental assessment

The fast increase in installed PV capacity is, aside from decreases in PV system prices, also largely due to incentive programs implemented by governments to

speed up the transition to renewable electricity generation, and make steps towards achieving GHG reduction targets. Compared to conventional electricity generation, electricity produced with PV systems has a very low GHG emission factor. While fossil fuel based electricity generation typically emits around 400-1000 gCO_2-eq/kWh depending on the fuel type, recent studies show that the GHG emissions associated with PV electricity are in the range of 10-85 gCO_2-eq/kWh, depending on the type of PV, primary electricity source, and production and installation location [35–37]. Thus, compared to fossil electricity generation, there is ample potential for GHG emission reduction, but compared to other renewable energy technologies like wind energy, with a GHG emission factor of about 3.0-45 gCO_2-eq/kWh [38], there is still room for improvement.

As mentioned before, R&D on PV technologies is still very active, and focused on increasing energy conversion efficiency, reducing the amount of input materials, and substituting scarce or expensive materials. SHJ solar cells, like conventional crystalline silicon solar cells, are based on silicon wafers. However, where the *pn*-junction in conventional silicon solar cells is formed with high temperature diffusion processes, this junction is made by deposition of doped amorphous silicon in a heterojunction configuration. This change in production process decreases the thermal budget and therefore the energy requirement of cell production [29], possibly resulting in reduced environmental impact and production costs.

The environmental impact of conventional crystalline silicon PV, as well as that of main thin-film technologies is well understood, as a large number of lifecycle assessment (LCA) studies have been performed. For relatively new or minor technologies, like SHJ, there has been little research performed on the environmental impact. Furthermore, there is a large variety of different SHJ cell designs being investigated, calling for a more in depth assessment of SHJ technology in general, and a comparison of the environmental impacts of different SHJ designs.

A related issue concerning the environmental impact of PV in general, is connected to the fast growth of the PV industry. The main impact of PV electricity is due to the production of the PV system components, and occurs before the beginning of a 30 year system lifetime producing environmental benefits by replacing high-environmental impact electricity from fossil fuel sources. Considering these up-front investments in PV systems, in terms of environmental impact, it takes some time *PBT* (payback time), to repay this environmental debt. When the growth of the PV industry is larger than $1/PBT$, the result is that the industry is at that moment a net emitter of environmental impact, while the aim with PV is to reduce the environmental impact of electricity generation. This effect can however be offset by periods of less strong growth in later stages. Therefore, in order to analyse the net environmental impact of the PV industry as a whole, one needs to take

into account the development over time of both the installed PV capacity, and the environmental impact of the production of PV systems.

1.6 Economic assessment

As mentioned before, the price of PV modules and systems has dropped dramatically over the last decade. The last few years, due to a large increase in PV module supply, prices have dropped so far that some PV producers, including major companies, are struggling financially. As a result, production cost reductions are very much needed. Furthermore, although the low price of PV has enabled direct competition with fossil fuel based electricity in some locations [39], and residential grid parity has been achieved in several countries worldwide [40], further cost reduction are needed to assure PV production is financially stable and PV electricity becomes competitive with bulk electricity generation in broad geographical areas.

The past cost reductions have been made possible predominantly by economies of scale and technological learning and innovations [33]. For crystalline silicon, main cost reductions resulted from using ever thinner wafers and decreasing silicon losses, and reducing the amount of silver used in cells. As the room for further improvement is becoming limited, and also to increase the efficiency of the cells, many alternative designs, like SHJ, are being investigated. SHJ cells are only produced on a large scale by Panasonic, and rely on large amounts of silver [33], making them quite expensive. In order to improve the economics of SHJ, the FLASH programme investigates several alternative SHJ cell designs, aiming to understand what exactly determines their quality, to replace expensive materials and simplify the production process. Aside from silver, current SHJ designs also rely on the application of indium, in a transparent conductive oxide (TCO) layer as indium-tin-oxide (ITO) [29], to improve the lateral conductivity of the cells. Indium is often regarded as being expensive, and there are doubts about the long-term availability of the material. With this in mind, many R&D projects focus on replacing the ITO layer by a TCO layer based on other materials, such as zinc oxide, or changing the design to completely omit the TCO layer or combine its function with other layers of the cell. Aside from current designs changes, there are also changes to be expected for prospective SHJ cell designs, such as replacing silver with copper-based metallisation, and a transition to altogether different cell and module layouts. There is currently almost no literature available on cost breakdowns of SHJ cells, which does not allow for an accurate assessment of the relative costs of different SHJ designs and the cost benefits and drawbacks of changing current and prospective cell designs.

1.7 Performance assessment

The energy output of PV panels is one of the key parameters determining both the environmental and economic costs of electricity produced with PV. Both for environmental footprint and economics, the majority of costs occur during production of the PV system, while during operation almost no environmental impact is released, and operation and maintenance costs are very low, especially for residential systems. Therefore, environmental and economic cost of electricity produced with PV is proportional to $1/E_{\text{lifetime}}$, where E_{lifetime} is the lifetime energy output of the PV system. Thus, the larger the energy output of a PV system in its lifetime, the lower the environmental impact and cost are of the electricity produced with it. Assessment of the performance of the SHJ panels is therefore essential in order to accurately assess the environmental and economic performance. Currently, the power output of PV modules is determined at standard testing conditions (STC), which comprise an irradiance of 1000 Wm^{-2}, a temperature (for the cells) of 25°C, and a spectral composition of the irradiance that conforms to the AM1.5G standard solar spectrum defined by IEC 60904-3 ed. 2. [41]. Furthermore, in many LCA studies on the environmental performance, standard figures for irradiance (1700 kWh/m^2) and performance (performance ratio *PR* of 0.75) are used to ensure different studies can be compared. However, in practical operation, these conditions hardly occur, and the performance of PV modules is affected by the deviation of practical operating conditions from STC values. Furthermore, the local weather conditions determine in what manner the operating conditions deviate from STC values, and thus the performance of PV can be very locally dependent. Each type of PV can respond differently to changes in different operational parameters. For instance, the yield of SHJ modules is often proposed to be superior to that of conventional crystalline silicon modules, as the adverse effect of temperature is smaller for SHJ modules. However, operation temperatures are likely to vary from one location to the other.

1.8 Thesis objectives and outline

This thesis' main focus is to perform a comprehensive ex-ante assessment of SHJ technology, in which the environmental footprint, economics and energy performance are assessed. As the market penetration of SHJ PV modules is still very limited, we aim to analyse the technology from these different perspectives, before it is possibly deployed at a larger scale. As PV is supposed to contribute to a transition from a non-renewable to a renewable energy supply system, we need to know in advance what the environmental and economic characteristics of the technology

are, and how they are related to the location where it is produced and installed. SHJ PV should be able to produce electricity at low cost, with low greenhouse gas (GHG) emissions as possible, in an energy-sustainable manner. A requirement for this is that the performance of the technology is comparable or better compared to other types of PV. Finally, to allow for large-scale deployment, the technology should be produced with materials that are not finite on human timescales. This thesis aims to answer the following research questions:

1) *What is the lifecycle environmental impact of different existing and conceptual SHJ cell designs and systems based thereon, and how do these compare to conventional crystalline silicon solar cells and systems?*
2) *What are the production costs of different existing and conceptual SHJ cell designs and modules based thereon, and how do these compare to conventional crystalline silicon solar cells and modules?*
3) *How do prospective design changes in SHJ cell designs affect environmental impact and economics?*
4) *How does the outdoor performance of SHJ modules compare to a variety of commercial alternatives?*
5) *How does the performance of SHJ modules vary as a function of geographical installation location, and how does the variation compare to a variety of commercial alternatives?*
6) *What is the contribution of the PV industry in reducing the environmental impact of electricity generation, in terms of both energy and GHG emissions?*

Table 1.1 shows an overview of the chapter topics, and the research questions that are adressed in each of the chapters. The sections below describe in detail the topics, aims and approaches of each of the chapters.

In **Chapter 2**, we focus on questions 1 and 3, and analyse the environmental footprint of SHJ technology, by comparing different SHJ cell designs and PV systems based on these designs. We analyse the production processes of each of the designs by means of Lifecycle Assessment (LCA), making an inventory of all the material and energy flows into and out of the life cycle of the respective designs. Furthermore, we compare the results for SHJ with those of a conventional monocrystalline silicon based PV system. For the SHJ designs, we gather new data detailing the material and energy flows in the production cycles of the SHJ cells. For background data (like input materials) and the monocrystalline silicon PV cells and system, we make use of preexisting LCA databases and research results. For all the designs studied we attribute an energy cost (cumulative energy demand;

CED) and greenhouse gas footprint to all material and energy flows based on established LCA methods [42–44]. The resulting data allows us to characterise the whole lifecycle of the different designs and PV systems, so we can identify the contributions of different processes in the production cycle to the overall environmental footprint. Subsequently, the total footprint for the whole lifecycle is used to determine the energy payback time (EPBT) and the GHG emission factor (in gCO_2-eq/kWh) of the studied PV systems, based on a standardised assumed energy yield and performance of PV systems. We analyse designs for a current and prospective cell architecture, and show which improvements that can be made to cell designs have major effect on decreasing the environmental footprint of PV. As there is little known about the environmental footprint of SHJ technology specifically, this research builds the bases for continued LCAs on this technology, and establishes the environmental footprint of SHJ, allowing for comparison with alternative technologies. Furthermore, pathways to future reduction of environmental footprint are identified.

In **Chapter 3**, we aim to answer questions 2 and 3, and use the lifecycle inventory data gathered in Chapter 2 to perform a cost analysis, comparing the different SHJ designs, again also with conventional monocrystalline silicon based PV. For all the material and energy flows analysed in chapter 2, we determine the associated costs. For all studied designs, we focus on the cells and modules, and gather data on the costs of materials, but also those of the production equipment used in the different process flows. Again, we study current and prospective cell designs, and highlight what the effect is of expected changes in cell and module designs on future cost reductions.

Table 1.1 · Overview of the topics of the chapters and the research question addressed in each of them.

Chapter	Main topic	Research questions					
		1	2	3	4	5	6
2	Environmental assessment of current and prospective SHJ cells, modules and systems	•		•			
3	Economic assessment of current and prospective SHJ cells and modules		•	•			
4	Outdoor performance characterisation and analysis of commercial PV modules				•		
5	Modelling of geo-spatial performance of commercial PV modules				•	•	
6	Analysis of environmental learning rates in PV and modelling of net environmental impact of PV industry as a whole						•

In **Chapter 4**, we analyse the outdoor performance of several different types of commercially available PV modules: SHJ, mono- and polycrystalline silicon, cadmium telluride (CdTe), copper indium selenide (CIS), copper indium gallium selenide (CIGS) and amorphous silicon (a-Si). We use data measured with a PV testing facility in Utrecht, the Netherlands, to establish the effect of different parameters on the performance of the different PV modules. We analyse the effect of variation with respect to STC conditions of irradiance, temperature, spectral composition and angle-of-incidence by performing curve fitting of models describing the effect of these parameters on performance of PV. The curve fitting is performed on datasets filtered to show variation only in the studied parameter. The resulting curves offer us empirical models to describe and analyse the effect of each parameter on a instantaneous, seasonal and annual basis. We show that the effect of variation in operating conditions with respect to STC conditions can have significant effects on the annual energy yield, and that these effects can be very different from one type of PV module to the other.

In **Chapter 5**, we expand the analysis of performance of PV from a very specific location (Chapter 4) into an analysis that covers a broad geographical range. In this chapter we use PV performance modelling, combined with a GIS irradiance and weather dataset that covers Europe, Africa and a large part of the Middle-East, to analyse the performance of different types of PV modules including SHJ modules, and make it geospatially explicit. First we establish the optimum tilts of PV systems at every location, by calculating the annual insolation that is received by inclined surfaces and determining the tilt with the highest annual insolation. Next, we model the irradiance components (direct, diffuse) on these inclined surfaces on a 15-minute timescale. Subsequently, we model the performance of 6 different types of PV for every location in the dataset using this 15-minute timeseries of direct and diffuse irradiance and the weather dataset, which contains wind speed and ambient temperature, to model the temperature of the PV cells. The resulting annual yields are then used to show the locational dependence of the environmental footprint of PV. As the energy yield of PV varies significantly at different locations, so does the environmental footprint of PV electricity. Furthermore, as PV is installed to replace fossil-fueled electricity production, it is interesting to analyse what the balance is between local energy mixes with varying degrees of renewable energy penetration, and the environmental impact of PV resulting from local PV energy yield.

In **Chapter 6**, we take a look at the PV industry as a whole, and analyse the development of environmental impact of PV over the last 40 years, to determine to what extent the fast growth of the industry in the last years has had adverse effects on the energy and GHG balance of PV. Using LCA studies conducted during this period, and data that detail the development of cumulative installed PV capacity,

we try to establish *learning curves* or *experience curves* for environmental impact of PV.

The established learning curves are used, in conjunction with data on the development of cumulative installed capacity, to establish the cumulative environmental impact of all installed PV capacity over time. Here, we also take into account production location and technology shares. Two PV performance scenarios combined with the development of cumulative installed PV capacity are used to calculate the (cumulative) electricity production from PV and the cumulative development of environmental benefits. In terms of environmental impact and benefits, we focus on energy (CED) ang GHG emissions of mono- and polycrystalline silicon based PV systems. The analysis also focuses on determining whether, and if so when, there is a break-even between the energy invested in PV and the resulting GHG emissions, and the energy produced with PV and the resulting GHG emissions avoided. We also perform a Monte Carlo analysis to analyse the effect of uncertainty in the established learning curves on our results.

In **Chapter 7**, we summarise the findings of of Chapters 2-6, revisit the main objectives of the thesis, and make a connection between the findings of the different chapters. We also reflect on and discuss our results and the methods we have used to obtain them.

2

Life-cycle greenhouse gas emissions and energy payback time of current and prospective silicon heterojunction solar cell designs

Published in: Prog. Photovolt. Res. Appl. 23 (10) 1406-1428 (2015)
doi: 10.1002/pip.2540

Abstract Silicon Heterojunction (SHJ) cells offer high efficiencies and several advantages in the production process compared to conventional crystalline silicon solar cells. We performed a life-cycle assessment to identify the greenhouse gas (GHG) footprint, energy payback time (EPBT) and cumulative energy demand (CED) of four different SHJ solar cell designs. We analyse these environmental impacts for cell processing and complete systems for both current and prospective designs. Based on in-plane irradiation of 1700 kWh/m^2, results for current designs show that life-cycle GHG emissions could be 32 gCO_2-eq/kWh for complete SHJ PV systems (module efficiencies of 18.4%), compared to 38 gCO_2-eq/kWh for conventional monocrystalline silicon systems (module efficiency of 16.1%). The EPBT of all SHJ designs was found to be 1.5 years, compared to 1.8 years for the monocrystalline PV system. Cell processing contributes little ($\leq$6%) to the overall environmental footprint of SHJ PV systems. Among cell processing steps, vacuum based deposition contributes substantially to the overall results, with 55-80%. Atomic layer deposition of thin films was found to have a significantly lower environmental footprint compared to plasma enhanced chemical vapour deposition and sputtering. Copper-based compared to silver-based metallization was shown to reduce the impact of this processing step by 74%-84%. Increases in cell efficiency, use of thin silicon wafers and replacement of silver-based with copper-based metallization, could result in life-cycle GHG emissions for systems to be reduced to 20 gCO_2-eq/kWh for SHJ systems and 25 gCO_2-eq/kWh for monocrystalline system, while EPBT could drop to 0.9 and 1.2 years, respectively.

2.1 Introduction

During 2012, the global installed photovoltaic (PV) capacity crossed the 100GW_p mark [45]. Up to 2012 we saw more than exponential growth of installed PV capacity, largely due to declining prices for PV systems throughout the world, and successful support schemes from governments. In 2012, the growth of the PV market more or less stabilized, as a similar amount of capacity was installed in that year, compared to 2011 [45]. Taking Germany as an example, this extreme growth now results in PV meeting roughly half of the peak electricity demand on sunny spring and summer days [46, 47]. When we examine the types of PV systems being sold, we see that the majority of panels sold are of the crystalline silicon type, which is a quite mature technology. However, research and development (R&D) of many different types of PV technologies is still intensively ongoing, in order to reduce costs, material use, to replace scarce materials, and to decrease the environmental impact of production.

This fast growth, aside from decreases in system prices, is also for a significant part due to the environmental profile of electricity generated with PV. Extensive research on the environmental impact of various PV technologies has shown that all PV technologies currently available to consumers, are effective in reducing greenhouse gas (GHG) emissions in electricity generation compared to current fossil fuel based alternatives. Fossil fuel based electricity generation typically emits some 400-1000 gCO_2-eq/kWh, depending on the type of fuel and power plant efficiency. In a recent review of 13 life cycle assessment (LCA) studies on the GHG emissions of crystalline silicon PV, an average$\pm$(standard deviation) of 52$\pm$29 gCO_2-eq/kWh was found, for LCAs harmonized to accord with IEA guidelines on PV LCAs [44]. With a similar harmonization approach, the GHG emissions for electricity from thin-film PV was found to be on average 14-38 gCO_2-eq/kWh for various thin-film technologies [48]. These values confirm the CO_2 emission reduction potential of PV technology, but also leave room for improvement, especially compared to for instance wind powered electricity generation, which was found to emit only about 20 gCO_2-eq/kWh [49].

As mentioned before, R&D on PV is still ongoing, in order to increase efficiency and reduce costs and environmental impact. One of the approaches to this end is the R&D on silicon heterojunction (SHJ) solar cells, which combine design elements from wafer based and thin-film silicon solar cells. Since the recent expiry of core patents describing the structure of silicon heterojunction (SHJ) solar cells with intrinsic thin a-Si layers, research on and development of such cells strongly increased [29]. An example of such research was the HETSI project, performed under EU grants [34]. A national follow-up programme is currently ongoing in

the Netherlands, called FLASH (Fundamentals and Application of Silicon Heterojunction solar cells). This programme aims to develop cost-effective SHJ solar cells based on abundant-only materials.

SHJ solar cells, like conventional crystalline silicon solar cells, are based on silicon wafers. However, where the *pn*-junction in conventional silicon solar cells is formed with high temperature diffusion processes, this junction is made by deposition of doped amorphous silicon in heterojunction cells. This change in production process decreases the thermal budget and therefore the energy requirement of cell production [29], possibly resulting in reduced environmental impact and production costs.

In general, research on solar cells is focused on replacing materials commonly used today, or decreasing the amounts of material used. Currently, silicon based solar cells often require several scarce and/or expensive materials, like silver (for the contacts) and indium (for a transparent oxide that increases conductivity). Furthermore, silicon wafers contribute strongly to the production costs and environmental impact of wafer-based solar cells, mainly due to the high energy requirements for purification of silicon and wafer sawing. In this context, the FLASH programme aims to replace scarce materials with abundant ones, and to decrease the amount of silicon used in SHJ cells by reducing the thickness of the wafers used.

Reports by (amongst others) De Wild-Scholten *et al.* [50], Fthenakis *et al.* [51] and Van der Meulen *et al.* [52] have pointed to the use of high global-warming-potential (GWP) fluorized gasses (like nitrogen trifluoride or, even more so, sulphur hexafluoride) in processes like chamber cleaning. All three studies found potential emissions of these gasses to significantly contribute to the life-cycle GHG emissions of PV modules. Furthermore, Fthenakis *et al.* [51] show the usage of NF_3 to be increasing in the last decade. Therefore, we take into account the application of the high GWP gases in chamber cleaning.

As mentioned before, the environmental performance of conventional, crystalline silicon PV is relatively well established, contrary to SHJ solar cells. To date, only one life cycle assessment (LCA) on SHJ cells has been published [53], which analyses cells and modules as developed within the HETSI project [6]. Therefore, a sub-project within the FLASH programme is focused on establishing the environmental performance of SHJ cells, taking into account the design changes investigated within FLASH. Furthermore, we hope to quantify the possible benefits, in terms of environmental impact, of the lower temperature processes (compared to conventional silicon solar cells) used during the production cycle, and quantify the effect of increased efficiency. Therefore, we performed an LCA on an existing SHJ solar cell design as well as potential future designs. In our study we assessed

the environmental impact (in terms of greenhouse gas emissions), the energy payback time (EPBT) and the cumulative energy demand (CED) of these cells. With our results we hope to be able to steer the R&D towards improved environmental performance of SHJ solar cells. Additionally, we take into account the effect of the application of high GWP greenhouse gasses for cleaning of process chambers. We analyse these parameters for a crystalline silicon system as reference, and for 4 different SHJ cell designs.

2.2 Methods

2.2.1 Life Cycle Assessment

The environmental performance of SHJ cells was determined by employing Life Cycle Assessment (LCA), to quantify the material and energy flows and associated emissions of e.g. greenhouse gases. LCA is a well-established method to analyse the environmental performance of products and services, and its application is standardized by ISO standards [42, 43]. In addition, the IEA PVPS Task 12 has published guidelines specific to LCA of photovoltaic systems [44]; these guidelines were followed in this study. According to the ISO standards, LCA consists of four distinct phases: 1) goal and scope definition 2) life cycle inventory 3) life cycle impact assessment and 4) interpretation. The second phase (life cycle inventory; LCI) consists of gathering and presenting the data used as input for the analysis of environmental impact. The data gathered here and our approach are detailed in section 2.2.3.

The life cycle inventory was prepared and the life cycles were modelled using SimaPro v7.3 [54], a widely applied LCA software tool. The life cycle impact assessment was also carried out using this software, which has built-in impact assessment methods. For life cycle GHG emissions we used the “IPCC 2007 GWP 100a” (v1.02) method, based on the 4th assessment report by the IPCC [55]. Cumulative energy demand (CED) was analysed with the “Cumulative Energy Demand” (v1.08) method. For more information on these impact assessment methods see section A.1.

Although a full LCA would include impacts assessment in other categories, such as human or ecosystem toxicity, we do not consider the data we have gathered suitable for such assessments. Furthermore, as in shown in [56], CED is a strong indicator for environmental impacts in other categories. Additionally, GHG footprint is arguably the most important indicator of the environmental performance of renewable energy technologies, as these technologies mainly enjoy public support for reducing the global warming impact of our energy supply.

Table 2.1 · Overview of processes and main data sources.

Process	Main data source	Remarks
Si feedstock + Wafer	Ecoinvent [57], literature [58]	Ecoinvent data from Jungbluth *et al.* [57] adjusted for wafer thickness and kerf loss based on [58].
Cleaning & texturing PECVD of a-Si TCO Deposition Metallization	Equipment data [59], Ecoinvent [57] Equipment data [61], literature [52] Equipment data [62], Ecoinvent [57] Equipment data [63, 64], Ecoinvent [57]	Energy and material consumption from equipment data, materials LCI and waste treatment based on Ecoinvent [57, 60].
Module	Ecoinvent [57], literature [65, 66]	SHJ module adapted from Ecoinvent based on [65]
Balance-of-System	Ecoinvent [57]	Area related parameters adapted based on assumed module efficiencies.

In this study, we assumed a performance ratio (*PR*) of the solar cells of 75%, at an insolation of 1700 kWh $m^{-2}y^{-1}$ (Southern European insolation), as recommended by IEA guidelines [44] with a lifetime of 30 years for all components except the inverter, for which 15 years was assumed, requiring one replacement of the inverter in the lifetime of the PV systems.

2.2.2 Scope definition

Figure 2.1 and Table 2.1 show the processes analysed in this study and the main data sources for each process. Although the main focus of this study is to analyse new solar cells, we report the environmental impact for a complete solar PV installation (with inverter, cabling, mounting structure, etc.), to comply with the IEA PVPS PV LCA guidelines [44]. Therefore, the functional unit in our LCA study related to greenhouse gas emissions is defined as “one kilowatt-hour of alternating current electricity delivered by a PV system”.

Related to the cumulative energy demand, the functional unit is a watt of (rated) peak output (W_p). As the delivery of electricity from solar cells requires a mounting structure, an inverter and other electronic components, these were also included in the analysis (the balance-of-system, BOS). Assuming decentralized grid connection (in the built environment), transmission losses were not included. Also, we did not account for the requirement of back-up or base-load power resulting from the intermittent character of PV electricity. For the functional unit mentioned, we assessed the cumulative energy demand in megajoule of primary energy per watt-peak (MJ_P/W_p) and the life cycle greenhouse gas emissions in carbon dioxide equivalent emissions per kilowatt-hour (gCO_2-eq/kWh). The energy pay-back time cannot be expressed in terms of the defined functional unit and therefore relates to the PV system composed of modules and BOS. All studied SHJ cell designs are assumed to use the same BOS.

Temporal scope

The main aim of the study is to analyse the solar cell designs investigated within FLASH, based on the application of current state-of-the-art production methods. However, a secondary aim is to analyse the solar cells in a prospective context. For the latter, we performed a prospective LCA to establish the potential environmental performance of the SHJ cell designs in the year 2020. To this end, we analysed developments in improved production processes and reduced material use. Taking

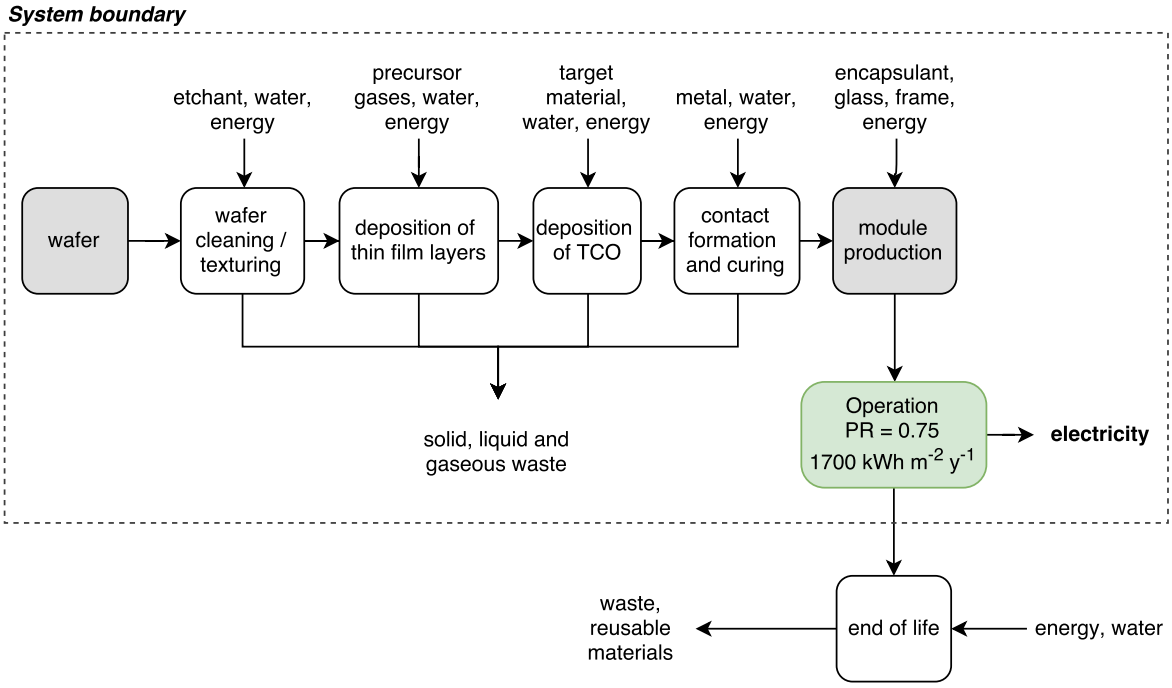

Figure 2.1 · Simplified process flow diagram of this study. Grey shaded boxes indicate processes analysed based on Ecoinvent (existing data). White boxes were analysed based on (at least partly) newly gathered data. The dashed line indicates the system boundary of this study.

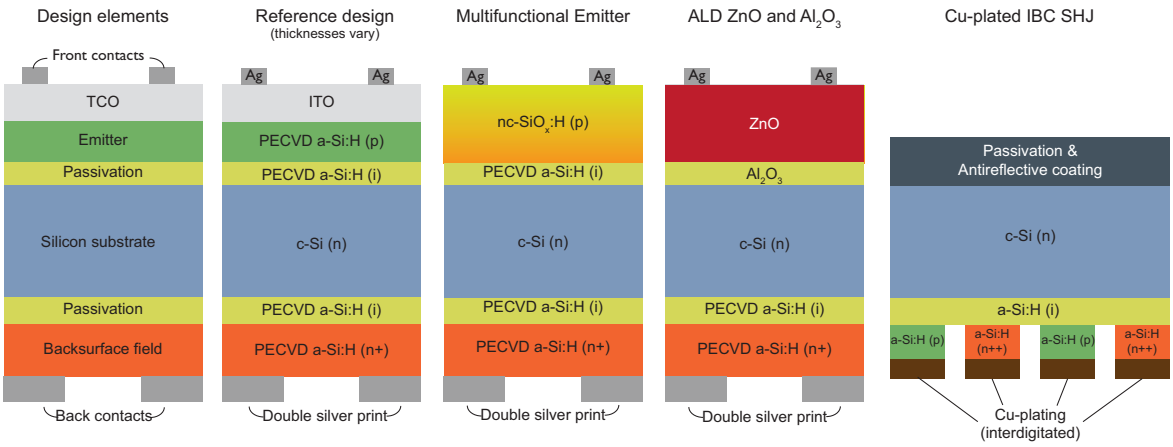

Figure 2.2 · Schematic representation of the four SHJ cell designs analysed in this study. Reference, Novel Emitter and ALD design based on: [67, 68]. Cu-plated IBC design based on [69] and [70].

these developments into account, we developed conceptual evolutions of the four current designs we discuss in the next section. In section 2.2.3, we discuss these conceptual designs and the rationale behind them.

Designs studied

In this study we analysed four different SHJ solar cell designs. Figure 2.2 shows a graphical representation of these designs, showing the structure of devices and the used materials. Table 2.2 lists the design elements for all cells. Although both cells in our project are still in a developmental stage, the analysis was performed for industrial scale production of these cells. In the analysis it was assumed that in all designs a monocrystalline Cz silicon wafer of 180 µm thickness is used. In the reference design (Figure 2.2) the cells consist of the wafer, with two layers of amorphous silicon on both sides (deposited by plasma enhanced chemical vapour deposition, PECVD) and a transparent conductive oxide (TCO) composed of indium-tin-oxide (ITO) layer on the top of the cells, deposited via sputtering.

First, saw-damaged is removed from the wafers, and the wafers are cleaned and textured. For all designs we assume a saw-damage removal using a sodium hydroxide (NaOH) bath, before a standard RCA clean and a hydrogen fluoride (HF) dip. After this, the (i) a-Si:H and (p) a-Si:H layers are deposited on the front side of the wafer. Next, the (i) a-Si:H and (n^{++}) a-Si:H layers are deposited on the backside, followed by deposition of the ITO on the front side. Metallization is then evaporated onto the backside, and screen-printed on the frontside. Curing is performed at low temperature of about 200°C [29].

The multifunctional emitter design is largely the same; with the exception that the emitter and TCO are combined in one silicon layer deposited via PECVD.

The third design again has a similar structure. Here, however, no a-Si:H is deposited, but instead, emitter and TCO are made with aluminium oxide (Al_2O_3) and zinc oxide (ZnO), deposited with atomic layer deposition (ALD) en sputtering, respectively.

The last design studied has a very different structure; it is an interdigitated back contacted (IBC) SHJ solar cell. The cell is again based on a silicon wafer and a-Si:H thin layers. The antireflective coating is formed by deposition (PECVD of SiN_x). Metallization for this design is achieved by copper plating. For the interdigitated structure, a production process was modelled based on a method developed by Q-Cells [69]. This process uses masks for selective etching and deposition of a-Si:H layers and deposition of the TCO and metallization.

The monocrystalline system was analysed based on data available in the Ecoinvent database. This data was modified only to correct for the use of 180 µm wafers,

Table 2.2 · Overview of cell design parameters for the different silicon heterojunction solar cell designs studied, for current and prospective designs.

	Reference SHJ		**Novel Emitter**		**ALD AlO ZnO**		**IBC Cu-plated**	
Cell parameters	*Current*	*Prospective*	*Current*	*Prospective*	*Current*	*Prospective*	*Current*	*Prospective*
Wafer type	mono-Si (n)							
Wafer thickness	180 µm	50 µm	180 µm	50 µm	180 µm	50 µm	180 µm	50 µm
Passivation	a-Si:H	a-Si:H	a-Si:H	a-Si:H	Al_2O_3	Al_2O_3	a-Si:H	a-Si:H
Emitter	a-Si:H (p)	a-Si:H (p)	nc-SiO_x	nc-SiOx	ZnO	ZnO	a-Si:H (p)	a-Si:H (p)
TCO	ITO	ZnO:B		-			ITO	ZnO:B
BSF	a-Si:H (n+)							
Metallization	Ag print	Cu print	Ag print	Cu print	Ag print	Cu print	Cu-plated IBC	Cu-plated IBC
Cell area (mm^2)	156×156							
Cell efficiency	20.4%	25%	20.4%	25%	20.4%	25%	20.4%	25%
Module efficiency	18.4%	23.5%	18.4%	23.5%	18.4%	23.5%	18.4%	23.5%

as Ecoinvent features thicker wafers.

Cell and module efficiency SJH cells offer high conversion efficiencies compared to standard monocrystalline cells. The current record SHJ cell has a conversion efficiency of 25.6%, the highest of any crystalline silicon based (non-concentrator) technology [71]. On a production scale, SHJ modules also offer high efficiencies, although the market-share of these modules is limited. Current production scale cells have conversion efficiencies of 21.6% [72], while SHJ module efficiency is on average 18.4% [73]. Standard monocrystalline modules are produced by a large variety of PV manufacturers, and as such the module area efficiency varies quite a lot. An average module introduced in 2012 had an efficiency of 16.1% [73]. For our study we assume module efficiencies of 18.4% and 16.1% for current SHJ and monocrystalline silicon modules, respectively. For cell efficiencies, we assume a constant cell to module efficiency loss of 2%-point, thus cell efficiency is assumed to be 20.4% and 18.1%, for current SHJ and monocrystalline silicon cells, respectively. Although it is reasonable to assume design changes will result in changes to rated cell efficiency, and thus each of the devices studied to have a specific efficiency, we have assumed all the studied SHJ cell designs to have equal cell efficiency. With the absence of accurate efficiency measurements of these designs that are still under development, this harmonization of cell efficiency highlights the effects of differences in cell processing on environmental performance.

Modules

For the most important parts, module design is similar for conventional crystalline and SHJ cell based modules, however, there are some differences. First of all, as the a-Si layers on SHJ cells are sensitive to heat and cannot be heated above 200°C [29], cell interconnection cannot be performed with traditional soldering,

but instead is made with conductive adhesive that is cured at low temperature. Furthermore, SHJ cells are more sensitive to moisture [65]. Therefore, the backsheet of SHJ cell based modules must have a much lower moisture vapor permeability. One way to obtain a lower moisture vapor permeability, is to embed a layer of aluminium foil in the backsheet, a method commonly used for thin film PV applications. Application of aluminium foil decreases the water vapor transmission rate significantly, from a value of 2.4 $g{\cdot}m^{-2}day^{-1}$ for standard backsheet (PVF-PET-PVF) to a value of $5{\cdot}10^{-4}$ $g{\cdot}m^{-2}day^{-1}$ [66]. In our analysis we assume standard module materials for c-Si based on ecoinvent [57], and replacement of traditional solder with conductive adhesive and addition of 100 µm thick aluminium foil in the backsheet for the SHJ designs.

2.2.3 Prospective 2020 Scenario

In this section we will develop a scenario for the future state of SHJ technologies. R&D for SHJ cells focusses on several aspects: replacing scarce or expensive materials, using thinner wafers, and optimising designs to reach higher conversion efficiencies. Apart from cell R&D, we expect more focus on BOS components, as these are becoming more significant in terms of overall system costs (due to decreasing module prices) and are significant in terms of environmental impact. Table 2.2 list the design elements for the current and prospective designs.

Developments in wafer production

Crystalline silicon wafers contribute significantly to both environmental impact and production costs of SHJ solar cells and PV systems. As a result, wafer manufacturers focus on decreasing high-quality silicon losses and wafer thickness. As Goodrich *et al.* [33] and Mann *et al.* [70] for instance show, wafer production is assumed to become kerf-less, with wafer thicknesses decreasing to under 50 µm. For the prospective scenario, we will assume production of wafers of 50 µm thickness with kerf losses of 50 µm.

Increased cell efficiency

Ongoing R&D on SHJ solar cells has increased the record cell efficiency from 12.3% [29] in its first implementation by Sanyo Corp in 1990, to 21.3% in 2001 [29] up to the current record of 25.6% announced in April 2014 [71], which is stated by Panasonic to be the highest of any crystalline silicon-based solar cell of over 100 cm^2 (with a thickness of 98 µm). Especially between 2001 and 2013, the trend of efficiency increase seems to be quite linear. However, future developments will

likely converge to a maximum if the basic technology does not undergo fundamental changes. For the 2020 scenario, we therefore assume a 25% cell area conversion efficiency in production and 1.5%-point cell to module losses, resulting in 23.5% module area efficiencies.

Chamber cleaning and abatement

Currently, PECVD tools commonly rely on the application of high Global Warming Potential (GWP) gases in order to clean the vacuum chambers of silicon and other contaminants deposited on the chamber surface. Emissions of these substanced can lead to a strongly increased GHG footprint of PV modules [52]. Cleaning regimes using low GWP gases such as fluorine (F_2) have been developed, leading to a strong reduction in the GHG footprint of chamber cleaning [74]. For the Prospective 2020 designs, we assume chamber cleaning to be performed with F_2 gas replacing the high GWP NF_3 used currently. We assume the same amount of F_2 is used as NF_3 in the current scenario.

Metallization

As mentioned before, current solar cell designs mainly rely on screen printed silver based metallization. The contribution of this silver-based metallization to the overall price of the solar cells is quite significant. Furthermore, the supply of silver is expected to become a main constraint when the PV industry keeps growing at the high rates we have seen over the last decade [75, 76]. Therefore, with respect to metallization, two movements are observed: 1) reduction of silver use in cells by improving metallization pastes and printing processes and 2) replacement of silver with copper. The first is a fairly straight-forward approach, but significant reductions in silver use are being reported [75]. The shift to copper based metallization is slightly more challenging, but here also promising results have been shown. Because of potential for oxidization of copper, copper printing techniques were dismissed earlier on. Especially during the drying process, exposure of copper pastes to (hot) air leads to significant degradation, but more recently, good results were obtained when copper pastes are dried in an inert atmosphere [77], although these results were obtained on aluminium oxide substrates, not yet on solar cells.

Scarce Materials

To replace the most scarce materials in the current SHJ cell designs, we have assumed all devices to be free of both silver and indium in the Prospective 2020

case. Silver screen printing is replaced with copper screen printing for the Ref-SHJ, NovelEmitter-SHJ, ALD-SHJ design. ITO is replaced with Boron-doped Zinc Oxide in the Ref-SHJ and Cu-IBC designs.

2.2.4 Sensitivity analysis

Various parameters influencing the environmental performance of SHJ solar cells and systems were varied in a sensitivity analysis to establish the impact of such variations on the overall result. In the sensitivity analysis we varied:

- Module area conversion efficiency
- The average annual insolation (kWh $m^{-2}y^{-1}$)
- The performance ratio (actual (AC) relative to rated (DC) electricity production)
- Source of electricity used in production processes

The impact of module area efficiency variability is investigated for two reasons: First, the aim of the FLASH programme and PV R&D in general is to achieve high efficiency PV cells. Furthermore, design changes could have adverse effects on cell efficiency.

The average annual insolation was varied to analyse the effect of using the PV systems at different locations. Annual insolation in Europe varies from about 2000 kWh·m^{-2}·y^{-1} in southern Greece, to less than 700 kWh·m^{-2}·y^{-1} at locations in northern Europe [78]. Within the context of this sensitivity analysis, we were especially interested in the results when using annual insolation figures for the Netherlands (about 1000 kWh·m^{-2}·y^{-1}).

The performance ratio determines the ratio between actual electricity production, and the theoretical production based on annual insolation. By standard, this value is assumed to be 75% [44]. However, research has shown that in practice, values for PR can be lower than 65% [79], but also higher than 90% [80].

Electricity consumption in the production process of solar PV cells and systems is one of the main contributors of PV life cycle GHG emissions. Large differences exist in the GHG intensity of country specific present and future electricity generation. In compliance with the standards for PV LCA studies [44], we assumed the use of European average electricity mix (UCTE), which has an emission factor of 531 gCO_2-eq/kWh. In this study we also investigated the impact of a variation in these emissions.

2.3 Life cycle inventory

For our study we have gathered data on material and energy use of several processes related to SHJ cell production. The Life Cycle Inventory (LCI) of all material and energy inputs were modelled based on the Ecoinvent life-cycle database [81].

For the monocrystalline system, which we analyse here as a reference case to compare the SHJ designs with, we have taken data from the Ecoinvent database v2.1 photovoltaics report [57]. This report gives life cycle data on the complete production chain of various photovoltaic cells, modules, and has a separate module for balance-of-system (BOS) components. It includes an analysis of the silicon feedstock and wafer production. The analysed SHJ cells we study here are assumed to be based on wafers as analysed in the Ecoinvent database. However, since Ecoinvent features 270 µm wafers, we have updated this data to be applicable to 180 µm wafers. In section 2.3.7 we will further discuss our approach.

Module materials and BOS components were also modelled with Ecoinvent data, but for SHJ modules we used a slightly different module structure (see Section 2.2.2. The amount of module materials needed was assumed to be directly related to module area.

For the SHJ specific processes, as much as possible, we have gathered new data. Table 2.1 shows an overview of the studied SHJ processes and main data sources. The following sections detail our approach for each cell processing step.

2.3.1 Wet etching: cleaning/texturing

Wet chemical etching is performed in order to clean the wafers, removing saw damage, metal particles and oxides formed on the wafer surface. Additionally, if required, wet etching can create a textured wafer surface to enhance light trapping, the latter being especially important for thinner wafers [29]. The cleaning process, including the chemicals used for cleaning, and the number of cleaning steps, can have significant effect on device performance [29]. For the processing step in which the wafers are cleaned, we analysed the material and energy use of several wet etching lines in a market survey [59]. All water and material used was assumed to be treated as industrial waste water, waste handling was analysed based on Ecoinvent data [57].

Wet etching is not as energy intensive as other cell processing steps, as electricity is mainly used for transportation of cells through the chemical baths and drying of the cells after treatment, and the processing occurs at low temperatures (ambient to 100°C). Common listed throughput rates are either 2400 wafers/hr or 3200 wafers/hr, with a maximum reported of 6450 wafers/hr. Energy use, ex-

pressed per 1000 wafers/hr of throughput, ranged from 3.13 to 37.5 kWh/h, and was on average 15.7±5.9 kWh/h, and thus 0.647 kWh per m^2 of cell area. Water consumption (de-ionised), expressed per processed wafer, ranged from 0.3 to 1.3 L/wafer, and was on average 0.8±0.2 L/wafer, or 33.4 L/m^2 of cell area.

Specifications on etchant consumption in the survey is quite limited, as for most tools it was reported to be dependent on customer requirements. Only for 4 tools it was mentioned and values reported ranged from <1mL to <2mL per wafer. As mentioned in section 2.2.2, we assumed a three step wet etching process: 1) A sodium hydroxide (NaOH) bath for saw-damage removal, 2) a standard RCA clean and 3) an HF dip. The NaOH consumption was modelled based on Ecoinvent, while the RCA clean and HF dip material consumption was based on the etchant consumption figures mentioned above, and own estimations. The input data for wet chemical etching treatment is summarized in Table A.1.

2.3.2 Thin film deposition - PECVD and ALD

For the PECVD process, we used specifications from 7 different PECVD tools designed to deposit amorphous silicon layers for thin film a-Si PV devices, that were reported in a market survey [61]. The survey lists the following specifications for several inline, turn-key PECVD lines from a variety of manufacturers:

- Throughput, which is expressed in substrates per hour
- Average energy consumption in kWh/h
- Water consumption in L/h
- Deposition rate in nm/s

We calculated energy and water consumption per unit of cell area with the approach detailed in Section A.2. Material (SH_4, H_2, O_2) consumption was modelled based on data from [52]. We assumed material use in this processing step to linearly scale with a-Si layer thickness. According to the specifications listed in the survey [61], the start-up for the PECVD process (pre-heating and creating the vacuum) accounts for a significant fraction of total PECVD related electricity consumption. Optimally, all a-Si layers are deposited without breaking the vacuum. However, many current production lines do not offer this possibility. For this study we assumed that the deposition is executed in two steps: one for each side of the solar cell, resulting in two load-deposition-unload cycles for the deposition of all a-Si:H layers. Process parameters for PECVD deposition is shown in Table A.2.

Chamber cleaning

As mentioned in the introduction, the cleaning of CVD chambers for thin-film deposition is often performed with high Global Warming Potential (GWP) fluorized gases, such as NF_3 and SF_6 [51]. To account for the application of these gases, we have included the effect of chamber cleaning in our study. The specifications listed in the survey of thin-film deposition equipment [61] list the employed cleaning gas and required downtime. For our study, we based the cleaning regime on that mentioned by Van der Meulen *et al.* [52], which investigates the application of NF_3 and for cleaning of PECVD tools, and the amounts of these gasses needed per m^2 of cell area. We have scaled these amounts to account for the thickness of the a-Si layer deposited, as the cleaning requirement is related to the amount of material (silane) deposited on cells and thus in the reactor. Furthermore, we assumed use of NF_3, not SF_6, as most of the tools in the survey [61] are specified to use NF_3 for the cleaning process.

2.3.3 Exhaust gas abatement

Data from a survey on point-of-use (POU) gas abatement systems [82] was used to calculate the energy and material requirement of gas abatement, during production as well as during cleaning of the reactors. Table A.3 lists the process data for gas abatement we have gathered in this study and used in our analyses. It was assumed that exhaust gases from both the PECVD and ALD reactors are treated in these POU abatement systems, while the exhaust gas from the TCO sputtering tool is assumed to be vented, as sputtering does not rely on gaseous precursors like silane or trimethylaluminium that are in the exhaust gas in high concentrations after deposition, but rather consists of argon with low concentrations of contaminants.

2.3.4 TCO sputtering

TCO deposition is performed on commercial scales with two technologies: sputtering and evaporation. For our study, we assumed TCO layers to be deposited with a sputtering tool. Data we took from a survey [62] gives the following equipment specifications:

- Throughput in terms of deposition area per hour
- Utilization rate of target material
- Water consumption
- Average power consumption

With this information, we calculated the energy and water consumption per wafer area processed. With an average throughput of 90.6 m^2/hour and an average power consumption of 564.6 kWh, we calculated the energy consumption per m^2 cell area to be 6.3 kWh. Water consumption (for cooling) was calculated to be 547.2 L m^{-2} cell area. The utilization rate (74%), combined with an assumed TCO layer thickness of 80 nm, was used to calculate the target material consumption per unit of cell area. An 80-nm thick layer of ITO on both sides, has a volume of 0.08 cm^3. With an ITO density of 7.14 g·cm^{-3} this results in an ITO consumption per m^2 wafer area of 1.54 gram. Of this 1.54 gram, 0.4 gram is lost (not utilized) during the deposition process. Cooling water consumption was reported to be on average 547 liters per m^2 cell area. The process parameters for TCO deposition are summarized in Table A.4.

Energy use of the different sputtering lines was found to be quite variable, leading to a large uncertainty in this parameter for TCO sputtering in general. An attributional LCA of SHJ solar cells where there is data on the specific tool used could improve the results for the sputtering process. However, as this is a prospective LCA focusing on comparing design alternatives, we have chosen to use average values for each production process. In section 2.7 we discuss the uncertainty in the data of various processing steps on the overall results.

2.3.5 Screen printing

For screen printing we took our data from a survey [63] which shows the specifications of 19 different screen printing tools from 8 different suppliers. These specifications listed:

- Throughput in wafers/hour
- Maximum power consumption in kW
- Compressed air consumption in liters per hour

We assumed power consumption to be at maximum for maximum throughput, and used the given values for throughput, wafer size and power consumption to calculate the energy use and compressed air use per m^2 of cell area. Power consumption was reported to be 0.133±0.05 kWh/m^2 cell area on average, ranging from 0.02 to 0.41 kWh/m^2. Compressed air consumption was reported to be 273±102 L/m^2. Process parameters for screen printing are listed in Table A.5.

Metallization paste use was based on data from ecoinvent, which states, including losses, a paste usage of 180 mg per wafer for the front side silver grid of a conventional crystalline silicon solar cell. We assumed the metallization to be equal for front and backside, but that metallization requirements to be double that of a

conventional crystalline silicon solar cell, resulting in a total use of 720 mg/wafer, which we consider to be a conservative estimate. We assumed the difference in terms of environmental impact between the conventional, high temperature silver pastes and the specific low-temperature pastes used for SHJ cells to be negligible, as over 99% of the environmental impact of the conventional paste in Ecoinvent is a result of the use of silver (which has high levels of embedded energy), which is still a main material in low-temperature pastes.

With screen printing, like with wet etching, energy use is not as significant an impact compared to for instance deposition processes. Material use in the form of the amount of silver consumed is however important, in terms of environmental impact because of the high level of embedded energy in silver [81], and furthermore in terms of cost as the silver paste used is expensive. Research and development of silver pastes and printing techniques focus on reducing silver consumed. We use a conservative estimate for the current designs.

2.3.6 Cu-plating

Copper electroplating is a technology that is not used in commercial solar cell production yet. However, as reduction of silver use and complete replacement of silver for contact metallization is being intensively investigated, many R&D groups are publishing on copper plated solar cells. A quite limited number of companies now offer commercial scale electroplating tools for solar cells. These tools commonly rely on a plating sequence in which layers of nickel, copper and silver or tin are plated onto a solar cell. The nickel layer serves as a seed layer for copper plating, and at the same time forms a barrier against copper diffusion into the cells. It has been stated however that the ITO layer used in SHJ cells also is effective in preventing copper diffusion. The last step of the plating process is to coat the copper gridlines with a thin layer of silver, to prevent corrosion of the copper while maintaining good conductivity. Cost considerations could result in using tin for this final step, however, tin is much less conductive compared to silver.

For the plating process we assume the complete process to consist of 3 steps, based on a paper by Tous *et al.* [83]. First, the barrier/seed layer (1 µm thickness) of nickel is plated onto the cells, after which a copper layer is plated (7 µm). Finally, the copper plated contacts are covered with a thin layer (0.1 µm) of silver to prevent corrosion of copper. The process material and energy requirements are based on the specifications of the Meco DPL plating tool [64] and personal communications [84].

The specifications of the Meco plating tool shows a throughput of 3000 wafers per hour at a maximum power consumption of 100 kW, resulting in an energy

consumption of (max) 1.37 kWh/m^2 of cell area. Rinse water consumption was reported to be 100 L/hr, or 1.37 L/m^2 cell area.

The material requirements mainly result from two factors, namely 1) electrolyte consumption due to deposition of metals on the cell and 2) electrolyte drag-out by the cells when they move out of the plating baths. Plating drag-out is mentioned in the process tool specifications in [64], but varies strongly from one tool to the other (from 0.003 mL/wafer to 0.5 mL/wafer). However, we assume that most of the electrolyte consumption is resulting from the deposition of the metals, and not from the drag-out. Assuming a line width of 50 µm and metal layer thicknesses as mentioned above, and an equal amount of gridlines compared to conventional screen printed metallization (resulting in a strong reduction of metal use per wafer compared to screen printing), we calculate the material consumption requirements to be:

- 3.66 mL/m^2 cell area of nickel electrolyte
- 23.9 mL/m^2 cell area of copper electrolyte
- 0.56 mL/m^2 cell area of silver electrolyte
- 1.3 L/m^2 cell area of rinsing water (de-ionised)

We assume all used rinsing water to be treated as liquid PV effluent waste. Process parameters for copper-plating are shown in Table A.6.

2.3.7 Wafers

The Ecoinvent database lists the requirements of wafer sawing from monocrystalline silicon ingots, including silicon use per wafer, electricity and heat use, sawing abrasives (silicon carbide) and materials for cleaning of wafers and treatment of sawing slurry. The data in Ecoinvent is based on wafer thickness of 270 µm, and kerf losses of 180 µm. We assumed kerf losses to be 130 µm per 180 µm wafer, based on a saw wire diameter of 120 µm [33, 58]. Therefore, total silicon consumption was adjusted by a factor (180 µm + 130 µm)/(270 µm + 180 µm), while processes and material consumption related to treatment of kerf losses were adjusted by a factor of (130 µm)/(180 µm). Energy use and requirements for packaging of the wafers were assumed to be unaffected by the assumed reduction in kerf losses.

Table 2.3 · Main life cycle inventory results for material and energy use of cell production processes of current SHJ cell designs.

Process input	Unit (per m2 cell area)	Ref-SHJ	NE-SHJ	ALD-SHJ	CuIBC-SHJ	Source
			Texturing/cleaning			
Water (deionized)	L	33.43	33.43	33.43	33.43	[59]
Electricity	kWh	0.647	0.647	0.647	0.647	[59]
Hydrogen Fluoride	kg	0.095	0.095	0.095	0.095	[59], *a*
Sodium Hydroxide	kg	0.156	0.156	0.156	0.156	[59], *a*
Hydrogen Peroxide	kg	0.056	0.056	0.056	0.056	[59], *a*
Hydrochloride Acid	kg	0.061	0.061	0.061	0.061	[59], *a*
Ammonia	kg	0.011	0.011	0.011	0.011	[59], *a*
Compressed Air	m^3	0.25	0.25	0.25	0.25	[85]
Fluid waste to treatment	L	33.5	33.5	33.5	33.5	Water and unused etchants
			Thin-film deposition			
PECVD of a-Si:H						
Electricity	kWh	6.59	7.14	3.29	9.88	[61]
Water	L	394	449	197	591	[61]
Silane	g	1.62	4.21	0.81	2.43	[52]
Hydrogen	g	2.42	6.29	1.21	3.63	[52]
Oxygen	g	0.26	0.68	0.13	0.39	[52]
Boron trifluoride	g	0[b]	0[b]	-	0[b]	[52]
NF_3 for cleaning	g	2.2	5.6	1.1	4.1	[52]
Gaseous waste to abatement	L	29.0	60.9	55.1	14.5	Unused inputs and NF_3
ALD						
Electricity	kWh			0.29		[62]
TMA[c]	g			0.19		[62]
Oxidant[d]	g			8.59		[62]
Nitrogen	kg			0.11		[62]
Water	L			23.11		[62]
Gaseous waste to abatement	L	-	-	360	-	Unused inputs
			TCO Sputtering			
Electricity	kWh	6.3	-	6.3	6.3	[62]
Water	L	511.82	-	511.82	511.82	[62]
ITO	g	2.74	-	-	1.37	[62][d]
ZnO	g	-	-	1.08	-	[62][d]
			Metallisation			
Screen printing						
Electricity	kWh	0.524	0.524	0.524		[63]
Compressed air	m^3	1.096	1.096	1.096		[63]
Silver paste	g	29.6	29.6	29.6		[33, 57]
Cu printing						
Electricity	kWh	0.131	0.131	0.131		[63]
Compressed air	m^3	0.274	0.274	0.274		[63]

Table 2.3 · (continued)

Process input	Unit (per m2 cell area)	Ref-SHJ	NE-SHJ	ALD-SHJ	CuIBC-SHJ	Source
Cu paste	g	29.6	29.6	29.6		
Cu plating						
Electricity	kWh				1.37	[64]
Ni plate solution	mL				3.66	[83, 84], [e]
Cu plate solution	mL				23.9	[83, 84], [e]
Ag plate solution	mL				0.56	[83, 84], [e]
Water deionised	L				1.3	[64]
Fluid waste to treatment	L				1.3	Water and unused electrolytes
Curing						
Electricity	kWh	0.31	0.31	0.31	n.a.[f]	
Gas abatement						
Electricity	kWh	0.045	0.11	0.033	0.085	[82]
Water	L	1.2	3.0	0.87	2.2	[82]
Oxygen	g	5.1	13	3.9	9.8	[82]
Nitrogen	g	4.3	11	3.3	8.2	[82]
Propane	g	3.3	8.6	2.5	6.3	[82]
Compressed Air	L	14	36	10	26	[82]

[a] Own estimations
[b] Assumed negligible
[c] Trimethylaluminium: a common precursor for thin film aluminium oxide deposition.
[d] Own calculation based on utilization rate in [62]
[e] Own calculations
[f] Included in Cu-plating

2.4 Results - Current Designs

2.4.1 Results for cell designs

The life cycle inventory (LCI) for the different SHJ designs is shown in Table 2.3. The resulting environmental impact is shown in Figure 2.3, modeled based on cell efficiencies of 18.4%. When we examine the production processes for the four different SHJ cells (Figure 2.3), we can see that all of the new SHJ designs improve upon the environmental performance of the reference design (in terms of GHG emissions per W_p). The Novel Emitter SHJ design shows the smallest GHG footprint, largely due to replacement of the sputtered TCO layer. However, the increased requirements of PECVD for nc-SiO_x:H layer slightly negate these benefits in terms of GHG emissions per W_p.

The CuIBC-SHJ design benefits from the replacement of silver with copper, but these benefits are offset due to increased PECVD requirements. Although total a-Si layer thickness is not increased for this design, startup of the PECVD equipment

(creating vacuum and preheating) is quite energy intensive, while the actual deposition process is quite short. Thus, preferably, the various PECVD processing steps should be performed in a single PECVD chamber or in multichamber tools without breaking vacuum.

The results for the ALD SHJ design show the decreased energy consumption of using ALD instead of PECVD as a thin-film deposition process. The energy consumption of ALD equipment (expressed per m^2 cell produced) is almost 90% lower according to the equipment data we reviewed [61, 62]. This results in a decreased environmental impact for the ALD design with ZnO/Al_2O_3.

Obvious for all silver metallization based designs is the large contribution of cell metallization. Copper-electroplating the contacts appears to significantly reduce this contribution, as can be seen from the results from the IBC Cu-plated design. This reduction is mainly due to the high amount of embedded energy (and thus GHG emissions) in silver compared to copper. For copper plating, a major contribution to the GHG footprint comes from the electricity used in the plating process.

The results for cumulative energy demand demonstrate a similar decrease in environmental impact of the new SHJ designs compared to the reference SHJ de-

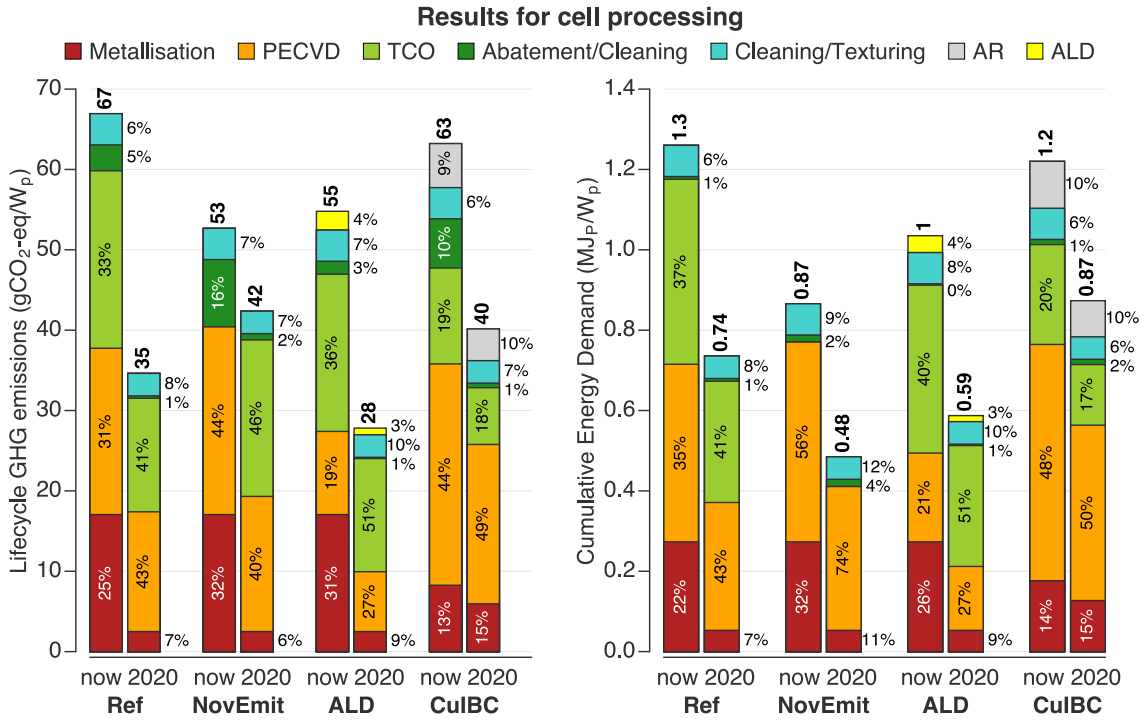

Figure 2.3 · Comparison of the lifecycle GHG emissions (left) and cumulative energy demand (right) caused by cell processing for the production of the SHJ cell design alternatives. Totals are indicated in bold above the bars. Results are modeled based on cell efficiencies of 20.4% and 25% for current and prospective cells respectively.

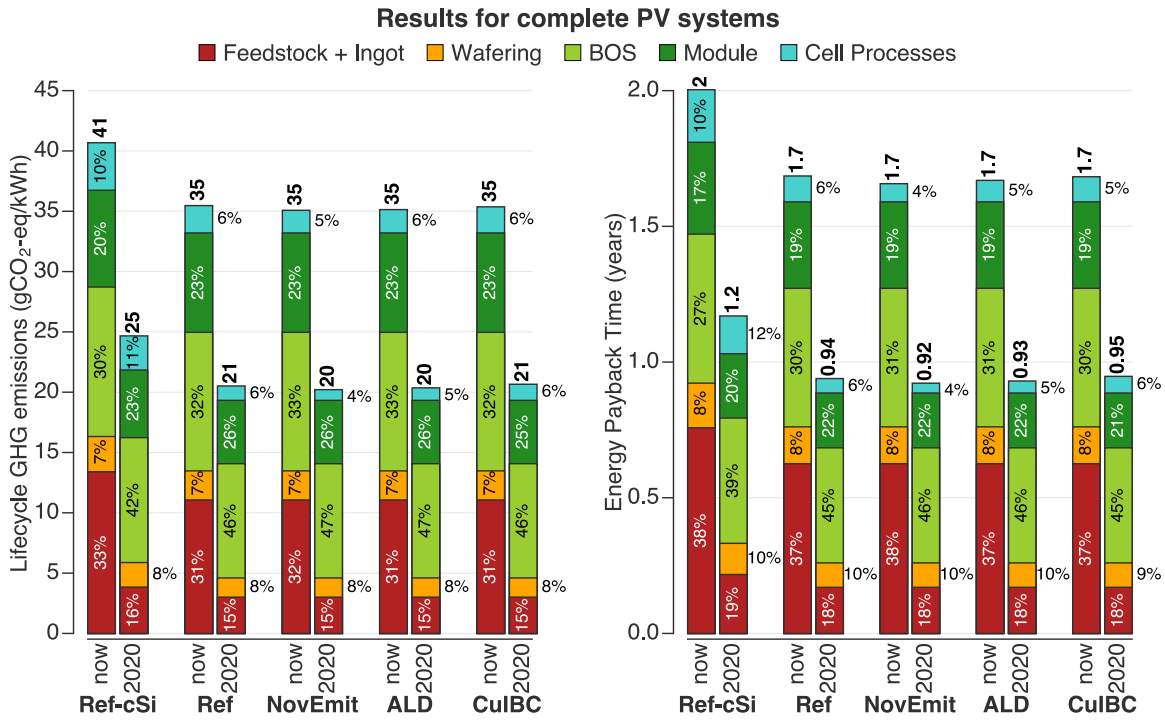

Figure 2.4 · Results for complete PV systems. Left: Comparison of the lifecycle greenhouse gas emissions of the monocrystalline and silicon heterojunction PV systems. Right: Comparison of the energy payback time of the monocrystalline and two silicon heterojunction PV systems. Totals are indicated in bold above the bars. Results are based on insolation of 1700 kWh $m^{-2}year^{-1}$, *PR* of 0.75 and module-area efficiencies of 16.1% and 18.4% respectively for current c-Si and SHJ modules and 19.5% and 23.5% respectively for prospective c-Si and SHJ modules.

signs, however, here, the improvement of the copper plated design relative to the reference SHJ design is smaller. This is due to the fact that the CED impact assessment only looks at primary energy used, and does not take into account the GHG intensity of the energy used. Energy intensive processes at the end of the process chain often have a lower GHG footprint per unit of energy compared to processes at the beginning of the process chain. As the copper plated IBC design requires more energy intensive (but less material embedded energy) processes, this results in a decrease of the improvement in terms of CED, compared to the reference SHJ design.

2.4.2 Results for complete systems

Life cycle GHG emissions for systems

The results for complete PV systems based on the designs studied are shown in Figure 2.4, for both GHG emissions per kWh as well as the Energy Payback Time (EPBT) of the systems. Additionally for this section, we compare the results to a conventional monocrystalline silicon (c-Si) PV system. The results obtained were

modeled based on an irradiance of 1700 $kWh \cdot m^{-2} \cdot yr^{-1}$, and a performance ratio of 0.75, resulting in an annual electricity yield from the PV systems of 1275 $kWh \cdot kW_p^{-1} y^{-1}$.

From Figure 2.4 it is quite obvious that the cell processing steps shown earlier do not contribute very much to the overall emissions and EPBT associated with the systems. The majority of the environmental impacts results from the silicon wafer and its feedstock (about 38-40%) the balance-of-system (about 30-33%) and the module materials (around 20-23%).

Compared to the monocrystalline system, the SHJ systems improve the environmental impact (both in terms of GHG emissions and EPBT) with 15%. Excluding the (non PV-type specific) BOS this difference increases to 17%. The difference between the monocrystalline system and the SHJ systems is mainly due to the increased efficiency of the SHJ designs, and only slightly due to the improvement of the production process (which is performed at a lower temperature). Thus, these results emphasize that in order to obtain significant reductions in the GHG footprint of PV systems, issues like module efficiency, silicon material usage and production efficiency, and module and BOS material and energy use need to be addressed.

EPBT for systems

Figures 2.4 also shows the results for energy payback time. These results show a similar trend, with higher environmental impact for the monocrystalline PV system compared to the SHJ systems. As we have seen above, feedstock, ingot, and BOS contribute most to the overall result. The strong similarities between the results for GHG emissions and CED/EPBT confirm the notion that CED can be an indicator for other environmental impacts, as described in literature [56, 86].

2.5 Results - Prospective 2020 Designs

As mentioned in earlier sections, we performed a prospective analysis of the four SHJ designs. For this prospective analysis, we assumed the use of thinner (50 µm) wafers, the use of more abundant materials (replacing silver and indium), and an increase of cell conversion efficiency due to optimization of cell processing steps. For a review of these prospective designs see Table 2.2 and section 2.2.3.

The results for the prospective analysis are shown in Figures 2.3 and 2.4. Figure 2.3 shows the results for cell processing, whereas Figure 2.4 shows the results for complete systems based on these prospective designs.

2.5.1 Prospective 2020 Cell Processes

Figure 2.3 shows that the prospective designs have a strongly improved environmental performance compared to the current designs, as GHG emissions per W_p drop by 44%, 48%, 46% and 29% and CED (in MJ_P/W_p) drops by 39%, 44%, 40% and 17% respectively for the Ref-SHJ, NovEmit-SHJ, ALD-SHJ and CuIBC-SHJ designs. The improvement is mainly due to the assumed increase of efficiency (which decreases the impact of all categories by a factor of $\eta_{\text{current}}/\eta_{\text{prospective}}$) and the replacement of silver with copper printing, which reduces the impact of metallization with 84% for copper printing compared to silver printing. The relative impact of thin-film deposition processes does however strongly increase. The environmental performance of the devices relative to each other do not change much, as the main improvements have an effect on all designs. The improvement of the Cu-IBC design is not as pronounced compared to the other designs, as the current Cu-IBC design already has copper based contacts. This shows that, based on our assumptions, copper printing has a lower environmental impact compared to copper plating, mainly due to lower energy use for the printing process.

2.5.2 Prospective 2020 Systems

The results for the systems based on the prospective designs (see Figure 2.4) show that the assumed increase of efficiency and strongly decreased silicon use (due to the thinner wafers) has a very strong effect on the environmental performance of the PV systems. From current to prospective systems, the GHG emissions per kWh are reduced with about 40% and the energy pay-back time is reduced with about 43-44%, for all systems. The environmental impact of the systems is 25 gCO_2-eq/kWh for the c-Si design, compared to 20-21 gCO_2-eq/kWh for the prospective SHJ designs, while EPBT is 1.2 years and 1 year, respectively. The relative contribution of BOS and module materials is however increased to well over half of the total GHG emissions and EPBT, emphasizing again the need for alternative module materials and improvements in the production of BOS components.

2.6 Sensitivity analysis

To analyze the effect of changes in various parameters on the overall results, we performed a sensitivity analysis. We varied insolation, Performance Ratio (*PR*), greenhouse gas intensity of electricity used during the production process, and cell efficiency. Table 2.4 summarizes the ranges over which we varied these parameters.

The results for the sensitivity analysis are shown in Figures 2.5 and 2.6. Figure 2.5 shows that for the ranges analysed, the results are most affected by changes in the annual insolation on the PV system, and to a lesser degree to the observed range of the performance ratio. Changes in these two parameters have the same effect on the overall results, as they both determine how much electricity is produced in the PV systems' lifetime. Therefore, the effect of these parameters relates to all system components. The results show that location, correct (optimal) installation, performance monitoring and maintenance are strongly influencing the life cycle GHG emissions associated with PV generated electricity. The analysis for insolation shows that emissions almost double for PV systems operated in the Netherlands compared to Southern Europe. However, we did not account for the lower operating temperatures, with concomitant larger *PR* values, that PV systems would encounter in lower insolation areas. The effect of changed efficiency on the overall result is much lower, as the range of efficiencies investigated is relatively much smaller.

Aside from insolation and PR, we analysed the effect of changes in module area efficiency, and the GHG intensity of the electricity used to produce the cells (direct electricity) and complete systems (all electricity). Changes in module area

Table 2.4 · Overview of the ranges investigated in the sensitivity analysis.

Parameter	Min	Baseline	Max
Insolation ($kWh \cdot m^2 \cdot y^{-1}$)	1000	1700	2500
PR	0.5	0.75	1.0
Electricity GHG (gCO_2-eq/kWh)	0	531	1060
Module efficieny (rel. to baseline[a])	75%	100%	125%

[a]Baseline module efficiency figures are 16.1% for the reference crystalline silicon design and 18.4% for the SHJ designs.

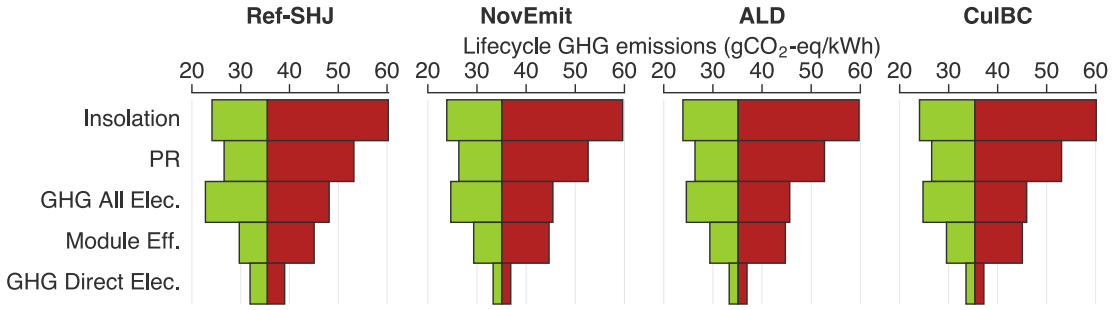

Figure 2.5 · Sensitivity analysis for the four SHJ designs for GHG intensity of direct electricity, module area efficiency, GHG intensity of direct and indirect electricity, performance ratio, and annual insolation. The tornado graphs show the sensitvity of the end result (in gCO_2-eq/kWh) as a function of changing these parameters. Left: RefSHJ, Middle-left: NovelEmitter, Middle-right: Al_2O_3/ZnO ALD, Right: Cu IBC.

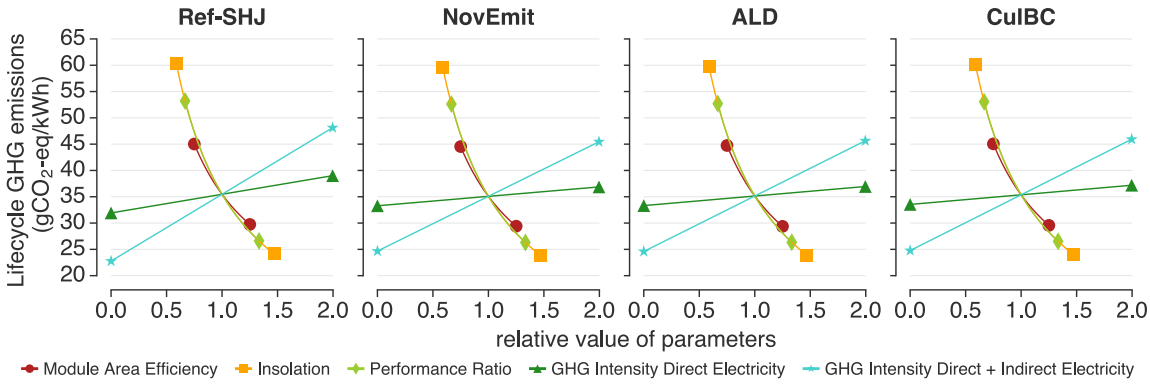

Figure 2.6 · Spider diagrams: sensitivity of the overall result to variation in five different parameters. The results are for complete systems. The x-axis indicates variation in each parameter, relative to the baseline values.

efficiency affect almost all components of the PV system, except for the non-area related components (inverter, cabling). Direct electricity use during cell processing accounts for over 5% of the GHG emissions of the SHJ systems, while electricity use for the production of the complete systems accounts for almost 30% of all GHG emissions. Therefore, when ranging GHG intensity of all electricity used for system production from 0% to 200% of baseline intensity, the overall emissions range from -30% to +30% relative to the baseline. This shows that a vertically integrated PV producer who has control over the type of electricity used for all processes, from silicon production to module production, can substantially reduce the environmental impact of the PV systems it produces. Furthermore, Reich *et al.* [87] have shown that when including the electricity use embedded in all processes and materials including auxiliary ones, the total contribution of electricity use to GHG emissions is over 50%. In Figure 2.6, it is shown that the results are most sensitive to changes in 1) insolation and PR and 2) module area efficiency.

2.7 Uncertainty

As discussed in section 2.3, the life cycle data for some of the processing steps was found to be quite variable, especially for electricity consumption of the various processing tools. As - for most cell processing steps - electricity consumption is the main driver of environmental impact, we have analysed the effect of uncertainty in electricity use for the processing steps involved. In this section we present the results of this analysis, and address how the observed ranges in the life cycle data affect the overall results. Figure 2.7 shows the data ranges found for the electricity consumption of five processing steps: wet etching, PECVD deposition of a-Si:H thin films, TCO sputtering, ALD and screen printing.

TCO Sputtering

As shown in Figure 2.7, the data for electricity consumption of TCO sputtering shows a quite large variation. For this study, as mentioned before in section 2.3, we analysed the specifications of 8 different TCO sputtering tools. The electricity consumption of these tools range from 1.1 to over 10.6 kWh/m^2 of cell area, and is on average 6.3 kWh/m^2. As the electricity consumption (assuming average consumption) determines 85% of the life cycle GHG emissions of this processing step, life cycle emissions of this processing step could increase by 44% for the worst case, or decrease by 79% for the best case. Overall results, for the cell processing of the Ref-SHJ and ALD-SHJ designs, would increase by 12.7 gCO_2-eq/W_p (+19%) and 11.3 gCO_2-eq/W_p (+20%), or decrease by 15.4 gCO_2-eq/W_p (-22%) and 13.6 gCO_2-eq/W_p (-24%), in these respective cases. For complete systems, this effect would be relatively much smaller (-1.5% to +1.2% and -1.4% to +1.1%, respectively). For the other designs the effect would be similar but smaller.

PECVD

For PECVD deposition of amorphous silicon thin films, we examined specifications of six different PECVD tools, and found electricity consumption to range from 1.7 to 5.3 kWh/m^2 cell area, and to be on average 3.2 kWh/m^2 cell area. From best to worst case, this would result in GHG emissions for cell processing to range from -18% to +26% for the most "PECVD-intensive" design, the Cu-IBC design. For a complete PV system, the changes would be only -1.2% to +1.6%.

Table 2.5 · Overview of the effect of data uncertainty on the overall GHG emissions for cell processing steps for the different SHJ designs studied.

	Uncertainty in process step:					
Design	**TCO Sputtering**	**PECVD**	**Wet etching**	**ALD**	**Screen printing**	**Total**
Ref-SHJ	-22% to +19%	-13% to +18%	-2.3% to +4.4%	n.a.	-2.0% to +5.0%	-40% to +46%
NovEmit-SHJ	n.a.	-18% to +25%	-2.9% to +5.6%	n.a.	-2.5% to +6.3%	-23% to +36.5%
ALD-SHJ	-24% to +20%	-8% to +11%	-2.8% to +5.4%	-1.3% to +2.1%	-2.5% to +6.0%	-39% to +44.6%
CuIBC-SHJ	-13% to +11%	-18% to +26%	-2.5% to +4.7%	n.a.	n.a.	-34% to +41%

Table 2.6 · Overview of the effect of data uncertainty on the overall GHG emissions for a kWh produced with complete PV systems based on the different SHJ designs studied.

	Uncertainty in process step:					
Design	**TCO Sputtering**	**PECVD**	**Wet etching**	**ALD**	**Screen printing**	**Total**
Ref-SHJ	-1.5% to +1.2%	-0.86% to +1.2%	-0.15% to +0.29%	n.a.	-0.13% to +0.32%	-2.6% to +3.0%
NovEmit-SHJ	n.a.	-0.96% to +1.4%	-0.16% to +0.31%	n.a.	-0.14% to +0.34%	-1.3% to +2.0%
ALD-SHJ	-1.4% to +1.1%	-0.45% to +0.63%	-0.16% to +0.30%	-0.07% to +0.12%	-0.14% to +0.34%	-2.2% to +2.5%
CuIBC-SHJ	-0.80% to +0.66%	-1.2% to +1.6%	-0.15% to +0.29%	n.a.	n.a.	-2.1% to +2.6%

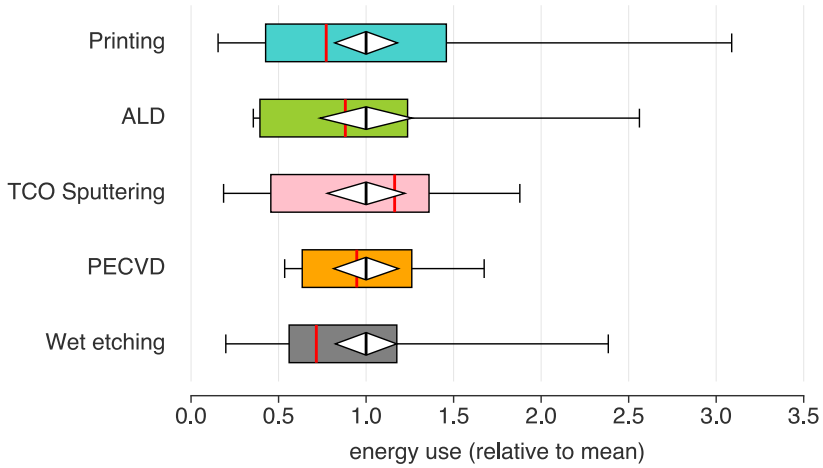

Figure 2.7 · Boxplots of the gathered data on electricity consumption (relative to the mean value) for 5 different cell processing steps. The diamonds indicate the standard error of the mean value. The red lines indicate median values.

Wet etching

For cleaning/texturing of the wafers, we examined specifications of 16 different etching tools, and found electricity consumption to range from 0.13 to 1.5 kWh/m^2 cell area, and to be on average 0.6 kWh/m^2 cell area. From best to worst case, this would result in GHG emissions for cell processing to range from -2.9% to +5.6% for the novel emitter design. For the complete PV system, the changes would be only -0.2% to +0.3%. For the other designs, the absolute effect is equal, but relatively to the overall result, the effect is smaller as these designs overall environmental footprints are higher.

ALD

Like other thin-film deposition processes, the environmental impact of ALD mainly results from electricity use of the deposition tool, as the material use in the form of precursors is quite low, and these materials have low embedded energy. For the deposition of the Al_2O_3 layer, some 66% of the environmental impact in terms of GHG emissions results from the use of electricity.

For the specifications we reviewed, average electricity use for deposition of an aluminium oxide layer was found to be 0.29 kWh/m^2 cell area, but ranged from 0.15 to 0.51 kWh/m^2 (-48% to +76%). As the ALD process is much less energy intensive compared to for instance sputtering, the effect of this process step on the overall result is quite limited. Regardless, when varying the electricity consumption from best to worst case, overall GHG emissions for cell processing for the ALD-SHJ design vary with -0.74 to +1.16 gCO_2-eq/W_p, or -1.3% to +2.1%. The effect on

overall PV system emissions are negligible.

Screen printing

Contrary to other cell processing steps, the environmental footprint of screen printing of silver contacts results mainly from the material use (silver paste), and not from electricity consumption. Of the overall GHG emissions for screen printing the contacts on both sides of an SHJ cell design, 9.6% results from electricity consumption. From best to worst case, the electricity consumption for the 19 tools we analysed ranged from 0.02 to 0.4 kWh/m^2 cell area processed, while the average value was found to be 0.13 kWh/m^2. From best to worst case, this would result in GHG emissions for cell processing steps to vary by -1.39 to +3.4 gCO_2-eq/W_p. For the novel emitter design (for which metallization emission are *relatively* the highest) this would mean a variation of -2.5% to +6.3%. For complete systems, the effect is quite limited and does not exceed -0.14% to +0.34%.

Combined effect of uncertainties

The uncertainty in the LCI data does not result in significant changes in the results for complete PV systems based on the analysed designs. For cell processing however, in best and worst cases, the results could be affected quite substantially. Table 2.5 shows the combined effect of uncertainty of the processes discussed earlier in this section, for each design separately. Table 2.6 shows the effect of data uncertainty on the results for complete systems, in terms of GHG emissions per kWh electricity.

As Table 2.5 shows, the effect of uncertainty in the data for sputtering and PECVD can have a profound effect on the results calculated for cell processing. The combined effect of all parameters could result in changes of the overall result by a maximum of -40% to +46%, for the Reference-SHJ design. For the other designs, the effect is similar.

As the contribution of cell processing to overall system environmental footprint is quite limited, the data uncertainty in the cell processing LCI does not result in substantial effects on overall results (see Table 2.6). For systems, when looking at GHG emissions per kWh, the effect of uncertainty on the overall result is at maximum -2.6% to +3.0%, for the Ref-SHJ based system. The overall effect on this design is the largest, because this design relies on all processing steps (except for ALD) and is thus affected by uncertainty in all the processing steps.

2.8 Discussion

The results indicate that the cumulative energy demand (CED), energy payback time (EPBT), and greenhouse gas (GHG) footprint of silicon heterojunction solar cells (module efficiency of 18.4%) is improved compared to conventional monocrystalline solar cells (module efficiency 16.1%). The main reason for this difference, as expected and also established in a previous LCA on SHJ cells [53], is the higher efficiency of SHJ modules. This observation is confirmed by the sensitivity analysis as it shows that the environmental impact of SHJ based systems quickly increases once module efficiency drops. For SHJ based systems with assumed equal module area efficiencies as mono-Si based systems, the improvement in environmental performance would be limited, as life cycle GHG emissions and EPBT would only be about 3% lower, compared to 15% when including the efficiency advantage of SHJ cells. From an environmental point of view, changes to designs can therefore only be justified it these changes do not lead to decreases in efficiency, as improvements of the impact of cell processing steps will very quickly be negated by decreased efficiencies. It also stresses that the results for conceptual solar cell designs are heavily reliant on accurate efficiency estimations.

Research on the environmental performance of SHJ cells has so far been quite limited. Our results for monocrystalline solar cells, based largely on existing data, show no large differences with commonly found results [88]. Thin-film solar cell systems are generally found to have lower environmental impact compared to crystalline silicon PV systems. A recent harmonized review however shows a broad range for amorphous silicon thin film systems among the analysed studies [48]. The same study shows the emissions for CdTe thin-film systems to be lower compared to both our results for SHJ cell systems and the monocrystalline system [48].

Compared to the existing LCA on SHJ cells [53] both lifecycle GHG emissions and EPBT/CED are significantly higher in our study (about 32 gCO_2-eq/kWh in our study compared to 20 gCO_2-eq/kWh in the study by Olson *et al.* [53]). Main reasons for this difference are that in the LCA study by Olson *et al.* BOS components are not included in the analysis. In our study, the BOS-components contribute 10.4 gCO_2-eq/kWh to the overall results, which largely accounts for the difference between our study and the results obtained in the study by Olson *et al.* Furthermore, our model results in higher emissions for cell processes like PECVD and TCO deposition. The differences for these latter processes are however very small. A more detailed comparison between the two studies is however difficult, as the paper by Olson *et al.* does not report a life cycle inventory for the SHJ specific processes analysed in that study.

2.8.1 Lifetime electricity production of PV systems

For this study, in accordance with IEA PVPS guidelines [44], we assume a system lifetime of 30 years with a single replacement of the inverter, a Performance Ratio of 0.75, and an annual insolation of 1700 kWh/m^2. As we have seen in section 2.6, insolation and performance ratio have a strong effect on the environmental performance of PV systems, due to their effect on annual and thus lifetime energy production of the system. The lifetime of the system components has the same effect by constraining the period in which the system produces power. Therefore, the results obtained for complete systems are highly dependent on location and system lifetime. Strong reductions in PV system prices could increase incentives for current system owners to replace their PV systems before end-of-life. Without proper recycling procedures, this could have an adverse effect on the environmental performance of PV systems.

2.8.2 Balance-of-System

As large contributors, BOS elements are of increasing interest in cost reduction strategies. The data from ecoinvent shows that in terms of environmental impact, largest contributions come from the mounting structure (45%-55%) and inverter (26.5%-32.1%). This data is shown in Table 2.7. With increasing module efficiency, the contribution of the mounting structure, which is area related, decreases, while the contribution of non-area related parameters like the inverter relatively increases. For our analysis, we assumed no changes in BOS components from the current to the prospective analysis. As the results show, improvements in BOS components has the potential to significantly improve the environmental impact of PV electricity. These improvements could be achieved by increasing the lifetime of the inverters, and reducing the amount of material used for the mounting structure, or replacing the aluminium commonly used for this by other, less energy intensive materials.

Table 2.7 · Contribution of BOS elements to total BOS environmental impact.

Module efficiency	**16.0%**	**19.5%**	**23.5%**
Mounting structure	55.0%	50.1%	45.4%
Inverter	26.5%	29.4%	32.1%
Transport & installation	18.5%	20.6%	22.5%

2.8.3 Data uncertainty

As we have shown in section 2.7, the data for many cell processing steps is characterized by a relatively large uncertainty. We have used average values for material and energy consumption for cell processing steps. From best to worst cases, the effect of the uncertainty in data could result in substantial changes to the results for cell processing, and to a much lesser degree to the results for complete systems (see also Table 2.5 and 2.6). Therefore, more a more accurate LCA of specific solar cell designs should be conducted at producers, where measurements could be performed to establish the material and energy use of specific tools and for specific designs in realistic production environments, that are possibly customized from the standard values reported in the equipment surveys [59, 61–64, 82] we used as input data. The uncertainty in the LCI data for especially TCO sputtering and PECVD energy use can have a profound effect on the results for cell processing (see section 2.7). In certain cases, this would affect the results to a degree that a comparison of the four SHJ designs would be somewhat different. For instance, the benefit of replacement of TCO sputtering for the novel emitter design is quite beneficial in our baseline results, but this benefit is almost non-existent when we assume the electricity consumption for sputtering to be the minimum of the dataset we reviewed. However, in many cases, data uncertainty would affect all designs in a similar manner, as some of the processes are needed for all designs studied. For complete systems, the effect of uncertainty in our LCI is quite limited.

2.8.4 Additional environmental impacts

Our study focuses on two environmental impacts: greenhouse gas emissions (gCO_2-eq), and primary energy use (Cumulative Energy Demand). Research has shown CED to be a reasonable proxy for environmental impact in other impact categories [56, 86]. However, direct waste emissions from PV production processes could have additional environmental impact not proportional to energy use during these processes. A more detailed study at specific PV production facilities should be performed to analyse the waste flows of the various cell processing steps. Furthermore, resource depletion is unlikely to correlate strongly with energy use during production of PV systems. Especially metal depletion is often mentioned as a possible constraint for PV technology [89–92]. Unfortunately, there is limited methodology available to assess metal depletion. For instance one such method, the ReCiPe method [93], includes a limited number of metals. Indium, which is produced commonly as a by-product of zinc manufacturing, is unfortunately not included. To be able to assess and compare the application of different metal alter-

natives in solar cells, a method would need to be developed that takes into account all metals used in PV manufacturing.

2.9 Conclusions

The results obtained from our analysis show that silicon heterojunction solar cell based PV systems can improve the environmental performance of solar PV compared to conventional monocrystalline silicon based PV systems. Electricity produced with four analysed SHJ systems results in the release of 32 gCO_2-eq/kWh, while the energy payback time is 1.5 years for these systems. Conventional monocrystalline silicon systems with cells with similarly thin (180 µm) wafers have a higher environmental impact at 38 gCO_2-eq/kWh and an EPBT of 1.8 years. The main reason for the improved environmental performance is the higher module area efficiency for SHJ modules (18.4%) compared to the monocrystalline module (16.1%).

When comparing the different SHJ designs on a PV system level, differences are very small, due to the relatively minor contribution of cell processing to overall GHG emissions and CED. As expected, the main contributors to overall GHG emissions and energy pay-back time of PV systems are the silicon feedstock and ingot, and the components used for the Balance-Of-System.

When examining purely the cell processing steps, differences are more readily observable. It is clear that “standard” silver metallization contributes significantly to the environmental footprint of cell processing due the high energy use in silver production. Copper based metallization is promising for reduction of this impact, although electricity use of copper plating was found to be much higher compared to screen printing.

The absence of TCO sputtering in the Novel Emitter design leads to a decreased environmental footprint, despite a slight increase in PECVD related GHG emissions and CED. The novel emitter does however eliminate the requirement for the scarce and expensive indium, and simplifies the production process by eliminating a process step, possibly resulting in cost reductions.

The ALD design also has a lower footprint compared to the reference design, due to decreased PECVD emissions and CED. Furthermore, as a thin-film deposition process, ALD is much less energy intensive due to the elimination of the requirement for operation at vacuum.

Due to the added PECVD steps in the process chain of the copper plated IBC design, its environmental footprint (when examining cell processes) is only slightly decreased compared to the reference design. This is mainly due to the requirement for stopping and starting the deposition process to change the deposition masks,

as starting up the PECVD reactors is as energy intensive as the deposition process itself, and takes more time. Cu-based metallization was however found to be quite promising in terms of reducing the environmental footprint of cell processing.

The analysis of the prospective designs shows that the environmental impact for both cell processing and complete PV systems can be substantially decreased due to an expected increase in cell efficiency. For the novel SHJ designs, GHG emission per kWh of electricity produced could drop to around 20 gCO_2-eq/kWh, while EPBT values could be around 1 year. The relative influence of BOS components does however substantially increase, however, we assumed no changes in this parameter. The use of novel mounting systems based on materials other than aluminium could result in a further decrease of the environmental impact of PV systems. For the Cu-IBC design, the decrease in the environmental footprint from current to prospective cell processing is not as pronounced, as the current design is already based on copper metallization.

Uncertainty in LCI data for several cell processing steps could result in a somewhat different comparison of the studied SHJ designs. Further research in this context should therefore focus on establishing accurate data on the electricity consumption of cell processing tools in a realistic production environment.

2.10 Acknowledgements

This work was performed under the FLASH programme, funded by Technology Foundation STW under project number 12172 (www.stw.nl/en/). We would like to thank Rob van der Meulen and Mariska de Wild-Scholten for their input on LCA of PV systems in general, Sander Mann for his help with SHJ specific LCA and Loic Tous from IMEC for his helpful input on copper plating for solar cells.

3

A cost roadmap for silicon heterojunction solar cells

Published in: Sol. Energ. Mat. Sol. Cells 147, 295-314 (2016)
doi: 10.1016/j.solmat.2015.12.026.

Abstract Research and development of Silicon Heterojunction (SHJ) solar cells has seen a marked increase since the recent expiry of core patents describing SHJ technology. SHJ solar cells are expected to offer various cost benefits compared to conventional crystalline silicon solar cells. This paper analyses the production costs associated with five different SHJ cell designs, including an interdigitated back-contacted (IBC) design. Using life-cycle costing, we analyzed the current cost breakdown of these SHJ designs, and compared them to conventional diffused junction monocrystalline silicon modules. Coupling the results for current designs with literature data on technological improvements, we also present a prospective analysis of production costs for the six SHJ cells and modules.

For current designs, module cost were calculated to be 0.48-0.56 USD per Watt-peak (W_p) for SHJ modules, compared to 0.50 USD/W_p for a conventional c-Si module. The efficiency bonus for SHJ modules compared to conventional c-Si modules is offset by a strong increase in metallization costs for SHJ designs, as comparatively large amounts of low temperature silver-paste are required. For module materials, the requirement for conductive adhesives results in a small cost penalty for SHJ modules compared to c-Si modules, which is more than balanced by the effect of higher efficiency in SHJ modules.

Our prospective study showed that improvements in cell processing and module design could result in a significant drop in production costs for all module types studied. The SHJ modules gain much advantage by reducing and replacing silver consumption, increased cell efficiency and thinner wafers and have prospective production costs of 0.29-0.35 USD/W_p. Conventional c-Si module cost is less sensitive to silver paste consumption, limiting the potential for cost reduction, and has prospective production costs of 0.33 USD/W_p. Replacement of indium-tin-oxide was not found to contribute substantially to a reduction in module costs.

3.1 Introduction

Concurrently with the strong growth in PV module production and sales, average PV module prices have dropped sharply over the last decade. Polysilicon, wafer, cell and module prices dropped especially sharp over the last few years, as shown in Figure 3.1. In the Netherlands, PV module prices including tax dropped by almost 50% between 2011 and 2013, from 2 EUR per W_p to 1.13 EUR per W_p [94], while global spot prices (excluding tax) for PV modules have dropped to 0.6 USD/W_p (see Fig. 3.1). Price decreases have long been following a learning curve that has been valid for multiple decades, however, more recently, due to decreased demand and resulting oversupply, prices have dropped below what could be extrapolated from the learning curve. As a result, PV producers are scrambling for opportunities to reduce production costs. On the other hand, although residential grid parity has been reached in several countries worldwide [40], PV electricity is as of yet not competitive with fossil electricity generation [95–99]. These two factors emphasize the need for further cost reductions in the PV industry, in order to assure PV production that is financially sustainable and competitive with bulk electricity generation.

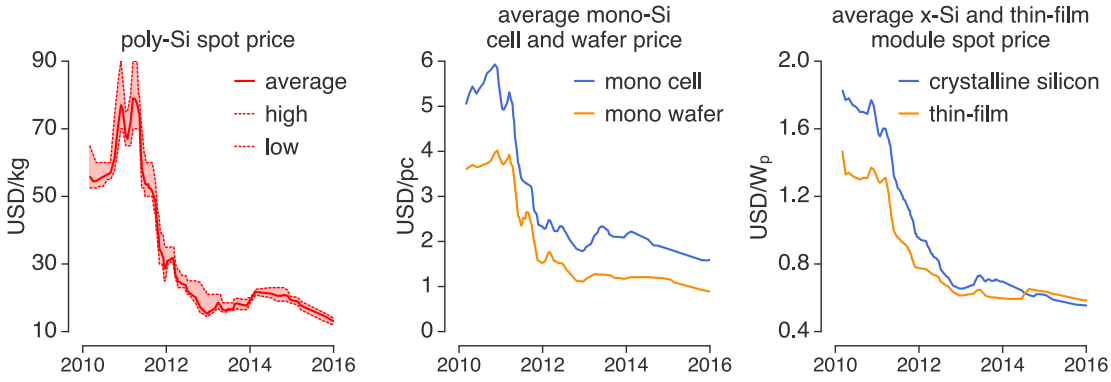

Figure 3.1 · Overview of development of prices for polysilicon (left, in USD/kg), monocrystalline cells and wafers (middle, USD/pc) and crystalline silicon and thin film modules (right, USD/W_p). Data: [100].

Photovoltaic systems offer us the possibility to produce electricity with low emissions of greenhouse gasses [48, 87, 88, 101, 102], low energy pay-back time, and low emissions of toxic or otherwise harmful substances, compared to traditional forms of electricity production. Its' modular nature allows for the application on a variety of scales, from small-scale decentralized and off-grid to large-scale, centralized electricity production. According to a recent International Energy Agency 'World Energy Outlook', PV will contribute significantly to a sustainable energy supply system [103]. Because of this expectation, adoption of PV is being supported by national governments worldwide, at sometimes high financial costs

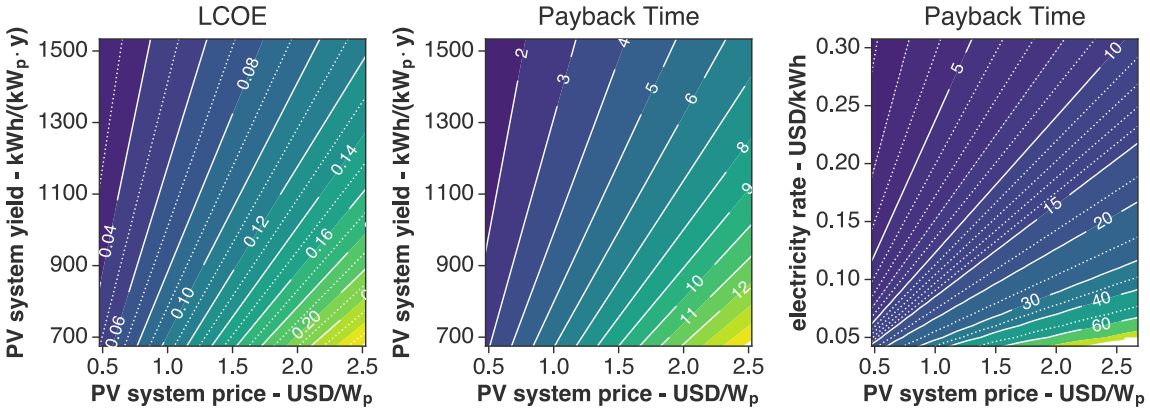

Figure 3.2 · Left: effect of PV system price and PV system yield on the levelised cost of electricity from a PV system. Middle: effect of PV system price and PV system annual yield on the investment payback time of a PV system, based on an electricity rate of 0.26 USD/kWh. Right: effect of PV system price and electricity price on the payback-time of a PV system, at a yield of 875 kWh/kW_p.

for society [104]. Cost reductions are thus of substantial societal importance when deployment of solar energy covers larger shares of total electricity generation.

In order for PV to become a competitive source of electricity production, the levelised cost of electricity (LCOE) from PV should decrease below residential electricity prices ("socket parity") and below wholesale electricity prices ("grid parity"). Furthermore, for PV to become a viable investment option for both consumers and businesses, the payback time (PBT) of investing in PV should drop to about 3-5 years [105]. Figure 3.2 shows the effect of PV system price and annual yield on LCOE and PBT. From this figure, we can deduce that, in order for PV to reach grid parity (instead of the already achieved socket parity) PV system prices still need to drop significantly. For PV to compete with combined-cycle natural gas and coal with a levelized cost of electricity (LCOE) of about 0.05 USD/kWh [106], we estimate that PV system prices need to drop below 0.60-1.00 USD/W_p, thus PV module prices should drop below 0.3-0.5 USD/W_p[1]

For a large part, cost reductions in PV production have been achieved due to economies of scale, and technological learning in the PV production supply chain [33]. More recently we have seen an increased focus on intrinsic cost reductions. General approaches for cost reductions have traditionally been to decrease material use or replace expensive materials with cheaper ones. For instance, silicon consumption per watt-peak (W_p) has decreased significantly due to increased efficiencies and the use of increasingly thin wafers, while silver use for metallization has also decreased over the years. Significant cost reductions have been obtained with this approach, however, more recently the room for further improvement has

[1] Assuming a PV system energy yield of 800-1400 kWh/(kW_p·year) and a module-to-system price ratio of 2.

decreased. This has resulted in a variety of approaches being researched, including a shift from the traditional diffused junction crystalline PV devices, towards alternative designs or technologies.

One of those "new" technologies is the Silicon Heterojunction (SHJ) solar cell technology. SHJ solar cells are produced from silicon wafers in a low temperature process that does not exceed 200°C. High temperature diffusion of the p-n junction is replaced with a low temperature deposition of a *p*-doped amorphous silicon layer on an n-type monocrystalline silicon wafer.

This technology is only produced on a large scale by Panasonic (by acquiring Sanyo), but a recent expiry of the core patents describing their SHJ technology has lead to a marked increase in R&D on this technology [29, 107]. The large interest is mainly due to the fact that [29, 107]: **1)** SHJ fabrication is a simple process with high efficiency cells as a result; **2)** the deposition of the thin film layers for SHJ cells can benefit from ample experience with these processes in the flat-display industry; **3)** SHJ modules have a low temperature coefficient which leads to higher energy yields compared to conventional c-Si modules, and **4)** SHJ cells benefit more from the application of thinner wafers, because the deposited thin-film layers allow for very good passivation of the wafer surface. Current R&D mainly focuses on improving device performance, but novel design structures and processing steps are also being investigated, aiming to lower production costs. Examples are alternative materials for the transparent conductive oxide (TCO), alternative metallization schemes and materials, and alternative passivation structures and materials [107]. Current SHJ cell designs rely on expensive materials (silver, indium) and processing steps.

In order to improve the economic performance of SHJ technology, the FLASH[2] programme investigates several alternative SHJ cell designs. The research focuses not only on replacement of expensive and high price volatility materials like indium (for the TCO) and silver (for metallization) but also on simplifying the production process. In this paper we present an analysis of the cost structure of PV modules based on six different SHJ cell designs, and, as a reference, conventional diffused junction monocrystalline silicon PV cells. Furthermore, we use the results obtained to evaluate a roadmap towards significant cost reductions in prospective SHJ modules. With the analysis of current production costs, we aim to establish a baseline, but also to compare and rank different SHJ cell designs in terms of cost, and to provide an upfront cost estimation of these different cell designs while they are still

[2]The FLASH programme (acronym for FundamentaLs and Application of Silicon Heterojunction solar cells) is a Dutch research programme funded by technology foundation STW under their *Perspectief* programme. *Perspectief* programmes aim to employ fundamental technical research to apply novel technologies in society.

under development. Together with previous work [102] focusing on the environmental performance of SHJ solar cells and modules, we aim to perform an ex-ante technological assessment of SHJ technology, and SHJ cell and module production on an industrial scale of designs currently in laboratory stage. To analyze where this technology could go in 10 years, we have also investigated a roadmap towards production of derivatives of the SHJ designs in 2025.

3.2 Methods

In a previous study we performed a life cycle assessment (LCA) of four of the six SHJ designs studied here, resulting in a detailed description of SHJ cell and module production [102]. LCA studies aim to establish the environmental impact of products, and are based on establishing a life cycle inventory (LCI): a detailed inventory of all material and energy inputs and waste outputs of production of a product. We used the life cycle inventory gathered in our previous study to perform a bottom-up cost analysis using life cycle costing (LCC), by attributing costs to all the material, energy and waste flows in the LCI. Some updates were made to our previous LCI. The LCI used in this study is shown, per processing step, in Tables B.2-B.7 in the appendix. The methodology for LCA is firmly standardised, both in general terms [42, 43] and for PV specifically [44]. For LCC, this methodology is not yet standardized [108], but in many ways very similar to LCA. We will follow the approach detailed by Rebitzer and Seuring [109] and Hunkeler and Rebitzer [110] for LCC, our previous study followed PV LCA guidelines by Fthenakis *et al.* [44].

3.2.1 Designs studied

In this study we compared the production of various different SHJ cell designs, and compared this with the production of a conventional crystalline silicon solar cell. The different designs studied here are shown in Fig. 3.3 and described in detail in Table 3.1. We assumed production with commercial scale (optimized for throughput) cell processing tools, with wafer throughputs of 3600 wafers/hr (or approximately 120-130 MW/yr dependent on cell efficiency). As in our previous work [102] we assumed the designs to be based on a 180 µm monocrystalline Cz Si wafer, passivated with intrinsic amorphous silicon (a-Si:H) on both sides, deposited via plasma enhanced chemical vapor deposition (PECVD). The reference design (see Figure 3.3) has a standard SHJ structure: an a-Si:H emitter and back surface field (BSF), and an indium-tin-oxide (ITO) transparent conductive oxide (TCO). Metallization is screen-printed silver on both sides. Compared to conven-

Table 3.1 · Overview of Design Parameters for the Current and Prospective Scenario Cell Designs. The abbreviations of the design names refer to the discussion of these designs in section 3.2.1 and are also shown in Figure 3.3.

Short name	**Ref-cSi**	**Ref-SHJ**	**PVD-SHJ**	**NE-SHJ**	**ALD-SHJ**	**IBC-SHJ**
			Current Designs			
Wafer type	p-type	n-type	n-type	n-type	n-type	n-type
Wafer thickness (µm)	180	180	180	180	180	180
Passivation		a-Si:H (i)	a-Si:H (i)	a-Si:H (i)	Al2O3	a-Si:H (i)
Emitter	diffused n-dopant	a-Si:H (p)	a-Si:H (p)	multifunctional layer	ZnO	a-Si:H (p)
TCO	-	ITO	ITO	ITO (back)	ITO (back)	ITO (back)
Metallization front	Ag print	Ag print	Ag print	Ag print	Ag print	-
Metallization back	Al print with Ag soldering pads	Ag print	Ag PVD	Ag PVD	Ag PVD	Ag PVD
Cell Area (cm^2)	239	239	239	239	239	239
Cell Efficiency[a]	19.4%	22.4%	22.7%	19.7%	19.5%	23.3%
Module Efficiency[a]	17.1%	19.7%	20.0%	17.3%	17.2%	20.5%
			Prospective Designs			
Wafer type	p-type	n-type	n-type	n-type	n-type	n-type
Wafer thickness (µm)	**100**	**100**	**100**	**100**	**100**	**100**
Passivation		a-Si:H (i)	a-Si:H (i)	a-Si:H (i)	Al2O3	a-Si:H (i)
Emitter	diffused n-dopant	a-Si:H (p)	a-Si:H (p)	multifunctional layer	ZnO	a-Si:H (p)
TCO	-	**ZnO**	**ZnO**	**ZnO**	**ZnO**	**ZnO**
Metallization front	**Cu print**	**Cu plate**	**Cu plate**	**Cu plate**	**Cu plate**	**-**
Metallization back	Al print with **Cu soldering pads**	**Cu plate**	**Cu PVD**	**Cu plate**	**Cu plate**	**Cu plate**
Cell Area (cm^2)	239	239	239	239	239	239
Cell Efficiency[a]	**20.7%**	**25.4%**	**25.3%**	**23.2%**	**23.0%**	**25.9%**
Module Efficiency[a]	**19.7%**	**24.1%**	**24.0%**	**22.1%**	**21.8%**	**24.6%**

[a] Cell and module efficiencies are monofacial efficiencies.

tional silicon cells, more silver paste is required for the front grid due to the low temperature curing process. As shown in [29], there is no single preferred metallization layout in SHJ research and development. Therefore, we have compared SHJ designs with different forms of metallization: the reference design with an Ag grid at the back (Ref-SHJ), and SHJ cells with a PVD deposited Ag layer at the back (PVD-SHJ).

Aside from these designs with only changes in metallization, we have studied three other designs: The Novel Emitter SHJ (NE-SHJ) design has no ITO or a-Si:H layers on the front, but instead has a multifunctional layer which aims to combine the function of passivation, emitter, TCO and antireflective coating in a single layer.

The atomic layer deposition design (ALD-SHJ) replaces the standard SHJ front side with ahole selective Al_2O_3/ZnO window layer. The aluminum oxide layer is deposited with ALD, while the zinc oxide layer is sputtered.

The final design studied is an interdigitated back contacted (IBC) SHJ cell (IBC-SHJ). The IBC structure is produced with masked plasma-deposition (PECVD) and -etching, while the contacts are formed at the back by masked PVD of ITO and silver.

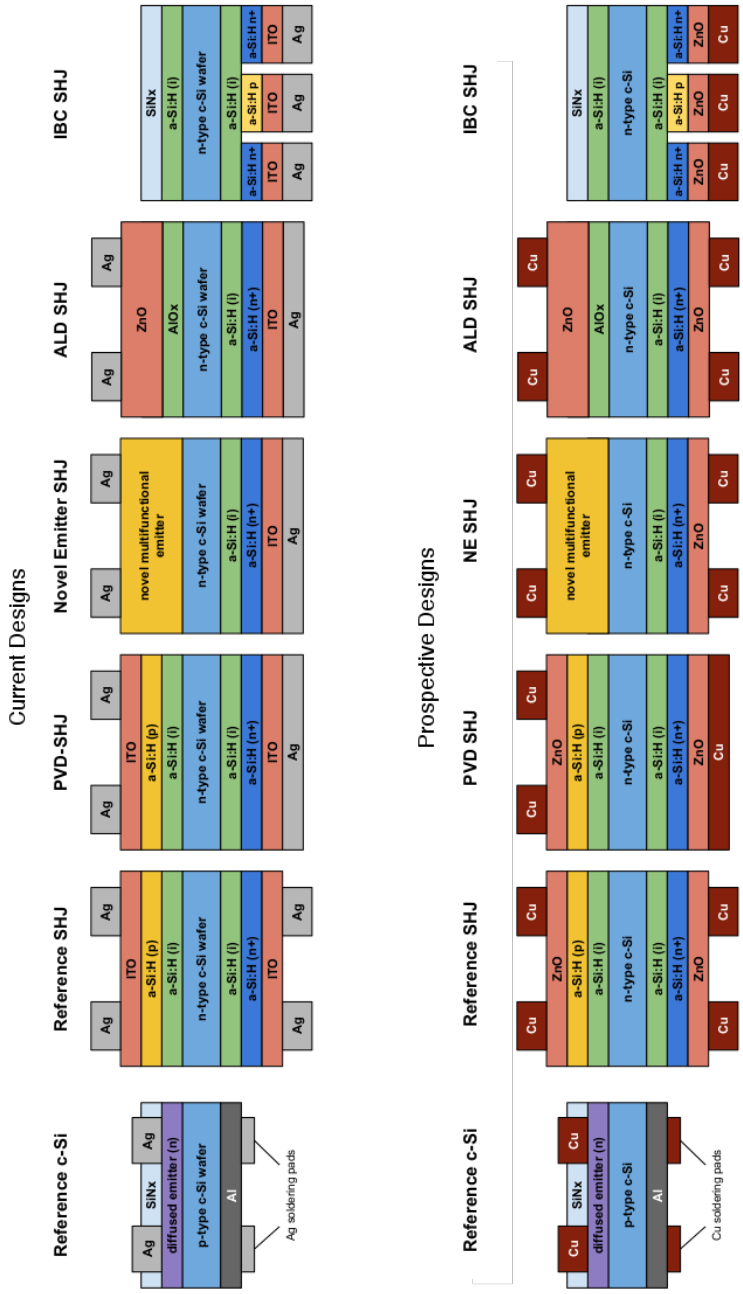

Figure 3.3 · Graphical representation of the current and prospective scenario cell designs analysed in this study. Based on designs from [102].

We compared these five SHJ designs with a conventional c-Si cell, with a p-type wafer and diffused emitter, aluminum BSF, SiN_x anti-reflective coating (ARC) and fired-through silver grid at the front, and silver soldering pads at the back.

Cell design efficiencies

This study presents productions cost for five different SHJ cell designs. For most of these designs, it is difficult to assign an accurate cell efficiency, as they are not being produced and tested at a large scale. With an approach similar to that in [33] we have calculated cell efficiencies for each of the SHJ designs, based on an assumed cell efficiency of 22.4% for the reference SHJ design, adjusting the efficiency for each alternative design based on the effect of changes in the cell structure on open-circuit voltage (V_{oc}), short-circuit current (I_{sc}) and fill factor (FF). The assumed efficiencies for each of the SHJ designs, and the assumptions made for their calculations are shown in Table 3.2.

3.2.2 Scope of the study

The aim of the study reported here was to quantify production costs for the six SHJ cell designs mentioned in the previous section, show a roadmap towards reduction of these costs in the future, and make a comparison with conventional c-Si modules. With the analysis we hope to be able to offer an ex-ante production cost assessment of different SHJ designs currently being developed, in order to be able to steer the R&D towards cost reductions. Furthermore, we hope to identify the importance of SHJ specific design elements in cell and module production to overall costs.

Fig. 3.6 shows the cell production cycles we have analyzed, which are detailed below in sections 3.3.1 and 3.3.2. The focus of our study was on production costs. We therefore established these costs for a functional unit defined as “one Watt of rated (peak) module power output” (USD/W_p). The aim of the study is to analyse these production costs based on a breakdown of the production cycles detailed in Fig. 3.6.

3.2.3 Cost data and calculations

The production costs for the designs studied were calculated by combining material and energy prices with a life cycle inventory (LCI) of cell production. The LCI gives a detailed bill of materials needed for production of the studied solar cells and modules. The LCI was taken from our previous work [102], while cost data was taken from a variety of sources. For an overview of input cost data, see Table B.9 in the appendix.

Table 3.2 · Overview of estimated SHJ cell performance parameters and the assumptions behind their calculation. Method based on the approach in [33].

Cell Parameter	Ref-SHJ	PVD-SHJ	NE-SHJ	ALD-SHJ	IBC-SHJ
			current cell designs		
Open-circuit voltage (V)	0.737	0.737	0.729 - No ITO at front side + No TCO/a-Si:H interface	0.715 - negative effect of TCO on Voc - front emitter changed	0.744 + Reduced recombination at front interfaces
Short-circuit current density (mA/cm^2)	0.380	0.382 + Increased reflectivity backside metal	0.356 + decreased parasitic absorption of ITO - decreased lateral conductivity emitter/TCO	0.358 - decreased lateral conductivity emitter/TCO	0.389 + Elimination of shadowing front + Decreased parasitic TCO absorption front
Fill factor	0.800	0.808 +Increased conductivity backside metal	0.760 - decreased lateral conductivity emitter/TCO	0.761 - decreased lateral conductivity emitter/TCO	0.803 + High contact coverage back
Cell efficiency	22.4%	22.7%	19.7%	19.5%	23.3%
Module efficiency	20.2%	20.5%	17.8%	17.5%	21.0%
			prospective cell designs		
Open-circuit voltage	0.760	0.760	0.756	0.746	0.768
Short-circuit current density	0.400	0.402	0.386	0.386	0.409
Fill factor	0.820	0.828	0.796	0.797	0.826
Cell efficiency	24.9%	25.3%	23.2%	23.0%	25.9%
Module efficiency	23.7%	24.0%	22.1%	21.8%	24.6%

The LCI data from our previous study [102], was gathered with the aim of analysing the environmental impact of solar cell production. Therefore, it is focused on material and energy in- an outputs, and emissions of harmful substances. As a result, it does not accurately reflect costs at all times. For instance, the price of silver and indium on the global market is not only a result of the materials and energy expended in acquiring them, but is also a reflection of the balance between the supply and demand of these materials. Also, as labor has no direct environmental impact (or one that is negligible), it is also not included in an environmental LCI, at least not on the basis of man-hours.

To account for this difference, we have supplemented the data with processes like labor, and have attributed cost at the highest level in de LCI. For instance, instead of calculating the cost of input energy and materials using life cycle costing (LCC), we have instead used the market price of these inputs. In this sense, our study deviates from a true LCC. For each step in the production chain, the processing costs were calculated as follows:

$$CoP = \frac{a \cdot I_{\text{total}} + \sum_{n=1}^{i} (cons_i \times price_i)}{T_{\text{annual}}} \tag{3.1}$$

where CoP is the cost of processing per unit of throughput, a is the capital recovery factor, I_{total} is the total investment expenditure for the processing tool, T_{annual} is the annual throughput of the processing facility, $cons_i$ refers to an annual amount of consumable input (material, labor, and energy inputs), $price_i$ refers to the price per unit of $cons_i$. The capital recovery factor a is defined as:

$$a = \frac{r}{1 - (1 + r)^{-D}} \tag{3.2}$$

where r is the depreciation rate and D is the depreciation period of the processing tool. The capital recovery factor expresses the annual depreciation and interest cost of the capital investment in the processing tool.

Cost data for process inputs was taken from a variety of sources. Equipment prices were taken from market surveys [59, 61, 62, 82, 111] for cell processing and from [33] for silicon and wafer production. For materials and energy we used data from literature, gathered average market prices, and included globally tradable products at international prices. The data gathered is summarized in Tables B.9-B.7 in the appendix.

3.2.4 Sensitivity and uncertainty analysis

The data we have gathered comes from a large variety of different sources, and as such can show large variety in both accuracy, quality and age. To investigate the

Table 3.3 · Overview of general economic input parameters. FTE refers to full-time equivalent.

Parameter	Unit	Value	Source
Depreciation rate	-	8.0%	[33]
Cleanroom cost	USD/m^2a^{-1}	200	[33]
Skilled labor	USD/(FTE·a)	70000	Own estimate
Unskilled labor	USD/(FTE·a)	50000	Own estimate

sensitivity of the overall result to variation in certain parameters, and to analyse the effect of uncertainty in the data on the overall result, we performed a sensitivity and an uncertainty analysis.

For the sensitivity analysis, we varied several parameters over a range defined by either historical data (for consumables, wafer price), or estimated ranges (cell or module efficiency). The resulting recalculated overall results are plotted to show the overall result as a function of change in the studied parameter.

For the uncertainty analysis, we performed a Monte Carlo simulation. From the results and sensitivity analysis parameters were identified that have a large effect on the overall result and have considerable uncertainty. We generated 100,000 random samples of these parameters from log-normal distributions with means of the base values, and sigmas reflecting the uncertainty in each parameter. After that, the results were recalculated for each of the generated samples. The resulting data was presented as boxplots showing the variation in the overall result that was obtained. We opted to use log-normal (instead of normal) distributions as we assumed the parameters under investigation, such as module efficiency and prices, to be more constrained on one side of the mean, and to have a longer tail on the other side, e.g. the uncertainty was assumed to not be symmetrically distributed around the mean. The variance of the lognormal distribution was chosen so the 95^{th} percentile of the distribution reflects the upper level of the uncertainty we want to investigate.

3.3 Production costs

3.3.1 Silicon, ingot and wafer production

The starting point for all of the devices analyzed in this study is a monocrystalline silicon wafer. Wafer production is generally an activity for dedicated wafer production companies, although supply-demand imbalances in the wafer production chain have resulted in an increased number of PV companies vertically integrating polysilicon, ingot and wafering in their activities [33]. Aside from more vertically integrated firms, the polysilicon production capacity has been expanded signifi-

cantly since the price of polysilicon peaked in 2011. This has resulted in polysilicon prices dropping sharply, from around 80 USD/kg in 2011 to around 20 USD/kg from the end of 2012 until now (see Figure 3.1).

The production chain for polysilicon, ingots and wafers is depicted in Figure 3.4. From silica (SiO_2), which costs around 20 USD/tonne [112], metallurgical grade silicon (MG-Si) is produced by reducing the silicon-oxide with coke at high temperatures (1900°C). As this process occurs in an electric-arc furnace, main inputs aside from the SiO_2 are electricity, and some form of carbon. This MG-Si has a purity of about 98.5%-99.5% [57], while much higher purity (99.99%-99.9999%) is required in the solar and especially electronics industry. To achieve these higher purities, the MG-Si is processed into polysilicon, commonly using (hydro)chlorination in a Siemens reactor. A less common alternative is the Fluidized Bed Reactor (FBR), although due to technical challenges this process is not common [33], and is also more capital intensive compared to the Siemens process [113]. In the Czochralski (Cz) process, the polysilicon is "pulled" into monocrystalline silicon ingots, which are sawn into wafers with wire saws. In this process, silicon is lost as kerf loss, due to the abrasive sawing of the ingots into wafers. The silicon usage per wafer is reduced by decreasing wafer thickness and kerf losses. Current wafers are generally 180 µm thick [114], and sawing losses amount to 130 µm of silicon per wafer [33].

For material and energy requirements in polysilicon, ingot and wafer production, we used a life cycle inventory (LCI) from the ecoinvent database [57]. This database analyses the full life cycle of production of a 270 µm Cz wafer. The data from this inventory were updated to account for the different wafer thicknesses we investigated. Furthermore, as ecoinvent data does not accurately reflect the cost of capital expenditures, we based equipment and facility costs on Goodrich *et al.* [33], who studied the polysilicon-ingot-wafer production chain as a basis for cost roadmaps for various types of c-Si based PV modules. By attributing costs to all the material and energy inputs from the LCI we calculated a cost structure for monocrystalline silicon wafers, from silica sand to wafer sawing. Table 3.4 shows the main input parameters for Cz ingot production. Figure 3.5 shows the calculated cost structures for wafers of various thicknesses. The 100 and 80 µm wafers were assumed to be sawn with diamond wire saws (see Table 3.5).

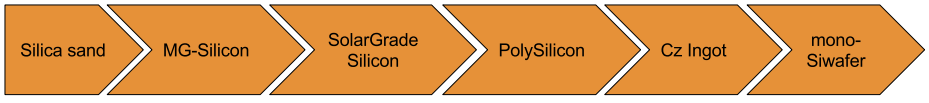

Figure 3.4 · Schematic overview of the silicon, ingot and wafer production chain studied here.

Table 3.4 · Main input parameters for Cz ingot production. Amounts per kg of Cz Silicon ingot produced.

Input	Amount	Unit	Source	Unit Cost	Source
PV Grade Silicon	1.07	kg	[57]	16.47	Own model
Electricity (hydro)	85.6	kWh	[57]	0.025	[33]
Argon	5.8	kg	[57]	0.714	Own survey

Table 3.5 · Main input parameters for wafer production

Input per m^2	wafer thickness 180	120	100	80	Unit	Unit cost (USD)	Source
Cz silicon	0.74	0.54	0.49	0.38	kg	27.36	Own calculations based on [57]
Electricity	8.0	8.0	8.0	8.0	kWh	0.07	[57], assumed constant for var. wafer thickness
SiC fluid	1.2	0.7			L	1.8	[33, 57]
- recycled	3.5	2.2			L		[57]
Cutting fluid			3.0	2.0	L	0.00[a]	Assumption, cost from [33]
Steel saw wire	5.0	5.0			km	0.5	[113]
Diamond saw wire			83.0	83.0	m	0.125	Estimate based on [115]

[a]Cutting fluid cost is 0.39USD/1000L

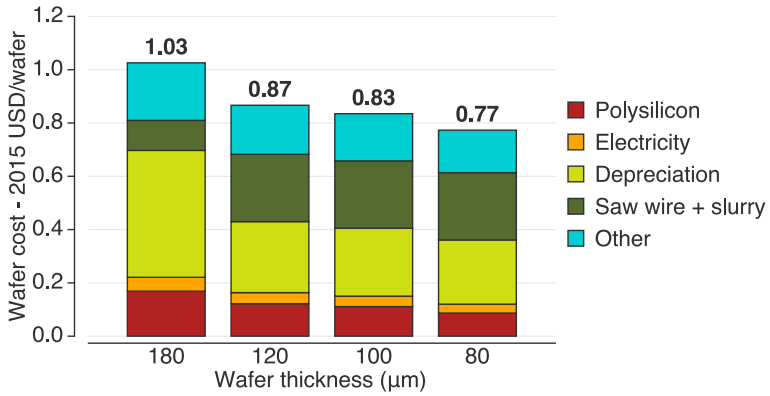

Figure 3.5 · Overview of wafer production costs for various wafer thicknesses. In this study, p-type and n-type wafers are assumed to have equal production costs.

3.3.2 Cell processing

The analyzed process flows are shown in Figure 3.6. The basis for all designs studied is an 180 µm monocrystalline silicon wafer, n-type for the SHJ and p-type for the c-Si reference design. For simplicity, wafer costs are assumed equal for p-type and n-type wafers. The following section discuss the cell processing flow for each of the studied designs.

Conventional *p*-type c-Si cell

The p-type c-Si cell is assumed to be produced according to a standard process flow. Wafers are treated for saw damage and textured, prior to emitter diffusion in a diffusion furnace. After diffusion, a wet chemical treatment step is performed for edge isolation and phosphosilicate glass (PSG) removal. The silicon nitride

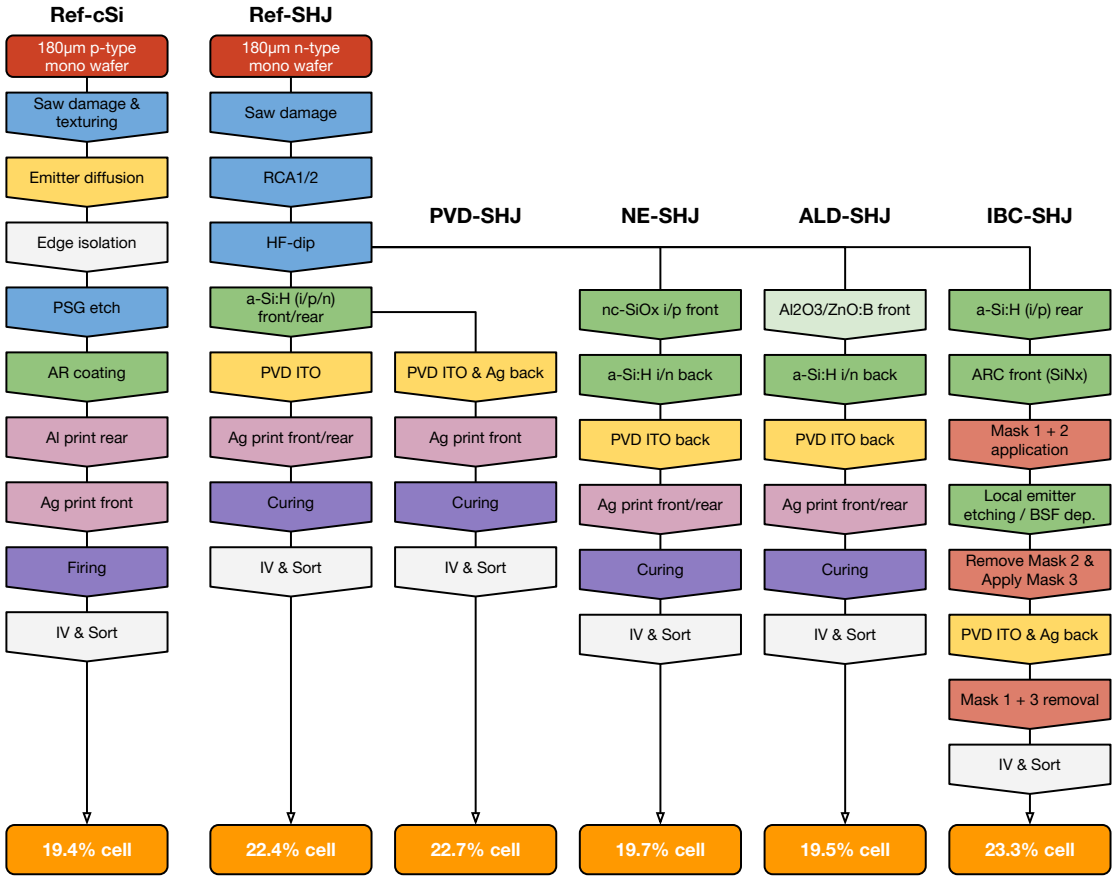

Figure 3.6 · Overview of cell processing steps for the different PV cell designs studied here. The process flow for the reference monocrystalline-silicon cell was based on [116].

(SiN_x) ARC is deposited with PECVD. Metallization is screen printed (Al with Ag soldering pads on the back, Ag grid on the front) and fired in a firing furnace at high temperature.

Reference SHJ cell

A reference case for SHJ cells was analyzed based on a conventional SHJ cell structure. The process flow for this Reference SHJ design (Ref-SHJ) is shown in Figure 3.6, while the cell design is described in Table 3.1 and Fig. 3.3. The Ref-SHJ cell has a symmetric layout, with wafer, intrinsic a-Si:H, doped a-Si:H, ITO and metallization.

To treat the wafers for saw damage, texture it to achieve better light-trapping, and remove oxides from the surface of the wafers, the first process in the cell processing is at wet chemical treatment. In our model, the wafers are treated with 1) Sodium hydroxide for saw damage removal, 2) A two step RCA cleaning procedure, and 3) a HF dip for oxide removal and texturing.

In terms of costs, this process main costs are consumables (the etchant solu-

tions), capital expenditures (CapEx) and waste treatment. A survey on wet chemical treatment tools [59] shows average CapEx to be 293±52 USD/(wafer/hr), resulting in a wafer processing cost of 0.017 USD/wafer for capital investments, while total cost-of-ownership (CoO) including consumables is 0.075 USD per wafer. The etchants used in this process account for over 30% of these costs.

After wet chemical treatment, the electronic structure of the SHJ cell is applied by deposition of thin a-Si:H layers on both sides of the wafers. On one side, an a-Si:H (i) layer is deposited, followed by a p-type a-Si:H layer. On the other side, an i/n^+ a-Si:H stack is deposited. Main consumables are electricity, silane, hydrogen, and water. Because of the very thin layers applied (5 nm for the intrinsic layers, up to 20 nm for the doped layers) the material consumption is very low. As a result, most of the cost of this process step results from the capital expenditures for the processing tools. CapEx for PECVD was based on equipment costs for PECVD tools used for a-Si:H deposition in the preparation of thin film modules. A survey [61] showed large variation in the cost of these tools (ranging from 1489 to 5393 kUSD/(wafer/hr), especially the older tools were found to have very high costs. PECVD tools for deposition of SiN_x ARC layers were found to have much lower costs, on average 882 USD/(wafer/hr) [111], but as this process occurs at higher pressures, we assume these tools to be cheaper compared to those for a-Si:H deposition. We have selected the two most recent tools from the survey [61] to calculate PECVD costs for a-Si:H deposition, and found these to be 1676 USD/(wafer/hr). Resulting processing costs were found to be 0.050 USD/wafer for capital expenses, or 0.078 USD/wafer including consumables and utilities.

PECVD is followed by the deposition of a TCO layer, in this case ITO, on both sides of the wafer. This transparent conductive oxide-layer is applied to improve lateral conduction in the device, while maintaining a high absorbance of light in the p/n region of the device. This deposition of ITO is commonly assumed to be expensive, as indium is a scarce and quite expensive material (750 USD/kg). According to our cost model however, this processing step is not as expensive as expected. The very thin layers deposited do not require much material (0.028 gram/wafer), and utilization factors in the sputtering tools are quite high (88%, resulting in ITO consumption of 0.032 gram per wafer). The cost of ITO target material was calculated to be about 0.85 USD/gram, although this is a rough estimation, and likely an overestimation, as we assume commercial targets to approach raw materials prices (0.75 USD/gram). Capital costs for the sputtering tools we reviewed were found to be on average 1573 USD/(wafer/hr) [62]. The total CoO of TCO deposition was found to be 0.087 USD/wafer, of which 0.027 USD/wafer (31%) was due to the consumption of ITO.

Silver-based metallization

A main cost factor in cell processing, as expected, was found to be the silver based metallization. As SHJ solar cells have to be processed at low temperatures (below 250°C), there is a need for low temperature silver paste. This paste is more expensive than conventional metallization paste, and more of it is needed to reach the required contact resistance values in the cells. We assume that the higher price of low temperature paste is mainly the result of a higher silver content in these pastes, but supply and demand dynamics possibly also play a role, as the market for low temperature paste is much smaller to that of regular (high temperature) paste.

Current silver paste cost were conservatively estimated at 820 USD/kg for high temperature and 1060 USD/kg for low temperature paste. Because of the lower conductivity of the cured low temperature paste, we assume that twice the amount of silver is required compared to high temperature silver paste metallization. A metallization grid is therefore assumed to require 200 mg silver per side of the wafer, or 250 mg of paste, assuming 80% loading of the paste with silver. For the reference SHJ design, we assume the application of a silver grid on both sides of the solar cell, thus the total paste requirement per cell is 0.5 grams. Total materials costs for metallization amount to 0.55 USD/wafer, or 0.10 USD/W_p. In current and past SHJ cell R&D many different metallization layouts have been studied for the backside of the cell, including silver screen printed grids, aluminium PVD back contact and silver PVD back contact. An aluminum backside would have the lowest material costs, but impacts the efficiency of SHJ cells severely as it is shown to result in a poor internal quantum efficiency in the infrared region of the spectrum without a more complex rear structure [117].

Silver PVD SHJ cell (PVD-SHJ)

The silver PVD SHJ cell (PVD-SHJ) is another design strongly based on the reference SHJ cell. Here, instead of a bifacial Ag grid, the backside contact is formed from PVD deposited silver. The cost of silver target material is lower compared to silver paste, resulting in a material cost decrease of 0.26 USD/wafer, to a total of 0.27 USD/wafer for metallization materials (0.059 USD/W_p). Here, we assumed the thickness of the PVD deposited layer to be 0.2 µm [117], while the utilization rate of the PVD tool is assumed to be 74% [62], resulting in a silver consumption of 0.07 g/wafer for the rear side metallization. Capital costs do increase by 0.04 USD/wafer due to the PVD tool, but the resulting costs for metallization are still considerably lower at 0.33 USD/wafer compared to 0.55 for the bifacial silver grid.

Novel emitter SHJ cell

The novel emitter design is an SHJ design that focuses on replacing the scarce and expensive ITO with abundant materials, at the same time simplifying the processing sequence by cutting out on process, namely TCO deposition. The process flow for this design is shown in Figure 3.6. As we can see from this figure, the basis of this design is very similar to the reference design. The changes occur however during the PECVD step. Instead of a p-doped a-Si:H layer, a transparent p-type conductive PECVD layer is deposited at the front side. The layer is deposited to function as both an emitter and a transparent conductive layer.

The replacement of the ITO layer on the front results in an increased requirement for PECVD. This does however not result in a strong decrease of throughput of the PECVD step as the p-layer is replaced by the combined layer and the main time-consuming factors are a result of creating and releasing the vacuum in the processing chambers, which is done once less. For the deposition of a total of 130 nm layer thickness, which is an increase in terms of total deposited layer thickness by a factor of 2.6, throughput drops with only about 4.5% compared to the reference design, based on throughput figures for a the selected PECVD tools mentioned in section 3.3.2. This results in an increase of processing cost for PECVD by 0.025 USD/wafer to a total of 0.10 USD/wafer. The absence of the ITO deposition on the front however gives an advantage of 0.03 USD/wafer, largely due to increased throughput and an ITO consumption cost reduction of 0.013 USD/wafer.

ALD Aluminum-Oxide/Zinc Oxide SHJ cell

The ALD aluminum-oxide/zinc-oxide SHJ cell design (see Fig. 3.6) is an R&D design that tries to address two issues with conventional SHJ cells, namely *1*) ITO replacement for more abundant ZnO and *2*) introduction of a thin-film deposition process that is less energy-intensive compared to PECVD and does not require operation at vacuum. The back-side of the cell is similar to that of the Reference SHJ and Novel Emitter SHJ design, with an i/n-stack of a-Si:H deposited with PECVD. On the front side, an Al_2O_3 passivation layer and ZnO window-layer are deposited with ALD and sputtering, respectively. Alternatively, this process could also involve MoO_3 as a high-workfunction hole-selective contact.

Average CapEx for the ALD tools surveyed [111] was found te be 796 USD wafer^{-1} hr^{-1}. As consumable consumption is low, the capital costs account for over 60% of the cost of processing a wafer with ALD. Another major factor is the cost of trimethylaluminium, which at 845 USD/kg accounts for over 20% of the cost of processing. Energy consumption in this atmospheric pressure process was found to be much lower compared to PECVD.

The relative cost of the PECVD deposition of the back-side i/n a-Si:H stack (25 nm total thickness) is quite high, as the throughput of the PECVD tool only increases by about 20% on average, while the capital related cost of processing only decreases by 11% compared to deposition of 50 nm of total a-Si:H layer thickness. As this cost advantage is minimal, the total cost of processing the ALD cell is slightly higher compared to that of the reference SHJ cell.

IBC-SHJ cell

The interdigitated back-contacted heterojunction (IBC-SHJ) cell is quite different from the reference design in terms of cell and module structure. The device has an assymetric structure, with interdigitated emitter and back-surface field and corresponding contacts. For this design we assume this interdigitated structure to be applied by using a masked PECVD deposition and etching process, based on a process described [69]. The process flow of this cell design is shown in Figure 3.6, and detailed below.

The IBC-SHJ cell undergoes the same wet chemical treatment as the other designs, however, after this step the differences are pronounced. First with PECVD, on the front side of the cell a passivation layer (intrinsic a-Si:H) and SiN_x antireflective coating (ARC) are applied, while on the backside an a-Si:H emitter is applied. Then, a base mask is applied, followed by the mask for local plasma etching of the emitter and deposition of the a-Si:H backsurface-field (BSF). The BSF mask is removed and replaced with a second mask for TCO deposition and deposition of the evaporated silver back-contact. We have assumed contact coverage at the rear side to be 80%, with a thickness of 0.4 micron, thus requiring 140 mg of silver target per wafer, assuming a 74% utilization rate in the sputtering tool.

We have assumed silver to be required for this IBC contact, as the reduced contact area would result in higher contact resistance when using aluminium.

The cost structure of production of this design is affected in three ways: **1)** more processing steps are required, leading to a higher cost of capital, **2)** replacement of the silver front grid with a silver PVD back-contact increases material costs for metallization, more silver is required for the back-contact. **3)** the application and removal of masks increases handling, yield losses and material requirements.

To calculate the cost of producing the IBC structure, we have made several (rough) assumptions: **1)** each process requiring a mask application or removal has a 10% lower throughput, **2)** a mask application or removal step induces a 2.5% yield penalty, and **3)** mask costs were estimated to be 0.05 USD/wafer.

The increased requirement of PECVD, coupled with the application and removal of masks, requires a three-step PECVD. This leads to a decreased throughput, and

as a result, a strong increase in capital costs. Furthermore, material requirements are much higher, and yield losses increase due to the number of handling steps when applying and removing the masks. The total cost of processing of PECVD therefore increases more than three-fold compared to the reference design, to 0.27 USD/wafer, of which 0.03 USD/wafer due to yield losses (compared to only 0.0011 USD/wafer for the reference SHJ design).

The replacement of the front-side silver grid made with low temperature silver paste with an interdigitated PVD silver contact decreases the cost of metallization by 0.33 USD/wafer compared to the Ref-SHJ design. This is mainly the result of the substitution of low temperature silver paste screen printed grid with a silver PVD metallization structure. We assume this metallization to be 0.4 micron thick, and to cover 80% of the rear side of the cell. As a result, 0.13 g/wafer of silver is used. Per watt-peak, metallization cost drop by 0.06 USD. Overall, CapEx costs increase by over 0.2 USD/wafer, but, due to the absence of low temperature silver paste, consumable costs decrease by over 0.3 USD/wafer, resulting in processing costs that are 0.019 USD/wafer lower compared to the reference design.

3.3.3 Modules

For the current designs (except the IBC design), SHJ module production is quite similar to that of regular crystalline silicon modules, with the exception that the soldering step cannot be performed for SHJ cells, as this would lead to too high cell processing temperatures [29, 65, 118]. Therefore, the stringing and tabbing is performed with conductive adhesive (CA), which is cured during the module lamination step [65]. For the IBC-SHJ designs, the 1.8 grams/module of CA is printed as dot-contacts, while for the other SHJ designs, 3.6 grams/module of CA is applied on the busbars.

Before module production, cells are tested and sorted according to their IV characteristics, so that they can be matched in 60-cell modules for an optimal power rating. Cells have to be handled to be layed up, tabbed and stringed and laminated into the module, in a sandwich of glass, backsheet and EVA. We reviewed CapEx for module production equipment [119–122] and found total costs for a module production line to be 4.8$\pm$0.7 million USD for a line with a throughput of 60 modules/hr, resulting in a CapEx cost of 0.006-0.007 USD/W_p.

Conductive adhesive is more expensive than regular solder, mainly because silver is often used as a conductive material (as opposed to cheaper tin and lead). At the same time, the resistivity of conductive adhesive compared to regular solder is a concern [65]. For the performance stability of SHJ modules and protection against moisture related degradation, we assume the backsheet to be a combination of

a standard Tedlar®-Polyester-Polyamide (TPA) backsheet and an aluminium foil moisture barrier. Table 3.6 lists the costs of various module components assumed in this study. Prices for glass, frame, backsheet and ethyl-vinyl-acetate (EVA) where estimated based on average market prices.

The module design for the IBC-SHJ design is quite different. The interdigitated contacts mean that regular tabbing and stringing cannot be employed for cell interconnection. Rather, the cells are interconnected by glueing them with conductive adhesive to a backsheet / foil with prestructured copper contacts on it. The conductive adhesive is printed onto the foil in small dots. The EVA foil on the backside is patterned, to make holes at the points where the conductive adhesive is printed. The sandwich of glass, EVA, cells, patterned EVA, conductive adhesive, and backsheet / foil is laminated in one step in which the conductive adhesive is simultaneously cured. Table 3.7 summarizes the differences between the three module layouts.

Figure 3.9 shows a breakdown of module costs. Glass, backsheet and frame contribute most substantially to the overall module costs, while the addition of conductive adhesive results in a cost penalty of 0.007-0.014 USD/W_p for the SHJ designs. The structured backsheet for the IBC design increases the module cost by about 0.06 USD/W_p.

3.4 Prospective Designs

The results for current designs indicate, as expected, main contributions for wafer and metallization to overall cell production cost. Other significant factors are PECVD and TCO sputtering while wet pretreatment of wafers contributes very little to overall production costs. In this paragraph we will detail, per processing step, a roadmap towards possible reduction of cell production costs. For this section we

Table 3.6 · Overview of module component costs. Costs specified in USD/module relate to modules of standard size (1.65 m × 0.99 m).

Component	Cost	Unit	Source
Frame	13.5	USD/module	Market survey
Glass	5.50	USD/m^2	[123]
Standard Backsheet	5.04	USD/m^2	Market survey
SHJ Backsheet with Al Foil	7.00	USD/m^2	Own assumption
IBC Backsheet with Cu foil	10.0	USD/m^2	[124]
EVA	1.85	USD/m^2	Market survey
J-Box	6.50	USD/module	[33]
Stringing/Tabbing	2.50	USD/module	[33]
Conductive Adhesive	750	USD/kg	[124]

Table 3.7 · Overview of difference in 60 cell module design and production between c-Si and SHJ modules.

	c-Si	**SHJ**	**IBC-SHJ**
Stringing	Soldering tabber/stringer	CA & tabber/stringer[a]	CA & lamination[b]
Backsheet	Standard TPA	TPA with aluminium foil[c]	TP with structured Cu foil

[a]Cell stringing is assumed to be performed with a conventional tabber/stringer, but with conductive adhesive (CA) instead of regular solder.
[b]For IBC modules, we assume cell interconnection to be made during lamination, when conductive adhesive (CA) that was printed onto the structured foil is cured together with the EVA sandwich.
[c]SHJ modules are assumed to require a backsheet that is more resistant to moisture ingress. We assume this backsheet to be composed of a standard PVF backsheet with an additional aluminium foil layer.

assume production in 2025.

3.4.1 Wafer costs

Logically, wafer prices are mainly influenced by two parameters: silicon usage per wafer, and silicon price per kg. Apart from a peak in the silicon price in 2008, silicon prices are relatively stable between 15 and 30 USD/kg (see Fig. 3.4). Cost reductions for silicon wafers therefore mainly focus on reducing wafer thickness and sawing losses. Goodrich *et al.* [33] project wafer prices to decrease significantly, due to these two cost reduction strategies, but also include the change from standard to diamond-wire saws, as this should increase throughput [114, 125]. Diamond wire saws furthermore are more durable and do not require silicon-carbide slurry but work with a much cheaper cutting fluid based on water and surfactant [33].

Regular tabbing-and-stringing of cells into modules puts the solar cells under significant amounts of mechanical stress. With decreasing wafer thickness, this mechanical stress increases up to a point at which the cost reductions achieved by thinning the wafers is matched by the added cost of production yield losses. Therefore, we assume a minimum wafer thickness of 100 µmm for all prospective modules.

In silicon production, a gradual shift from Siemens to Fluidized Bed Reactor (FBR) process that is already started is expected to continue, leading to a FBR market-share of just over 30% in 2025 [125]. FBR is currently a new technology and as discussed in section 3.3.1, is quite complex. Cost reduction with this technology is therefore not currently expected [33]. Therefore, we modeled prospective silicon costs based on continued use of the Siemens process.

As shown in Fig. 3.5, even with conservative assumptions regarding silicon and wafer production, wafer cost can decrease substantially from the current modeled cost of 1.03 USD/wafer to 0.83 USD for diamond-wire sawn 100 µm wafers and

0.77 USD for 80 µm diamond-wire sawn wafers. However, it is not expected that module technology will be compatible with wafers below 100 µm by 2025, especially for monocrystalline cell based modules [125]. Therefore, we have based our prospective modules on wafers of 100 µm, for all cell designs. Although the low temperature processing of SHJ cells is more compatible with thinner wafers than the higher temperature processing of standard c-Si cells, we have not assumed different wafer thicknesses to avoid bias in cost due to different wafer thicknesses.

3.4.2 Metallization

Cost reductions in solar cell metallization focus on two aspects: **1)** reduction of material consumption and **2)** substitution of high-cost metallization materials. Because of the high cost of silver-based metallization, the amount of silver used per cell has decreased, and is expected to continue decreasing for the coming years [114]. Although silver use per cell is constrained by minimum conductivity requirements [75], it is expected to decrease from 100 mg per cell in 2015 to about 40 mg/cell in 2025 [125]. This material use reduction alone results in significant cost reductions if application to all designs would be possible. For the conventional mono-crystalline cell, reduction from 100 to 40 mg/cell of silver would drop metallization costs by 36%, or 0.02 USD/W_p. A reduction to 40 mg/cell of silver would actually mean that the Al-back paste would contribute the majority of metallization costs. However, as the Al paste is essential for the Al-BSF in the Ref-cSi design, the backside metallization of this design remains the same.

As the silver related metallization costs are much higher for the current SHJ designs (aside from the IBC design), the effect of this strong reduction in silver use per cell is very substantial. For the SHJ designs, metallization costs drop by 58% (Ref-SHJ), 49% (PVD-SHJ) and 45% (NE-SHJ and ALD-SHJ) or by 0.03 to 0.06 USD/W_p.

Further cost reductions can be obtained by replacing silver with copper. Copper has similar conductivity at only a fraction of the cost of silver. Currently, the cost of copper is less than 2% of the cost of silver. However, copper oxidizes much more easily compared to silver, and diffusion of copper into the silicon substrate is also an issue, as copper atoms diffusing into the silicon can negatively affect performance [126], through a variety of mechanisms [127]. Copper diffusion can be prevented by a nickel barrier layer, while oxidation is prohibited by covering the copper with a thin layer of silver applied with electroplating. Another approach to reduce copper oxidation is to dry/cure the applied metal contact lines in an inert (nitrogen) atmosphere [77]. Printed copper busbars that were printed on top of a SiN_x ARC and cured at low temperature in a $<$10ppm oxygen atmosphere were

shown to result in high module efficiencies, while subsequent thermal cycling and damp heat test showed no copper diffusion into the silicon [126]. Other recent results have furthermore demonstrated a newly developed copper paste that offers similarly low contact resistance compared to silver-based pastes, and can be cured at low temperature in "normal" atmosphere after screen printing [128]. However, line resistances were found to be much higher compared to both low temperature silver paste and high temperature silver paste [128].

In the area of copper metallization, copper electroplating is often mentioned as the prime candidate, as it has been shown to offer the possibility of high-efficiency, silver-free heterojunction solar cells, at a large cost-advantage compared to silver screen printed SHJ cells [83, 129]. However, a electroplating is a multi-step process, consisting of screen-printing and curing a plating resist ink [33], plating different metal layers, and stripping the resist ink in a wet chemical tool. Despite this added complexity, the cost of plating is indeed significantly decreased compared to silver screen-printed contacts [129].

Although adoption of copper metallization in mass production of PV is not expected before 2018 [114], we have modelled our prospective designs with copper plated contacts, as we feel silver substitution is not only advisable for cost reductions, but also necessary, as silver is becoming an increasingly scarce material [75, 130–132], so an upwards trend of the silver price is likely. The copper plated metallization assume a metal stack of nickel, as a seed layer and copper diffusion barrier, copper, as the main contact metal, and silver, as a capping layer which prevents oxidation of the copper. Electrolyte costs were modelled based on their composition, with the cost of plating equipment was taken from [129].

The cost reductions resulting from subsitution of silver with copper result in additional cost savings of 0.01 USD/W_p for the Ref-cSi design, 0.03 USD/W_p for the Ref-SHJ design and 0.02 USD/W_p for the other SHJ designs.

3.4.3 TCO sputtering

Especially for SHJ solar cells, Indium-Tin-Oxide (ITO) is a commonly used TCO material. Because of the high cost and perceived scarcity of Indium, replacement of ITO with other materials is under investigation in many R&D projects. Zinc oxide, doped with boron or aluminium is a commonly named alternative [33]. Our results show that the deposition of ITO layers does not contribute much to the overall costs of cell and module production, as the amount of material used is very low. Still, we assume our prospective designs to be ITO-free, as there are concerns about the availability of indium [90, 91] and ZnO targets were calculated to be slightly cheaper. Due to the higher resistance of ZnO compared to ITO, this replacement

does however result in an efficiency penalty, due to an increased series resistance (R_s). Also, the workfunction of ZnO is sub-optimal for contacting a p-type a-Si:H layer. Aside from materials, TCO sputtering seems to be a mature process, with relatively low capital costs and high throughput.

3.4.4 Modules

Module design and materials have been largely the same for quite some time, and it is expected that the marketshares of alternative module designs will remain limited up until 2025 [114, 125]. Material use is expected to slightly decrease in the coming years, due to a step from 3.2 to 2 mm thick glass, decreasing EVA and backsheet thickness, and reduced aluminium usage in module frames [114]. For the aluminium frame we assume that the cost is reduced proportionally to the mass decrease shown in [114]. For the other materials, accurate data could not be found. Increased light transmission and trapping for the modules results in a slight increase of cell-to-module power ratio [114].

On the other hand, because of the high price of silver, the silver content of conductive adhesive will likely decrease further. Another development is the increasing attention for frameless and/or bifacial modules. In these modules, the backsheet is replaced with another pane of glass, and, possibly, the frame is also omitted.

The Ref-SHJ, NE-SHJ and ALD-SHJ designs in our prospective study are bifacial by design, thus, their prospective module layouts are assumed to be bifacial, replacing the backsheet with a pane of glass. For the Ref-cSi design and the other SHJ designs, we assume a standard module layout, with a backsheet. We assume all modules to have an aluminium frame, which is, as discussed above, decreased in weight and cost.

3.5 Current and Prospective Cell and Module Production Costs

Cell production costs (in USD/W_p) are shown in Figure 3.7. As expected, a main contributor to cell production costs is the wafer, for all designs. The SHJ designs have cell production costs ranging from 0.31-0.35 USD/W_p, while the cell production cost for the c-Si cell was found to be 0.31 USD/W_p. The IBC design benefits strongly from its high efficiency and subsitution of silver paste with PVD silver, which offsets the cost penalties for lower yield and throughput, while the bifacial Ref-SHJ cell shows a strong cost-penalty for requiring a large amount of low temperature silver paste. The novel emitter and ALD SHJ designs are affected by their lower efficiency, and thus have higher production costs compared to the reference

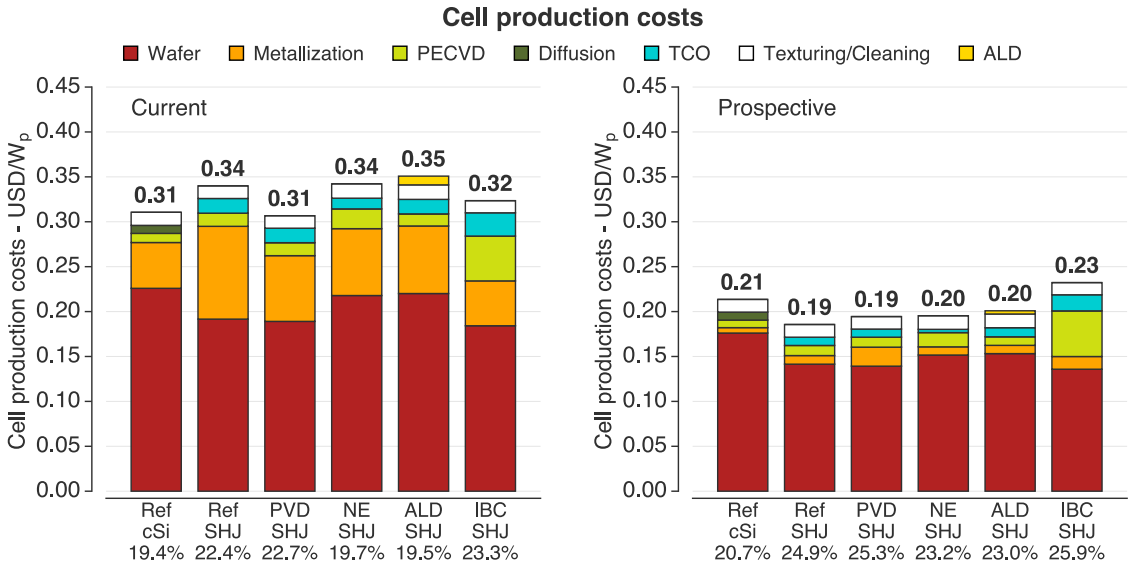

Figure 3.7 · Overview of cell production costs for the four silicon heterojunction designs and a conventional monocrystalline silicon device. Left: current production costs; Right: prospective production costs. The percentages below the labels indicate cell efficiencies.

design. The PVD-SHJ design has the lowest cost of the SHJ designs, as it benefits from high efficiency and substitution of low temperature silver paste.

Comparing the Ref-cSi cell with both the Ref-SHJ and PVD-SHJ designs shows that the choice of metallization layout likely determines the competitiveness of SHJ technology. There is a strong cost penalty for using silver paste on both sides of the SHJ cell, that cannot be offset by the increase in efficiency.

When intercomparing the SHJ designs, we see that the replacement of the front ITO in the NE-SHJ design does not result in a cost reduction compared to the Ref-SHJ design, as there is a significant assumed efficiency penalty for this novel SHJ design. For the ALD-SHJ design, this effect is also shown.

As indium is a relatively expensive material, the effect of replacing the ITO layer was expected to be larger. However, the LCA model [102] already showed that only very small amounts of indium are required as the layer thickness is very small. For two 80 nm layers of ITO, slightly over 0.03 grams of ITO was calculated to be required per cell (based on typical utilization rates, density of ITO, and the volume of the layer). The increased requirement for PECVD in the novel emitter design slightly decreases the advantage obtained by having no sputtered TCO layer, as the increased a-Si layer thickness leads to a slightly decreased throughput, and thus an increased cost of processing (*CoP*, see equation 3.1). The main determinant for higher production costs of the NE-SHJ design is however the decreased efficiency compared to the Ref-SHJ design.

3.5.1 Module Costs

Figure 3.8 shows the costs of complete PV modules based on the designs studied, while Figure 3.9 shows the cost of the module materials. The requirement of conductive adhesive results in a small cost penalty for SHJ modules, while the structured back foil required for the IBC-SHJ design results in a larger cost increase for this particular module. These added costs compared to conventional modules are cannot completely be balanced by the increased module efficiencies. Especially for the NE-SHJ and ALD-SHJ designs, the relative increase in efficiency is to small to offset added costs of cells and module components. For the Ref-SHJ design, the expensive metallization layout results in higher module costs.

As a result, only the PVD-SHJ design has lower total module costs of 0.48 USD/W_p compared to 0.50 USD/W_p for the Ref-cSi module. The other SHJ designs have cost ranging from 0.51 for the IBC-SHJ design, to 0.56 USD/W_p for the ALD-SHJ design.

For the SHJ designs, the wafer and module contribute about 36-39% and 35-38% of the overal costs, respectively. Cell processing contributes 23-24%, for the designs with an PVD Ag back contact (PVD-, NE- and ALD-SHJ), 27% for the IBC-SHJ module, and 28% for the Ref-SHJ module. For the reference c-Si module, due to lower efficiency and cheaper cell processing, the contribution of wafer and module cost (46% and 37%) is much larger compared to that of cell processing (17%).

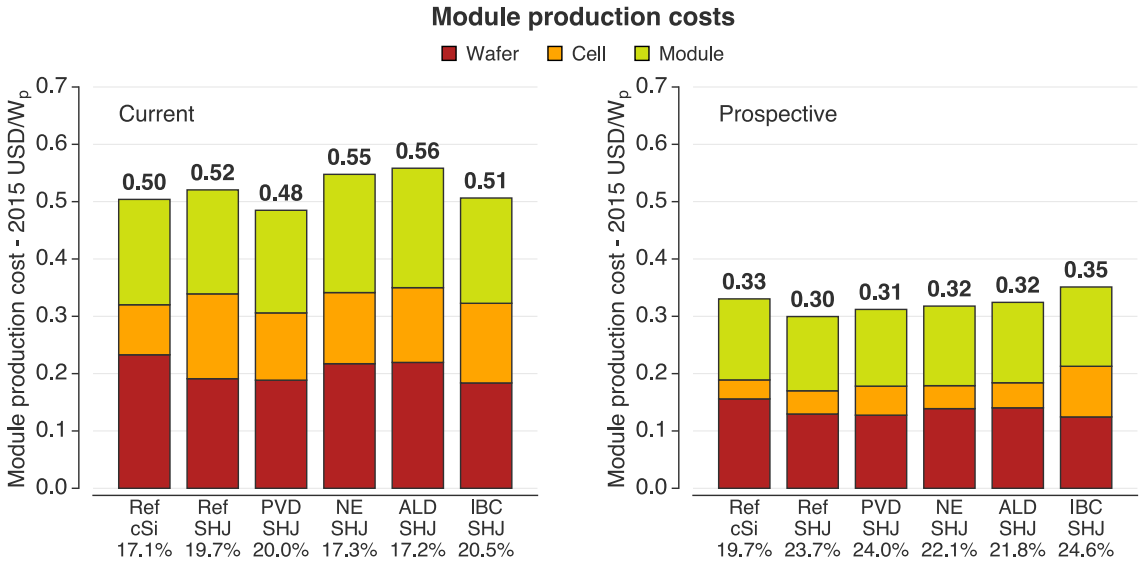

Figure 3.8 · Summary of total module cost for the monocrystalline silicon and SHJ designs. Totals are indicated in bold above the bars. A breakdown of cell costs is shown in Fig. 3.7. For a breakdown of the cost of module elements see Fig. 3.9. The percentages below the labels indicate module efficiencies.

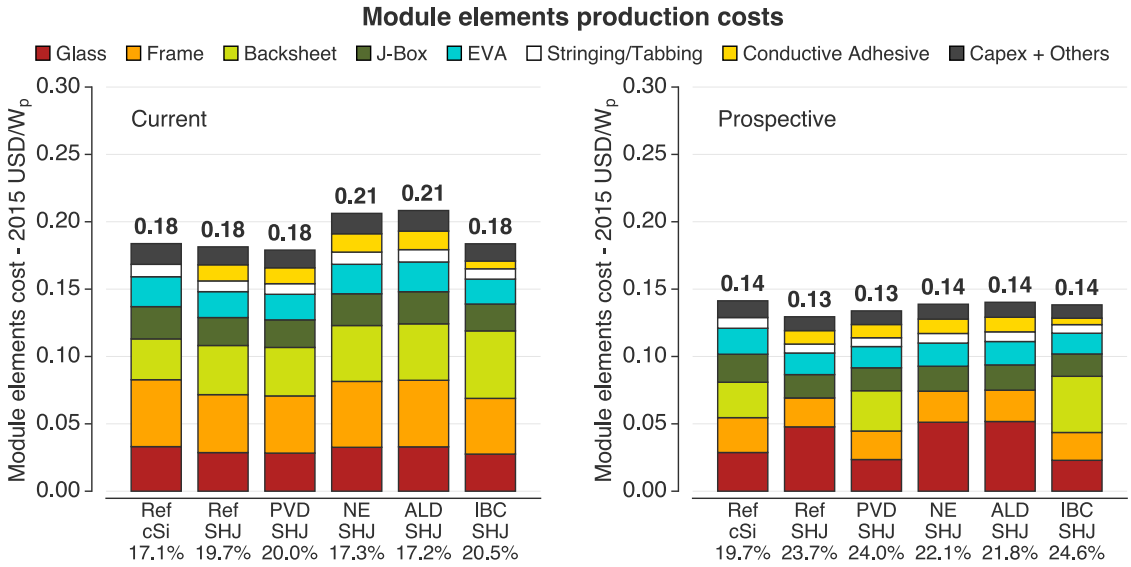

Figure 3.9 · Breakdown of the cost of module elements. Totals are indicated in bold above the bars. The percentages below the labels indicate module efficiencies.

3.5.2 From Current to Prospective Production Costs

In section 3.4 we identified several developments and pathways towards reduction of PV production costs. To summarize, these were: **1)** Increased cell and module efficiency for all designs **2)** Decreased cost of wafers due to higher silicon utilization (thin wafers, less kerf loss) **3)** Reduction of silver usage per cell followed by **4)** Substitution of silver with copper **5)** Replacement of ITO with ZnO, and **6)** Slight changes to the module frame.

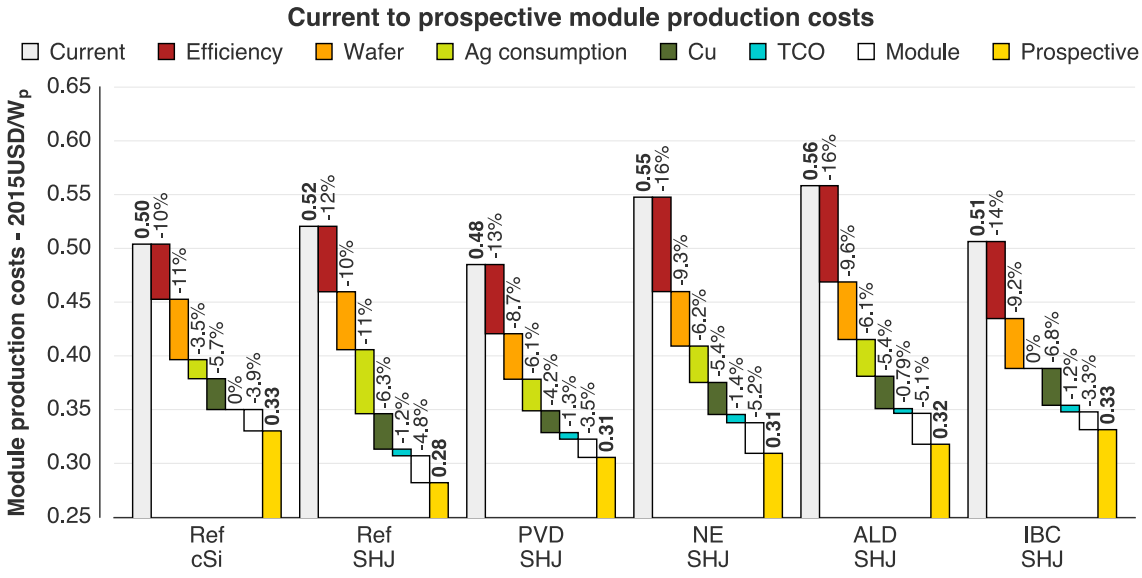

Figure 3.10 · Stepped bar chart showing the possible cost reductions achieved by changes in various parameters, from current to prospective designs.

Table 3.8 · Effect of design changes on module production costs

	effect,on production costs (USD/W_p)					
Improvement	**Ref-cSi**	**Ref-SHJ**	**PVD-SHJ**	**NE-SHJ**	**ALD-SHJ**	**IBC-SHJ**
Efficiency	-0.051	-0.060	-0.064	-0.088	-0.089	-0.071
- Increased Cell Efficiency	-0.048	-0.057	-0.060	-0.083	-0.084	-0.067
- Increased Cell to Module Power Ratio	-0.003	-0.003	-0.004	-0.005	-0.005	-0.004
Wafer	-0.056	-0.054	-0.042	-0.051	-0.054	-0.046
Metallization	-0.046	-0.093	-0.050	-0.064	-0.064	-0.034
- Ag paste reduction	-0.018	-0.060	-0.029	-0.034	-0.034	0.000
- Ag replacement with Cu	-0.029	-0.033	-0.020	-0.030	-0.030	-0.034
ITO replacement with ZnO	0.000	-0.010	-0.010	-0.008	-0.009	-0.010
Module Layout	-0.020	-0.025	-0.017	-0.028	-0.029	-0.017
- Frame cost reduction	-0.020	-0.017	-0.017	-0.020	-0.020	-0.017
- Bifacial module		-0.008		-0.009	-0.009	
Total	-0.174	-0.234	-0.182	-0.230	-0.235	-0.178

Figure 3.10 shows the effect of these changes on the five module designs studied here. Major cost reductions can be obtained by improved cell efficiency and lower wafer production costs. The increased efficiency of the prospective SHJ designs leads to a cost decrease of 12-16%, while this figure is 9.6% for the reference c-Si design. Higher silicon utilization due to thinner wafers, produced with less silicon kerf losses, allow for a reduction in cost of 9-10% for the SHJ designs (11% for c-Si). The reduction of silver consumption projected by the International Technology Roadmap for Photovoltaics [125], of about 60% in 2025, would allow for a cost reduction of 11% for the silver-heavy Ref-SHJ designs, and 6% for the remaining SHJ designs with screen printed Ag grids. Substitution of silver with copper-based metallization would allow for a further decrease of 4-7%. Silver use reduction (-4%) and substitution (-6%) would not decrease the production costs of the conventional c-Si module as much, as the contribution of metallization cost to overall costs is much lower (see Fig. 3.7). Replacement of TCO would allow for cost reduction of around 1%, while reduction in the amount of aluminium used for the module frame and a switch to bifacial modules where possible, would allow for a further cost reduction of 3-5% for all designs.

Combined, these developments result in a significant expected drop in cell production costs and total module costs. Cell processing costs drop by 62% for the Ref-cSi design, 73% for the Ref-SHJ design, 67-68% for the ALD-SHJ and NE-SHJ designs, 57% for the PVD-SHJ design, and 36% for the IBC-SHJ design. Total module costs drop by 34% for the c-Si module, 31% for the IBC-SHJ module and, 36-42%, for the other SHJ modules. As Figures 3.7 and 3.8 show, they would thus

allow for cell production cost of 0.19-0.23 USD/W_p and 0.21 USD/W_p for SHJ and c-Si cells respectively, and 0.30-0.35 USD/W_p and 0.33 USD/W_p for SHJ and c-Si modules, respectively.

The IBC module shows the least potential for cost reduction as its' prospective costs are hampered by the requirement for the structured backsheet, the high capex costs, and the high yield and throughput losses incurred by the complex processing sequence.

3.6 Sensitivity and Uncertainty

The cell and module production costs shown above rely heavily on a few major parameters: **1)** Uncertainty in cell and thus module efficiency; **2)** Historical variation in wafer cost; **3)** Variation in silver paste price and uncertainty in silver consumption per cell, and **4)** Uncertainty in prices of consumables. We performed a sensitivity and uncertainty analysis, to show the sensitivity of the overall results to changes in these parameters and to assess the effect of uncertainty in these parameters on the overall result. To analyse the sensitivity of the overall results to these parameters, we varied the parameters and plotted the resulting module costs in Fig. 3.12. For the uncertainty analysis, we performed a Monte Carlo simulation: random samples for each parameter were generated from a log-normal distribution, and the overall module cost was recalculated with these random samples. For instance, we generated 100,000 module efficiencies randomly from a log-normal distribution and recalculated module costs with these 100,000 samples. The resulting ranges of results are represented as box plots in Fig. 3.13 showing the distribution of obtained module costs.

Table 3.9 shows the parameters we investigated, the ranges over which we varied them, and the standard deviation we used to generate the random samples for the Monte Carlo simulations. The results of the sensitivity and uncertainty analysis are shown in Fig. 3.12 and Fig. 3.13 respectively.

3.6.1 Cell and Module Efficiency

As the novel SHJ designs studied here are still under development, accurate measurements of cell efficiency in mass production or even pilot production are not yet available. Furthermore, as shown in section 3.5.2 and Figure 3.10, a large fraction of prospective cost reductions relies on an assumed increase in cell and module efficiency. Recent development of varying designs show significant variation in SHJ cell efficiency [29].

Table 3.9 · Overview of parameter ranges studied in the sensitivity analysis (min-max range) and Monte Carlo simulation (σ)

Parameter		Ref c-Si	Ref-SHJ	PVD-SHJ	NE-SHJ	ALD-SHJ	IBC-SHJ
module efficiency	base	17.1%	19.7%	20.0%	17.3%	17.2%	20.5%
	min	16.2%	18.2%	17.9%	14.7%	14.5%	17.9%
	max	17.9%	21.2%	22.0%	20.0%	19.8%	23.1%
	σ^a	0.4%	0.8%	1.0%	1.4%	1.3%	1.3%
wafer price	base	1.03	1.03	1.03	1.03	1.03	1.03
	min	0.80	0.80	0.80	0.80	0.80	0.80
	max	2.00	2.00	2.00	2.00	2.00	2.00
	σ	0.128	0.255	0.255	0.255	0.255	0.255
ag paste price/consumption	base	100%	100%	100%	100%	100%	100%
	min	50%	50%	50%	50%	50%	50%
	max	200%	200%	200%	200%	200%	200%
	σ	0.128	0.255	0.255	0.255	0.255	0.255
consumable price/consumption	base	100%	100%	100%	100%	100%	100%
	min	50%	50%	50%	50%	50%	50%
	max	150%	150%	150%	150%	150%	150%
	σ	0.255	0.255	0.255	0.255	0.255	0.255

[a] the sigma (standard deviation) was calculated assuming the respective min-max ranges to be the lower and upper bounds of the 95% confidence interval

We assigned an efficiency range to each of the studied designs, assuming that the efficiency of the Ref-cSi design has the smallest uncertainty, being the most established cell design. For the SHJ designs, the range in efficiencies analysed is larger, especially for the conceptual NE-SHJ and ALD-SHJ designs. The ranges studied are shown in Table 3.9. These ranges were estimated roughly, based on the deviation of the designs' layout and processing cycle from that of the Ref-SHJ design.

As shown in Figure 3.12a, module cost is quite sensitive to changes in module efficiency. When we varied cell efficiency over the ranges described in Table 3.9, costs change with a factor of the inverse of the relative efficiency change. The figure clearly shows that the c-Si design has a pronounced processing cost advantage, that is offset only by strong efficiency increases in the PVD-SHJ and IBC-SHJ designs. The other SHJ designs need further efficiency improvements to approach Ref-cSi module costs. At similar efficiency, the SHJ would be more expensive compared to the c-Si module, due to the high cell and for the IBC design also module costs.

3.6.2 Wafer Cost

Wafer prices are strongly linked to polysilicon prices, which have shown to be quite volatile. Current (June 2015) spot prices for wafers are about 1.01 USD/wafer, with polysilicon prices at around 15.7 USD/kg [100]. After many silicon producers

shutting down the last 1.5 years due to an oversupply, prices were estimated to stabilize and rise slightly to a price of about 20-25 USD/kg [133]. More recently, polysilicon capacity was increased, leading to the possibility of another polysilicon oversupply situation with further price decreases. Polysilicon price is thus quite uncertain. Taking into account the price range of polysilicon for the last 5 years and possible further price decreases, we investigated the effect on the overall results of a wafer price in the range of 0.60 USD/wafer to 2.0 USD/wafer.

Figure 3.12b shows that all designs are quite sensitive to variation in wafer cost. The effect of changes in wafer cost is similar for all devices, although the effect is more pronounced as the module efficiency decreases, as the wafer cost contributes more to the overall costs at lower efficiencies. This is especially apparent in the results for the Ref-cSi module, and to a lesser degree for the ALD-SHJ and NE-SHJ modules.

3.6.3 Silver paste price and consumption

Another strong contributor to overall cell manufacturing cost is the price of silver paste used for metallization. As shown in Figure 3.11, silver prices are quite volatile, with prices ranging from about 500 USD/kg to over 1700 USD/kg over the last five years, with a current (Oct 2015) price of about 520 USD/kg. This silver price variation could account for very large increases in the cost of silver paste, to almost 1500 and 2000 USD/kg for high and low temperature paste, respectively.

Figure 3.11 · Silver price, and estimated high- and low temperature silver paste price from October 2005 to October 2015. Silver price data: [33, 134].

Because of the requirement for relatively large amounts of silver in low temperature paste, the SHJ designs are quite sensitive to changes in paste price or paste consumption per cell, especially the bifacial Ref-SHJ design. A doubling of the paste price would raise the production costs of this designs by up to 20%. The

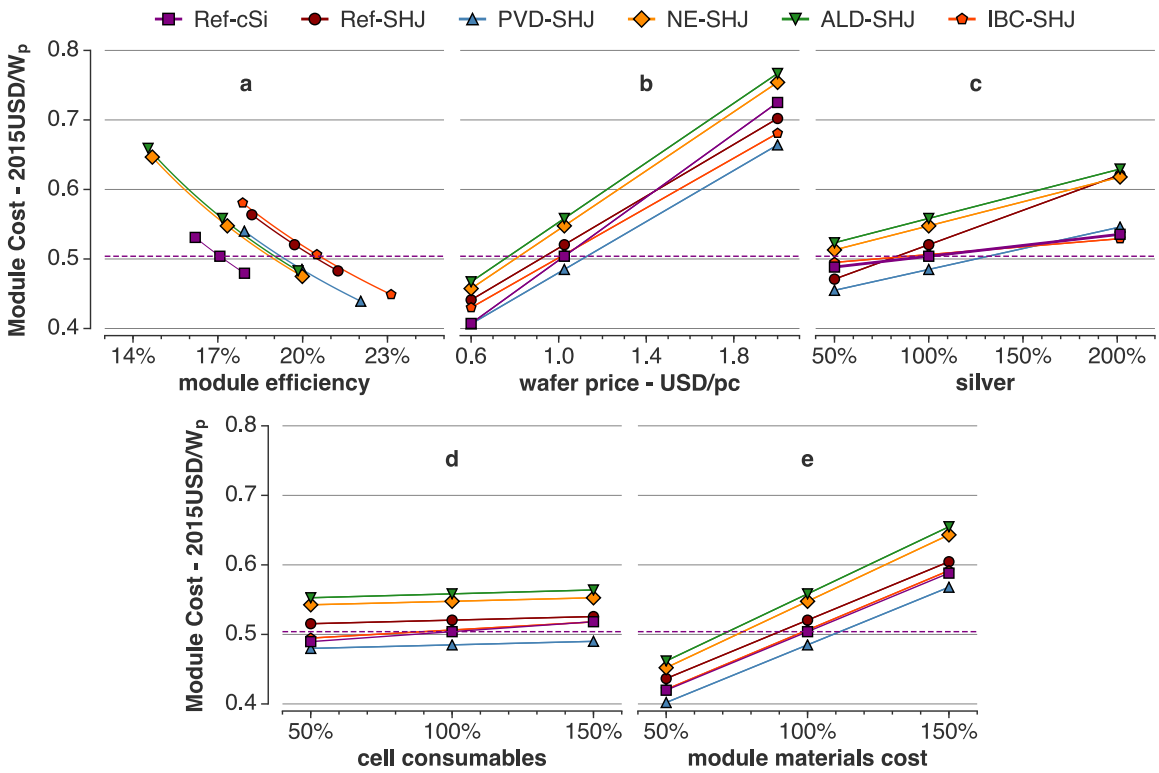

Figure 3.12 · Results of the sensitivity analysis. The graphs indicate the change in overall results as a function of change in module efficiency, wafer price, silver price or consumption and consumable price or consumption. The colored markers indicate the minimum, base and maximum results for each of the studied designs. Module efficiency was varied over a range we estimated. Wafer price and silver price was varied over a range reflecting these parameters' historical (5 year) variation. Consumable prices were varied over a range we assumed to account for most variation found on the market.

effect is not as strong for the c-Si design, as this design is based on cheaper, high temperature paste.

3.6.4 Other Consumable Prices

Price variation can of course occur not only for silver, but for all **other** material consumables that are required to produce the solar cells and modules. Therefore, we studied the effect of variation in the prices of cell consumables other than silver paste and wafers, and of module materials on the overall results. As seen in Fig 3.12d, the effect of changes in cell consumable prices is limited, as these consumables only account for around 2-5% of SHJ module prices and 9% of the Ref-cSi module. The results are however very sensitive to changes in the cost of module materials (see Fig. 3.12e, as they contribute around 30-40% of total module cost.

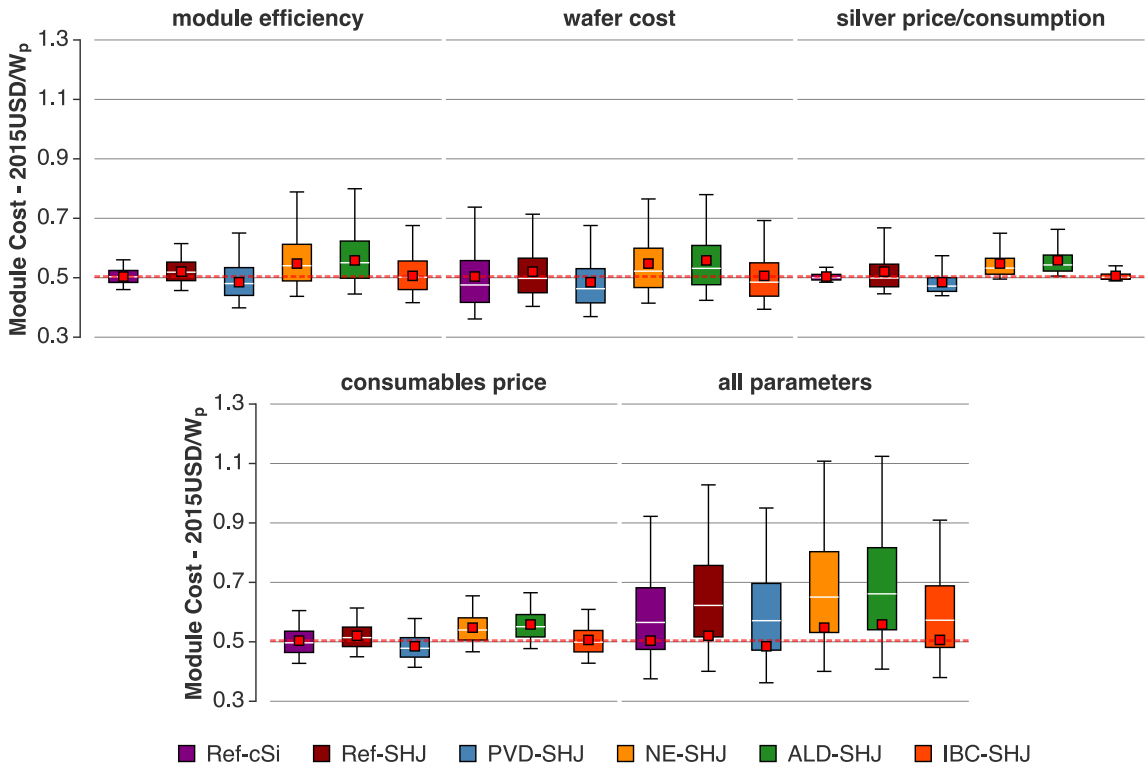

Figure 3.13 · Results of the Monte Carlo uncertainty analysis. The box plots indicate the range in overall results obtained when varying efficiency, wafer price, silver price or consumption and consumable price or consumption. The red squares and white lines indicate mean and median values respectively, while the boxes indicate 25th and 75th percentiles, and the whiskers indicate minimum and maximum values. The dashed red line indicates the main result for the Ref-cSi design.

3.6.5 Monte Carlo uncertainty

The results of the Monte Carlo simulation to assess the effect of uncertainty in the data is shown in Fig. 3.13. This figure shows the distribution of relative cost of the SHJ designs compared to the Ref-cSi design. This figure shows that especially uncertainty in module efficiencies can alter the results (absolute and relative) significantly. Uncertainty in the cost of wafers, silver, and other consumables also has a pronounced effect on module prices (as shown also in Fig 3.12b-e) but changes in these parameters would likely affect all designs similarly and thus not significantly changes the relative results.

3.7 Discussion and Conclusions

The main aim of this study is to perform a bottom-up analysis of the relative cost of different silicon heterojunction (SHJ) based PV modules, and to compare current and prospective costs of these modules with those of a conventional monocrystalline silicon module. The aim is to develop a methodology that allows for

ex-ante screening of R&D cell concepts. We performed a life cycle costing analysis to analyse in detail the cost structure of the production of PV modules, and found current SHJ modules to be comparable in price compared to conventional monocrystalline silicon modules, but cost penalties incurred by using more expensive materials need high efficiencies to be offset. Thus, especially designs that minimize the use of low temperature silver paste benefit from the efficiency advantage of heterojunction technology.

The life cycle costing (LCC) method shows its' usefulness in determining the contribution of each process and material input to the overall production cost of different cell and module designs. Our research has confirmed that for all designs investigated wafer and metallization contribute the majority of overall cell production costs, while for complete modules, the module materials are also a very significant cost factor. Reductions in wafer thickness, silver paste usage, or subsitution of silver with copper-based metallization allows for significant cost reductions. The strong effect of module efficiency on module price (USD/W_p) however shows that changes in cell and module design that have a negative effect on module efficiency will likely result in a relative cost increase. Futhermore, as Fig. 3.12a shows, the efficiency advantage of the studied SHJ designs is the main reason for there lower production costs (in terms of USD/W_p). This indicates that: **a)** the uncertainty in cell and module efficiency for the SHJ designs results in significant uncertainty of the overall result (see Fig 3.12 and 3.13). **b)** changes in cell processing that decrease cell efficiency are likely to result in cost increases, even if they reduce cell processing costs. **c)** accurate cost calculations for SHJ cell concepts should preferably rely on cell efficiency data from gathered from (pilot) production lines.

3.7.1 Wafer cost

To calculate the wafer production cost, we performed an LCC analysis of wafer production from silica to sawn wafers. Our model results for current wafers (1.03 USD/pc) results in slightly higher costs compared to the current wafer spot price (1.01 USD/pc) [100]. This likely is the result of the fact that the life-cycle data on silicon production we used for our calculations is already some years old (from 2007), although we have updated this as much as possible, as progress has been made especially in reducing the energy budget of silicon production. A different issue with our model is that we have used a single cost model for the wafer used, e.g. we have not distinguished between *n*-type and *p*-type wafers. It is sometimes assumed that *n*-type wafers are likely to be more expensive compared to *p*-type wafers because of lower yields, more complex processing and added capital expenses, however this has been disputed [33].

3.7.2 Metallization

In PV industry and research, it is common knowledge that metallization is a main contributor to PV module costs. R&D on alternative metallization schemes is therefore a very active field of research. The amount of silver used per wafer has already dropped significantly [114], a trend which is expected to continue. Our results indicate that a projected reduction in silver use per cell [114] could decrease the costs of the silver-based SHJ modules studied here by about 6% for most designs, but up to 11% for a design with high silver consumption. As conventional c-Si cells use cheaper silver paste, containing less silver, this cost reduction potential is smaller (-4%) for this technology.

Aside from material use reduction, replacement of silver with copper is also being heavily researched, mainly through research on copper-plating. Copper offers similar conductivity, at only a fraction ($\sim$2%) of the cost. Furthermore, the supply of copper is less constrained, although not impervious to price volatility. Our results show that silver substitution could decrease module cost by an additional 4-7% for SHJ modules, or 6% for c-Si modules. In our prospective designs, the contribution of metallization is already low, as we assume paste consumption per wafer to substantially decrease.

The adoption of copper in the manufacturing process is however not without issues: copper rapidly oxidizes during thermal curing, and can diffuse into the silicon cell substrate [77, 114, 128]. Recent results have however shown that contact curing can be performed with minimal oxidation in inert or low-oxygen curing atmospheres [77, 126], or in normal atmospheres using a specially developed paste [128]. Furthermore, the ITO layer applied in SHJ solar cells is stated to be an effective barrier to metal diffusion [135]. Especially copper-plated contacts however, in conjunction with a nickel seed layer and silver capping layer, show prospects for high efficiency SHJ solar cells [83].

An issue with our current model for metallization costs is the cost-structure of metallization pastes. There is limited information on the cost of these pastes, but the available data shows that these pastes are much more expensive than pure silver. This indicates that a significant fraction of metallization paste cost is non-silver related (460 and 580 USD/kg for high- and low temperature paste). For aluminium pastes, this does not seem to be the case, as these pastes are much cheaper ($\sim$50 USD/kg). It does however seem to indicate that the cost in front-side metallization paste (especially low temperature) cannot only be reduced by reducing the silver content or replacing silver with another metal. Alternative forms of metallization, such as SmartWire Connection Technology [136], inkjet or stencil printing or electroplating could possibly offer further metallization cost reductions.

3.7.3 ITO replacement

From a cost perspective, replacement of ITO has very limited benefits, as the total amount of indium needed for the thin transparent conductive oxides is very low. Alternative TCO's that are cheaper but less conductive, are likelier to increase the module cost due to decreased cell efficiency. As one of the options, we have also modelled replacement of ITO with ZnO, which offers a very modest cost decrease.

At current price levels (June 2015, 750 USD/kg), ITO contributes about 0.8-1.8% of cell costs and 0.5-1.1% of total module costs. As we have possibly overestimated the cost of ITO target material (see section 3.3.2), this contribution could be smaller. Thus, from a cost perspective, ITO replacement does not seem to be that important. At a 100% price increase for ITO, the contribution increases slightly to 1.0-2.2% of module costs. The development of alternative TCOs should however still be researched, as the availability of indium could become a concern [90, 91].

3.7.4 Module Design and Materials

Our results indicate that module materials already contribute a large fraction of overall module cost, and will likely contribute the majority of module costs as wafer and cell production become cheaper. Cost reduction possibilities in module design are likely limited, as the production of the materials used is already very mature, and there is thus limited possibility for technological learning. For current modules, main costs are glass, frame and backsheet. Prospective glass-glass modules can be somewhat cheaper compared to modules with an aluminium frame, because of the replacement of the backsheet with a sheet of glass. The cost of the glass on the backside of the prospective modules is likely overestimated, as lower quality glass can be applied here compared to the front-side. This could significantly lower the price of the backside of the module. Furthermore, the costs calculated here are based on monofacial efficiencies, and thus do not reflect the additional energy yield than can be obtained from bifacial PV modules.

3.7.5 Concluding Remarks

Our results show that silicon heterojunction (SHJ) technology offers the potential for cost reductions in PV manufacturing compared to conventional crystalline silicon solar cells and modules, especially for prospective PV modules. Heterojunction module production costs were found to range from 0.48-0.56 USD/W_p, compared to 0.50 USD/W_p for a conventional monocrystalline silicon module. Heterojunction modules incur a strong cost penalty because of the requirement for low temperature silver paste. High-efficiency SHJ designs that minimize the use of this

paste can be competitive with standard crystalline silicon PV modules. As the designs studied are conceptual, the validity of the results will strongly benefit from more accurate determination of the efficiency of SHJ cells and modules from large-scale production. Variation of material prices can also have a large influence on the cost of SHJ modules, but these variations will likely affect all designs similarly and thus not alter the relative results.

Our results confirm that the choice of metallization has a substantial impact on the cost of SHJ modules compared to conventional crystalline silicon modules. This is mainly due to the high cost of low temperature paste needed for SHJ cell processing, and the increased amount of paste required due to its lower as-cured conductivity. This results in higher cell costs for SHJ designs (USD/cell), that is offset partly by the high efficiency of heterojunction technology.

Our prospective analysis indicates that a reduction in paste consumption and replacement of silver with copper paste could alleviate this problem, e.g., the cost-advantage of SHJ cells becomes less dependent on the efficiency advantage. However, these results are based on the assumption that progress in reduction of silver consumption is also applicable to SHJ cells. A more promising approach seems to be the replacement of screen printed silver grids with copper-electroplated contact, minimizing the amount of silver used in SHJ cells. For all studied prospective modules, the module materials contribute significantly more to the overall module cost than they do now.

Interdigitated back-contacted (IBC) design are often mentioned as a promising low-cost (future) module technology. Our results however show that for now, the requirements for this technology during cell processing and module production cannot be completely offset by the large efficiency advantage obtained through the improved cell structure.

As the prospective cost reductions that we have modelled are very dependent on reductions and eventual elimination of silver use in SHJ cells, further research should keep addressing these issues, by establishing a metallization process based on copper that is compatible with industrial scale production without adding complexity to the production process. Furthermore, increasing attention should go towards reducing the cost of module elements.

Acknowledgements

This work was performed within “FLASH”, a *Perspectief* programme funded by Technology Foundation STW (www.stw.nl/en) under project number 12172. The authors would like to thank the reviewers for their very detailed and helpful comments, as they feel these comments strongly contributed to the quality of the paper.

4

Comprehensive characterisation and analysis of PV module performance under real operating conditions

Published in: Prog. Photovolt. Res. Appl. (2016)
doi: 10.1002/pip.2848

Abstract The specifications of PV modules show performance under standard testing conditions (STC), but only limited information relating to performance at non-STC conditions. While performance is affected by irradiance, temperature, spectral composition of irradiance, angle-of-incidence of the irradiance, and other parameters, specifications only partly give detail to consumers or retailers about the effect of irradiance and temperature.

In this study, we characterise and analyse the performance of eight different, commercially available PV modules. We establish the effect of four different parameters on module performance: irradiance, temperature, spectral composition of irradiance (via the parameter average photon energy), and angle-of-incidence, by performing linear and nonlinear optimisation of physical or empirical models. Furthermore, we characterise the operating conditions, and analyse the seasonal and annual development and contribution of the four parameters to energy losses or gains relative to STC operating conditions. We show a comprehensive way of presenting the deviation of performance from STC, combining the variation in operating conditions and the resulting variation in performance.

Our results show that some effects on performance are attributable to the semiconductor material used in the modules (spectral composition and temperature) while especially angle-of-incidence effects seem more related to the type of glass used on as the front cover of the module. Variation in irradiance and module temperature generally affect performance the strongest, resulting in a performance effect ranging from +2.8% to -3.2% and -0.5% to -2.2%, respectively. The combined effect of all parameters results in an annual yield deviation ranging from +1.2% to -5.9%.

4.1 Introduction

The current market for photovoltaic modules is quite homogeneous, with 90% of the market consisting of conventional, diffused junction mono- and polycrystalline silicon modules [19]. More advanced types of PV modules are only gradually entering the market, but are expected to gain larger market shares in the medium to long term future. One of those alternative module types is the silicon heterojunction module, currently produced mainly by Panasonic (since their acquisition of Sanyo) as the Heterojunction with Intrinsic Thin-layer (HIT™; [137]) module. Other alternative PV modules include those based on thin-film amorphous silicon (a-Si), cadmium telluride (CdTe), copper indium gallium selenide (CIGS) and copper indium selenide (CIS), and on the longer term, perovskites. This variety of available module types means that selecting the right module type for the right location becomes more complex, as the optimal balance between module cost and energy yield determine the best business case, among other parameters.

The specifications of PV modules commonly show performance under standard testing conditions (STC), which are: irradiance of 1000 W/m^2, spectral composition of light conforming to an airmass of 1.5 and a module temperature of 25°C [138]. Testing at these conditions results in a measurement of the rated power output or watt-peak power of the PV module. Additionally, specification sheets report some performance parameters at non-STC conditions: the nominal operating cell temperature (NOCT), the temperature coefficient of power, current and voltage, and sometimes the performance of the module as a function of light intensity as well. Although these specifications thus accurately describe the performance of the module under STC conditions, and give some information on the effect of variations in some parameters, they do not offer much insight in the energy yield of the modules under realistic, outdoor conditions. Furthermore, the effect of other parameters on module performance, like spectral variation, angle-of-incidence and effect of increased relative amounts of diffuse irradiance, is not described by these specifications.

In this study we compare the performance of eight different PV module technologies, and aim to establish the effect of four different parameters on PV module performance for all eight PV modules, namely irradiance intensity, module temperature, average photon energy (APE; [139]), angle-of-incidence and the ratio of direct to total irradiance. Furthermore, we characterise the operating conditions under which the PV modules operate for our test-facility in Utrecht, the Netherlands, to show the effect of deviation from STC conditions on the performance of the PV modules, and the annual energy yield compared to a reference yield that can be calculated based on the rated watt-peak power output and annual insola-

tion. We analyse the performance as a function of each parameter by filtering data around STC conditions and varying only the parameter investigated. The data was obtained over a period of approximately 1.5 years of continuous measurements between July 2014 and January 2016.

With this study we aim to characterise the operating conditions at a North-Western European location and compare the performance of a variety of PV module technologies under these conditions. We propose a general method that can be used to characterise PV modules under realistic operating conditions, not restricted to location. The resulting method should allow for a more accurate determination of which type of PV module is most suited for the respective installation location.

4.2 Methods

4.2.1 Test system and data acquisition

The measurements for this study were performed at the campus of Utrecht University, Utrecht, the Netherlands, with the Utrecht Photovoltaic Outdoor Test facility (UPOT) described in [140]. The test facility is located at the top of an eight storey building, at a height of about 36 meters, at a longitude of 5.2°E and latitude of 52.1°N. The facility operates year round, 24 hours per day, performing measurements on a set of PV modules, with a variety of irradiance and atmospheric sensors. Measurements of PV module performance is performed at in-plane irradiance values above 50 W/m^2.

PV modules

The test facility is equipped with 23 different modules, of a variety of PV technologies. Commercial modules of technologies like mono- and poly-crystalline PV modules are installed, including one pair of the same n-type mono-crystalline silicon modules. Thin film technologies are represented in the form of amorphous silicon (a-Si/a-Si tandem), cadmium telluride (CdTe), and copper indium (gallium) selenide (CI(G)S). Also, a pair of the same silicon heterojunction (SHJ) modules is installed. Table 4.1 below gives a description of the main STC parameters of all the modules observed. All modules are installed on a frame of roughly 12 by 3.6 meters that is tilted by 37° with respect to the horizontal plane. From the PV modules, we measure current-voltage (IV) curves at time intervals of 2 minutes, with an Eko Instruments MP160 IV Curve tracer [141]. In between IV curve measurements the modules are kept at MPP by module-level power optimizers. Combined with the measurement of the IV curve, back-of-module (BOM) temperature is obtained by measurement with a thermo-couple sensor fixed to the back of each PV module,

and an irradiance measurement is taken from an Eko Instruments pyranometer installed in the plane of the PV modules.

Table 4.1 · Overview of the modules installed at the Utrecht Photovoltaic Outdoor Test facility. Data taken from the module specification sheets.

Parameter	H1	M1	P1	P2	A1	CT1	CG1	CS1
Type	SHJ	mono	poly	poly	a-Si/a-Si tandem	CdTe	CIGS	CIS
Area (m^2)	1.39	1.63	1.58	1.64	1.45	0.72	1.07	1.09
Rated Power P_{mpp} (W)	245	265	225	240	100	77.5	110	120
Current at rated power I_{mpp} (A)	7.14	8.55	7.69	8.03	5.71	1.61	5.61	2.79
Voltage at rated power V_{mpp} (V)	34.4	31.0	29.7	29.9	17.5	48.3	19.6	43.1
Short-circuit current I_{sc} (A)	7.73	8.93	8.25	8.47	6.79	1.84	6.70	3.18
Open-circuit voltage V_{oc} (V)	42.7	39.0	37.1	37.0	23.8	60.7	25.1	59.7
I_{sc} temperature coefficient α (%/K)	0.03	0.04	0.04	0.05	0.08	0.04	0.00	0.00
V_{oc} temperature coefficient β (%/K)	-0.25	-0.33	-0.36	-0.32	-0.33	-0.24	-0.36	-0.37
P_{mpp} temperature coefficient γ (%/K)	-0.30	-0.42	-0.43	-0.41	-0.20	-0.25	-0.45	-0.39

Table 4.2 · Overview of ranges used to filter data for investigation of the effect of different parameters on PV module performance.

Parameter investigated	Irradiance (W/m^2)	Temperature (°C)	APE[a] (eV)	AOI (°)	Clear-sky Index
Irradiance (W/m^2)		20.5-29.5	1.848-1.904	0-57	
Temperature (°C)	950-1050		1.848-1.904	0-57	0.9-1.1
APE (eV)	950-1050	7.5-42.5		0-57	manual[b]
AOI (°)	950-1050	20.5-29.5	1.848-1.904		manual[b]

[a] APE was determined from spectra that were measured in the wavelength range from 350 to 1050 nm

[b] For analysis of effect of APE and AOI we manually selected measurements from clear sky days. See section 4.2.3 for a discussion

Sensors

Aside from the module measurements, UPOT gathers data with a variety of sensors. In-plane we measure irradiance with three pyranometers, the measurements of which are used for cross-validation. Also, solar spectral irradiance is measured with a spectroradiometer that measures spectral irradiance in the wavelength range of 350-1050 nm. On the horizontal plane, another pyranometer is installed for measurements of global horizontal irradiance, and a sun tracker with pyrheliometer and pyranometer with shading assembly is installed for measurement of direct and diffuse irradiance. Aside from the irradiance sensors, a weather station is installed that measures ambient temperature, precipitation type and intensity, relative humidity and wind-speed and direction. A more detailed description of the measurement system is given in [140].

Data acquisition, filtering and analysis

The data from the different sensors is obtained at different frequencies. Weather and irradiance data and spectral data is measured at 30 second intervals. An IV curve is measured for all 23 installed PV modules in a series of measurements that starts every 2 minutes.

The data is processed in LabView software [142] and subsequently stored in a MySQL database. During the processing in LabView and before insertion in the MySQL database, several filtering steps are performed to flag PV measurements that do not fulfil several quality criteria: **1)** stable irradiance during the measurement is ensured by checking irradiance before and after the measurement of an IV curve and flagging measurements with a deviation of more than 5%; **2)** some snowy days have manually been flagged, since the partial snow cover causes irregular I-V curves, and/or incorrect irradiance measurements if the snow covers the pyranometers, and full snow cover of either pyranometers or PV modules also causes incorrect measurements.

In this study we analyse the effect of different operation parameters on PV module performance. We do this by taking the complete dataset measured over the period of July 2014 through December 2015, and filtering the data to investigate the effect of each parameter separately. For each parameter, we apply a filter that restricts the values of all other parameters to around their STC values. Hence, we filter data for irradiance, temperature, spectral irradiance, angle-of-incidence and clear-sky index[1]. The range of each filter parameter is shown in Table 4.2. To describe the performance effect of each parameter, we perform a fit of the selected data to a model (physical or general) that will describe the performance of the PV module as a function of the investigated parameter. We have used the Python programming language in conjunction with the *SciPy curve_fit* module [143] to process the data. The *curve_fit* module performs least-squares fitting of data using the *Levenberg-Marquardt* algorithm. The models used for fitting the different parameters, and our model optimisation approach are detailed below.

4.2.2 Model optimisation with second iteration

The filter ranges discussed above and shown in Table 4.2 were chosen to limit the variation to values around STC, except for the parameter currently investigated. However, in some cases, the filter ranges need to be broadened. For instance, for the analysis of angle-of-incidence effects, filtering of irradiance and APE around STC values would exclude most of the angle-of-incidence measurements greater than

[1] Clear-sky index is calculated here as the ratio between measured direct normal irradiance (DNI) and modelled clear-sky DNI

15°. As a result of these broadened filter ranges, the effect of irradiance and APE could be reflected in the data – and resulting model fits – for angle-of-incidence. Furthermore, even with datasets filtered more closely around STC, the effect of variations in the filtered parameters could still be present in the data and thus affect the resulting model fits. To account for this problem, we perform a second iteration of the model fitting, by correcting the raw data with the models obtained in the first model fit iteration. For example, for angle-of-incidence, we correct the data using the models obtained for irradiance, temperature and APE, and perform a second model fit using this correct data. We assess the change in the quality of the fit by comparing the root-mean-square error of the model fit before and after the model optimisation.

4.2.3 Main performance functions

In this study we analyse the effect of deviations from STC in terms of irradiance, module temperature, spectral composition of irradiance, and angle-of-incidence. Although module performance is also affected by module stability [144], especially amorphous silicon modules [145–147], and there is some evidence of module stability fluctuations in our dataset for a limited number of modules, we neglect this effect in our study, as we assume the amplitude of the effect of stability variation at our test site to be limited because the devices have been light-exposed for more than one year before the start of the dataset, and the effect of thermal annealing is likely limited at Northern-European locations [147, 148].

We have fitted the datasets to models describing the PV module performance. From here on we define performance as the instantaneous performance ratio *PR* or relative-to-STC power P_{rel}:

$$PR = P_{\mathrm{rel}} = \frac{mP_{\mathrm{mpp}}}{P_{\mathrm{STC}}} \cdot \frac{1000\ \mathrm{W/m^2}}{G_{\mathrm{poa}}} \tag{4.1}$$

where mP_{mpp} and P_{STC} are the measured and STC rated maximum power, respectively, and G_{poa} is the in-plane irradiance.

For irradiance and temperature, we have used physical models for fitting the data, however, in the case of spectral composition and angle-of-incidence we have used polynomial models based on the approach in [149]. In the following sections we discuss the models used and their background. The effect of irradiance, temperature, APE and angle-of-incidence is described by the factors f_{irr}, f_{temp}, f_{APE}, and f_{aoi} respectively. These factors are detailed in the sections below.

Irradiance

The effect of irradiance on the power output of PV modules is almost linear, and is very reasonably approximated by the function:

$$P_{\text{mpp}} = G_{\text{poa}} \cdot \frac{P_{\text{stc}}}{1000\ \text{W/m}^2} \tag{4.2}$$

The short-circuit current increases linearly with irradiance, but in the one diode model for an ideal solar cell without shunt or series resistances, the open-circuit voltage (V_{oc}) increases logarithmically with irradiance:

$$V_{\text{oc}} = \frac{kT}{q} \ln\left(\frac{I_{\text{sc}}}{I_0} + 1\right) \tag{4.3}$$

where k is the Boltzmann constant, T the temperature, q the elementary charge, I_{SC} the short-circuit or light-generated current and I_0 the diode or dark saturation current. As irradiance decreases, I_{sc} decreases linearly, and the efficiency of the PV modules thus becomes lower due to the decrease of V_{oc} with I_{sc}.

The efficiency as a function of light intensity is also affected by the shunt (R_{sh}) and series R_{s}) resistance in the solar cells and the PV module. As shown in the two-diode model [150], efficiency decreases at high light intensity because of the effect of series resistance, and decreases at low light intensity due to the effect of shunt resistance:

$$\begin{aligned} I = I_{\text{SC}} &- I_{0_1}\left(\exp\left(\frac{V + IR_{\text{s}}}{kT}\right) - 1\right) \\ &- I_{0_2}\left(\exp\left(\frac{V + IR_{\text{s}}}{2kT}\right) - 1\right) \\ &- \frac{V + IR_{\text{s}}}{R_{\text{sh}}} \end{aligned} \tag{4.4}$$

where I_{0_1} and I_{0_2} are the diode saturation currents for the two diodes. In practical operating conditions the combined effect of V_{oc}, R_{s} and R_{sh} on module output power means that in most cases, the relation between irradiance and power is linear, but at low light (below 200-300 W/m^2), the P_{mp} deviates from this linear relation [151, 152]. Various models exist to describe this behaviour, here we follow the example of Dirnberger *et al.* [153] by using the model from Heydenrich *et al.* [154] as it was found to accurately describe low-light behaviour of the PV modules considered here [153]:

$$f_{\text{irr}} = PR(G) = aG + b\ln(G+1) + c\left(\frac{\ln^2(G+e)}{G+1} - 1\right) \tag{4.5}$$

where f_{irr} is a factor describing the change in *PR* as a function of irradiance, a, b, and c are empirical parameters that describe the low-light behaviour of the PV modules, and e is Euler's number. We have adjusted the model to fit performance ratio *PR* as a function of irradiance, instead of efficiency. To analyse the effect of irradiance on *PR* and energy yield, and establish these parameters, we have selected measurements from our dataset with a BOM temperature within 4.5°C from STC (25°C), an APE between 1.848 eV and 1.904 eV, and an angle-of-incidence below 57°, which was found to be a "critical" angle for angle-of-incidence effects [155]. As mentioned before, we aim to filter data around STC conditions, and vary only the investigated parameter. To obtain a full range of irradiance measurements between 0 and 1500 W/m^2 however, we need to include measurements at high diffusivity. Therefore, we have not used clear sky index as a filter parameter in this case.

Temperature

Another parameter influencing the performance of PV modules is temperature. As the temperature of PV cells increases, the open-circuit voltage decreases due to temperature dependence of the dark saturation current I_0, as is shown in this derivation of the single diode equation (see eqn 4.3) for an ideal diode: As I_0 is a function of the intrinsic carrier concentration, which in turn is a function of temperature, it can be expressed as:

$$I_0 = CT^3 \exp\left(-\frac{E_{g0}}{kT}\right) \tag{4.6}$$

where C is a temperature-independent constant, and E_{g0} is the band gap of the material, extrapolated to absolute zero temperature. As can be seen in the equations (4.3) and (4.6), the term T in the exponent of equation (4.6) makes that the temperature dependence of I_0 has more effect on V_{oc} than the term T outside of the natural logarithm in equation (4.3) and thus the result is a negative dependence of V_{oc} on temperature. Also shown in (4.3) is that the temperature dependence of a PV module is as related to the band gap of the used material. Generally speaking, the effect of temperature on PV module performance decreases with the band gap of the material. High band gap technologies, such as a-Si and CdTe thus have lower specified temperature coefficients than crystalline silicon and CI(G)S PV modules.

We have in this study assumed a linear relation between temperature and performance:

$$f_{\text{temp}} = PR(T) = 1 + (T_{\text{BOM}} - 25) \times \gamma_{P\text{rel}} \tag{4.7}$$

where f_{temp} is a factor describing the change in PR as a function of temperature, T_{BOM} is the back-of-module temperature, and $\gamma_{P\text{rel}}$ is the STC temperature coefficient of P_{rel} (which is equal to the temperature coefficient of P_{mpp}). As shown in Table 4.2, we have selected data from an irradiance range from 950-1050 W/m^2, with a clear sky index between 0.9 and 1.1 and APE within 1% of STC. The used fit model thus corrects power for irradiance assuming them to be linearly proportional in the considered irradiance range.

Spectrally distributed irradiance

The STC conditions at which PV modules are rated also prescribe the spectral composition of the light source used to determine STC power output of the module. The spectral distribution should conform to the AM 1.5G standard solar spectrum as defined by IEC 60904-3 ed. 2 [41]. For the wavelength range of the spectroradiometer used in this study (350-1050 nm), the AM1.5 average photon energy (APE) is 1.876 eV. The effect of spectral variation on PV device performance is a result of multiple factors: **1)** the band gap of the material used for the PV module determines a minimum photon energy that can generate free carriers in the PV cells, **2)** above this threshold, the absorption of and carrier generation by photons varies as a function of their wavelength. **3)** the energy in photons above the band gap threshold is not converted into current but rather dissipated as heat in the PV cells.

The effect of these parameters is reflected in Figure 4.1, which shows examples of the internal quantum efficiency (IQE) and spectral response (SR) of various types of PV modules. The IQE shows the relative amount of carriers generated for each photon wavelength (energy). The spectral response shows the resulting current generated per watt of irradiance at each photon wavelength. The spectral response is calculated by multiplying the IQE with the ratio of the band gap to the photon energy. Spectral shifts towards the red region of the spectrum (low photon energy, large wavelength) usually result in lower generated current, as more photons are below the band gap threshold, and thus the IQE and SR are lower. The effect of spectral variation on PV device performance is thus most pronounced for technologies with a narrow spectral response, such as CdTe and a-Si. Especially for a-Si, there is much evidence in the literature of this effect [144, 158–164]. As two-dimensional data, the measured spectra are an inconvenient way to

present the effect of spectral variation on PV performance. Therefore researchers often analyse the performance of PV as a function of a one-dimensional parameter representing the spectra. Examples are the useful fraction (UF) [165–167], the spectral factor (SF) or spectral mismatch factor (MMF) [144, 158, 159, 168] and the average photon energy (APE) [139, 168, 169]. The useful fraction, spectral factor and spectral mismatch factor require that a researcher knows the spectral response of the PV module under study. This data is not available publicly for commercial PV modules. In contrast, the average photon energy is an external parameter, as it represents the average energy of an incoming photon. It is calculated as:

$$APE = \frac{\int_a^b E(\lambda)d\lambda}{q\int_a^b \varphi(\lambda)d\lambda} \tag{4.8}$$

where $E(\lambda)$ is the photon energy, $\varphi(\lambda)$ is the photon flux at wavelength λ, and a and b are the limits of integration, which are 350 and 1050 nm for the spectroradiometer used in this analysis. A number of studies have confirmed the applicability of APE as an indicator of unique spectra [170–174]. The APE varies both on a daily and seasonal basis, due to increased airmass at sunrise and sunset compared to noon, and in winter compared to summer. For instance, before sunrise and after sunset, as there is only diffuse light from the atmosphere, the spectral irradiance is blue-shifted, and APE is high. When the sun is close to the horizon, the light is red-shifted, and APE is low. During the day APE increases again to a maximum around noon. As the sun has a lower zenith at noon in winter compared to summer, the APE is lower in winter compared to summer months. Furthermore parameters like cloud cover, atmospheric water and aerosol content affect APE by absorption and

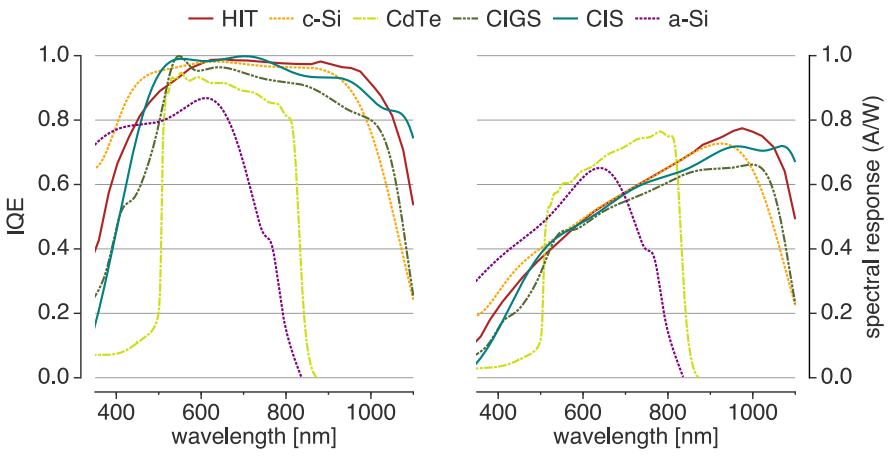

Figure 4.1 · Illustrative example of the internal quantum efficiency (IQE) and spectral response (SR) of six different PV cell technologies. Data courtesy of [156] and [157].

scattering of solar insolation.

For limited ranges of APE values, and for some PV module types the effect of APE on performance seems to be linear. However, considering a full range of APE measurements, the relation is non-linear. Here, we have used the approach described by [149] for airmass and angle-of-incidence effects, which is to use an empirical polynomial model to fit the data. As variations in the spectrum affect the power output indirectly, but current generation directly, we have analysed performance in terms of the normalised short-circuit current, nI_{SC}:

$$nI_{\text{sc}} = \frac{mI_{\text{sc}} \cdot (1 + a_{I_{\text{sc}}} \cdot (T_{\text{BOM}} - 25))^{-1}}{G_{\text{poa}} \cdot (G_{\text{STC}})^{-1} \cdot rI_{\text{sc}}} \tag{4.9}$$

where mI_{sc} and rI_{sc} are the measured and STC rated short-circuit current, and $a_{I_{\text{sc}}}$ is the temperature coefficient of short-circuit current. As shown in this equation, we use the module specifications to correct the measured short-circuit current for temperature, as the temperature coefficients obtained with the analysis of section 4.2.3 refer to those for module power and thus cannot be used to correct the data for measured short-circuit current. We fitted data for the performance ratio of the short-circuit current to a polynomial model:

$$\begin{aligned} f_{\text{APE}} &= PR(APE) = \\ &a_0 + a_1 \cdot APE + a_2 \cdot APE^2 \\ &+ a_3 \cdot APE^3 + a_4 \cdot APE^4 + a_5 \cdot APE^5 \end{aligned} \tag{4.10}$$

where f_{APE} is a factor describing the change in PR as a function of APE, a_n are a set of empirical parameters, APE is the measured APE value, and f_{APE} is the relative effect on performance.

Angle-of-incidence

STC power ratings of PV modules are performed with a beam of light that is perpendicular to the PV modules surface. As a consequence of the (apparent) movement of the sun across the Earth's sky, the sun's light hits the PV modules at different angles throughout the day, as solar zenith and azimuth change. Because of the Earth's inclination, there is also a strong seasonal variation in the course of zenith and azimuth throughout the day. Combining the solar zenith, azimuth, and the slope and orientation of the PV module, we can calculate the angle-of-incidence between the beam component of solar irradiance and the PV module surface. In Twidell and Weir [175], it is defined as :

$$\cos\theta = \cos\theta_z \cdot \cos\beta + \sin\theta_z \cdot \sin\beta \cdot \cos(\varphi_s - \varphi) \tag{4.11}$$

where θ is the angle-of-incidence, θ_z is the solar zenith, β is the PV module slope, φ_s is the solar azimuth, and φ is the orientation of the PV modules (by definition $\varphi = 0$ for a panel oriented to the south in the northern hemisphere).

A higher angle-of-incidence results in a decrease of light coupled into the PV cells [155, 176–178]. To analyse the effect of angle-of-incidence on the performance of the PV modules we have fitted a polynomial model from [149] to the data:

$$\begin{aligned} f_{AOI} = PR(AOI) = \\ a_0 + a_1 \cdot AOI + a_2 \cdot AOI^2 \\ + a_3 \cdot AOI^3 + a_4 \cdot AOI^4 + a_5 \cdot AOI^5 \end{aligned} \tag{4.12}$$

where f_{AOI} is is a factor describing the change in PR as a function of angle-of-incidence, a_n are a set of empirical parameters, and AOI is the angle-of-incidence. The filter ranges were adjusted to allow for a larger range of APE values and lower irradiance measurements, as STC values for irradiance and APE are generally only measured at very low angles-of-incidence. Previous research suggests a strong decline in performance at high angles-of-incidence [179–181], mainly (after correcting for irradiance) because of increased reflectance at high angles-of-incidence [180].

4.2.4 Seasonal and annual effect of parameters

The fit models obtained are used to calculate the effect of each parameter on module performance, for all the measurements in the complete dataset and for the complete period. This allows us to track the effects over time, and to analyse the contribution of each parameter to seasonal and annual energy yield.

To combine both the variation in operating conditions, and the effect of these variations on PV performance, we analyse and plot the performance deviation as a function of the percentile of data measured for each parameter. This allows us to visualise, for instance, that although the effect of temperature on performance is very pronounced, the resulting variation in performance, taking into account a full year of module temperature variation, is low, as the majority of measurements have temperatures around STC values, much lower than NOCT, because of an exceptionally large amount of low-irradiance measurements (see section 4.3 and Fig. 4.2).

The calculated parameter effects also allow us to show the seasonal variation of performance as a result of the variation in operating conditions. We aggregate this data per four weeks, and use weighting so the graphs show the effect on energy yield. For irradiance, temperature and APE we use in-plane irradiance for

weighting, for angle-of-incidence we use direct irradiance (as we have many measurements with high levels of diffuse irradiance). We also analyse the effect on an annual basis in a similar way, but aggregating all data for one year.

4.3 Characterisation of operating conditions

Figures 4.2 and 4.3 show the characterisation of weather conditions at the Utrecht Photovoltaic Outdoor Test facility (UPOT). Data for irradiance, average photon energy, ambient and module temperature and angle-of-incidence show that realistic operating conditions for a North-Western European location hardly ever agree with standard testing conditions (STC), especially for irradiance and angle-of-incidence.

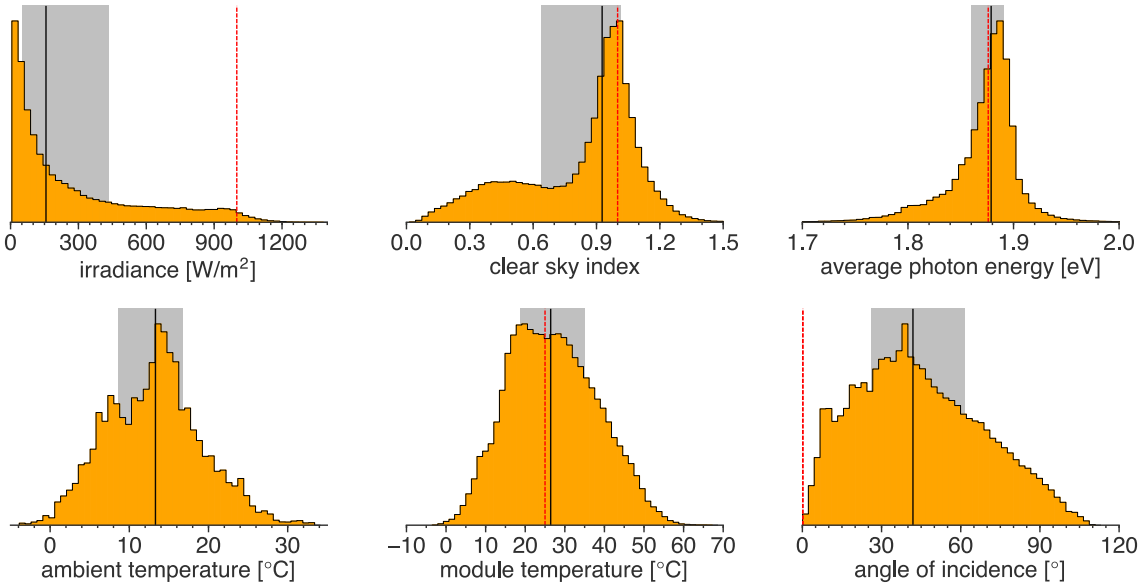

Figure 4.2 · Distribution of irradiance, clear sky index (CSI), average photon energy (APE), ambient temperature, module temperature (back-of-module temperature T_{BOM}), and angle-of-incidence (AOI) at the Utrecht Photovoltaic Outdoor Test facility (UPOT) in Utrecht, the Netherlands, for the year 2015. The y-axis shows the relative probability of occurrence. CSI, APE, were weighted by irradiance, T_{BOM} by module power, and AOI by direct irradiance. Dashed red lines indicate STC. Shaded areas indicate the interquartile ranges, the solid black lines the medians.

In our location, module temperature is almost normally distributed around STC (25 °C), although the variance is quite large. This is striking as the nominal operating temperature is between 40-50 °C for the studied modules. However, our location is characterised by large amounts of low irradiance measurements, well below the 800 W/m^2 at which NOCT is established, with concurrently low operating temperatures. The distribution of average photon energy (APE) is more or less around STC, but with very long tails, especially on the lower side. Almost no measurements have an STC angle-of-incidence, and almost 98% of measurements have an irradiance lower than 1000 W/m^2. The development of insolation, mean

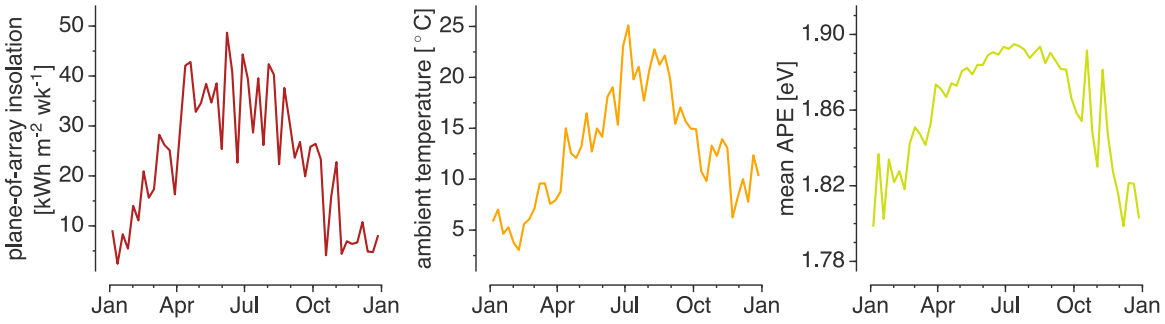

Figure 4.3 · Weekly insolation (H_{poa}), mean temperature (T_{ambient}) and mean average photon energy (APE) at the Utrecht Photovoltaic Outdoor Test facility (UPOT) in Utrecht, the Netherlands, for the year 2015. Ambient temperature and APE where weighted by irradiance.

air temperature and mean APE is shown in Fig. 4.3. This figure shows that there is a very strong seasonal variation of all three parameters. It shows that only a small portion of the APE measurements are around STC.

These results indicate that for the location investigated, practically all measurements deviate significantly from STC, and as a result, the performance of PV modules could very well be significantly affected, especially on a seasonal basis. In the following sections we investigate the effect of variation in irradiance, APE, module temperature and angle-of-incidence on the performance of different types of PV modules.

4.4 Model fit quality

Table 4.3 shows the results of the initial model fits, and the model optimisation, which corrects the initial fit for each parameter, with the fit models from the other parameters (see section 4.2.2). The table shows the root-mean-square error (RMSE) of the data to the models, for each module separately. The largest errors in the initial fit are found for irradiance and angle-of-incidence. For temperature and APE, the RMSE is around 1% for most modules, while for irradiance and angle-of-incidence, the error is around 3% but up to almost 5%. In most cases, the model optimisation improves the fit of the models. Notable exceptions are the P2, CG1 and CS1 modules, which show a deterioration for the fits in half or more of the cases. The most notable improvements of the fitted model occurs for the angle-of-incidence fits.

Table 4.3 · Overview of root-mean-square errors (RMSE) of the model fit to the data for four parameters and eight devices. For each parameter the top row indicates RMSE before, while the lower row indicates RMSE after optimisation and correction. Colours are used as a visual aid to indicate improvement (green) or deterioration (orange) of the fit.

	device							
parameter	**H1**	**M1**	**P1**	**P2**	**A1**	**CT1**	**CG1**	**CS1**
irradiance	2.85%	3.28%	4.87%	3.08%	3.43%	3.52%	3.32%	4.10%
	2.48%	2.50%	2.80%	2.65%	2.11%	2.75%	3.11%	3.66%
temperature	1.02%	0.93%	2.34%	0.91%	1.57%	1.35%	1.49%	1.39%
	0.99%	0.80%	0.97%	0.94%	1.00%	1.23%	1.50%	1.47%
APE	1.03%	1.05%	1.26%	1.10%	1.15%	1.59%	1.42%	1.26%
	1.03%	1.01%	1.27%	1.11%	1.06%	1.50%	1.49%	1.29%
angle-of-incidence	2.69%	3.23%	3.25%	3.15%	2.12%	2.98%	4.25%	4.11%
	1.21%	1.75%	1.84%	1.61%	1.11%	1.34%	1.54%	1.22%

4.5 Module performance

4.5.1 Irradiance

To analyse the effect of variation in irradiance intensity on PV performance, we have filtered data around STC conditions, varying only the irradiance in the range of 50 - 1400 W/m^2 (see Table 4.2). Due to the high time resolution of the measurement, the datasets include a significant number of irradiance measurements well above 1000 W/m^2, due to cloud-induced super-irradiance. The results of the analysis are shown in Fig. 4.4. The selected data were used to fit the model of equation 4.5. For four types of modules we find that deviation away from STC irradiance leads to a small increase of performance (H1, M1, P2, A1) relative to STC conditions. Below approximately 175-200 W/m^2 however, performance of these modules starts to deteriorate. Contrary, for module P1 we do not see the performance increase, likely because of a lower series resistance in this module. For the cadmium telluride and CI(G)S modules, lowered performance is measured at lower irradiance values. Especially for the CIS module this effect seems very pronounced. These results are striking, considering that it is often reported that thin-film modules operate better at low light conditions compared to crystalline silicon modules. The strong decrease of performance could be due to a relatively low shunt resistance in the modules [182], as the adverse effect of low shunt resistance on performance is greater as irradiance is lower.

The results show that the filtering still results in large datasets with a large spread around the model fits. As a result, compared to the analyses for other parameters, the fit errors (RMSE) are relatively high. The model optimisation

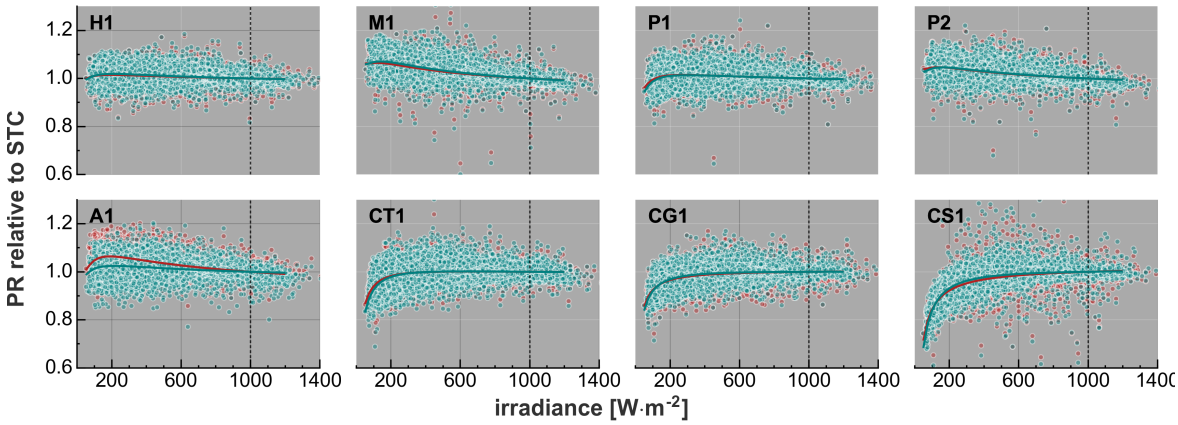

Figure 4.4 · Performance ratio (PR) relative to STC conditions as a function of irradiance, for 8 different modules. Module names are indicated in the top left corner of the plots and refer to section 4.2.1 and Table 4.1. The graphs show the non-linear model of equation 4.5 fitted to the measured data. The red datapoints and curve indicate the raw data and fitted model, the blue datapoints and curve are the corrected data and optimised fitted model. Most red datapoints are not visible as they are plotted behind the blue ones. The dashed vertical line indicates STC irradiance.

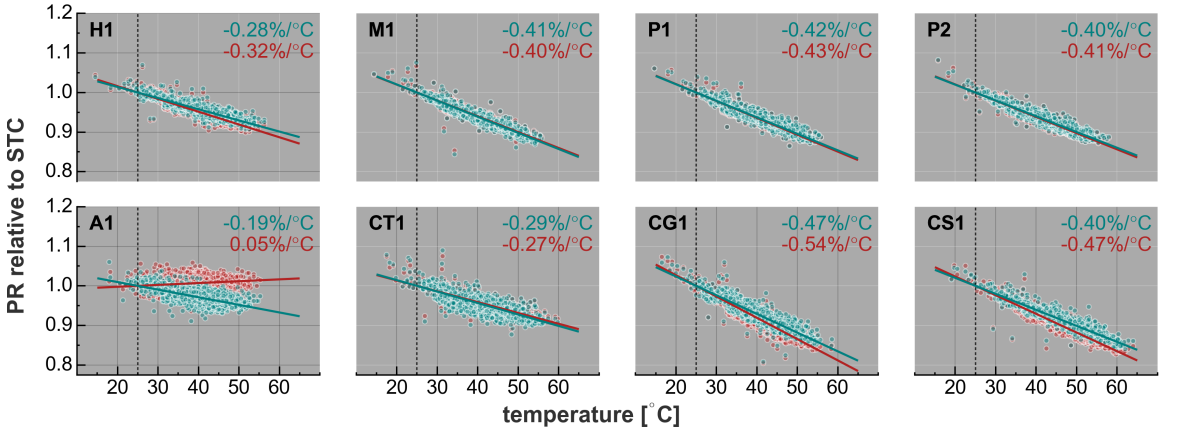

Figure 4.5 · Performance Ratio (PR) relative to STC conditions as a function of back-of-module temperature, for 8 different PV modules. Linear models were fitted to the data (solid red and blue lines). The red datapoints and lines indicate the raw data and fitted model, the blue datapoints and lines are the corrected data and optimised fitted model. The temperature coefficient of module power is shown in the top right corner for raw and corrected data. The dashed vertical line indicates STC temperature.

decreases the fit errors, however the effect on the data and the fits is not as visible in Figure 4.4.

4.5.2 Temperature

The effect of temperature on PV module performance was estimated by filtering data around STC irradiance, APE and AOI and varying only back-of-module temperature. For the filter ranges see Table 4.2. The results of our analysis, shown in Fig. 4.5, indicate for each module type the temperature coefficient at maximum power. The values obtained from this outdoor, long term measurement

mostly agree quite reasonably with those reported by the manufacturer in the module specification sheets. Notable exceptions are the A1, CS1, and CG1 modules. The thin-film a-Si/a-Si tandem A1 module shows a temperature coefficient of +0.05%/K for raw data, while module specifications indicate a negative coefficient of -0.20%. After the model optimisation however, the fit is shifted towards a value of -0.19%, which is very close to the module specifications. The positive value obtained for raw results is predominantly caused by variation in spectral irradiance, which have quite a strong effect on the performance of this module (see section 4.5.3). The importance of considering the spectrum for outdoor determination was also shown by Makrides *et al.* [183].

For the CS1 and CG1 (CIS and CIGS) modules, we observe a much stronger negative coefficient of maximum power (-0.54%/K and -0.47%) for raw data, than in the module specifications (-0.45% and -0.39%). After correction, the coefficients are -0.47%/K and -0.40%/K, and the difference with module specifications is 0.07%/K smaller for both modules, mainly due to correction for APE and irradiance. From the results we can also observe that the CS1 module seems to operate at higher temperatures compared to the other modules investigated, even though the specified normal operating cell temperature (NOCT) does not indicate this. For the CT1 module, the difference in fitted and specified coefficient is not very big for the raw data, but is bigger for the corrected data. This is likely an overcorrection for APE or the results of a temperature mismatch between back-of-module and cell.

The values obtained for the M1, P1, and P2 modules are quite close, but somewhat smaller (less negative) compared to the specified values. The data fitting indicate that each module seems 0.01%/K less affected by temperature change than the module specifications show, however, this difference is likely within the margin of error. The effect of data correction and model optimisation is small for these modules. The coefficient obtained for the H1 module is also close to module specifications, but is larger in the raw data, and smaller in the corrected data. This might be due to an overcorrection of the data.

4.5.3 Spectral variation

The effect of spectral variation (here analysed by means of APE) on the performance of the eight investigated PV modules is shown in Figure 4.6. The figure shows data measured at manually selected clear sky days, and a polynomial model fitted to this data. The results indicate as expected a strong effect of varying APE on the performance of the A1 (a-Si/a-Si tandem) module, while the effect is limited for crystalline silicon based modules (M1, P1, P2) and the H1 (heterojunction) module. In the low end of APE values, the CT1 module shows lowered perfor-

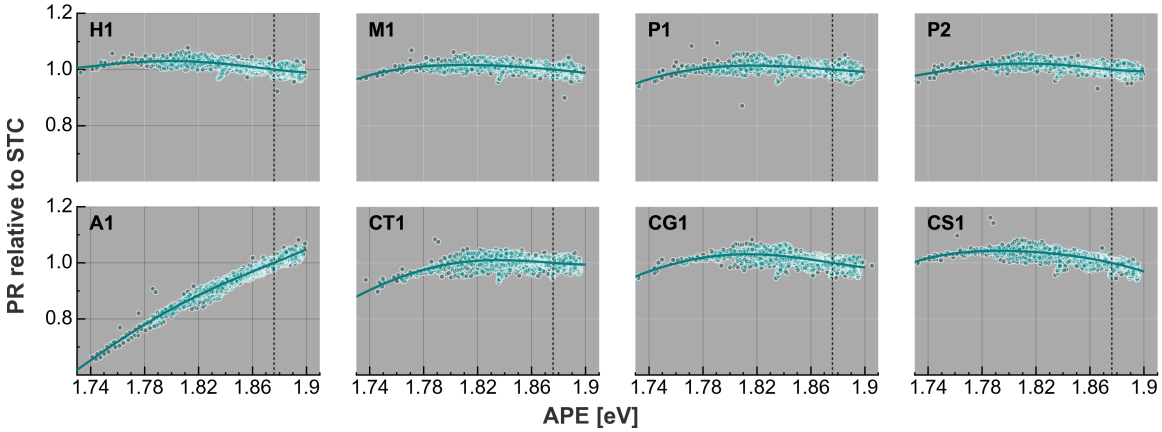

Figure 4.6 · Performance Ratio (PR) or short circuit current relative to STC conditions as a function of average photon energy (APE), for 8 different PV modules. Polynomial models were fitted to the data (solid red and blue curves). The blue datapoints and curves are the corrected data and optimised fitted model. The dashed vertical line indicates STC APE. Although the plots contain the raw data like Figures 4.4, 4.5 and 4.7, this data is obscured by the corrected data after correction as the effect of the correction is minimal.

mance, although the number of datapoints in this region is very small. Very low APE values are normally measured at high airmass and thus (for these fixed tilt modules) high angles of incidence. However these datapoints are filtered from the data for this analysis to avoid the data representing the effect of both parameters on PV module performance. For the crystalline silicon based modules (H1, M1, P1, P2) and the CI(G)S modules (CG1 and CS1) we observe a slight decrease of performance as the APE increases. This is likely related to the low band gap and the peak of spectral response at long wavelengths (Fig. 4.1). At very low APE values we do however observe a slightly decreased performance for these modules. For the CI(G)S modules this effect is stronger compared the crystalline silicon based modules. The model optimisation does not seem to affect the model fits. For all modules except the A1 module, the peak of performance is at a lower APE than STC conditions specify.

4.5.4 Angle-of-incidence

Figure 4.7 shows the effect of angle-of-incidence on the performance of the studied PV modules. The red and blue curves indicate the polynomial model fitted to the data (see equation 4.12). For all modules investigated, there is a strong decrease in performance at high angles of incidence, although the magnitude of the effect slightly differs from on module to the other. The effects of high angles-of-incidence do not necessarily depend on the semiconductor material in the module, but likely more on the optical structure of the whole device, and as such the type of glass used as front cover of the module, and the applied laminate [180]. This seems to be confirmed by our results, which distinguish the modules with a smooth glass

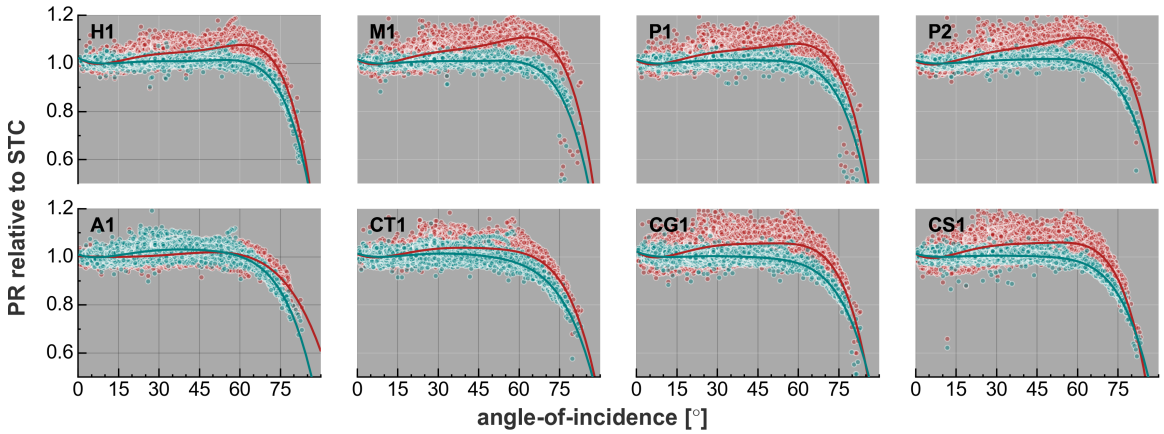

Figure 4.7 · Performance Ratio (PR) relative to STC conditions as a function of angle-of-incidence, for 8 different PV modules. Polynomial models were fitted to the data (solid red and blue curves). The red datapoints and line indicate the raw data and fitted model, the blue datapoints and line are the corrected data and optimised fitted model.

front cover (CT1, CG1, and CS1) from the textured glass modules (H1, M1, P1, P2). In the latter case, the onset of angular losses is at a higher angle-of-incidence, but the decline is sharper, compared to the more gradual effect observed in the smooth glass modules. The fit for the A1 module seems affected by a large spread in both the raw and uncorrected data.

The data correction and model optimisation substantially affects the data and resulting model fits. The raw data and their fits clearly exhibit the effect of low irradiance and low temperature, at high angles of incidence. Correction for these parameters, and APE, significantly improves the model fit for all modules investigated (see Table 4.3). For the crystalline silicon based modules M1 and P2 we clearly observe enhanced performance at low irradiance levels that coincide with large angles of incidence. This is visible at the "knee" of the graphs in Fig. 4.7. As a result of the model optimisation, this effect is reduced significantly, and the graphs become nearly horizontal up to roughly 60°. For the CG1 and CS1 modules, an opposite effect is observed, where the correction for low performance at low irradiance shifts the angle-of-incidence fit and data to the right (Fig. 4.7).

4.5.5 Module comparison

Figures 4.8 and 4.9 show a comparison of the effects of the investigated parameters for the eight investigated PV modules. Fig. 4.8 shows the fitted models from Figures 4.4-4.7. In this figure we can clearly see that: **1)** low irradiance most substantially affects the performance of the CS1 module, but the CG1 and CT1 modules also show strongly decreased performance at low irradiance conditions, contrary to what is often reported for CI(G)S modules. The performance increases

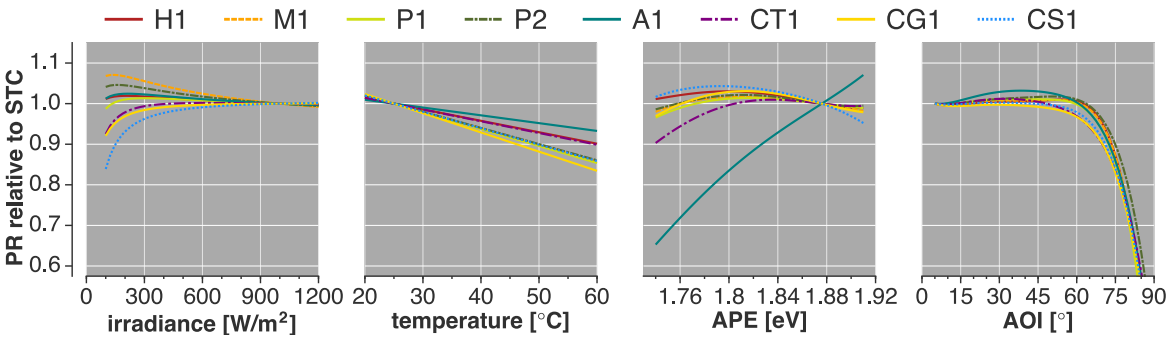

Figure 4.8 · Comparison of Performance Ratio (relative to STC) of 8 PV modules as a function of irradiance, temperature, average photon energy (APE) and angle-of-incidence.

at low irradiance for the P2 and especially the M1 module; **2)** increased module temperature has the most effect on the CG1 module (-0.47%/°C), slightly less for the M1, P1, P2 and CS1 modules (-0.40 to -0.42%/°C), and significantly less for the H1 (-0.28%/°C), CT1 (-0.29%/°C) module and A1 (-0.20%/°C) module; **3)** the effect of spectral variation is very pronounced for the A1 module, and most limited for the crystalline silicon based modules; **4)** the angle-of-incidence losses are significant for all modules, but the effect is different for smooth glass modules (CT1, CG1, CS1) compared to textured glass modules (H1, M1, P1, P2). The fit for the A1 module seems negatively affected by noise in the data.

Figure 4.9 combines the fitted models from Figures 4.4-4.7 and the measurements presented in Fig. 4.2. It shows the performance deviation as resulting from variation of the four investigated parameters as a function of the relative occurrence of the variation in each parameter. The dashed vertical lines indicate the location of STC values for each parameter. The figure makes visible that for some modules, the observed variation in operating conditions does not result in strong deviation of performance relative to STC. This is true mainly for H1 and P2, and to a lesser extent for M1 and P1. Especially for the CS1 module, but also for the CG1 and CT1 modules, strong deviation from STC performance is observed as a result of observed variation, mainly irradiance and temperature. The effect of observed variation in spectral composition of irradiance is especially clear for the A1 (a-Si/-a-Si tandem) module, because the optimal current matching between the two cells in the tandem module is affected as the APE shifts away from STC conditions [172, 184]. Thus, this effect does not so much depend on the module material, but rather on the tandem structure.

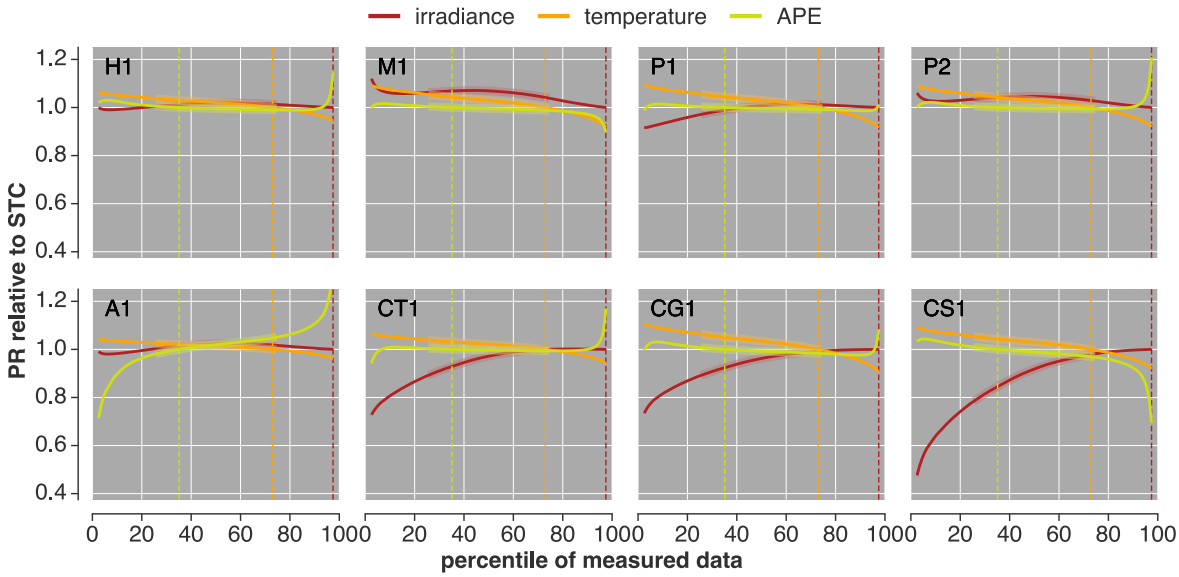

Figure 4.9 · Comparison of Performance Ratio (relative-to-STC) of 8 PV modules as a function of the measured percentiles for irradiance, temperature, and average photon energy (APE). The interquartile range is indicated by the thicker portion of the curves. The dashed vertical lines shows the percentile location of STC conditions for each parameter. Angle-of-incidence is omitted from this figure, as its effect on overall performance is also affected by the fraction of direct light.

4.6 Effect on seasonal and annual energy yield

We have analysed the effects of observed variation in operation conditions on both seasonal and annual performance. The results of this analysis are shown in Figures 4.10 and 4.11. Fig. 4.10b shows that especially variation in module temperature leads to a substantial seasonal variation in performance for all modules, although the effect is of course smaller for the modules with lower temperature coefficients. Because of high operating temperatures, performance is decreased in summer. In winter, module temperatures are so low performance is increased above STC values (although energy yield in this period is low due to low insolation). Variation in average photon energy (APE) also results in seasonal variation of performance, especially for the A1 module, showing a peak in summer (high APE) and strongly

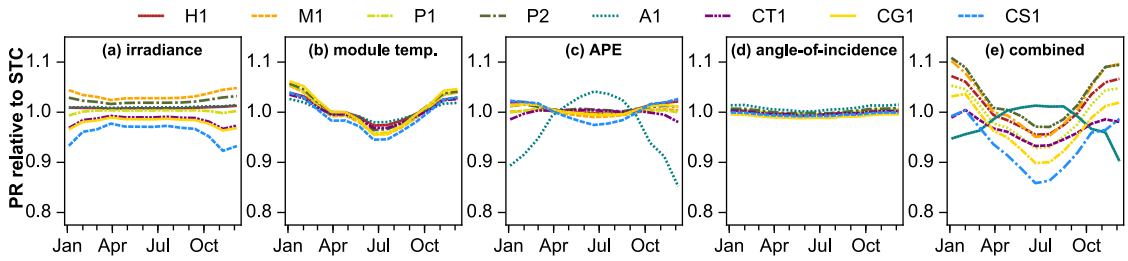

Figure 4.10 · Overview of the effect of variation of four parameters, and their effects combined, on the seasonal performance of eight PV modules. For the module specifications refer to Table 4.1.

decreased performance in winter (low APE) in Fig. 4.10c. Low APE values observed in winter can lower the performance of this module by almost 15%. For the (non-tandem) CT1 module this seasonal effect is similar but much less pronounced. Fig 4.10a shows that because of deviations in irradiance, some modules, most obviously the CS1 modules, operate at lower performance compared to STC year-round, while other modules, like the M1 module, benefit from year-round lower-than-STC irradiance. The effect of angle-of-incidence on seasonal performance variation is small, as this effect is compensated by an increase of diffuse irradiance, and the majority of measurements performed have a high fraction of diffuse irradiance.

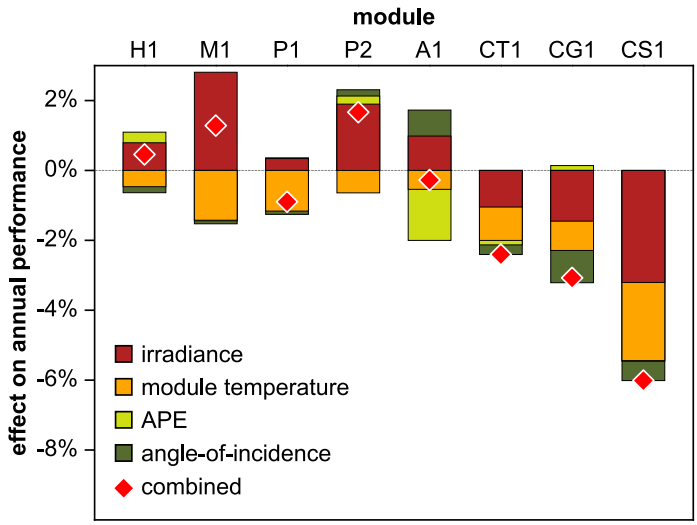

Figure 4.11 · Stacked bar chart showing a comparison of the effects of variation in four parameters on annual module performance. The red diamonds indicate the combined effect of all four parameters. For the module specifications please refer to Table 4.1.

The contribution of observed variation in operating conditions to annual performance is shown in Figure 4.11. This figure indicates that for all modules there is a negative effect of module temperature and angle-of-incidence on annual performance, except for the A1 and P2 modules, that appear to get a small performance bonus from deviation of angle-of-incidence values which we cannot conclusively explain. For both modules the angle-of-incidence models fitted show slightly (P2) or significantly (A1) increased performance between roughly 15° and 65°. For the A1 module, this might be due to increased absorption in the thin silicon film as a result of the longer trajectory of light in the absorbing layer. For the P2 module it seems outliers in the dataset (visible in Fig 4.7) could have affected the model fit.

Deviations of irradiance from STC conditions results in enhanced performance for five modules: H1, P1, P2, A1 and especially M1, while the other thin-film modules show poor low-light performance and thus are affected negatively by irradi-

ance in terms of annual output.

Especially the CS1 module, which operates generally at higher temperatures compared to the other modules, temperature losses are large. This module is also very strongly affected by the low irradiance operating conditions, and angle-of-incidence effects. On an annual basis, most modules are (almost) unaffected by variations in spectral composition of irradiance. The one exception is the thin-film a-Si/a-Si tandem A1 module.

4.7 Conclusions

We have characterised and compared the performance of different types of PV modules, under realistic operating conditions observed in a North-Western European installation location, in the context of an R&D project focussing on the development and assessment of silicon heterojunction (SHJ) technology. We have analysed the effect of deviations from standard testing conditions (STC) observed for irradiance, module temperature, spectral composition of irradiance and angle-of-incidence. Our results show that the effect of observed variations in operating conditions affect modules very differently according to module type (semiconductor material) but also the materials used in the modules, such as the type of glass used in the front cover of the module.

In our study a copper-indium-selenium module (CIS) was most affected by variations of operating conditions. This module exhibited, on an annual basis, a negative effect of variations in all investigated parameters, and an especially strong effect of irradiance and temperature variations on annual performance. The combined effect of all parameters was a decrease in annual energy yield of more than 6%, of which 3.2% caused by low irradiance and 2.2% by high temperature operation of the module. angle-of-incidence effects amounted to a performance loss of around 0.5%. The other modules investigated were much less affected by variations in operating conditions, with the annual combined effect ranging from -3.1% to +1.6%.

Focusing on the SHJ module, our results show that this module performs very similar to other crystalline silicon based modules in the study. The benefit of SHJ's small temperature dependence is confirmed by lower temperature related losses, and there is no substantial difference in the response to varying spectral conditions.

Examining the effects in the context of PV module types (semiconductor materials), we see that not all effects seem to be related to semiconductor material, but also to the type of glass on the front of the module, and other module parameters, such as a tandem or single junction structure, or the packaging in the module (warm or cool packaging).

By supplying more information on the effect on PV module performance of different operating parameters, like spectral irradiance, low irradiance conditions, and angle-of-incidence, PV producers could improve the estimates installers make on the expected energy yield of the PV systems they install, especially when they can connect this with data on local operating conditions. We argue that the addition to the module datasheets of spectral response data, and data showing the performance of the modules as a function of irradiance and angle-of-incidence would improve the estimates of installers substantially.

Acknowledgements

This research was funded by *Stichting Technologische Wetenschappen* within the FLASH *Perspectief* programme under project number 12172.

5

Geospatial analysis of the energy yield and environmental footprint of different types of PV modules

Submitted to: Solar Energy

Abstract The majority of currently installed photovoltaic (PV) systems are based on mono- and polycrystalline silicon PV modules. Manufacturers of competing technologies often argue that due to the characteristics of their PV technologies, PV systems based on their modules are able to achieve higher annual energy yield, due to a smaller effect of temperature on module performance and/or a better performance at low light intensities. While these benefits have been confirmed in local studies many times, there is still limited insight as to the locations at which a particular technology actually performs best.

In this study we have analysed the performance of a large set of PV modules, based on irradiance time series that were taken from satellite measurements. Using these data, and combining it with a PV performance model, we have made a geospatial analysis of the energy yield of different types of PV modules. We aim to make the energy yield of the investigated modules spatially explicit, allowing PV system installers to choose the best module type for every location investigated. Our results show that there is large geographical variety in the performance of PV modules, in terms of energy yield but also in terms of relative performance or performance ratio. While some technologies clearly exhibit a decrease in performance ratio at locations where they operate at higher temperatures, for some technologies this effect is much smaller. As a result of the variation in performance, the environmental footprint of PV modules also shows large geographical variations. However, even at low irradiance locations the environmental footprint of PV modules in general is much lower compared to that of fossil fuel based electricity generation.

5.1 Introduction

The past decade saw exponential growth of installed photovoltaic (PV) solar energy system capacity. While at the end of 2005 cumulative global installed PV capacity was only around 5 GW_p, by the end of 2015, almost 230 GW_p of PV was installed [17, 19]. The growth has been concurrent with strong reductions in the cost of PV systems, and support mechanisms in countries like Germany and later China have also strongly stimulated growth of installed capacity, and have helped push prices down. The levelised cost of electricity (LCOE) from PV has dropped to values below that of conventional, fossil fuel based electricity production in some locations [39]. Furthermore, in many countries, PV electricity has achieved socket or grid parity [40].

The majority ($\sim$90%) of installed PV systems are based on either mono- or polycrystalline silicon based PV modules [185], while the remainder of systems are mostly based on cadmium telluride (CdTe) or copper-indium-gallium-selenium or copper-indium-selenium (CIGS or CIS) type modules [185, 186]. Other module technologies with small market shares are silicon heterojunction (SHJ) and thin-film amorphous silicon (a-Si). Manufacturers of technologies competing for market share with the incumbent crystalline silicon technologies often argue that their modules show superior energy yield in outdoor operation, due to better low-light performance [187] and/or lower temperature coefficient of module power [187–190]. For instance, while the performance of crystalline silicon modules normally decreases from its nameplate capacity with around 0.4% for every degree the module operates above 25°C, for SHJ modules this figure is normally below 0.3%/°C [189], and even lower for CdTe and a-Si modules [188, 191]. Especially considering the fact that PV modules normally operate at temperatures much higher than at which the nameplate capacity is determined, the manufacturers often argue that in most locations their technology will outperform conventional crystalline silicon PV modules.

In many PV performance studies, the benefits of the characteristics of these ”alternative” technologies have been confirmed. For instance it was shown that SHJ modules achieve higher energy yield compared to crystalline silicon because of a lower detrimental effect of high operating temperatures [192–194]. For a-Si and CdTe, this is also been established for certain locations [193–195]. However, while we have information that in some specific cases one technology might outperform the other, there is limited information available that makes the performance of different types of PV geospatially explicit. Furthermore, as the environmental impact of PV is largely dependent on the energy yield over the lifetime of a PV system, the environmental impact of a PV system will also be location-dependent.

In this study we aim to use detailed modelling of the performance of different PV module technologies to determine the geospatial performance of PV, in terms of energy yield, performance relative to the nameplate capacity, and environmental performance. The results should offer insights in which technology performs best at which location, in terms of these several criteria, and can be applied by system installers, investors and policy makers to make sound decisions on choosing technology types for a specific location.

5.2 Methods

For this study, we used irradiance, air temperature, and wind speed time series from satellite measurements to model the performance of different types of PV modules. First we used the irradiance time series to calculate the optimum tilt of the PV module array for every location in our analysis. Then, we modelled plane-of-array irradiance time series for these tilted planes, and used these plane-of-array time series to model PV power output and energy yield. Finally, we used the resulting data to present energy yield, performance ratio (*PR*), energy payback time (*EPBT*), greenhouse gas (GHG) emission factor (gCO_2-eq/kWh), and GHG payback time (GHGPBT) for a broad geographical scope.

5.2.1 Irradiance and weather data

We obtained global horizontal irradiance time series with a temporal resolution of 15 minutes, and a geographical resolution of 0.5° by 0.5°, from measurements of the HelioClim satellite, for the year 2005 [196]. We also obtained wind speed and temperature measurements with the same geographical resolution, and a temporal resolution of 6 hours [197]. The geographical scope of the data includes most of Europe, all of Africa, and the Middle-East.

5.2.2 Optimum tilt and plane-of-array irradiance

The global horizontal irradiance data was converted to plane-of-array (POA) irradiance time series using the Hay-Davies model [198], which calculates plane-of-array irradiance from global horizontal, direct normal, diffuse horizontal and extraterrestrial direct normal irradiance. The direct normal irradiance (DNI) was calculated from the global horizontal irradiance (GHI) using the DIRINT model [199]. The extraterrestrial DNI was calculated according to [200, 201]. The beam component of the DNI was calculated for a horizontal plane to establish the diffuse horizontal irradiance (DHI). The optimum POA tilt was assumed to be the tilt at

which the annual POA irradiance is at its maximum. Therefore the POA irradiance was calculated in several iterations for every location, until a maximum was found. The determination of optimum tilt was performed with irradiance time series downsampled to hourly resolution to reduce computation time. The resulting optimum tilt was used to calculate 15 minute POA time series using the previously described approach. The dataflow for the determination of optimum tilt is shown in Figure C.1. The resulting optimum tilts and plane-of-array irradiance sums are shown in Fig. 5.1. The figure shows that there is as expected a large, predominantly latitudinal, variation of POA insolation, with POA insolation ranging from under 1000 $kWh \cdot m^{-2} \cdot yr^{-1}$ to over 2500 $kWh \cdot m^{-2} \cdot yr^{-1}$.

5.2.3 PV performance modelling

The POA irradiance time series obtained in the previous step are comprised of global, direct, sky diffuse and ground diffuse irradiance in the plane-of-array. These datasets are used as input in the PVLIB-python implementation [202] of the Sandia Array Performance Model (SAPM). SAPM was developed by Sandia National Laboratories and models the performance of PV modules based on module specifications, direct and diffuse POA irradiance, cell temperature, airmass and angle-of-incidence of the direct irradiance on the module plane [149]. Aside from the normally listed modules specifications, the model uses empirically determined module coefficients that take into account the effects of airmass and angle-of-incidence on

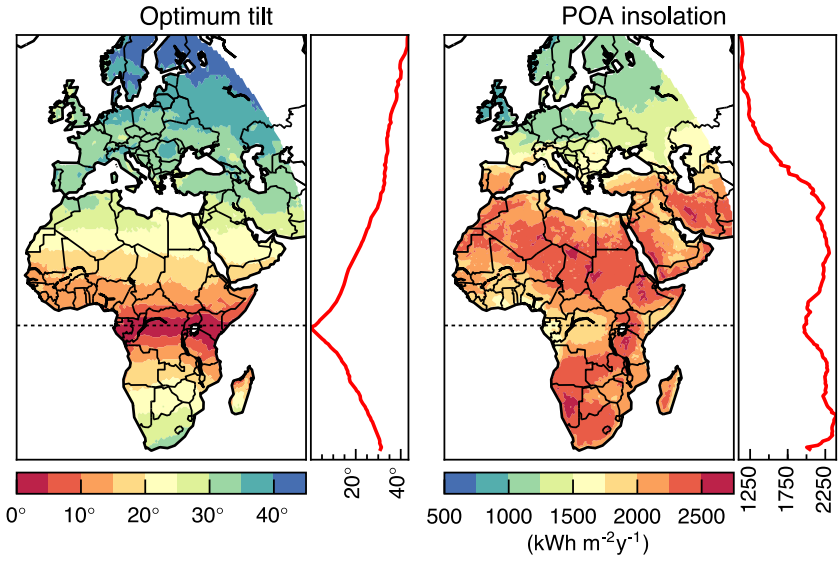

Figure 5.1 · Global optimum plane-of-array (POA) tilts and POA insolation for optimally tilted surfaces, calculated from global horizontal irradiance time series for the year 2005, converted to POA using the Hay-Davies model. The curves on the right side of the map indicate average tilt and POA insolation as a function of latitude.

module performance. The effects of these parameters was established for a wide range of modules by performing a fit of a polynomial model. The dataflow of the PV performance model is shown in Figure C.1.

The cell temperature is calculated based on an empirical model also developed by Sandia National Laboratories which is included in the PVLIB-python SAPM implementation. It takes into account total POA irradiance, ambient temperature, wind-speed, and the type of module backside (glass, polymer, steel) and the type of installation (open-rack, roof-mounted, etc.). For this study we use the default setting, e.g. an open rack installation, but accounted for the type of module (glass or polymer backside).

The output of the SAPM model is a time series of the direct-current (DC) characteristics of the modelled module, and includes short-circuit current (I_{sc}), maximum power point current (I_{mpp}), open-circuit voltage (V_{oc}), maximum power point voltage (V_{mpp}), and maximum power point power (P_{mpp}).

5.2.4 Annual energy yield and performance ratio

The SAPM time series are used to establish the performance of the modelled PV modules on an annual basis. The annual energy yield is calculated from the time series as:

$$E_{\text{annual,DC}} = \sum P_{\text{mpp}}(t) \cdot \Delta t \tag{5.1}$$

where E_{annual} is the annual energy yield and Δt is the time step between measurements (15 minutes). Because our primary aim was to compare different PV technologies, we focus on the DC output of the modules, to exclude any influence of the inverters applied to convert the DC power to AC power that can be fed into the grid. The performance ratio (PR) is defined as the ratio between the actual energy yield E_{annual} and the yield that is expected when we take only into account the rated power of the module (P_{STC}) and the annual insolation at the module plane. It is calculated for each module as:

$$PR_{\text{DC}} = \frac{E_{\text{annual}}}{P_{\text{STC}} \cdot H_{\text{POA,annual}} \cdot (G_{\text{STC}})^{-1}} \tag{5.2}$$

where $H_{\text{POA,annual}}$ is the insolation (annual irradiance sum) at the POA, and G_{STC} is the STC irradiance at which the P_{STC} is determined. The PR is normally calculated for actually measured energy yield, but here we calculate it using the modelled annual energy yield of the PV modules.

Table 5.1 · Overview of loss factors of PV systems assumed in this study for the calculation of EPBT, GHG emission factor and GHGPBT.

Loss parameter	Losses	Source
Soiling	2.0%	Assumption
Module mismatch	1.71%	[203]
Wiring losses	1.25%	[80]
Connection losses	0.5%	Assumption
Light-induced degradation	1.5%	Assumption
Total combined losses	6.78%	

5.2.5 Environmental indicators

The annual energy yield of PV modules is of course very important for investment decisions, but it also determines the environmental impact of PV, as normally this impact is expressed in relation to the functional output of a PV system, e.g., the amount of electricity a PV system produces over its lifetime. Here, we analyse the geo-spatial variation of three environmental impact indicators, energy payback time (EPBT), life-cycle greenhouse gas (GHG) emissions and GHG payback time (GHGPBT).

The energy payback time is defined as the time it takes for a PV system to produce the same amount of energy that is consumed during its whole lifecycle. For PV systems, by far the most energy is consumed during the production of the PV system components. In general, the EPBT is calculated as:

$$EPBT = \frac{E_{\text{prod}} + E_{\text{tran}} + E_{\text{inst}} + E_{\text{EOL}}}{E_{\text{annual}} \cdot f_{\text{deg}} \cdot f_{\text{loss}} \cdot \eta_{\text{inv}} \cdot (\eta_{\text{G}})^{-1} - E_{\text{OM}}} \tag{5.3}$$

where the terms in the numerator are the energy invested for production (E_{prod}), transport (E_{tran}), installation (E_{inst}), and end-of-life treatment (E_{EOL}), all expressed in MJ of primary-energy equivalent energy (MJ_{P}). E_{annual} is the annual energy output of the PV module under study, f_{deg} is a factor expressing the decrease in energy output of PV systems as a result of (internal) degradation, f_{loss} are other system related losses, η_{inv} is the average inverter efficiency, and E_{OM} is the energy invested during operation and maintenance. The factor f_{loss} describes the effect of assumed system losses for soiling, module mismatch, wiring and connection resistance, and light-induced degradation. Table 5.1 shows an overview of the loss-parameters included here. Total system losses are estimated to be 6.8%, thus f_{loss} is estimated at 93.2%. The factor f_{deg} was calculated for the PV system lifetimes of 30 years, based on an assumed degradation rate of 0.67% per year (20% degradation in 30 years) for all technologies, thus f_{deg} amounts to 0.9.

The parameter η_{G} is the primary energy to electricity conversion efficiency for the grid where the PV system is installed [204]. As described in the *Methodol-*

ogy Guidelines on Life Cycle Assessment of Photovoltaic Electricity [204], there are two main options for determining the value of η_G: **1)** by assuming the installed PV systems electricity production replaces the average grid mix of electricity at the point of installation (normal EPBT) **2)** by assuming the installed PV system replaces only non-renewable electricity at the point of installation (non-renewable EPBT). In terms of capacity additions and decommissioning, there is support to assume the latter, as the newly installed capacity is mainly in the form of renewable electricity, while the capacity that is decommissioned is likely mostly non-renewable. However, considering the intermittent nature of electricity production from PV one could also argue that at the time of generation PV is more likely to replace flexible electricity supply, like natural gas fired power plants, especially at high PV penetration grades and in the absence of sufficient flexible storage capacity or demand response. In this study we analyse the "normal" EPBT. For η_G we take country average values where available, otherwise we take values for a larger geographical scope. The energy demand for production of the various types of PV was taken from a recent life cycle assessment (LCA) study [35].

The greenhouse gas (GHG) emissions of PV electricity are normally expressed per kWh of electricity generated with a PV system. It is calculated by summing all the CO_2 emissions that originate during production, transport, installation, operation and end-of-life treatment of the PV system and dividing this figure by the lifetime energy output of the PV system. Similarly to the EPBT, one can also calculate a GHG payback time (GHGPBT). As with EPBT, this requires some assumptions on which type of electricity is replaced by PV, and thus, what amount of GHG emissions can be considered to be avoided.

To analyse the geospatial distribution of GHG emissions from PV, we took GHG emissions data for the studied module technologies from a recent LCA study that analysed all different module technologies studied [35]. From these studies, we established the GHG emissions related with producing a PV system expressed per unit of PV system capacity (gCO_2-eq/W_p). The yield figures modelled here where then used to calculated a GHG emission factor (gCO_2-eq/kWh):

$$G_{\text{elec}} = \frac{G_{\text{prod}} + G_{\text{tran}} + G_{\text{inst}} + G_{\text{EOL}}}{E_{\text{annual}} \cdot f_{\text{deg}} \cdot f_{\text{loss}} \cdot \eta_{\text{inv}} \cdot T_{\text{life}}} \tag{5.4}$$

where G_{elec} is the GHG emission factor in gCO_2-eq/kWh, G_{prod}, G_{tran}, G_{inst}, G_{EOL} are the GHG emission associated with production, transportation, installation, and end-of-life treatment of a PV system, respectively, E_{annual} is the annual energy production (modelled here), T_{life} is the expected lifetime of the system (assumed to be 30 years for all module types).

Similar to EPBT, we also calculate the time in which the GHG emissions re-

leased during the various stages of the PV systems' lifecycles are payed back by replacing electricity produced from the average electricity grid, the GHG payback time (GHGPBT). The GHGPBT is calculated as:

$$\text{GHGPBT} = \frac{G_{prod} + G_{\text{tran}} + G_{\text{inst}} + G_{\text{EOL}}}{E_{\text{annual}} \cdot f_{\text{deg}} \cdot f_{\text{loss}} \cdot \eta_{\text{inv}} \cdot \left(G_{\text{gridavg}} - G_{\text{elec}}\right)} \tag{5.5}$$

where G_{gridavg} is the country average grid GHG emissions factor. This factor was calculated by combining GHG emission data from [205] and electricity production data from [206]. For countries where data is missing, or where the GHG emission factor is above the 95$^{\text{th}}$ percentile of all countries analysed, we assume the average value for all countries.

It is to be noted that the GHG emission factor G_{elec} and the GHGPBT we show below do not represent point-of-generation GHG emissions, but rather represent what emission can be attributed to PV produced elsewhere, when installed in each location shown on the maps. Thus, the emissions from PV production are associated with a fixed production location, and the variation in G_{elec} comes from the variation of performance of PV at different locations. Furthermore, for GHGPBT we assume a grid emission factor that is constant within each country. Especially for larger countries, the shown GHGPBT does not necessarily reflect local conditions. The results are thus considered to be indicative, but shown nonetheless, to indicate that the energy yield of PV at different locations can result in significant variation in G_{elec} compared to the results obtained in LCA studies that assume a specific energy yield of (normally) 1275 kWh·kW$_{\text{p}}^{-1}$y^{-1} [44, 204, 207]. We also aim to show indicatively how the combination of local attainable energy yield from PV and local grid emission factors results in the ability of PV to contribute to decarbonisation of electricity generation.

5.2.6 Selection of studied modules and comparison of PV technologies

In this study we analyse six different PV technologies: SHJ, mono-Si, poly-Si, CdTe, CI(G)S, and tandem a-Si. For each PV technology we have analysed eight recent types of PV modules for which we were able to obtain the SAPM performance coefficients. We present our results per technology, by taking the average result for the studied modules. For each module technology we also investigate the variation in the obtained results between the eight modules selected per technology.

5.3 Comparison of PV module technologies

The results of our modelling analyses are shown in Figures 5.2-5.5 for energy yield, performance ratio, energy payback time, GHG emission factor, and GHG payback

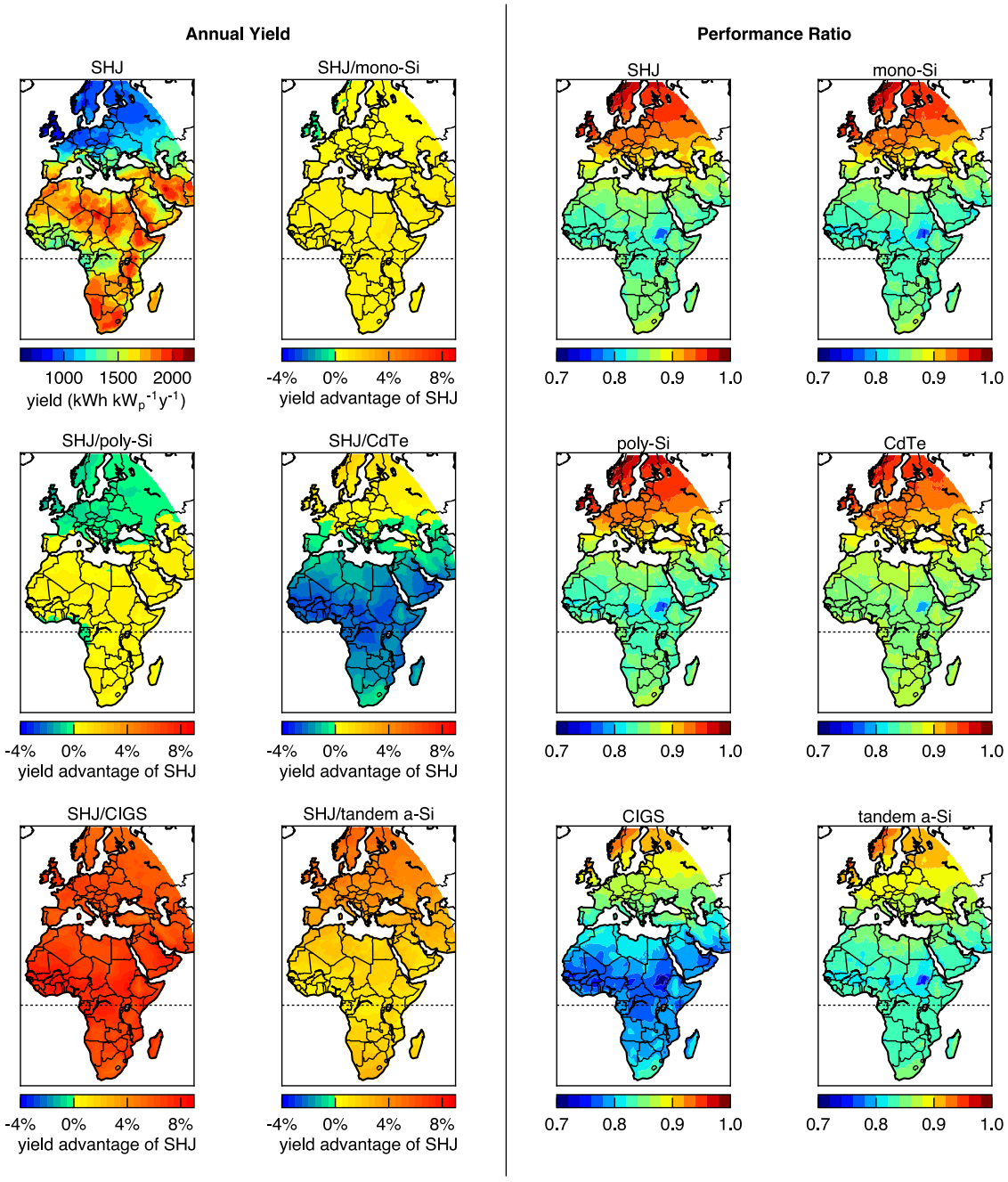

Figure 5.2 · Left: Overview of the annual energy yield in kWh/kW_p (SHJ) and relative yield of SHJ compared to other technologies. Right: the performance ratio PR_{DC} of optimally tilted PV systems. Results for the year 2005, calculated with the Sandia Array Performance Model [149] using 15-min resolution plane-of-array irradiance time series [196] and 6-hour ambient temperature and wind-speed time series [197].

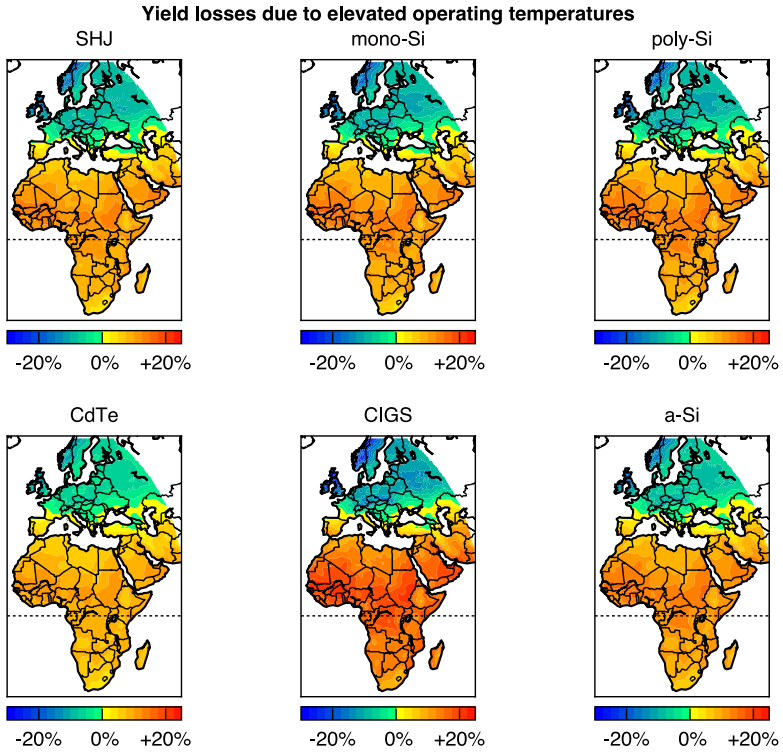

Figure 5.3 · Overview of the modelled energy payback time (EBPT) of optimally tilted PV systems in years, calculated with the Sandia Array Performance Model [149] using 15-min resolution plane-of-array irradiance time series [196] and 6-hour ambient temperature and wind-speed time series [197] for 2005.

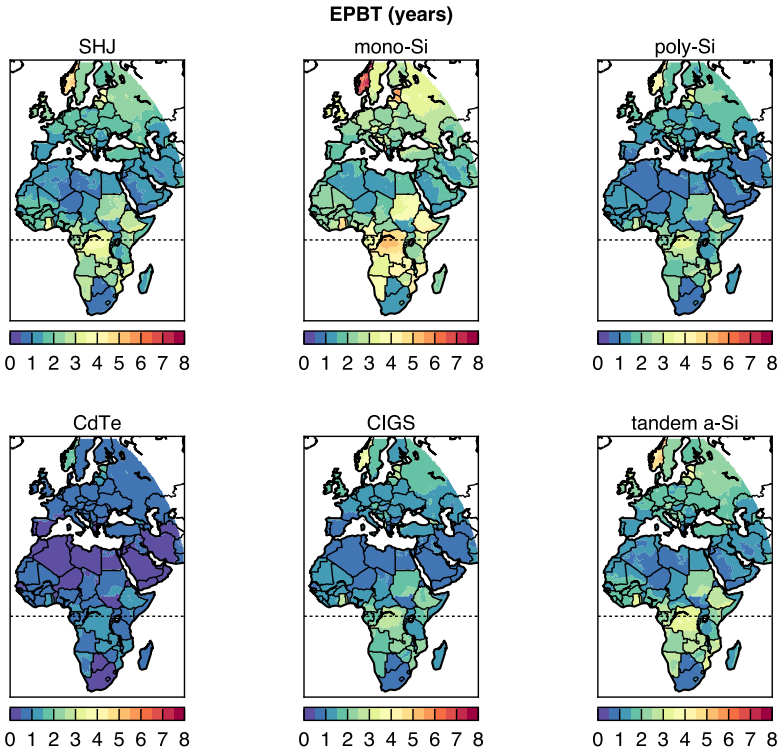

Figure 5.4 · Overview of the modelled energy payback time (EBPT) of optimally tilted PV systems in years, calculated with the Sandia Array Performance Model [149] using 15-min resolution plane-of-array irradiance time series [196] and 6-hour ambient temperature and wind-speed time series [197] for 2005.

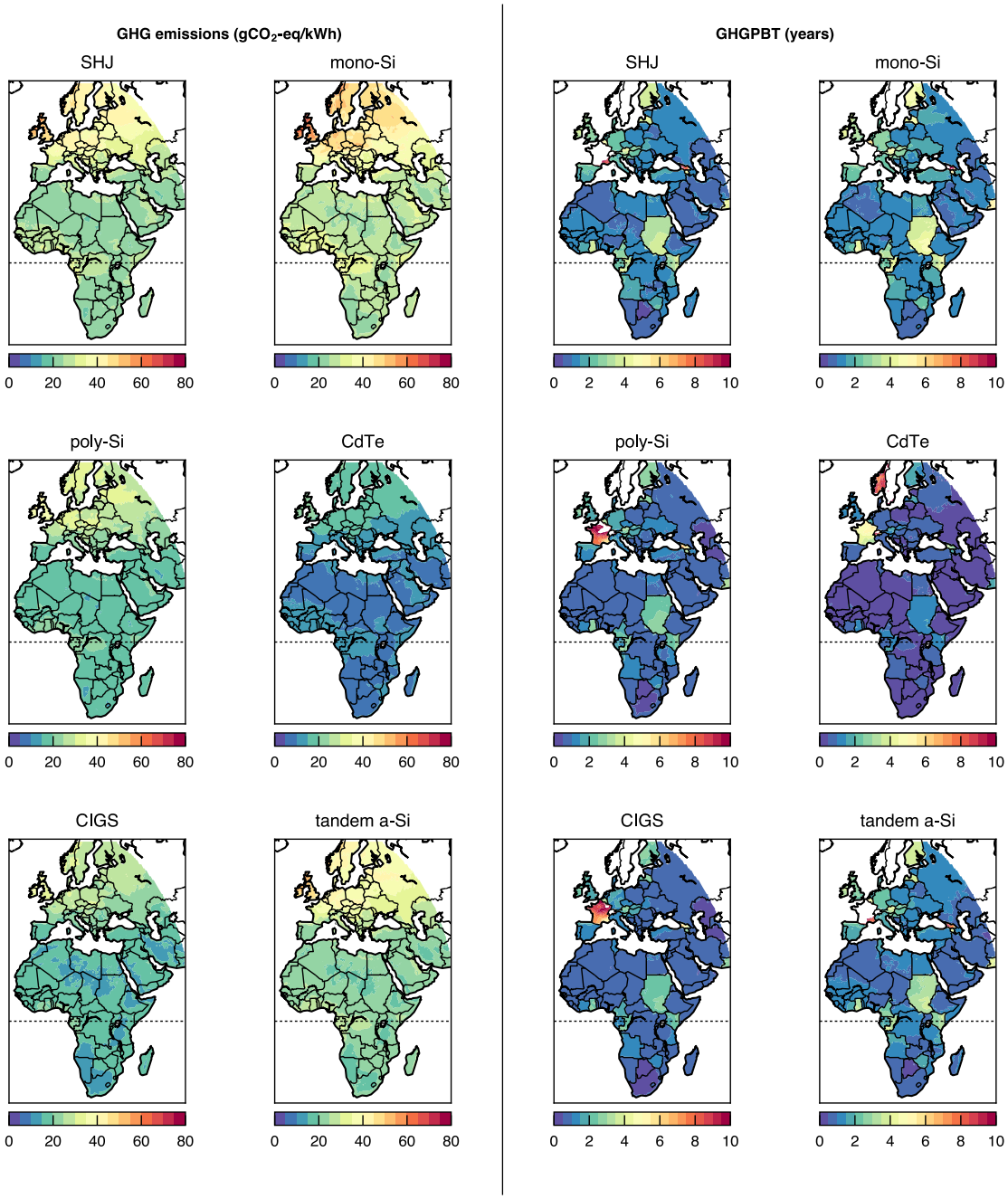

Figure 5.5 · Overview of the modelled greenhouse gas emission factor (left) and payback time GHGPBT (right) of optimally tilted PV systems in gCO_2-eq/kWh, calculated with the Sandia Array Performance Model [149] using 15-min resolution plane-of-array irradiance time series [196] and 6-hour ambient temperature and wind-speed time series [197].

time. Figure 5.2 (left) shows the annual energy yield of SHJ modules, and the relative yield of SHJ modules compared to modules of 5 other types of PV. The results indicate that for the modules studied, the SHJ modules outperform all module technologies aside from the CdTe modules in most locations. The results for the mono- and especially the poly-Si modules furthermore indicate that the yield advantage of SHJ modules becomes larger in locations closer to the equator, likely due to higher operating temperatures and the smaller effect of temperature on SHJ's performance. The yield of PV systems, calculated from modelled DC performance taking into account degradation, loss factors, and inverter efficiency as described in Section 5.2.5, ranges from under 750 $kWh \cdot kW_p^{-1} y^{-1}$ in locations with low irradiance to almost 2250 $kWh \cdot kW_p^{-1} y^{-1}$ in high-irradiance locations. Fig. **??** shows the performance ratio of the studied PV systems. Taking into account the losses described in Section 5.2.5, the *PR* ranges from under 70% to over 98% for all technologies. As performance ratio is essentially energy yield corrected for irradiance, Fig. 5.2 (right) more clearly shows the latitudinal variation of performance. For most technologies the main variation in *PR* is likely due to variations in operating temperature. Figure 5.3 shows the effect of temperature on annual PV yield. Comparing with Fig. 5.2 (right), it is shown that the decrease of *PR* at low latitudes can largely be attributed to temperature related yield losses.

Figure 5.4 shows that the energy payback time of PV modules shows large variation, not only from high to low latitudes, but also from one country to the other. This is due to the fact that EPBT is calculated using the country average grid efficiency. Countries with high shares of renewable electricity (especially hydropower) with high primary energy to electricity conversion efficiency show high payback times. Norway is a notable example of this phenomenon, not only because of the low irradiance, but because a very large fraction of the electricity produced there is from hydropower. Another notable example is the DR Congo, which also has a high share of hydropower in its electricity supply, and as a result shows high EPBT even though PV yields are quite high.

CdTe based systems show the lowest EPBT, which is below 0.5 years in many locations, especially on the African continent, but even in some southern European locations. Although SHJ modules show higher yield compared to poly-Si, CIGS and a-Si, the latter have lower EPBT in most locations due to a much lower energy consumption during their production and installation. Mono-Si systems, with the highest energy demand for production and installation, have relatively highest EPBT in all locations.

The GHG emission factors and GHGPBT are shown in Figures 5.5. Figure 5.5 (left) shows that for very large geographical ranges the GHG emissions factors are around or below 20 gCO_2-eq/kWh, and for CdTe modules, large areas even show

emission factor around or below 10 gCO_2-eq/kWh due to high performance and low GHG emissions from manufacturing, while the monocrystalline silicon devices show the highest GHG emission factors, due to comparatively high GHG emissions from manufacturing. The highest GHG emissions are thus those associated with mono-Si modules in areas with low insolation, and are below 80 gCO_2-eq/kWh, and thus well below fossil fuel alternatives, even those equipped with carbon-capture-and-storage systems. For most locations and technologies the emission factor of PV is around or well below 30 gCO_2-eq/kWh.

Fig. 5.5 (right) shows that there is large variation in the GHGPBT. For countries with high grid emission factors, the GHG PBT can be very short (below 2 years). Especially for lower latitude countries and for CdTe systems, the GHGPBT can be below 0.5 years. Some countries with very low grid GHG emission factors, like France, Norway and Sweden, most technologies show GHGPBT of over 10 years, because the difference between the GHG emission factor of PV and that of the average grid electricity is very small. This is due to high shares of hydropower (Norway) or nuclear energy (France, Sweden). Because of its very low GHG footprint, CdTe still shows GHGPBTs below 10 years in some of these locations.

Figure 5.6 shows the variation of the obtained results (for annual yield, PR_{DC}, EPBT and GHG emission factor) for all locations, in order to generally compare the different module technologies. Shown here is the very large variation in annual yield, EPBT and GHG emission factors, while the variation in PR_{DC} is much smaller. The plots indicate that a large fraction of the locations have an annual yield above 1500 $kWh \cdot kW_p^{-1} y^{-1}$, for all module technologies, although especially for CIGS modules the mean annual yield is lower compared to the other technologies. For all technologies the majority of locations show GHG emission factors below 30 gCO_2-eq/kWh, and EPBT below 3 years. The distribution of PR_{DC} results for the poly-Si, CIGS and a-Si indicate that there is larger variation within the technology module groups, indicate by two distinct peaks in the distribution. For all three of these technologies, there was one module that showed consistently higher power outputs compared to the other modules.

5.4 Comparison of specific locations

Figure 5.7 shows a comparison of the annual energy yield and *PR* of the six studied module technologies in different specific locations around the globe: **1)** Utrecht, a city in the center of the Netherlands representative for north-western Europe, **2)** Seville, a city in the south of Spain representative for southern Europe, **3)** Aouzou, a village in Chad in the central Sahara, and **4)** Kinshasa and Brazzaville in the DR Congo and Congo respectively, in the tropics of central Africa, representing north-

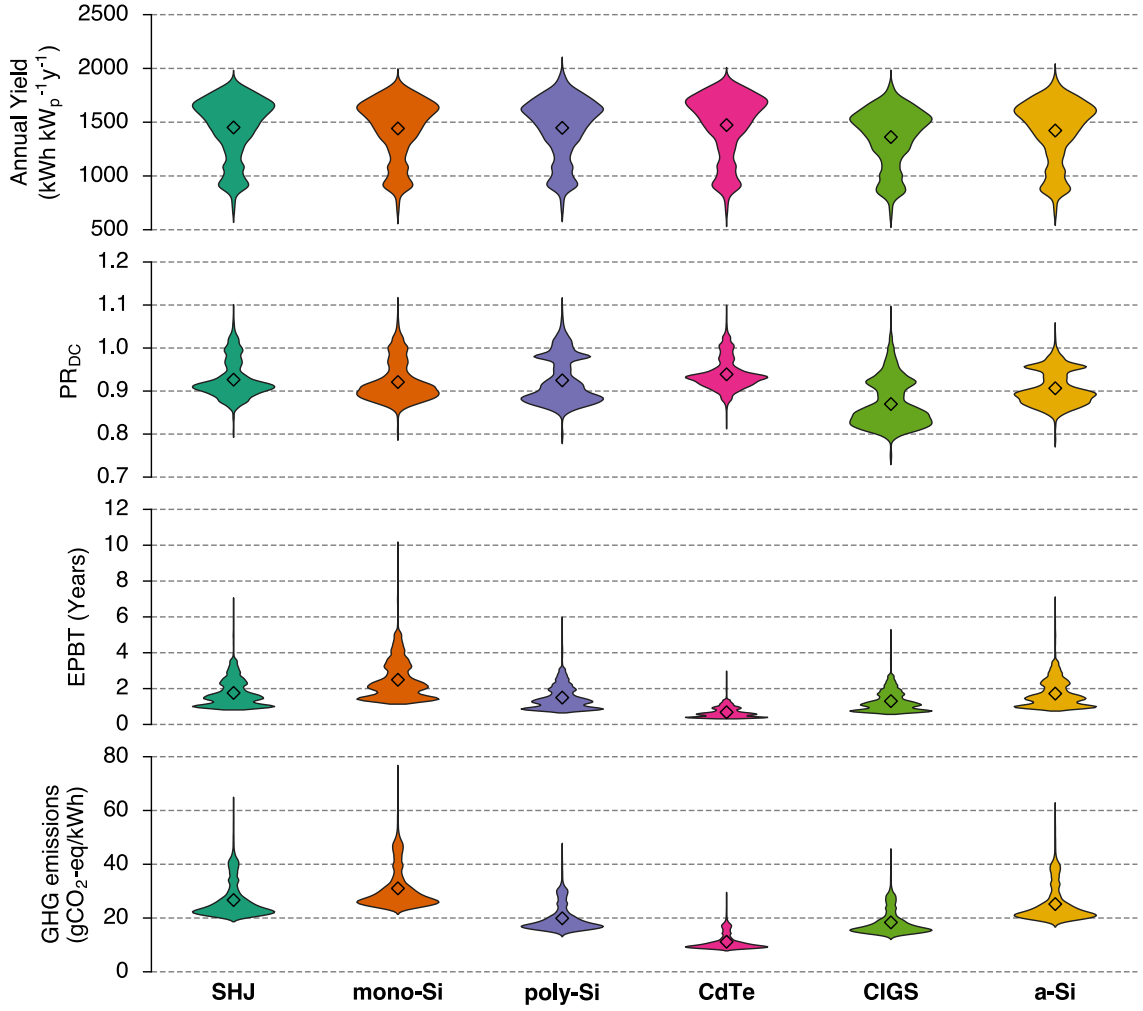

Figure 5.6 · Plots indicating the distribution of the obtained results, per technology, for all locations and modules, for annual yield, DC performance ratio, energy payback time (EPBT) and GHG emission factor. The diamond shaped markers indicate the overall means.

western European, southern European, desert and tropical climates, respectively. The yield is highest for the modules in the Sahara which has a very high annual insolation (see Fig. 5.1), and relatively low for the location in NW Europe. Although the southern European location is of much higher latitude compared to the tropics location, the annual yield is much higher, as this location is semi-arid, with a low degree of cloud cover. The figure also indicates the variation (min-max range) of performance modelled for each module type and location. It indicates that especially for the Sahara and Tropics location, the variation of modelled performance is significant, especially for the poly-Si and CIGS modules. The variation of modelled performance of the mono but especially the SHJ modules is very limited in all locations.

The performance ratio in Fig. 5.7 of the six module technologies shows that the relative performance (yield relative to annual insolation) is highest for the north-

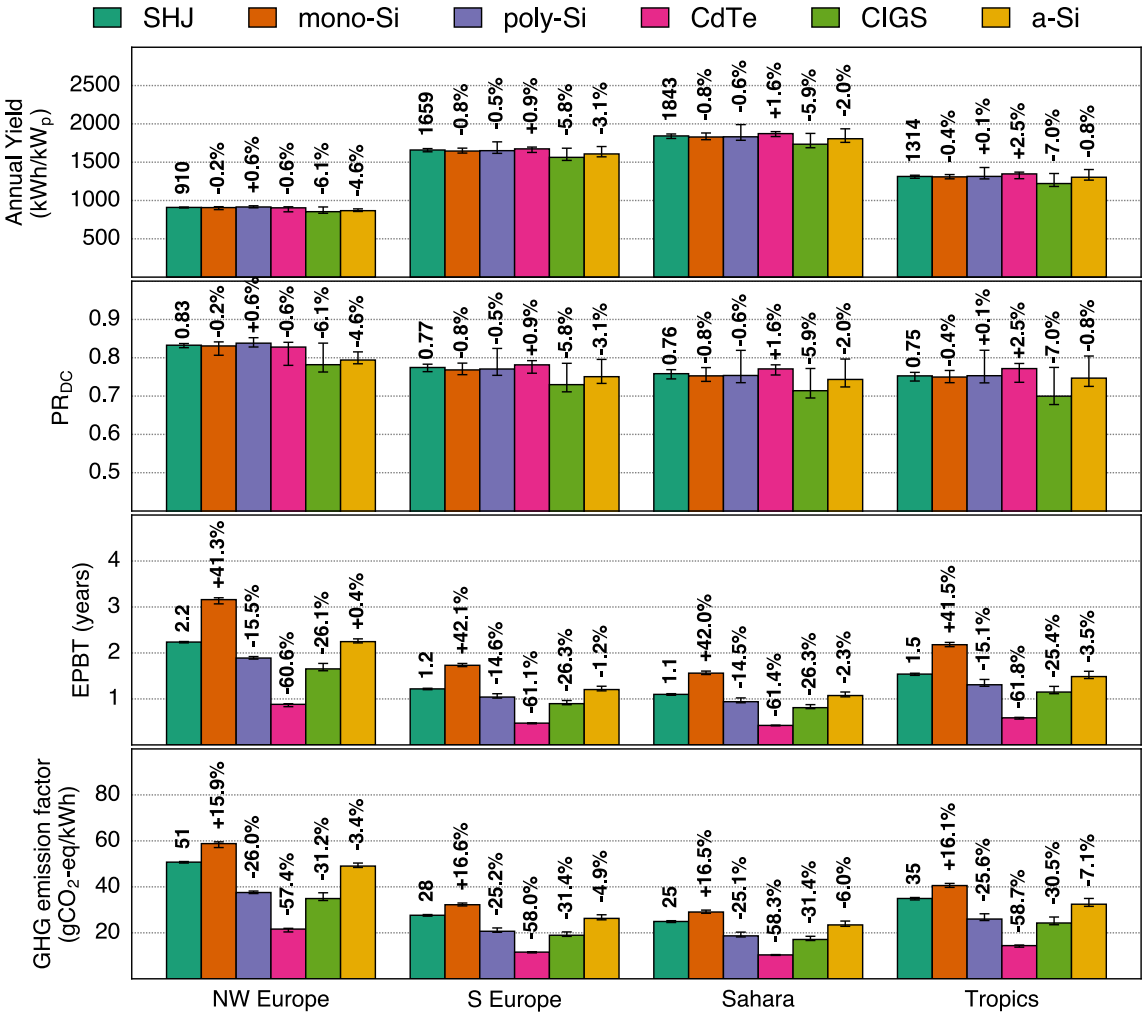

Figure 5.7 · Average annual yield, performance ratio, energy payback time and GHG emission factor of the six module technologies at four specific locations. The error bars indicate the minimum and maximum yield calculated for the eight modules for each module type and location.

western European location, and is around 0.83 for most technologies, but lower for CIGS and a-Si. The lowest PR_{DC} is modelled for the tropical location, which is characterised by high operating temperatures and a high degree of cloud cover. High operating temperatures also significantly decrease the PR_{DC} for the southern European and Saharan locations.

5.5 Discussion

In this paper we presented an analysis of the performance of PV systems based on different module technologies, to make the performance, in terms of energy yield and environmental performance geospatially explicit. Our results indicate that there is considerable variation of PV performance between module technologies, and considerable geographical variation in performance. The latter variation is not

only due to variations in the available solar irradiance at different locations, but also due to variations in operating conditions, mainly temperature.

Out of the six studied module technologies, cadmium telluride (CdTe) based systems seem to offer the best energy yield, and lowest environmental impact, in most locations, while the results of our modelling indicate that CIGS based systems show lower performance compared to the other module types over a broad geographical range. The results furthermore indicate that compared to conventional crystalline silicon modules (mono and poly), silicon heterojunction based systems offer a slightly increased performance, mainly due the smaller detrimental effect elevated operating temperature has on its power output. Especially at lower latitudes, the performance of SHJ modules is higher compared to mono- and poly-crystalline silicon based systems.

In terms of environmental impact, all module types show that they have short payback times, in terms of energy and greenhouse gas emissions, for most locations. At locations with low irradiance and/or locations with an efficient electricity grid or grids with high shares of renewable electricity, energy payback times are approaching ten years, while in some locations with very low grid emission factors, greenhouse gas payback times are over ten years. The greenhouse gas emission factors of all technologies is however below 80 gCO_2-eq/kWh for all locations, and below or around 30 gCO_2-eq/kWh for a broad geographical range. The environmental impact results are based on a lifecycle assessment study that analysed typical or average modules for each technology, and thus not necessarily represent any specific PV module of the same technology. Also, as is shown in [35], the production location, or rather the source of electricity used during production, has a pronounced effect on the environmental performance of PV.

A large part of the variation in the performance of PV at different locations can be attributed to variation in operating temperature. For our analysis, cell temperature was modelled based on the approach developed by Sandia National Laboratories for SAPM, and we assumed open-rack systems. Modelled cell temperatures are possibly lower compared to what would be measured for roof-mounted PV systems, which are also often used, especially in urban areas.

The results we have calculated here are based on assumed system losses, optimally oriented PV modules, and a yearly degradation rate of 0.67% for all studied module technologies. In practice, system losses, for instance due to soiling, shading, cabling and inverter losses could be higher. Furthermore, research has shown that some technologies have lower degradation rates than assumed here, while others exhibit higher degradation rates [208]. However, for some of the technologies studied, degradation rates and modes are not fully understood, or are calculated based on very small datasets as for some module types there is limited data with a

sufficiently large time range.

The comparison of the six PV module technologies is based on performance modelling of eight types of modules for each technology, and the results for each technology are based on the average performance of these eight modules. For some technologies, there is considerable variation between the eight analysed modules, while for other technologies this variation is very limited. Fig C.2 shows the variation (standard deviation) of the modelled annual energy yields for the different module sets. Especially the results for poly-Si and CIGS show much higher standard deviation compared to the other module sets, especially at high-irradiance locations. For SHJ, mono-Si, and CdTe the results of the eight studied modules are however very similar (low standard deviation). For CdTe this is likely due to the fact that all studied modules are from the same supplier, as there is a very limited amount of producers making CdTe modules.

5.6 Conclusions

Using the open source PV performance modelling tool PVlib-python, that implements the Sandia Array Performance model, and datasets of the global horizontal irradiance, air temperature and wind speed, we modelled the performance of six different types of PV modules for a broad geographical range including most of Europe, Africa and the Middle-East, and used the resulting figures for annual yield and literature data to calculate the environmental footprint of the studied PV module technologies over the described geographical range.

Our results indicate that for most locations, cadmium telluride PV modules offer the highest performance, although the difference with silicon heterojunction and mono- and polycrystalline silicon PV modules is small (within 2% yield difference). In our modelling results, a-Si and especially CIGS modules show considerably lower performance (4-8% in terms of annual electricity yield) compared to the other types of PV modules, over broad geographical ranges. When correcting for irradiance, performance of all module types was shown to have strong predominantly latitudinal variation, mainly due to differences in operating temperature. Annual yields of up to around 1850 $kWh \cdot kW_p^{-1} y^{-1}$ are attained in very sunny locations, while in North-West Europe yields of around 900 $kWh \cdot kW_p^{-1} y^{-1}$ are shown.

In terms of environmental impact the differences between the module types are greater, as the production of especially monocrystalline silicon wafer based PV modules is much more energy and greenhouse gas intensive than the production of thin film PV modules. As a result, the CdTe modules have lowest energy payback times (EPBT) and GHG emission factors. For all PV module technologies however,

EPBT is below 2 years and GHG emission factors are below or around 30 gCO_2-eq/kWh for large geographical ranges.

Acknowledgements

This research was funded by *Stichting Technologische Wetenschappen* within the FLASH *Perspectief* programme under project number 12172.

6

Re-assessment of net energy production and greenhouse gas emissions avoidance after 40 years of photovoltaics development

Published in: Nature Communications 7:13728 (2016)
doi: 10.1038/ncomms13728

Abstract Since the 1970's, installed solar photovoltaic capacity has grown tremendously to 230 gigawatt worldwide in 2015, with a growth rate between 1975 and 2015 of 45%. This rapid growth has led to concerns regarding the energy consumption and greenhouse gas emissions of photovoltaics production. We present a review of 40 years of photovoltaics development, analysing the development of energy demand and greenhouse gas emissions associated with photovoltaics production. Here we show strong downward trends of environmental impact of photovoltaics production, following the experience curve law. For every doubling of installed photovoltaic capacity, energy use decreases by 13% and 12% and greenhouse gas footprints by 17% and 24%, for poly- and monocrystalline based photovoltaic systems, respectively. As a result, we show a break-even between the cumulative disadvantages and benefits of photovoltaics, for both energy use and greenhouse gas emissions, occurs between 1997 and 2018, depending on photovoltaic performance and model uncertainties.

6.1 Introduction

Cumulative installed solar photovoltaic (PV) capacity (CIPC) grew from less than 1 MW in 1975 to around 180 GW at the end of 2014 [19, 209, 210], with a compound annual growth rate (CAGR) of 45%. As shown in Figure 6.1, major installation markets at the beginning of the 1990's were Japan and Italy, but from 2005 to 2014 Germany was the leading PV market in terms of CIPC [18]. It is expected that China will surpass Germany as the country with the largest CIPC during 2015 [211]. The strong growth can largely be attributed to successful government support schemes, like Germany's feed-in tariff, but also to rapidly falling prices of PV systems.

PV electricity has large social and governmental support, as during its operation no harmful emissions are released. Over the whole life-cycle of a PV system, it pays back the energy invested and greenhouse gas (GHG) emissions released during its production multiple times [35, 36, 101, 102]. As PV systems operate over a period of up to 30 years, there is a significant time-lag between the investments, in terms of cumulative energy demand (CED) and GHG emissions, and the benefits obtained due to delivery of electricity and replacement of high-environmental impact electricity from fossil fuel sources. Coupling the rapid growth of PV with this context of upfront investments has led to some concerns, regarding the PV industry's environmental sustainability. A fast growth of installed PV capacity could result in the creation of an energy sink, as the PV industry could embed energy in PV systems at a rate outpaced by these system's ability to deliver it back. The same can be true for GHG emissions, when the production of PV systems releases more GHG emissions than the electricity produced with PV can offset by replacing more GHG intensive electricity. Although there is evidence that shows that CED

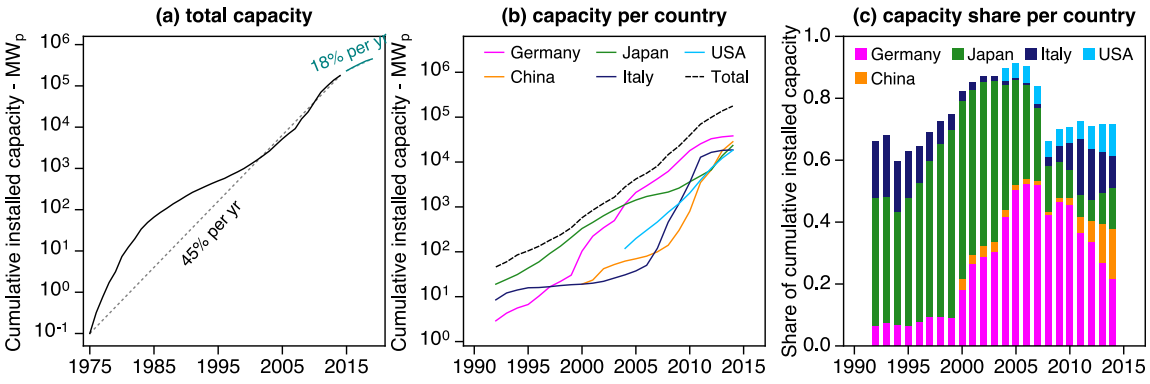

Figure 6.1 · Historical PV market developments. (**a**) Development of total Cumulative Installed PV Capacity (all PV technologies) from 1975-2014 with a CAGR of 45%; data taken from [19, 20, 185, 209, 210, 212], and expected development from 2015-2020 (CAGR: 18%, [209]). (**b**) Development of CIPC from 1992 - 2014 for 5 main markets; data taken from [19, 20]. (**c**) Development of total capacity share from 1993 - 2014 for 5 main markets; data taken from [19, 20].

and GHG emissions are correlated[56], this is not necessarily the case.

To avoid the creation of an energy and/or GHG sink, in general, the growth of the industry should be limited by $1/PBT$ [213, 214], where *PBT* (payback time) is the time in which upfront investments in either CED or GHG emissions are paid back. However, energy and GHG sinks from periods of growth exceeding $1/PBT$ can be offset by decreased growth rates (or decreasing *PBT*) in later stages. Thus, the dynamics of growth need to be taken into account, rather than always aiming for a $1/PBT$ limited growth, as is discussed by Emmott et al. [215]. The concept of the PV industry as an energy sink, and more recently GHG sink is well known in the PV community. Grimmer et al. [213] have been one of the first to address this issue in terms of energy, stating that to maximise the (positive) impact of solar technologies, they should have short energy payback time (EPBT) and long lifetime. When the growth of the PV industry started to accelerate, others indicated the necessity of strong decreases in energy payback time [214]. Others have also analysed the relation between industry growth and EPBT and concluded that for mono-crystalline PV, a sustainable growth rate should be limited to around 7% [216], however this result was based on a static measurement of the energy footprint of PV systems, and thus did not account for the decrease of the energy footprint of PV systems over time. More recent studies have also analysed GHG sinks [215, 217].

We review the development of environmental impact of production of PV systems over time, focusing on greenhouse gas emission and energy demand, and analysing only mono- and polycrystalline silicon based systems, as these cover over 90% of total installed capacity [185]. We gather results from a total of 40 life-cycle assessment (LCA) studies of PV systems (including inverters and support structure) conducted from 1976 to 2014, and couple these results to development of cumulative installed capacity figures, to show the development of energy demand and greenhouse gas emissions from PV production as a function of installed capacity, and to establish experience curves and learning rates [218] for these parameters. The models obtained are used in conjunction with scenarios on performance of PV in order to calculate net contributions of the PV industry as a whole, in terms of energy and greenhouse gas emissions, and to calculate when break-even between environmental investments and benefits occurs. A similar approach was used before by Dale and Benson [219], who focused on net electricity, and analysed studies in a narrower timeframe between 1990 and 2010. The authors concluded that cumulative break-even will occur somewhere before 2020. Other studies have focused on GHG emissions [215] even taking into account the gradual effect of GHG emissions on radiative forcing [217]. The latter two studies however focused on case studies or PV installation targets. Here, we want to combine approaches, by

taking into account actual PV industry growth, and analysing the environmental impact using LCA studies from a wider time period.

Here we show that there are strong downward trends for both energy demand and GHG emission from PV production, and that these trends follow the experience curve law. For every doubling of installed PV capacity, there is a decrease in energy use of 13% and 12% and in greenhouse gas footprint of production of 17 and 24%, for poly and monocrystalline based PV systems, respectively. As a result, there is a break-even since 2011 between the cumulative detriments and benefits of PV, in terms of both energy use and greenhouse gas emissions for a scenario that takes into account PV production location over time and a realistic PV performance scenario. Taking into account a worst-case PV performance scenario and model uncertainties, break even occurs in 2017 for net energy, and in 2018 for greenhouse gas emissions avoidance.

6.2 Results

6.2.1 Historical development of cost and environmental footprint

The development of cost and environmental footprint over the period 1975-2015 is shown in Fig. 6.2. Within this period, with an installed capacity increase from less than 1 MW to almost 180 GW, prices dropped from almost 100 USD/W_p to around 0.64-0.67 USD/W_p at the end of 2014.

Data for environmental footprint of PV systems does not go back that far, and furthermore shows a less clear trend over time. Still, especially for energy pay-back time (which is calculated from reported system CED according to the procedure described in the Methods section) a clear decrease of environmental footprint over

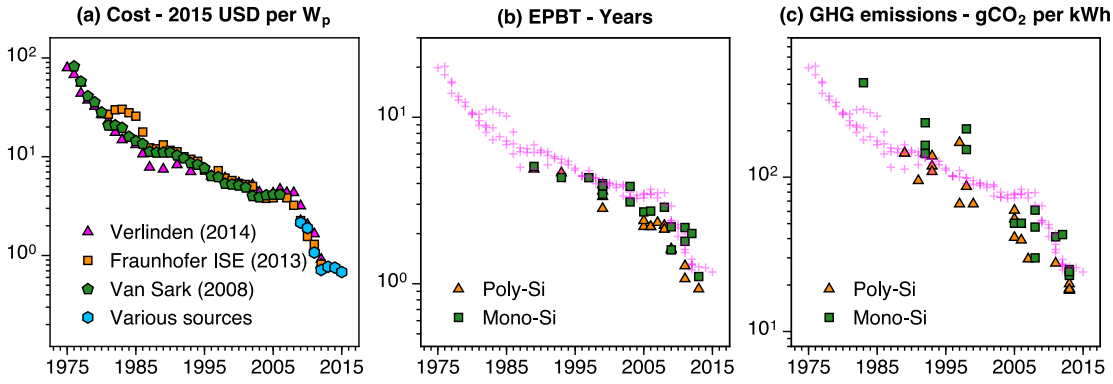

Figure 6.2 · Development of cost and environmental impact of PV. **(a)** Development of average module selling price over time, in 2015 USD per W_p. Data from [76, 185, 212, 220, 221].**(b)** Development of energy payback time over time. **(c)** Development of greenhouse gas emissions from PV electricity over time. The magenta crosses in (b) and (c) are an overlay of the cost data from (a).

time can be observed. Energy pay-back times drop from around 5 years in 1992 to around just under 1 year for poly-Si and just over 1 year for mono-Si PV systems currently [36]. Greenhouse gas emissions from photovoltaics, expressed in grams of CO_2-equivalent per kilowatt-hour (gCO_2-eq/kWh) , show large variations, even for studies analysing PV systems from the same year. This large variation is likely due to a variety of approaches in calculating the GHG emissions. More recent studies seem to use more congruent methods, resulting in a smaller variation of calculated GHG footprint. The current GHG footprint (harmonized data) is around 20 gCO_2-eq kWh^{-1} for poly-Si PV systems, and around 25 gCO_2-eq kWh^{-1} for mono-Si PV systems [36], down from 143 gCO_2-eq kWh^{-1} for poly-Si in 1992 [222] and 409 gCO_2-eq kWh^{-1} for mono-Si in 1986 [223]. For determining the EPBT and the GHG footprint per kWh of produced electricity, the energy yield of the systems, and thus insolation and consequently location, are of great importance. The values here refer to standardised conditions: insolation of 1700 kWh $m^{-1}y^{-1}$ and a performance ratio (*PR*) of 0.75, based on methodology guidelines from [44]. Recent meta-analyses of LCA studies on crystalline PV systems established average values for environmental footprint of PV systems, and found energy payback times to be 3.1 and 4.1 years for poly and mono-Si, respectively [224], based on studies conducted between 2005 and 2013. In a recent study Ferroni and Hopkirk [225] presented figures for energy return on energy invested that are equivalent to energy payback times that were much higher compared to what is found in other recent studies, or even much older studies. The study was not well received within the PV research community, and was found to severely lack in the applied methodology. For instance, the authors strongly overestimated the energy required for PV production, and at the same time underestimated the energy yield and lifetime of PV systems. A large group of leading PV scientists has written a critical response, for more details see [226].

Another meta-analysis found GHG emissions to be 44.3 and 79.5 gCO_2-eq kWh^{-1} for poly and mono-Si, respectively, based on studies from 2004 to 2014 [227]. Comparing this to the values mentioned earlier, that were reported for current PV systems by Wetzel [36], we see that the developments in the past decade have been so significant that the GHG footprint of state-of-the-art poly and monocrystalline silicon based PV systems is already 55% to 69% lower, respectively, compared to the averages of roughly the last decade (2004-2014) mentioned at the beginning of this paragraph.

6.2.2 Learning Rates

Figure 6.3 shows the data we have obtained for the average selling price of PV modules, and CED and GHG footprint of mono- and polycrystalline silicon-based PV systems, including inverter and support structure. It also shows the fitted experience-curve models, and an uncertainty range around this fitted model. As was established before [76, 185, 212], there is a very clear correlation between the price of PV and the cumulative PV production. In the price-experience curve in Fig. 6.3 we can observe two events: First, a price plateau appears when installed capacity was around 10 GW, due to a polysilicon feedstock supply shortage around 2008, and secondly, a strong drop of price is observed after this plateau to levels below the learning curve, due to oversupply of polysilicon and PV modules resulting from production capacity expansions. From 2012 onwards, prices have stabilised and are thus returning to values projected by the learning curve. Over the whole period, a learning rate of 20.1$\pm$0.5% can be observed (error bars refer to the standard deviation of the fitted parameter).

For CED, both technologies show a downward trend of CED *versus* installed capacity, with learning rates of 12.6$\pm$0.85% and 11.9$\pm$1.04% for poly and mono-Si systems. An earlier study indicates learning rates specific for rooftop and ground-mounted PV systems, a distinction not made in our analysis, and reports learning rates of 13% and 11% for ground mounted and 18% and 14% for rooftop-mounted poly and monocrystalline silicon based PV systems, respectively [228].

The quality of our fit is lower for CED compared to that for cost, likely due to a variety of methods employed to calculate the CED, such as different system boundaries or assumptions of energy usage during PV production. Especially over time these methods likely have changed considerably. However, many of the datapoints for CED also do not necessarily reflect a market average, contrary to the price data, but are often studies on specific producers, thus there is no convergence of the CED like there is for price in a globally operating PV market.

For greenhouse gas emissions from PV production, we also observe an even clearer downward trend for both technologies with increasing installed capacity, with learning rates of 16.5$\pm$2.31% and 23.6$\pm$1.86% for poly- and monocrystalline based systems respectively. As reflected by the higher errors in the learning rates and wider confidence intervals, the quality of the fit is somewhat lower compared to that for CED and especially cost, and would likely benefit from data that is more evenly spread over time. Especially for poly-Si, a large number of studies was performed between 1995 and 1999, after which there is a gap in the data between up to 2005. A more even dispersement of studies over a longer period of time would likely result in higher fit quality and lower parameter error. We observe

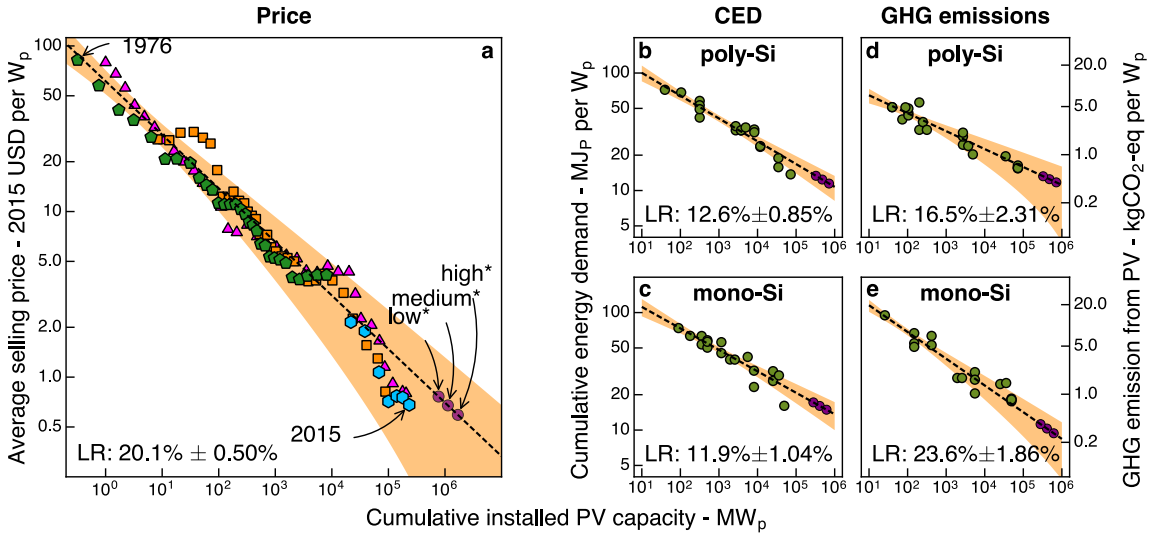

Figure 6.3 · Experience curves for cost and environmental footprint of mono- and polycrystalline PV modules and systems. **(a)** Experience curve for average module selling price. Magenta triangles: data from [76]; Orange squares: data from [185], Green pentagons: data from [212]; Blue hexagons: data from [220, 221]. **(b-e)** Experience curves for cumulative energy demand and GHG emissions from production of mono- and polycrystalline silicon based PV systems. The purple circles indicate the predicted cost, based on forecasted values of cumulative installed PV capacity for the year 2040. These values were obtained by adjusting the starting points of the 2014 IEA 'World Energy Outlook' [229] long term scenarios to the more recent 'Global Market Outlook for Photovoltaics 2015-2019' short-term scenarios [209]. **(a-e)** The experience curves are indicated by the dashed black lines. The shaded areas show a 95% confidence interval for the fitted models. **(d-e)** The graphs for GHG emission show data harmonised for lifetime and annual yield and degradation (right) as described in the Methods section.

a stronger learning rate for mono- compared to polycrystalline silicon-based PV systems. This is likely due to the fact that mono-crystalline silicon PV module production is more energy intensive, and thus benefits not only from energy usage reduction, but also, more than poly-Si, from reduction of the GHG footprint of energy used as input in the production processes, that occurs independently over time as show in the data from the UN [206] and the World Resources Institute[1].

6.2.3 Outlook for cost and environmental impact

The future development of PV is very difficult to predict, as every year of development seems to exceed our expectations. Forecasts for installed capacity in 2040 by the IEA in their World Energy Outlook 2014 range from 0.6-1.4 TW_p, figures we have adjusted to 0.7-1.6 TW_p based on more recent developments of installed capacity and short term forecasts [209]. Extrapolating the learning curves obtained from historical data to these cumulative PV capacity values, PV module costs are calculated to be 0.59 to 0.76 (2015 USD)W_p^{-1}, of which the high end of the range

[1] http://cait.wri.org

is actually well above current module factory gate selling prices of 0.68 USDW_p^{-1} for crystalline silicon modules [230]. This seems to confirm that current module prices are quite far below what we would have expected from about 40 years of price development.

For environmental impact, cumulative energy demand drops to 11.5-13.3 MJ_P W_p^{-1} for poly and 14.9-17.2 MJ_P W_p^{-1} for mono-crystalline based PV systems, equating to energy pay-back times of 0.8-0.9 and 1.0-1.2 years, respectively. Greenhouse gas emissions are extrapolated to drop to 0.40-0.49 and 0.27-0.37 $kgCO_2$-eq W_p^{-1} or 12-14 and 8.0-11 gCO_2-eq/kWh for poly- and monocrystalline systems, respectively. Note that in this latter case monocrystalline systems actually have lower environmental impact compared to polycrystalline systems, contrary to what is observed presently, due to the higher learning rate calculated. The projections indicate that in order to make such low GHG footprints possible, there is likely a need for a strong reduction of the GHG intensity of the energy inputs of PV production. Although many governments have put into place targets to achieve this, it remains to be seen if this will be the case.

6.2.4 Net Societal Contributions of PV

Figure 6.4 shows the development of net energy use and net avoided emissions, respectively, for the two PV performance scenarios, and for three production location scenarios (see Methods section). The solid curves show results for the 'Increasing *PR*' scenario, while the dashed curves show results for the 'Low *PR*' scenario. In the 'Increasing *PR*' scenario, *PR* of PV systems increases over time from 1975 to 2015 and remains constant thereafter, while in the 'Low *PR*' scenario, we assume a constant, worst-case *PR* (see Methods section). Figure 6.4a shows that a break even in terms of net primary energy has likely already occurred. Even for the 'Low *PR*' scenario, the mean simulation shows break-even before 2015. In the 'Increasing *PR*' scenario, break-even occurs before 2012 for all production location scenarios. For GHG emissions, break-even also has likely been reached already, during 2011 for the 'Increasing *PR*'/'Global Production' scenario combination. In the 'Low *PR*' scenario, break-even occurs during 2013. After the respective break-even points, the net energy output and emission avoidance increase rapidly. Considering we based the study on data for mono- and polycrystalline based PV system only, and the environmental footprint of other technologies is generally smaller [48], the break-even points possibly occur even sooner. We expect this effect to be small however, as the contribution of other technologies to total installed capacity has been and will likely remain limited to under 10%, and the effect on the environmental footprint of the total installed PV capacity will thus be small as well.

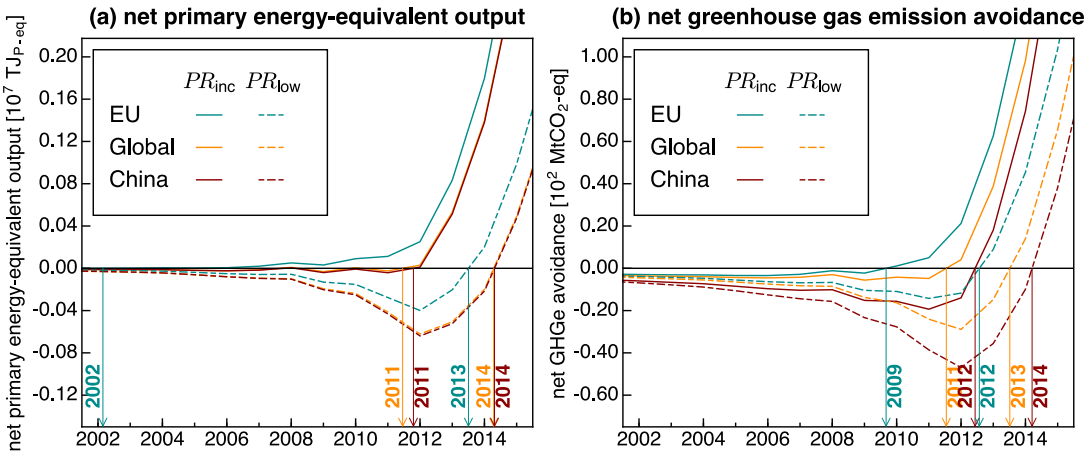

Figure 6.4 · Calculated cumulative net environmental impact of cumulative installed PV capacity. (**a**) Cumulative net energy output, in terajoules of primary energy equivalent. (**b**) Cumulative net greenhouse gas emissions avoidance, in megatonnes (Mt) of CO_2-equivalent. Results are shown for 2 PV performance scenario's: 'Increasing *PR*' and 'Low *PR*', and 3 production location scenarios (see Methods section).

We analysed the effect of uncertainty in the learning curve models by means of Monte Carlo analysis. The results, plotted in Fig 6.5, show that for the 'Global Production' scenario, break even in terms of energy occurs with a likelyhood of 95% between 1997-2015 and between 2009-2018 for the 'Increasing *PR*' and 'Low *PR*' scenarios, respectively. For GHG emissions, the respective ranges are 2001-2016 and 2005-2019.

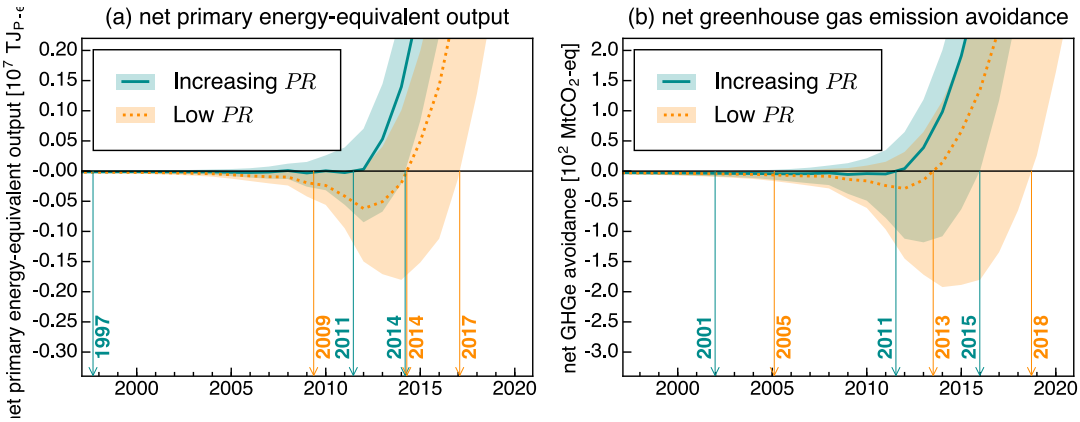

Figure 6.5 · Results of the Monte Carlo uncertainty analysis on the net contribution of PV. Results are shown for the 'Global Production' scenario and two PV performance scenarios. The solid curves show the mean simulation result, while the bands indicate a confidence interval of 95% around the mean simulation. (**a**) Monte Carlo simulation for cumulative net energy output. (**b**) Monte Carlo simulation for cumulative net greenhouse gas emissions avoidance.

6.3 Discussion

In this study we have analysed the development of the PV industry in terms of cost, cumulative energy demand, greenhouse gas emissions, and cumulative installed PV capacity. We have used this data to determine the net contribution of the PV industry in terms of CED and GHG emissions. Our analysis relies on a chain of (sometimes interdependent) data that can be difficult to accurately determine. For instance, development of cumulative installed PV capacity is not a measured quantity, but often rather estimated at country levels by performing surveys among select PV suppliers and extrapolating the resulting data. Some, but not all countries require registration of all installed PV systems and thus have more accurate data. The complete dataset is thus an aggregate of more and less accurate data.

Another main factor is the performance of PV systems over time, which is used to determine both the energy production and GHG emission avoidance of the total installed PV capacity. The performance of PV systems can be measured directly, or inferred from high-level statistics databases showing both installed PV capacity and generated electricity, such as the EIA[2] and UN databases [206]. The former are studies that result in detailed and accurate assessment of PV performance, but of a limited subset of PV systems. The latter can result in very unrealistic values for PV performance when the databases for PV capacity and PV electricity production are not aligned. For instance, for the year 1992 the calculated yield of PV systems from the UN database [206] in the US is over 17000 kWh kW_p^{-1}, while typical annual yields are currently in the range of 1400-1500 kWh kW_p^{-1}. Furthermore, in many cases PV electricity production is estimated from installed capacity figures by means of an estimate of the specific yield of PV capacity, rather than measured from actual production. As mentioned in the Methods section, this makes it difficult to ascertain the accuracy of the values for all countries and years. To address these issues we have analysed two performance scenarios (see Methods section): a worst-case and a realistic case. In Figure 6.6 we show a comparison between the different datasets for electricity production, installed capacity and inferred global average specific yield of PV capacity (kWh kWp^{-1}). Focusing on electricity production (Fig. 6.6a) we see that although the trends look very similar for the period between 1997 and 2014, our 'Increasing *PR*' scenario shows somewhat higher electricity production in the last years compared to the two databases, while the 'Low *PR*' scenario shows lower electricity production. The higher electricity production from the 'Increasing *PR*' scenario is partly due to the fact that the installed capacity numbers in both the EIA and UN databases are lower, compared to the data

[2] http://www.eia.gov/beta/international/browser/

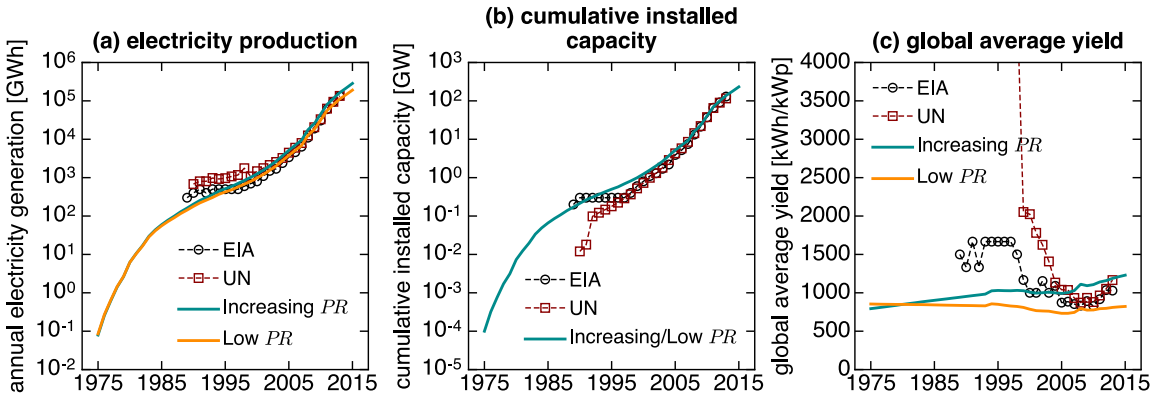

Figure 6.6 · Comparison of different PV performance data sources. (a) Comparison of the electricity generation as estimated by different sources of data: EIA database (http://www.eia.gov/beta/international/browser/), UN database [206] and 'Increasing *PR*' and 'Low *PR*' scenarios used in this study. (b) Comparison of the cumulative installed capacity from different data sources: EIA database, UN database and the data used in this study. (c) Comparison of the calculated global average electricity yield by using the different data sources or scenarios shown in (a) and (b).

we use in this study (shown in Fig. 6.1). Examining the yield inferred from the different datasources (Fig. 6.6c) we see that especially in the years before 2005 the EIA database but especially the UN database data results in unrealistically high average yield numbers. Furthermore it is shown that the time-range of the data is insufficient to cover the whole time horizon of our study. Taking into account the data from Fig. 6.6a, we argue that it is likely that the 'Increasing *PR*' and 'Low *PR*' scenarios cover a range of results that includes those that would be obtained by using one or both of the statistics databases.

For determining the net GHG emission avoidance, we need to make assumptions on what kind of electricity is used during production of PV systems, and replaced (or avoided) by produced PV electricity, and what the GHG emission factors are of both. For PV production, we assumed the use of average grid mixes of the producing countries. We have also assumed that electricity from PV replaced the average grid electricity mix. We deem this to be a conservative estimate, as new PV capacity (and other renewable electricity sources) is more likely to replace older, fossil fuelled power plants as they are decommissioned, mainly coal fired power plants [209], and thus avoided emissions could be larger. On the other hand, considering the timing of electricity production from PV, it could also replace electricity from more flexible sources of generation than baseline coal-fired power plants, such as gas fired power plants. As these are also often fossil fuel powered, especially in the major PV markets, we assume that using the grid average is a reasonable approximation. As the share of PV and other renewables in the electricity mix increases, the average grid GHG emission factor will decrease, and as a result, the GHG emission avoidance also decreases. Finally, increasing amounts of inter-

mittent electricity sources like PV will require either storage or back-up capacity. In the absence of sufficient storage capacity, back-up power plants, possibly fossil-fuel fired, might limit net GHG emission avoidance. Furthermore, storage options will contribute to the environmental footprint of PV electricity as their production of course requires the input of energy and materials, but they will decrease the requirement for back-up generation.

Our results show that from 1975 onwards, there are clear trends in reduction of cost, CED, and GHG emissions, concurrently with a rapid growth of installed PV capacity. While cost decreases with 20.1% for each doubling in capacity, CED decreases with 11.9-12.6% and GHG emissions with 16.5-23.6%. The rapid growth of the PV industry has resulted in the creation of a temporary net primary energy sink, as well as it being a temporary net emitter of GHG emissions. However, because of the trend of decreasing environmental footprint concurrent with the growth of CIPC, according to the 'Increasing *PR*' scenario, this debt was likely already repaid in 2011 for both CED and GHG emissions. For the worst case scenario, which is the 'Low *PR*' scenario, the 95% confidence interval shows break-even before 2018 for CED and 2019 for GHG emissions.

6.4 Methods

6.4.1 Data for cost, CIPC and environmental footprint of PV production

For the study conducted here we needed several different sources of data: **1)** historical data on the development of cumulative installed PV capacity (CIPC) including PV technology market shares, **2)** PV cost data for the period under investigation, **3)** forecast of the development of CIPC and PV technology market shares, **4)** life-cycle assessment (LCA) results for PV for the period studied.

Historical data for CIPC was obtained mainly from the IEA PVPS reports [18, 21, 231], reports from SolarPowerEurope (formerly EPIA) [209, 232] and other literature data [76, 185, 212]. Cost data was taken from [76, 185, 212, 220, 221]; all cost data in this paper is corrected for inflation by means of the Consumer Price Index [233] and expressed in 2015 USD. Data for PV technology market shares was taken from [185]. Environmental impact data was obtained from LCA studies conducted between 1976 and 2014, shown in the Supplementary Information in Supplementary Tables 1-5. Data was filtered only to exclude "worst-case" or "best-case" scenarios, prospective studies, and studies that did not include results for complete PV systems (see also Supplementary Methods).

For the studies on the energy payback time and greenhouse gas footprint of PV module production, it is sometimes difficult to ascertain in retrospect whether the

studies were performed using a consistent method, especially for the older studies selected here. Other meta-reviews of PV LCA's employ a stringent screening process eliminating most of the studies available [48, 88]. As we are interested in development of environmental footprint over time, a similar procedure would exclude most of the studies conducted before 2000. Therefore, we have adopted a simpler screening process: the LCA studies should report CED and/or GHG emissions for a complete PV system with enough meta-information to convert the reported units to our harmonised units (see section 6.4.2), and should analyse existing production processes (not prospective, worst or best case processes).

6.4.2 Harmonization of environmental footprint data

In the timeframe we are analysing, the environmental footprint of PV has been studied many times. The earliest study in our analysis dates from 1976, although most studies are from after 2000. The approach with which the environmental footprint of PV was determined has been steadily improving over the years. Only in 2009, standardised methodology guidelines specifically for PV systems were published [207] as a result of an IEA PVPS project specifically focusing on the environmental impact of PV (Task 12). These guidelines were updated in 2011 [44], although the practice of performing a Life Cycle Assessment (LCA) was standardised first in 1997.

For CED, we investigate megajoules of primary energy per watt-peak of PV system capacity (MJ_P/W_p). For GHG emissions, we analyse the GHG emission associated with the production of a watt-peak of PV system capacity (gCO_2-eq/W_p) but often report emissions per kWh of generated electricity as well (gCO_2-eq/kWh), as this is the unit most commonly used to express the GHG impact of PV. Where needed, conversion to the desired units was performed using harmonisation criteria based on LCA guidelines from [44]: a conversion factor from primary energy to electricity of 0.311; an insolation of 1700 kWh·m^{-2}·year; a performance ratio of 0.75; a module degradation rate of 0.7%/year; and the reported system capacity (W_p). The performance ratio *PR* is defined as [80]:

$$PR = \frac{Y_f}{Y_r} \tag{6.1}$$

where Y_f is the final energy yield of a PV system per unit of capacity, and Y_r is the reference yield per the same unit of capacity. Y_r is calculated as H_{POA}/G_{STC}, where H_{POA} is the plane of array irradiance, and G_{STC} the irradiance at which PV system capacity is determined (STC). Thus, the annual energy yield is given by:

$$E_{annual} = PR \times \frac{H_{POA}}{G_{STC}} \times C_{PV} \tag{6.2}$$

where C_{PV} is the system capacity. The ratio H_{POA}/G_{STC} gives us a figure that represents equivalent annual full load hours, and thus this calculation is not dependent on the efficiency of the PV systems investigated, but only the considered system capacity. The lifetime energy yield, corrected for the assumed (linear) degradation of performance is calculated as:

$$E_{\text{lifetime}} = E_{\text{annual}} \times T_{\text{lifetime}} \times \left(1 - r_{\text{deg}} \cdot \frac{T_{\text{lifetime}}}{2}\right) \tag{6.3}$$

6.4.3 Experience Curve

The production costs of PV decrease with increased cumulative production, based on the theory of technological learning. The relation between cost and cumulative units of production is described by the experience curve [234]:

$$C_n = C_1 n^{-a} \tag{6.4}$$

where C_n is the cost of the n-th unit of production, C_1 is the cost of the first unit of production, n is the cumulative production volume and a is the 'experience parameter' [218]. The 'experience parameter' describes the decrease in cost as a function of increased cumulative production. In the context of experience curves, there is often mention of the 'learning rate', which is the cost decrease for a doubling of cumulative production. This 'learning rate' can be obtained by rewriting equation 6.4:

$$C_n = C_1 n^{\log_2(1-l)} \tag{6.5}$$

where l is the 'learning rate'. The logarithm (base 2) in the exponent shows us that for each doubling of production volume, the cost of produced units decrease with a factor l. In this paper, we use this relation to establish the learning rate for PV price, CED, EPBT and LCGHG emissions, by performing orthogonal distance regression analysis of the environmental impact data to this non-linear model, using the open source Python library 'SciPy' [3]. Production volume for photovoltaics is most accurately reported in terms of cumulative installed PV capacity in watt-peak (W_p), so we will use this metric instead of cumulative number of produced units (cells, modules, systems). We have used the 'Delta method' to calculate confidence intervals for the fitted models [235].

As discussed in [218], the relationship between price and cumulative production is indirect (while that between production cost and cumulative production

[3] http://www.scipy.org

is direct), as market dynamics can influence the margin between cost and price. Only in a stable market phase does the price-experience curve have the same slope as a cost-experience curve [218]. However, as only price data is available for the period under study, we focus on the price-experience curve.

6.4.4 Production location

Both the production and installation location of PV influence its environmental impact. The production location mainly because the environmental impact of the electricity used in production is very locationally dependent, and as a result, production of PV in China has, for example, almost twice the GHG footprint compared to production in Europe [35, 236, 237]. For CED the difference is smaller but still significant. For installation, the environmental benefit of PV is larger where the environmental footprint of local electricity is greater, as it is assumed that the production of electricity from PV replaces electricity from fossil sources.

In our analysis, we have investigated the effect of production location in three scenarios: First, production in Europe; secondly, globally dispersed production, based on actual production location data from [185]; and thirdly, production in China.

To account for production location, we have combined data on the development of main PV production regions with the development of environmental impact of electricity production in those locations. For CED and GHG, we calculated a correction factor which is the average of the relative CED or GHG-footprint of electricity in each location, weighted by the share of production in each location. As the production has shifted from the US, to Europe and more recently to Asia (mainly China), this factor was calculated for each year. We also accounted for the development of the GHG-footprint of electricity over time, based on data from the UN [206] and the World Resources Institute [4]. No data was found suitable to include the development of CED of electricity over time, so the relative CED for each location was assumed constant over time and was based on [238]. For production in China, the factor is based on only the relative CED and GHG-footprint of Chinese electricity (over time). For production in Europe, the factors are set to 1, as the results from the environmental impact studies are mostly based on production in Europe.

[4] http://cait.wri.org

6.4.5 Projections and Net Contribution

From the data we have analysed we have established fitted models of development of CED, life cycle GHG emissions as a function of CIPC and their development over time. These models combined were used to calculate the total CED of PV production by integrating the learning curve. For instance, the environmental impact of production of a unit of PV in a certain year is given by:

$$EI_t(y) = \frac{\int_{y-1}^{y} EI_{1;t} \cdot C_t(y)^{\log_2(1-l_t)} dy}{C_t(y) - C_t(y-1)} \tag{6.6}$$

where $EI_{1;t}$ is the environmental impact of the first unit of production of technology t (see also C_1 in equation 6.4), C_t is the cumulative installed PV capacity of technology t in year y, and l_t is the learning rate of that technology. For each year, the environmental impact is calculated for mono- and polycrystalline silicon-based PV systems. To calculate the total annual environmental impact from PV we extrapolate the results for mono- and polycrystalline PV to total installed capacity, and for production location:

$$EI_{\text{released}}(y) = \sum_{t,i} EI_t(y) \times {}^{p}C_{t,i}(y) \cdot f_{EI;t;i}(y) \tag{6.7}$$

where ${}^{p}C_{t,i}(y)$ is the PV system capacity of technology t produced in country i in year y, and $f_{EI;t,i}(y)$ is a factor relating the environmental impact of production of PV in location i to the baseline results obtained from the learning curve, and is calculated as:

$$f_{EI;t;i}(y) = \left(\left(\frac{EI_{\text{elec};t;i}(y)}{EI_{\text{elec};t;\text{base}}} - 1 \right) \cdot f_{\text{elec};t;\text{PV}} + 1 \right) \cdot EI_t \tag{6.8}$$

where $EI_{\text{elec};t;i}$ and $EI_{\text{elec};t;\text{base}}$ are the environmental impact of electricity production in country i and the baseline scenario, respectively, and $f_{\text{elec};t;\text{PV}}$ is the fraction of environmental impact related to electricity use in production, taken from [239]. For GHG emissions EI_{elec} is calculated from databases from the UN [206] and the World Resources Institute [5], for CED historic data was not available, and we assumed a constant factor between countries based on data from the ecoinvent database [238]. Thus, we account for the effect of production location on environmental impact by varying the impact of electricity production. We assume here that direct electricity use in the lifecycle of PV production, from silicon to PV system, is changed from the baseline to the country average.

[5] http://cait.wri.org

The cumulative net environmental impact of PV is then calculated, for CED and GHG separately as:

$$EB_{\text{net;cumulative}} = \sum_{y=1975}^{y_{\text{end}}} EI_{\text{avoided}}(y) - EI_{\text{released}}(y) \tag{6.9}$$

where $EI_{\text{avoided}}(y)$ is calculated based on installed capacity shares from [19, 20, 22] and given by:

$$EI_{\text{avoided}}(y) = PR \times \sum_{i} \frac{H_i}{G_{\text{STC}}} \cdot C_{\text{active};i}(y) \cdot EI_{\text{elec};i} \tag{6.10}$$

where PR is the Performance Ratio, H_i is the population weighted plane of array insolation in country i, G_{STC} is the standard testing condition irradiance (1000 W/m^2), and $C_{\text{active};i}$ is the active installed PV capacity in country i. See also equations 6.1-6.2. The active capacity was calculated by correcting the cumulative installed capacity figures with an assumed degradation rate of 0.7% and a lifetime of 25 years.

The PR is an important metric relating the actual yield of a PV system to the theoretical yield calculated with just the annual insolation and the systems' rated (peak) power. It takes into account loss factors like higher operating temperatures, inverter and cabling losses, and other losses such as due to soiling, periods of outages, and suboptimal orientation. There likely is a trend of PR versus time, as increasing knowledge about and monitoring of PV performance, as well as improved system design and inverter efficiencies have led to a increase in system yields, as shown in [80, 240]. Accurate data on the actual performance of CIPC is however practically non-existent. There are in general two approaches in determining the actual PR of CIPC figure: a top-down analysis combining installed capacity figures with electricity production figures for PV installations, and a bottom-up, detailed analysis of PV performance using dedicated test facilities or a limited number of PV systems. Data for the former approach is readily available, but lacks in geographical and temporal scope. For instance, statistics from both the U.S. Energy Information Administration[6] and the UN statistics database [206] are insufficient to result in timeseries, from 1975 to now, of country-specific PR values, or other metrics that allow us to calculate historical energy generation from CIPC. The data goes back only to 1990, and for most countries, data is only available from 2010 onwards. Furthermore, especially for the older data, accuracy seems to be very low as unrealistic yield figures are obtained especially from the UN database (see also the Discussion section). Bottom-up studies result in very reasonable PR figures (around 75-85%) but their scope is even more limited (in terms of period

[6] (EIA, http://www.eia.gov/beta/international/browser/)

and geography). More recently, due to improved output monitoring of PV systems (e.g. by embedded monitoring solutions in PV inverters) the amount of available data has increased and studies are published on the performance of large numbers of privately owned PV systems [241, 242]. Unfortunately, the results from these studies are also (still) very limited in geographical but especially temporal scope, due to unavailability of older data. As *PR* is a very significant factor in determining annual yields, we have analysed two separate scenarios for the development of *PR* over time, which we consider represent a worst-case and more-likely scenario:

- A constant low-*PR* scenario with a *PR* of 0.5 based on the lowest estimate mentioned in literature referring to general PV performance.
- A increasing *PR* scenario, with *PR* increasing linearly with respect to time from 0.5 in 1975 to a maximum of 0.8 for the years 2015 and later, for all countries.

Aside from a trend in time for PR, there is also a variation of PR per location, as ambient temperature, but also spectral variations have effect on the performance of PV systems. Statistics on the actual performance of systems in all countries analysed, for the whole period studied, are however much too limited or inaccurate. Therefore we have assumed an equal *PR* for all locations.

Insolation data (H_i) was taken from [243]. We opted to use data that gives population-density weighted country insolation for surfaces with a fixed tilt and optimal orientation.We thus assume most systems to be installed in or near population centra, as is common at least in large parts of Europe. For some locations this might not be accurate. For instance, in the USA, large PV installations are built at locations in the South-West of the country, while population centres can be more confined to lower irradiance area's like the 'Boston-Washington Corridor', which has a population of almost 50 million, or 15.4% of the total US population.

6.4.6 Monte Carlo analysis

The parameters of the nonlinear models fitted to the data (EI_t and l_t in equation (6.6)) have a certain standard error as a result of deviation of the data from the fitted model, which are established by the fitting tool by determining the covariance of the fit parameters. We use Monte Carlo simulation to analyse the effect of these fit errors on our results. For each calculation, we generated 10,000 random samples of the parameters from a normal distribution for which the mean is the fitted parameter value and the standard deviation is the calculated error in the parameter. We then recalculated the results using these samples, and present the

intervals that cover the range from 2.5th percentile to the 97.5th percentile of the results, e.g. a 95% confidence interval around the main result.

Acknowledgements

This work was performed within “FLASH”, a *Perspectief* programme funded by Technology Foundation STW (www.stw.nl/en) under project number 12172.

7

Conclusions

7.1 Context

Our current energy supply systems relies heavily on fossil fuels. Because of this, we are releasing large amounts of CO_2 and other greenhouse gasses, distorting the natural carbon and GHG cycles, leading to a strong increase in the concentration of GHGs in our atmosphere. As a result, global land and ocean surface temperatures are rising at unprecedented rates, leading to severe problems like an increase in severe weather events, loss of biodiversity, and shrinking of polar icecaps and alpine glaciers. To limit the temperature increase and the problems originating from it, there is a strong need for decarbonisation of our energy supply, by increasing the efficiency of our energy system, and by shifting from energy sources with a high GHG intensity to sources with low associated GHG emissions. Thus we need to drastically increase the share of renewable sources in our energy supply, among which photovoltaics (PV) are a main technology.

In the last decade, the PV industry and markets have seen a dramatic growth. Installed PV capacity has grown from under 5 GW_p in 2005 to around 230 GW_p by the end of 2015. Major markets where PV is installed are China, Germany and Japan. Production of PV currently is located mainly in China and other South-East Asian countries. The cost of PV modules has dropped drastically from around 4 EUR/W_p in 2005 to well under 1 EUR/W_p in 2015, and as a result, PV is competitive with retail electricity prices in many countries, and in some countries the levelised cost of electricity of PV is even lower compared to fossil fuel generated electricity.

The strong growth of PV has resulted in it generating over 1% of our global annual electricity demand, while in some countries this share exceeds 7%. Projections for the development of installed PV capacity show that this figure will likely increase drastically in the coming years. As cumulative installed PV capacity is expected to increase from around 230 GW_p by the end of 2015 to 490-716 GW_p by the end of 2020. New PV technologies are being developed in order to keep increasing the energy conversion efficiency of PV modules and to achieve lower production costs. One of the promising technologies is the silicon heterojunction (SHJ) PV technology, which builds on experience in both crystalline silicon and thin-film PV technologies.

In this thesis, a broad ex-ante techno-economic assessment was performed of si-

licon heterojunction PV technology from multiple perspectives. The study included an analysis of the environmental, economic and energy performance aspects of SHJ PV cells and modules, and a study on the broader context of the development of environmental performance of the PV industry as a whole.

7.2 Answers to research questions

In this section the research questions defined in Chapter 1 are answered, by summarising the results from Chapters 2-6.

1) What is the life cycle environmental impact of different existing and conceptual SHJ cell designs and systems based thereon, and how do these compare to conventional crystalline silicon solar cells and systems?

In **Chapter 2**, the environmental performance of SHJ technology was analysed, for cells, modules and complete PV systems, for both current and prospective scenarios. A combination of pre-existing lifecycle inventories and newly gathered data for SHJ specific processes was used to determine the cumulative energy demand and GHG footprint of different SHJ cell designs, and modules and systems based on these cells. The newly gathered data was mainly obtained from the specifications of PV cell production equipment and previous research.

The results indicate that SHJ cells have comparable or lower environmental impact compared to conventional monocrystalline silicon solar cells, modules and systems. Based on an annual irradiance sum of 1700 kWh/m^2 and a performance ratio *PR* of 0.75 (resulting in an annual energy yield of 1275 kWh kWp^{-1}), it was determined that the energy payback time is 1.5 years, while the GHG emission factor was found to be 32 gCO_2-eq/kWh for the different SHJ cell based PV systems. For conventional monocrystalline silicon based systems, we find an EPBT of 1.8 years, and a GHG emission factor of 38 gCO_2-eq/kWh. A main factor determining the difference between SHJ and monocrystalline silicon is the increased conversion efficiency that is observed for SHJ solar cells.

Investigating the breakdown of environmental impacts, it shows that cell processing contributes relatively little ($\leq$ 6% for SHJ cells, 9-10% for c-Si cells) to the overall environmental footprint of PV systems. As a result, the differences between the SHJ designs, which have different cells but equal module layouts, are very small on a system level. Main factors determining the environmental footprint are the silicon feedstock (around 30%) the balance-of-system (BOS) components (around 30%) and the module materials (around 20%), for all SHJ designs and the c-Si reference, and for both EPBT and GHG emissions. Comparing cell processes for SHJ

cells it was found that vacuum based deposition (PECVD, sputtering) and metallisation contribute significantly to the environmental footprint of the cells because of high direct electricity use and use of high-footprint materials like silver, while the contribution of cleaning and texturing the wafers, and atmospheric-pressure deposition processes like ALD is much more limited. For modules it is shown that the slightly different structure of SHJ modules, which use conductive adhesive instead of solder for cell interconnection and a backsheet with an additional moisture protection layer, does not result in a large penalty in terms of environmental footprint, again mainly due to the higher efficiency of SHJ technology.

To investigate the sensitivity of the results to changes in certain parameters, a sensitivity analysis was performed, for which the change in the overall results was investigated, when we vary the energy yield (through variation in insolation, *PR* and module efficiency) and the GHG emission factor of the electricity used in the production of the PV cells and modules. The parameters affecting the energy yield had a most pronounced effect on the overall result, as both the EPBT and GHG emission factor of PV are proportional to $1/E_{\text{lifetime}}$, where E_{lifetime} is the lifetime energy output of the PV systems. The GHG emission factor of input electricity had a less strong but still significant effect on the overall results, especially when varying not only direct electricity inputs (cell and module production) but also indirect electricity inputs (silicon feedstock production). The data that was gathered for the SHJ cell production processes exhibited quite some variation in the energy consumption of the cell processing tools. Therefore, the effect of uncertainty in the energy consumption of screen printers, atomic-layer-deposition tools, TCO sputtering tools, PECVD reactors and wet etching equipment was investigated. While the effect of uncertainty in the energy consumption of these tools had a pronounced effect on the environmental footprint of the produced cells (with the uncertainty effect ranging maximally from -40% to +46% of the baseline results), the effect on the environmental footprint of the complete PV systems was very limited (-2.6% to +3.0%).

2) What are the production costs of different existing and conceptual SHJ cell designs and modules based thereon, and how do these compare to conventional crystalline silicon solar cells and modules?

In **Chapter 3**, the economic performance of SHJ technology was investigated, taking the information obtained for the analysis in Chapter 2, and again investigating a variety of SHJ cell and module designs, for current and prospective scenarios. The cell designs were refined compared to the designs studied in Chapter 2, based on new insights and feedback received. The LCI data from Chapter 2 was used to

attribute costs tot all material and energy flows occurring over the production cycle of the SHJ cells and modules, and again a comparison was made with conventional monocrystalline silicon cells and modules.

The results showed that the production costs for SHJ modules are comparable with c-Si module production costs. For current SHJ modules, the production costs were found to be 0.48-0.56 USD/W_p, while the cost calculated for the c-Si reference was found to be 0.50 USD/W_p. The variation in the production costs for the different SHJ cell designs was mainly a result of varying efficiency of these designs, and a variation in the amount (and type) of silver used to make the cell contacts. Because of the low-temperature processing required for SHJ cells, more silver is needed to achieve contacts without decreasing cell efficiency. As a result SHJ cells are generally more expensive compared to the c-Si reference. The increased efficiency of the SHJ designs compared to the c-Si reference was able to partly offset the more expensive cells, and also partly offset the slightly more expensive module materials needed for SHJ modules (silver-based conductive adhesive for cell interconnection and a different backsheet).

The sensitivity and uncertainty analysis showed that main parameters affecting the module production costs in USD/W_p are the wafer cost and module efficiency. The silver price also has significant effect on especially the SHJ designs, with the effect being almost as large or larger compared to variation in the price of all other consumables used during cell production.

3) How do prospective design changes in SHJ cell designs affect environmental impact and economics?

The environmental footprint analysis of prospective cell and module designs in **Chapter 2** showed that there is significant room for improvement of both the EPBT and GHG emission factor of SHJ and c-Si cells, modules and systems. With improvements in cell design, the EPBT can drop to below 1 year for SHJ and to 1.2 years for c-Si based systems, while the GHG emission factors drop to 20 and 25 gCO_2-eq/kWh, respectively. The improvement is mainly a result of increased prospective efficiency, but is also due to the use of thinner wafers and thus reduction of input silicon feedstock, and a shift from silver to copper based metallisation. In the prospective scenario, the contribution of especially BOS elements, which are for a significant part not scaling with module efficiency, is further increased to around 45% for the SHJ designs, and around 40% for the c-Si design.

In **Chapter 3**, the analysis of production costs of prospective designs showed that improvements in cell processing and module design could significantly lower production costs for all module types studied. Especially the substitution of silver

with copper based metallisation, increases in cell efficiency and the use of thinner wafers can strongly benefit SHJ cells, resulting in prospective production costs of 0.30-0.35 USD/W_p for modules. The module cost of the c-Si reference is less sensitive to silver paste consumption, which limited the potential for cost reduction, resulting in a prospective module cost of 0.33 USD/W_p. Replacement of indium-tin-oxide layers was not found to contribute substantially to a reduction in module costs.

4) How does the outdoor performance of SHJ modules compare to a variety of commercial alternatives?

Chapter 4 presents an analysis of the performance of SHJ modules and various other types of PV modules, to investigate the effect of variations in different operational parameters on the instantaneous, seasonal and annual performance and energy yield. PV module and weather condition measurements were gathered over the period July 2014 - December 2015, with measurements including current-voltage (IV) curves measured at 2 min. intervals and back-of-module temperatures for each PV module, plane-of-array, global-horizontal diffuse and direct normal irradiance, and spectral irradiance in the plane-of-array. The effect of variations (away from STC conditions) of irradiance, module temperature, spectral irradiance using average photon energy (APE) as a metric, and angle-of-incidence on the performance of the studied PV modules was studied, by filtering the complete dataset for each separate investigated parameter, and allowing only variation in one parameter, while the others were kept close to STC. Then curve-fitting of linear (for temperature) and non-linear (for the other parameters) models was performed with the dataset with least-squares regression. The models describe the instantaneous effect of a parameter on module performance, and were also used to investigate the seasonal and annual effect of the operating conditions on energy yield.

The results indicate that for the location investigated (Utrecht, the Netherlands), PV module performance was most affected by variations in irradiance and temperature, and the effect varies significantly between the different modules. Angle-of-incidence effects were smaller, largely due to the cloudy nature of the measurement location. Spectral effects were only substantial for one module type: the tandem a-Si module. Out of 8 modules investigated, 3 were positively affected by variations in operating conditions, while 5 were affected negatively, with the effect of variation in conditions ranging from -6% for a CIS module to +1.6% for a monocrystalline silicon module. The analysis indicated that the effect of certain parameters on module performance are not necessarily technology specific,

but rather depend on the module materials used, like the front cover glass, and packaging of the module (warm or cool package).

5) How does the performance of SHJ modules vary as a function of installation location, and how does the variation compare to a variety of commercial alternatives?

In **Chapter 5**, PV performance modelling was employed in conjunction with a large GIS irradiance and weather dataset to investigate the geo-spatial performance of six different PV module technologies, including an analysis of the environmental performance, in Europe, Africa and the Middle-East. The irradiance dataset contained global horizontal surface irradiance measurements on a 15-min time resolution, which was used in conjunction with various irradiance models to calculate the optimum tilt of a surface receiving the highest amount of annual irradiance. Subsequently, the PV performance modelling tool *PVlib-python* was used to calculate the performance of 6 different PV technologies (represented by 8 different modules for each technology) on these tilted planes, for every location in the GIS dataset, taking into account not only the irradiance characteristics on the tilted planes, but also cell temperature, which was modelled based on the irradiance, ambient temperature and wind speed datasets.

The results indicate that as expected a large geographical variation in the performance of PV was modelled, with the annual yield ranging from around 600 $\mathrm{kWh{\cdot}m^{-2}{\cdot}yr^{-1}}$ in Northern-European locations, to almost 2200 $\mathrm{kWh{\cdot}m^{-2}{\cdot}yr^{-1}}$ in locations in Saharan Africa and the Middle-East. When correcting for insolation, it was shown that the performance ratio is highest in Northern-European locations, and lower in locations with high irradiance, because of the detrimental effect higher operating temperatures have on the power output of PV modules. Temperature related losses are up to around 20% in hot regions, depending on the module type, while the coldest regions actually show temperature related *gains* in performance of up to 20%. The effect varied between the technologies because technologies like SHJ and CdTe have smaller temperature coefficients compared to, for instance, crystalline silicon and CIGS. The highest performance (in terms of annual energy output per unit of PV system capacity) is generally achieved with CdTe modules, closely followed by SHJ modules. The analysis was able to confirm the benefit of SHJ's smaller temperature coefficient, although the difference in energy yield compared to crystalline silicon is relatively small, especially in colder locations.

As a result of the geographical variations in performance, the environmental impact of PV also significantly varied over the studied regions. As the environmental impact is a function of $1/E_{\mathrm{lifetime}}$, the impact is highest in Northern locations,

and lowest in the locations with high annual irradiance and thus energy yield. For all module types and locations, the maximum GHG emission factor attributed to PV electricity was found to be under 80 gCO_2-eq/kWh, but roughly from Southern Europe downward, the emission factor is below 30 gCO_2-eq/kWh for all technologies. The lowest GHG emission factors are observed for CdTe modules, because of relatively high energy yields, and the lowest GHG emissions from manufacturing.

The trends for energy payback time (EPBT) are slightly more complicated. A local EPBT depends not only on the local energy yield, but also on the efficiency of the local electricity grid. It was assumed a kWh from PV replaces one from the average countrywide electricity mix, and this mix varies significantly from country to country. Thus, although, generally speaking, the EPBT decreases with increased energy yields in locations closer to the equator, it is also much higher in countries with large shares of hydropower (which has a very high efficiency from primary energy to electricity) compared to countries with large shares of especially fossil-fueled electricity production (which is generally of much lower efficiency from primary energy to electricity). Roughly the EPBT ranges between less than 0.5 years for CdTe modules in the Sahara, to around 8 years for monocrystalline silicon modules in Northern Europe. Similarly to EPBT, a GHG payback time (GHGPBT) was calculated, based on replacement of locally generated electricity by PV electricity. Here a similar issue was observed: countries with high shares of low-emission factor electricity had comparatively large GHGPBTs. In most countries and for all technologies, the GHG PBT is around or well below 2 years. However, in for instance France and Norway, where there are large shares of respectively nuclear and hydropower, the GHGPBT is around or well over 10 years, as it the average emission factor of existing electricity generation is lower or comparable to that of PV electricity.

6) What is the contribution of the PV industry in reducing the environmental impact of electricity generation, in terms of both energy and GHG emissions?

In **Chapter 6**, the broader context of the development of cumulative installed PV capacity, and the development of the environmental impact of PV was investigated. The aim was to analyse the development of the environmental footprint of PV coupled to the development of cumulative installed capacity, e.g. to construct *experience curves* for environmental footprint of PV. The analysis covered the period between 1975 and 2015. The experience curves would then be used to model the cumulative net environmental impact of PV, to see at which point in time a break-even would occur between the cumulative impact of PV production and the cumulated benefit of PV by means of electricity production. Furthermore, the study

took into account two different scenarios on the energy output of PV over time, and the locations where PV was manufactured and the development of manufacturing locations over time. For this study, a variety of data was gathered: historical data on the yearly development of cumulative installed PV capacity, historical data on the environmental impact of PV production, in terms of energy demand (CED) and GHG emissions, and historical data on the locations where PV was being manufactured.

The results of the analyses showed that there are clear downward trends in the environmental footprint of PV, for both mono- and polycrystalline silicon based PV systems. For every doubling of cumulative capacity, the energy demand of PV production decreases by around 13 and 12%, while GHG emissions drop by 17 and 24% for poly- and monocrystalline silicon based PV systems, respectively. The energy demand of PV production now is about ten times lower compared to 1975, while the GHG emissions from production have decreased by a factor 12.5-25. The strong growth of cumulative installed capacity resulted in a temporary energy sink and GHG emissions surplus from the PV industry, but already since 2011 we are most likely past a break-even point between the cumulative energy use and GHG emissions of PV production and the energy produced and GHG emissions avoided by electricity from PV systems. The latest break-even point from Monte Carlo uncertainty analysis and a worst-case PV performance scenario showed break-even in 2017 for energy, and 2018 for GHG emissions.

7.3 General conclusions

This thesis aimed to perform a comprehensive assessment of silicon heterojunction PV technology, from an environmental, economic and energy performance point-of-view. The research performed in Chapters 2 and 3 focused on getting a detailed inventory (life cycle inventory) of all the material and energy flows in and out of the production and life cycles of different SHJ cell designs, and using the resulting information to gain insight in the environmental footprint and economics of SHJ cells. The life cycle inventories obtained allow for identification of main contributions to the life-cycle environmental impact and overall production costs of different SHJ designs, and to compare these designs amongst each other and with conventional crystalline silicon PV. In terms of both cost and environmental impact, main contributions are formed by a few input materials. Both the monocrystalline silicon wafer, and the silver based metallisation of current SHJ designs contribute significantly, while the contribution of most other input materials is quite low, at least when referring to the cells only. Compared to reference crystalline silicon technology, SHJ technology benefits from high efficiency, but

especially for costs the higher amount of silver needed for the low-temperature metallisation means that SHJ cells incur a cost penalty. The shift from silver to copper based metallisation for prospective designs, increases in efficiency and enhanced material utilisation (less silicon per watt) results in significant decreases of both the environmental footprint and production costs of future SHJ solar cells and modules.

In order for SHJ technology to benefit from the simplified, low temperature production chain and high conversion efficiency, the performance of the technology needs to be comparable with or better than the available alternatives. In Chapter 2, the results for energy payback time and GHG footprint, of both the different SHJ designs and the conventional crystalline silicon reference design, are calculated based on an assumed PV system energy yield of 1275 $kWh \cdot kW_p^{-1}y^{-1}$ for all the designs investigated, based on a standardised methodology. In real operating conditions, the performance of different designs and PV technologies is affected by variations of the operating conditions from the standardised operating conditions that are used to establish the rated power output of PV systems. Chapter 4 shows that although there is significant variation between the performance of different types of PV, the SHJ modules that were tested performed very similar to both mono- and polycrystalline PV modules. However, these results are based on measurements at a specific location. In Chapter 5, the energy yield of different types of PV, including SHJ modules, was modelled for a broad geographical range. The results obtained here indicate that the difference in performance of SHJ modules compared to crystalline silicon modules is generally small, although there is some geographical variation. Especially in warmer climates, the SHJ modules benefit from the smaller negative effect of cell temperature on power output. The overall energy yield of modules is however a function of more parameters, like the module materials, degradation and soiling, so the difference in performance can be smaller than would be expected from the temperature effect alone.

The variation in PV module performance shown in Chapter 5 indicates that both the environmental footprint and cost of PV electricity is very dependent on installation location. A PV system installed in a Northern-European location has approximately 50% of the yield of a PV system in locations near the equator, due to the much lower solar insolation at higher latitudes. As a result, the environmental footprint also shows large geographical variation. The environmental footprint is however also affected by other local conditions (aside from operating conditions) as for instance the local electricity mix determines to what extent PV can contribute to reductions in GHG emissions.

The environmental footprint of the PV industry as a whole is not only determined by fixed measurements of the environmental impact of PV production and

estimations or measurements of energy yield from PV, but also by historical developments in both these parameters, and in the growth of the PV industry. Continued and fast growth of the PV industry could lead to large investments in terms of energy and GHG emissions, which could result or could have resulted in the creation of an energy sink or net GHG emissions instead of a positive energy balance and net reduction of GHG emissions. In Chapter 6, these considerations were taken into account, and the net energy production and GHG emission avoidance of the PV industry as a whole was investigated. The results indicate that although the fast growth of cumulative installed PV capacity resulted in a temporary negative contribution in terms of energy and GHG emissions, there is now already a break-even between these investments and the environmental benefits of producing electricity with PV, which is remarkable considering the very strong growth of installed PV in the last decade and the relatively minor contribution of PV to overall electricity generation. The energy payback time and GHG emission factor of PV electricity has decreased substantially over the last 40 years, and as a result, the positive contribution of the PV industry is now growing quite fast. Furthermore, at industry growth rates below 50% at the short-medium term, the net energy balance and GHG emission reduction from the PV industry will continue to grow.

The results of this thesis offer comprehensive knowledge on the environmental footprint, economics and energy performance of SHJ technology, and show how these parameters are interrelated and spatially dependent. The combination of results is not only valuable to gain insight in the technology, but, as the different parameters are interrelated, also necessary to assess whether the technology can contribute to improving the sustainability of our energy supply. The use of the combination of methods as employed in this work can be extended to any new technology contributing to the decarbonisation of our energy supply system.

7.4 Recommendations

- The accuracy of both life cycle assessments and cost calculations of PV cell and module designs relies heavily on good quality input data for life cycle inventories. PV manufacturers are generally not transparent about the production processes and material and energy in- and outputs.
  - Further research on these topics could benefit from cooperation of scientists from many disciplines related to PV, and also a strong(er) cooperation between PV manufacturers and the scientific community.
  - Policy makers should take into account transparency of PV manufactures when setting up incentive schemes for PV (and renewable energy technologies in general), to ensure manufacturers are encouraged to disclose information and critically look at their production cycles from an environmental point of view.
- The environmental footprint of PV varies significantly over time, which should be taken into account in scientific studies for several reasons.
  - When performing an LCA study it is important to realise that although (background) data might be considered quite new compared to other technologies, developments in the PV industry likely mean that complete life cycle inventories need to be updated at a minimum every 5 years.
  - Reviews or other studies trying to establish average PV GHG emission factors or EPBTs should critically look at the time-range from which studies are taken to calculate the average. Studies trying to reflect average environmental footprint of the currently installed PV based should use a larger time horizon but take into account weighting for when capacity was produced. Average emission factors for estimations of future energy systems should have a restricted time horizon (as recent as possible) or be based on other approaches like experience curves or prospective LCAs.
- The environmental footprint of PV depends on location because of variations in energy performance and because the environmental impact of PV production varies significantly with production location. Especially studies that take into account broad geographical and/or temporal ranges should take into account development of both installation and production locations. Installation and production location of PV should also be taken into account in scenario studies on future energy supply systems.

- In order to significantly reduce the environmental footprint of PV systems in the future, R&D focused on increasing cell and module efficiency and reducing production costs in the PV cell and module processing remain important. However, the impact of BOS elements, especially those not area-related, also should receive substantial attention, as the relative contribution of these elements to overall PV system environmental impact is increasing.

- The environmental impact of auxiliary technologies that enable high penetration of PV in electricity grids should be as critically analysed as the PV systems themselves. Technologies like electricity storage (battery or otherwise) and back-up electricity generation should ideally be included in LCA studies.

- The environmental impact of PV is not only determined during the production of PV, but also by the type of electricity that is being replaced. To measure the success of PV incentive schemes, both the increase in PV installations and electricity generation from PV, but also the associate decrease in other electricity technologies should be taken into account, including possible adverse effects like the use of more fossil fuel for back-up electricity generation in locations where more sustainable flexibility options (like hydropower) are not available.

- Further analyses of the sustainability of silicon heterojunction technology specifically, and PV technologies in general, should include an assessment of the resource availability of different materials used in the production of these technologies, taking also into account the projected or required growth of PV capacity that results from the demand to decarbonise our energy supply.

- Accurate data on the development of installed capacity and performance of PV allow for valuable studies on for instance the net contribution of the PV industry to increasing the sustainability of our energy supply, or calculating the total GHG emission reduction from country-wide PV installations. Especially the performance of PV is however poorly monitored in many countries. Efforts should be made to increase the accuracy of monitoring of both how much PV installed, and how these PV systems perform in real operation.

- The performance of PV systems in outdoor operation is affected by more parameters than current standardised testing procedures take into account. Manufacturers should work together with certification agencies to increase the availability of information for consumers and PV system installers to determine the real-life output of specific PV modules.

- The introduction of new technologies aiming to contribute to improving the sustainability of our energy supply, should as a minimum be preceded by a similar analysis as is performed in this thesis, that includes an assessment of the environmental footprint, economics and energy performance, and as these are interrelated, also an assessment of the spatial variation of these three parameters.

8

Nederlandse samenvatting en conclusies

8.1 Context

Ons huidige energiesysteem is voor een groot deel afhankelijk van fossiele brandstoffen. Als gevolg hiervan komen er momenteel grote hoeveelheden CO_2 en andere broeikasgassen vrij, wat resulteert in een ernstige verstoring van de natuurlijke koolstof- en broeikasgascycli. Dit leidt vervolgens tot een sterke toename van de concentratie van broeikasgassen in onze atmosfeer. Het gevolg hiervan is dat oppervlaktetemperaturen aan land en op de oceanen wereldwijd toenemen met een snelheid die niet eerder is vastgesteld, wat leidt to ernstige problemen zoals een toename van extreem weer, verlies aan biodiversiteit, en het krimpen van de ijskappen op de polen en gletsjers. Om de temperatuurstijging en de gevolgen daarvan te beperken, is het noodzakelijk dat we de energievoorziening minder broeikasgasintensief maken, door de efficiëntie van het systeem te verhogen, en door energiebronnen met een hoge broeikasgasemissie te vervangen door bronnen met een lage broeikasgasemissie. Hiervoor moeten we het aandeel van hernieuwbare energiebronnen in onze energievoorziening sterk vergroten. Zon-fotovoltaïsche (PV) energie is één van de belangrijkste hernieuwbare energiebronnen.

In het laatste decennium is de PV industrie en markt enorm gegroeid. De hoeveelheid geïnstalleerde PV capaciteit is toegenomen van minder dan 5 GW_p in 2005, tot ongeveer 230 GW_p eind 2015. De grootste markten qua installatie van PV zijn China, Duitsland en Japan. De productie van PV vindt met name plaats in China, en andere landen in zuidoost-Azië. De kosten van PV modules zijn sterk gedaald van ongeveer 4 EUR/W_p in 2005, tot ver onder 1 EUR/W_p in 2015, en als gevolg hiervan is stroom van PV systemen concurrerend met consumentenprijzen voor elektriciteit, en in sommige landen zijn de productiekosten van PV-elektriciteit zelfs concurrerend met de opwekking van stroom met fossiele brandstoffen.

De sterke groei van PV heeft er toe geleid dat meer dan 1% van de wereldwijde elektriciteitsproductie van PV afkomstig is, in sommige landen is het aandeel meer dan 7%. Prognoses voor de ontwikkeling van geïnstalleerd PV vermogen laten zien dat dit getal zeer waarschijnlijk snel zal toenemen in de komende jaren. Het cumulatief geïnstalleerd PV vermogen zal waarschijnlijk toenemen van ongeveer 230 GW_p eind 2015, tot 490-716 GW_p eind 2020. Nieuwe PV-technologieën worden ontwikkeld om de efficiëntie van PV-modules te vergroten en om lagere produc-

tiekosten mogelijk te maken. Een veelbelovende PV-technologie is de silicium heterojunctie (SHJ) technologie, waarin eigenschappen van zowel kristallijn silicium als dunne-film silicium worden gecombineerd.

Voor dit proefschrift is een brede, ex-ante techno-economische beoordeling van silicium heterojunctie technologie uitgevoerd vanuit meerdere perspectieven. Dit werk bevat een analyse van de milieuvoetafdruk, economische aspecten en energieopbrengst van SHJ PV cellen, modules en systemen, en een studie van de bredere context van ontwikkeling van de milieu-voetafdruk van de PV industrie als geheel.

8.2 Antwoorden op de onderzoeksvragen

In dit onderdeel worden de onderzoeksvragen zoals gedefinieerd in Hoofdstuk 1 beantwoord door de resultaten van Hoofdstukken 2-6 samen te vatten.

1) Wat is de milieuvoetafdruk van verschillende bestaande en conceptuele SHJ celontwerpen en systemen gebaseerd daarop, gegeven de volledige levenscycli, en hoe vergelijkt deze milieuvoetafdruk zich met conventionele kristallijn silicium cellen en systemen?

In **Hoofdstuk 2** is de milieuvoetafdruk van de SHJ technologie bestudeerd, voor zowel huidige als toekomstige SHJ cellen, modules en systemen. Er is gebruik gemaakt van een combinatie van reeds bestaande levenscyclus-inventarisaties, als nieuw verzamelde data voor SHJ-specifieke productieprocessen. Hiermee is de cumulatieve energiebehoefte en broeikasgasvoetafdruk bepaald voor verschillende SHJ celontwerpen, en modules en systemen die hierop gebaseerd zijn. De nieuw verzamelde data zijn vooral verkregen uit specificaties van PV celproductieapparatuur en gepubliceerd wetenschappelijk onderzoek.

De resultaten laten zien dat de SHJ technologie een vergelijkbare of lagere milieuvoetafdruk heeft vergeleken met conventionele monokristallijn silicium zonnecellen, modules en systemen. Gebaseerd op een jaarlijkse instralingssom van 1700 kWh/m^2 en een *performance ratio* (*PR*) van 0.75, laten de resultaten zien dat de energieterugverdientijd (EPBT) 1.5 jaar is, terwijl de broeikasgasemissiefactor 32 gCO_2-eq/kWh is voor PV systemen gebaseerd op de verschillende SHJ celontwerpen. Voor conventionele systemen gebaseerd op monokristallijn silicium werd een EPBT van 1.8 jaar en een broeikasgasemissiefactor van 38 gCO_2-eq/kWh gevonden. Een belangrijke verklaring voor het verschil tussen SHJ en monokristallijn silicium systemen is de verhoogde efficiëntie van de SHJ cellen.

Wanneer de opbouw van de resultaten wordt bekeken, wordt duidelijk dat de celproductie weinig bijdraagt aan de algehele milieuvoetafdruk ($\leq$ 6% voor SHJ

cellen, 9-10% for monokristallijn silicium cellen). Als gevolg daarvan zijn de verschillen tussen de SHJ ontwerpen klein op systeemniveau. Belangrijke factoren van de milieuvoetafdruk zijn de grondstof silicium (rond 30%) de systeemcomponenten (rond 30%) en de modulematerialen (rond 20%), voor alle SHJ ontwerpen en voor het monokristallijne referentiesysteem, zowel voor EPBT als broeikasgasemissies. Wanneer de celfabricage processes in detail worden beschouwd, word duidelijk dat vacuum verwerking (PECVD en *sputtering*) en celcontactering substantieel bijdragen aan de milieuvoetafdruk van de cellen aangezien bij deze processtappen veel direct electriciteitsgebruik plaatsvindt, en gebruikte materialen als zilver een hoge milieuvoetafdruk hebben. De bijdrage van andere processen, zoals het schoonmaken en textureren van de *wafers*, en processen die bij atmosferische druk plaatsvinden zoals ALD, is veel beperkter. Voor de modules zien we dat de SHJ ontwerpen een iets andere samenstelling hebben dan de monokristallijn silicium modules, aangezien een geleidende kleefstof wordt gebruikt in plaats van soldeer om de cellen onderling te verbinden, en er een onderlaag aan de achterzijde van de module wordt gebruikt die een additionele vochtbarriere heeft. Deze extra posten leiden echter niet tot een grote verhoging van de milieuvoetafdruk, wederom omdat de SHJ-technologie hogere efficiëntie kent.

Om de gevoeligheid van de resultaten voor variatie in bepaalde parameters te onderzoeken is een gevoeligheidsanalyse uitgevoerd, waarbij de verandering in de algehele resultaten wordt onderzocht als gevolg van veranderingen in de energieopbrengst en de broeikasgasintensiteit van de elektriciteit die gebruikt is bij productie van de PV-cellen en modules. Variaties in de energieopbrengst hebben de grootste invloed op de algehele milieuvoetafdruk, aangezien zowel de EPBT als de broeikasgasvoetafdruk proportioneel zijn met $1/E_{\text{levensduur}}$, waar $E_{\text{levensduur}}$ de energieopbrengst over de gehele levensduur is. De broeikasgasintensiteit van de elektriciteit voor productie van de cellen en modules had een minder sterk maar toch uitgesproken effect op de algehele resultaten, vooral wanneer niet alleen werd gevarieerd voor direct elektriciteitsgebruik tijdens cel- en moduleproductie, maar ook voor indirect elektriciteitsgebruik voor de productie van de silicium grondstof. De data verzameld voor de SHJ celproductieprocessen vertoonde redelijk wat variatie voor wat betreft het energieverbruik van de productieapparatuur, en daarom is ook een onzekerheidsanalyse uitgevoerd. Deze liet zien dat hoewel de onzekerheid in het energiegebruik van deze apparatuur een uitgesproken effect had op de milieuvoetafdruk van de celproductie (variatie van de resultaten van -40% tot +46% ten opzichte van de basisresultaten), was het effect op de resultaten voor complete systemen beperkt (-2.6% tot +3.0%).

2) Wat zijn de productiekosten van verschillende huidige en toekomstige SHJ celontwerpen en modules, en hoe vergelijken deze zich met conventionele kristallijn silicium zonnecellen en -modules?

In **Hoofdstuk 3** zijn economische aspecten van de SHJ technologie onderzocht, op basis van de informatie verzameld voor de analyse van Hoofdstuk 2, wederom voor diverse SHJ cel- en module-ontwerpen, voor zowel huidige als toekomstige scenario's. De celontwerpen zijn verfijnd ten opzichte van Hoofdstuk 2, op basis van nieuwe inzichten. De levenscyclusinventarisatie van Hoofdstuk 2 is gebruikt om kosten toe te wijzen aan alle materiaal- en energiestromen die plaatsvinden tijdens de levenscyclus van de SHJ cellen en modules, en wederom werd een vergelijking gemaakt met conventionele monokristallijn silicium cellen en modules.

De resultaten laten zien dat de productiekosten voor SHJ modules vergelijkbaar zijn met die voor monokristallijn silicium modules. Voor huidige SHJ modules worden de kosten vastgesteld op 0.48-0.56 USD/W_p, voor de monokristallijne referentiemodule op 0.50 USD/W_p. De variatie in productiekosten voor de SHJ modules is vooral een gevolg van de verschillende conversierendementen van deze ontwerpen, en de variatie in de hoeveelheid en het type zilver (pasta of *sputtering targets*) dat wordt gebruikt voor het vormen van de elektrische contacten op de cellen. Vanwege het lage-temperatuurproces waarbij de SHJ cellen worden gemaakt, is meer zilver nodig voor het vormen van deze contacten zonder rendement in te leveren. Als gevolg hiervan zijn SHJ cellen in algemene zin duurder, maar de verhoogde efficiëntie zorgt voor een (gedeeltelijke) compensatie voor deze duurdere cellen. Een andere nadelige factor voor de SHJ ontwerpen is dat de benodigde modulematerialen iets duurder zijn.

De gevoeligheids- en onzekerheidsanalyse liet zien dat de modulekosten met name afhankelijk zijn van variaties in de kosten voor de *wafers*, en de module-efficiëntie. De zilverprijs heeft ook een significant effect op met name de SHJ ontwerpen, waarbij het effect van variatie nagenoeg even groot is als de variatie in de kosten van alle andere tijdens celproductie gebruikte materialen.

3) Hoe beïnvloeden toekomstige veranderingen in SHJ celontwerpen de milieuvoetafdruk en productiekosten?

The analyse van toekomstige SHJ cell en module ontwerpen in **Hoofdstuk 2** toont aan dat er significante verbeteringsmogelijkheden zijn om de milieuvoetafdruk van de SHJ en monokristallijne cellen, modules en system te verlagen. Door verbetering in celontwerp en -efficiëntie daalt de EPBT tot minder dan 1 jaar voor SHJ en tot 1.2 jaar voor monokristallijn gebaseerde systemen, terwijl de broeikasgasemissiefactor afneemt tot respectievelijk 20 en 25 gCO_2-eq/kWh. Deze verbeteringen

zijn vooral het resultaat van toenemende efficiëntie, maar ook van het gebruik van dunnere *wafers* en dus het afgenomen gebruik van silicium, en een vervanging van zilver door koper voor de celcontactering. In het toekomstige scenario is de bijdrage aan de milieuvoetafdruk van systeemelementen (omvormer en installatiematerialen) die voor een aanzienlijk deel niet schalen met module efficiëntie, verder toegenomen tot ongeveer 45% voor de SHJ ontwerpen, en 40% voor het monokristallijn referentieontwerp.

In **Hoofdstuk 3** wordt uiteengezet dat de productiekosten van toekomstige celontwerpen sterk kunnen dalen voor alle bestudeerde modules. Met name de vervanging van zilver door koper voor de celcontactering, toename in celefficiëntie en het gebruik van dunnere *wafers* zijn van belang voor de SHJ ontwerpen, en resulteren in modulekosten van 0.30-0.35 USD/W_p. De productiekosten van het monokristallijn referentieontwerp zijn minder gevoelig voor zilvergebruik, waardoor het potentieel voor kostenreductie kleiner is, en toekomstige modulekosten van 0.33 USD/W_p kunnen worden bereikt. Vervangen van indium-tin-oxide blijkt geen sterk effect te hebben op de productiekosten van SHJ cellen.

4) Hoe verhoudt de energieopbrengst van SHJ modules onder operationele condities zich tot die van een variëteit aan commerciële alternatieven?

In **Hoofdstuk 4** wordt de energieopbrengst van SHJ modules en diverse alternatieven onderzocht om het effect vast te stellen van variaties in verschillende operationele parameters op de instantane, seizoensgebonden en jaarlijkse werking en energieopbrengst. Metingen van PV modules and weersomstandigheden van de periode juli 2014 - december 2015 werden verzameld, waaronder stroomspanning (IV) curves elke 2 minuten, moduletemperatuur per module, instraling in het vlak van de modules en op het horizontale vlak, diffuse en directe instraling en spectrale samenstelling van het licht in het vlak van de modules. Deze gegevens werden gebruikt om het effect van variaties in deze parameters ten opzichte van standaard test condities (STC) te bepalen door middel van het filteren van de complete dataset op waarden rond STC, en het variëren van iedere onderzochte parameter afzonderlijk. Vervolgens werden krommen gefit door middel van *de kleinste kwadratenmethode* om analytische, empirische modellen te koppelen aan het gedrag van de modules. Deze modellen beschrijven het instantane effect van variatie van elke parameter op de modulewerking, en werden ook gebruikt om het effect van variaties van de operationele condities op de seizoensgebonden en jaarlijkse energieopbrengst te bepalen.

De resultaten laten zien dat voor de bestudeerde locatie (Utrecht) de energieopbrengst van PV-modules met name wordt beïnvloed door variaties in intraling

en temperatuur, en dat het effect sterk kan verschillen voor de verschillende bestudeerde modules. De instralingshoek had een kleiner effect, vooral doordat op de bestudeerde locatie een hoog aantal metingen bij een hoge bewolkingsgraad werden gedaan. Effecten van de spectrale samenstelling van het licht zijn klein, behalve voor de dunne-film silicium module. Van de 8 bestudeerde moduletypen, werden er 3 positief beïnvloed door de variaties in operationele condities, terwijl 5 een negatief effect ondervonden. Op jaarbasis varieerden de effecten van -6% voor de CIS-module, tot +1.6% voor een monokristallijn silicium module. De analyse liet verder zien dat het effect van bepaalde operationele parameters niet zo zeer met de specifieke technologie te maken heeft, maar meer met de gebruikte modulematerialen, zoals het glas aan de voorzijde van de module, en de thermische opbouw van de module.

5) Hoe varieert de energieopbrengst van SHJ modules als functie van de installatielocatie, en hoe vergelijkt deze variatie zich met een variëteit aan commerciële alternatieven?

In **Hoofdstuk 5** wordt modellering van de energieopbrengst van PV, samen met een grote *GIS* instralings- en weerdataset gebruikt om de geospatiële variatie in werking, waaronder de milieuvoetafdruk, van zes verschillende PV-moduletypen te onderzoeken, voor Europa, Afrika en het midden-oosten. De instralingsdataset bevat instralingsmetingen op een horizontaal vlak met een tijdsresolutie van 15 minuten, welke met behulp van diverse instralingsmodellen werdt omgezet naar instralingswaarden in het optimaal georiënteerde vlak. Vervolgens werd het PV-modelleerprogramma *PVlib-python* gebruikt om de werking van 6 verschillende PV technologiën (vertegenwoordigd door 8 verschillende modules per technologie) in deze optimale vlakken te modelleren voor elke locatie in de *GIS*-dataset. Hierbij werd niet alleen de instraling, maar ook de celtemperatuur in acht genomen, die werd gemodelleerd op basis van de instraling, omgevingstemperatuur en windsnelheid.

De resultaten laten zien dat er zoals verwacht een grote geografische variatie in de energieopbrengst van de PV modules is, waarbij de jaarlijkse opbrengst varieert van 600 $kWh{\cdot}m^{-2}{\cdot}yr^{-1}$ op Noord-Europese locaties, tot bijna 2200 $kWh{\cdot}m^{-2}{\cdot}yr^{-1}$ op locaties in de Sahara en het Midden-Oosten. Wanneer er gecorrigeerd wordt voor instraling, zien we dat de *performance ratio* het hoogste is op Noord-Europese locaties, en lager op locaties met hoge instraling, vanwege het nadelige effect van hogere celtemperatuur op het geleverde vermogen van de PV modules. Temperatuurgerelateerde verliezen lopen op tot 20% in warme regio's, afhankelijk van moduletype, terwijl de koudste regio's temperatuurgerelateerde *toename* van ener-

gieopbrengst laten zien tot 20%. Het effect varieert per PV technologie aangezien technologiën als SHJ en CdTe een kleinere temperatuurcoëfficient kennen, ten opzichte van bijvoorbeeld monokristallijn silicium en CIGS. De hoogste energieopbrengst op jaarbasis wordt over het algemeen gemodelleerd voor CdTe modules, gevolgd door SHJ modules. Het positieve effect van de kleine temperatuurcoëfficient van SHJ modules werd aangetoond, hoewel de verschillen in energieopbrengst ten opzichte van kristallijn silicium modules relatief klein zijn, met name op koudere locaties.

Als gevolg van de geografische variatie in energieopbrengst, varieert ook de milieuvoetafdruk van PV modules significant binnen het bestuurde gebied. Aangezien de milieuvoetafdruk proportioneel is aan $1/E_{\text{levensduur}}$, is de voetafdruk het hoogst in noordelijke locaties, en het laagst op locaties met hoge jaarlijkse instraling. Voor alle module-typen en locaties is de maximale broeikasgasemissiefactor lager dan 80 gCO_2-eq/kWh, maar zuidwaarts vanaf ongeveer Zuid-Europa is de emissiefactor lager dan 30 gCO_2-eq/kWh voor alle technologiën. De laagste broeikasgasemissiefactoren worden gemodelleerd voor de CdTe modules, door relatief hoge energieopbrengsten en de laagste broeikasgasemissie tijdens fabricage.

De variatie in energieterugverdientijd (EPBT) zijn ingewikkelder te omschrijven. Een lokale EPBT hangt niet alleen af van de lokale energieopbrengst, maar ook van de efficiëntie van het lokale elektriciteitsnetwerk. In deze studie wordt aangenomen dat een kWh opgewekt met PV-systemen een kWh vervangt van de gemiddelde nationale energiemix, en deze energiemix varieert sterk tussen de landen. Daarom, al neemt de EPBT algemeen gezien af met toegenomen energieopbrengst op locaties dichter bij de evenaar, kan deze ook veel hoger zijn in landen met bijvoorbeeld een hoog aandeel waterkracht in de elektriciteitsvoorziening (aangezien waterkracht een hoge omzettingsefficiëntie heeft van primaire energie naar elektriciteit). Ruwweg varieert de EPBT tussen minder dan 0.5 jaar voor CdTe modules in de Sahara, tot ongeveer 8 jaar voor monokristallijn silicium modules in Noord Europa. Vergelijkbaar met EPBT is ook de broeikasgasterugverdientijd (GHGPBT) berekend, gebaseerd op vervanging van lokaal gegenereerde elektriciteit door PV-elektriciteit. Hier nemen we eenzelfde fenomeen waar als voor EPBT: landen met een hoog aandeel van lage-emissie elektriciteit hebben een relatief hoge GHGPBT. In de meeste landen, en voor alle technologiën, is de GHGPBT rond of ruim onder de 2 jaar. Echter, in bijvoorbeeld Frankrijk en Noorwegen, landen met een groot aandeel van respectievelijk kernenergie en waterkracht, is de GHGPBT rond of ruim boven de 10 jaar, aangezien de gemiddelde emissiefactor van de huidige elektriciteitsgeneratie vergelijkbaar is met die van PV-elektriciteit.

6) Wat is de toegevoegde waarde van de PV-industrie voor het reduceren van de milieuvoetafdruk van elektriciteitsopwekking, in termen van zowel energie als broeikasgasemissies?

In **Hoofdstuk 6** wordt de bredere context van de ontwikkeling van cumulatief geïnstalleerd PV-vermogen beschouwd, evenals de ontwikkeling van de milieuvoetafdruk van PV in het algemeen. Het doel was om, door de ontwikkeling van het cumulatief PV-vermogen te koppelen aan de ontwikkeling van de milieuvoetafdruk zogenaamde leercurves (*experience curves*) te bepalen, voor de periode tussen 1975 en 2015. De leercurves werden gebruikt om de cumulatieve milieuvoetafdruk van de PV-industrie als geheel te bepalen, om zo te kunnen nagaan wanneer de cumulatieve milieu-nadelen van productie van de systemen in balans zijn met de cumulatieve milieu-voordelen van de elektriciteitsopwekking uit deze systemen. Om de elektriciteitsopwekking te benaderen werden twee PV-energieopbrengstscenario's opgesteld. Bovendien werd er rekening gehouden met zowel de fabricagelocatie als de installatielocatie en veranderingen hierin gedurende de beschouwde periode. Er werd dus data verzameld over de historische ontwikkelingen van geïnstalleerd PV-vermogen, historische ontwikkelingen van de milieuvoetafdruk van PV (energiegebruik en broeikasgasemissies tijdens fabricage), en historische data over de fabricage- en installatielocaties.

De resultaten van de analyse laten zien dat er een duidelijke neerwaartse trend is van de milieuvoetafdruk van PV, voor zowel mono- als polykristallijn gebaseerde PV-systemen. Voor elke verdubbeling van het cumulatief geïnstalleerd vermogen, neemt het energieverbruik voor fabricage af met respectievelijk 13% en 12%, terwijl de broeikasgasemissies met 17% en 24% afnemen. Het energieverbruik tijdens PV-fabricage is nu ongeveer 10 keer minder dan in 1975, terwijl de broeikasgasemissies zijn afgenomen met een factor 12.5-25. De sterke groei van de PV-industrie en cumulatief geïnstalleerd PV-vermogen heeft geleid tot een tijdelijke situatie van netto energieverbruik en broeikasgasemissies vanuit de PV-industrie, maar in 2011 waren de milieu voor- en nadelen hoogstwaarschijnlijk in balans, en heeft de PV-industrie sindsdien een netto positieve bijdrage. In een Monte Carlo onzekerheidsanalyse voor een scenario waarin de PV-energieopbrengst zeer laag wordt ingeschat, vindt deze omslag op zijn laatst plaats in 2017 voor energie, en in 2018 voor broeikasgasemissies.

8.3 Algemene conclusies

Dit proefschrift had als doel het uitvoeren van een complete beoordeling van de silicium heterojunctie PV technologie, vanuit oogpunten als milieu, economie, en

energieopbrengst. Het onderzoek uitgevoerd in Hoofdstukken 2 en 3 richtte zich op het vaststellen van een gedetailleerde levenscyclusinventaris van alle materiaal- en energiestromen die plaatsvinden tijdens de productie van diverse SHJ ontwerpen, en het gebruiken van deze informatie om inzicht te krijgen in de milieuvoetafdruk en productiekosten. Met de inventaris is het mogelijk om de factoren vast te stellen die de grootste bijdrage leveren aan de milieuvoetafdruk en productiekosten voor de verschillende SHJ ontwerpen, en om de verschillende ontwerpen met elkaar en andere alternatieven te vergelijken. In termen van zowel kosten en milieuvoetafdruk overheersen enkele materialen voor het grootste deel de resultaten. De silicium *wafer* en het zilver gebruikt voor de celcontactering hebben een grote invloed, terwijl de invloed van andere materialen binnen het celproductieproces klein is. Vergeleken met de monokristallijn silicium technologie, heeft de SHJ technologie voordeel van de hogere efficiëntie, maar op de kosten heeft vooral het hoge zilvergebruik in de SHJ cellen een negatieve invloed. De vervanging van zilver door koper-gebaseerde celcontactering in toekomstige ontwerpen, toenames in cel-efficiëntie en verbeterd materiaalgebruik (minder silicium per watt) resulteren in significante afnames van zowel de milieuvoetafdruk als de productiekosten van toekomstige SHJ cellen en modules.

Als de SHJ technologie wil profiteren van het versimpelde, lage-temperatuur productieproces en hoge cel-efficiëntie, is het noodzakelijk dat de energieopbrengst van geïnstalleerde modules vergelijkbaar of beter is dan de beschikbare alternatieven. In Hoofdstuk 2 zijn de resultaten voor energieterugverdientijd en broeikasgasemissiefactor gebaseerd op een aangenomen standaard energieopbrengst van 1275 $\mathrm{kWh{\cdot}kW_p^{-1}y^{-1}}$ voor alle bestudeerde ontwerpen. Onder praktische operationele condities, wordt de energieopbrengst echter beïnvloed door variaties in omgevingsparameters die afwijken van de standaardcondities waarin modulevermogen wordt vastgesteld. Hoofdstuk 4 laat zien dat hoewel er duidelijke variatie is tussen de werking van diverse PV-technologiën, de SHJ technologie vergelijkbaar presteert met zowel mono- als polykristallijn silicium modules. Deze resultaten zijn echter gebaseerd op metingen op één specifieke locatie.

Daarom wordt in Hoofdstuk 5 een modellering uitgevoerd van de energieopbrengst van verschillende PV-technologiën voor een groot geografisch gebied. De resultaten van deze analyse laten zien dat het verschil in energieopbrengst tussen SHJ enerzijds en mono- en polykristallijn silicium anderzijds in het algemeen klein zijn, hoewel er wat geografische variatie is. Met name in warmere klimaten halen de SHJ modules voordeel uit het feit dat ze minder worden benadeeld door hogere werkingstemperaturen. De algehele energieopbrengst van PV-modules is echter afhankelijk van meer parameters, zoals modulematerialen, degradatie en vervuiling, dus het verschil in werking kan kleiner zijn dan wordt verwacht op basis van

het temperatuureffect alleen.

De variatie in de werking van PV-modules in Hoofdstuk 5 duidt aan dat zowel de milieuvoetafdruk als de kosten van PV-elektriciteit erg afhankelijk kunnen zijn van de installatielocatie. Een PV-systeem geïnstalleerd in Noord Europa heeft ongeveer 50% minder energieopbrengst dan een systeem nabij de evenaar, door de veel lagere zoninstraling op hogere breedtegraden. Als gevolg daarvan vertoont de milieuvoetafdruk ook significante geografische variatie. De milieuvoetafdruk is echter ook afhankelijk van andere lokale omstandigheden aangezien bijvoorbeeld de lokale elektriciteitsmix bepaalt in hoeverre PV-systemen kunnen bijdragen aan reductie van broeikasgasemissies.

De milieuvoetafdruk van de PV-industrie als geheel is niet alleen afhankelijk van vaste metingen van de milieuvoetafdruk van PV tijdens fabricage en schattingen of metingen van energieopbrengst, maar ook van historische ontwikkelingen in deze parameters en in de groei van de PV-industrie. Voortdurende en snelle groei van de PV-industrie veroorzaakt grote investering in termen van energie en broeikasgasemissies, wat vervolgens zou kunnen leiden tot een netto energieverbruik en netto broeikasgasemissie, in plaats van een positieve milieu-bijdrage van PV. In Hoofdstuk 6 worden deze overwegingen in beschouwing genomen en wordt de netto energieopbrengst en broeikasgasemissiereductie van de PV-industrie als geheel bepaald. De resultaten tonen aan dat hoewel de sterke groei van het geïnstalleerd PV-vermogen tot tijdelijke negatieve effecten heeft geleid, er nu reeds een omslag is geweest, en de PV-industrie als geheel een positieve milieubijdrage levert. Dit is opmerkelijk, gezien de zeer sterke groei van het cumulatief geïnstalleerde PV-vermogen in de laatste jaren en de nog zeer beperkte bijdrage van PV in de totale elektriciteitsvoorziening. De energieterugverdientijd en broeikasgasemissiefactor van PV is de laatste 40 jaar substantieel afgenomen, en als gevolg groeit de positieve milieu-bijdrage van de PV-industrie nu snel. Bovendien zal deze positieve bijdrage blijven groeien, mits op korte tot middellange termijn de groei van het geïnstalleerde vermogen beneden de 50% blijft.

De resultaten in dit proefschrift bieden brede informatie over de milieuvoetafdruk, economie en energieopbrengst van de SHJ technologie, en laten zien hoe deze parameters met elkaar verbonden zijn, en afhankelijk zijn van locatie. Het combineren van de resultaten is niet alleen waardevol voor het verkrijgen van inzicht in de technologie, maar, aangezien de verschillende parameters met elkaar verbonden zijn, ook noodzakelijk om te beoordelen of de technologie kan bijdragen aan een verduurzaming van onze energievoorziening. Het gebruik van de combinatie van methodes zoals in dit proefschrift kan dan ook worden toegepast voor elke nieuwe technologie die wil bijdragen aan de verduurzaming van onze energievoorziening.

Appendix A

Supporting information for Chapter 2

A.1 Impact Assessment

Following the IEA PVPS guidelines on LCA of PV systems, we assess the GHG emissions, the CED, and the EPBT of the various cell types studied. GHG emissions (gCO_2-eq/kWh) and CED (MJ_P/W_p) can be seen as indicators for a variety of environmental impacts. Life Cycle GHG emissions were assessed based on the IPCC 2007 report [55] The lifecycle GHG emissions are calculated by the software tool used (SimaPro) but can be represented by the following formula:

$$\mathrm{gCO_2\text{-}eq} \cdot \mathrm{kWh}^{-1} = \sum \frac{m_i \cdot GWP_i}{E_{\mathrm{lifetime}}} \tag{A.1}$$

where m_i indicates emissions (in grams) of substance i, GWP_i indicates the global warming potential (GWP) of substance i, and E_{lifetime} indicates the lifetime electricity production (in kWh) of the studied PV cell or system. For this analysis, all GHGs and their GWPs described by the IPCC in their latest assessment report [55] are taken into account. The energy payback time is related to the CED but expresses the amount of time in which an electricity source produces the same amount of primary energy that was used to produce it. The electricity delivered by the PV systems is converted to primary energy with an average grid efficiency factor as CED is also expressed in primary energy:

$$EPBT = \frac{E_{CED}}{E_{PV,annual}} \cdot \eta_{grid} \tag{A.2}$$

where E_{CED} is the CED for production of a PV system, module or cell, $E_{\mathrm{PV,annual}}$ is the annual electricity production of the considered PV system, module or cell and η_{grid} is the average grid conversion efficiency from primary energy to electricity (0.315, from ecoinvent [57]). The calculation of $E_{\mathrm{PV,annual}}$ depends on whether the analysis is for PV cells, modules or complete systems. For cells and modules, we express the CED per 1 m^2 so we calculate $E_{\mathrm{PV,annual}}$ by multiplying the yearly irradiation with cell or module efficiency and performance ratio (PR):

$$E_{\mathrm{PV,annual}}\ (\text{cells and modules}) = G \cdot A \cdot \eta_{\mathrm{conv}} \cdot PR \tag{A.3}$$

where G is the annual insolation, η_{conv} is the module area conversion efficiency, and PR is the performance ratio. For complete systems, for which we express the CED

per W_p, we calculate $E_{PV,annual}$ by multiplying 1W with the yearly amount of full load hours (yearly insolation divided by standard testing conditions irradiation) and the *PR*:

$$E_{PV;annual}\ (\text{systems}) = 1\text{W} \cdot \frac{G}{1000\text{W/m}^2} \tag{A.4}$$

A.2 PECVD process parameters

For our analyses of PECVD deposition of a-Si:H layers we have calculated total batch time, deposition time, and load-unload time with the data given in Table A.2. To calculate deposition vs. load-unload time, we assumed that the given throughput figures for each line were based on deposition of a 300 nm a-Si layer, which is a typical thickness for a-Si thin-film solar cells [70]. With given deposition rate and calculated load-unload time we were able to calculate the energy use of deposition of varying a-Si layer thickness with given average electricity consumption figures:

$$E_{\text{PECVD}}(x) = E_{\text{load-unload}} + \frac{x}{\xi_{\text{deposition}}} P_{avg} \tag{A.5}$$

where x is the layer thickness, $\xi_{\text{deposition}}$ is the deposition rate, P_{avg} is the average power consumption of the PECVD tool, and

$$E_{\text{load-unload}} = E_{\text{PECVD}}(300\text{ nm}) - \frac{300\text{ nm}}{\xi_{\text{deposition}}} P_{\text{avg}} \tag{A.6}$$

where $E_{PECVD}(300\text{ nm})$ was calculated as

$$E_{PECVD}(300\text{ nm}) = T_{\text{batch}} P_{\text{avg}} \tag{A.7}$$

where T_{batch} is the process time for a complete load-deposition-unload cycle as given for each PECVD tool in [61]. $E_{\text{PECVD}}(x)$ was calculated for each separate PECVD tool, and the mean of these values was used in our analysis. A similar approach was used to calculate water consumption. The process parameters are show in Table A.2.

A.3 Input data

Table A.1 · Process parameters of wet chemical etching. MSE indicates the standard error of the mean.

Parameter	Unit	Value	MSE	Remarks/references
Electricity consumption	kW	30	3.3	Average from [59]
Water consumption	L/h	1750	217	Average from [59]
Throughput	wafer/h	3160	36	Average from [59]
Wafer breakage	%	0.1	–	Average from [59]
Etchant usage[a]	mL/wafer	2	–	Limited data, conservative estimate based on specifications for 3 tools listed in Photon

[a] Etchant usage is not reported for the majority of the tools listed in [59]. For a limited number of tools approximate values were reported. We took a conservative estimate.

Table A.2 · Process parameters for PECVD of amorphous silicon thin films. MSE indicates the standard error of the mean.

Parameter	Unit	Value	MSE	Remarks/references
Throughput	m^2/h	37.7	8.3	Average from [61]
Deposition rate	nm/s	0.57	0.29	Average from [61]
Electricity consumption[a]	kW	204	67.7	Average from [61]
for 25 nm	kWh/m^2	3.33	0.57	Calculated
for 45 nm	kWh/m^2	3.47	0.55	Calculated
Water consumption[b]	L/h	21990	9590	Average from specifications listed in [61]
Silane consumption[c]	$mg/(nm\ m^2)$	32.3		Calculated from [52]
Hydrogen consumption[c]	$mg/(nm\ m^2)$	48.3		Calculated from [52]
Oxygen consumption[c]	$mg/(nm\ m^2)$	5.23		Calculated from [52]
NF_3 for chamber cleaning[d]	$g/(nm\ m^2)$	0.043		Calculated from [52]

[a] Electricity use for varying layer thicknesses was calculated based on the assumption that the electricity consumption and throughput values in [61] are valid for deposition of a 300 nm a-Si:H layer. With reported deposition rates and this assumed layer thicknesses we calculated deposition time and load unload time for the 300nm layer. To calculate deposition requirements for varying layer thicknesses we assumed load/unload times to remain constant, and deposition time and thus energy consumption to scale linearly with layer thickness. Equation A.5-A.7 show how we have calculated these values.
[b] Water consumption was assumed to be constant, as it is used for cooling and we assumed continuous operation of the tools. Therefore, water consumption for different layer thicknesses was scaled according to total process time (load/unload time + deposition time)
[c] Material use was taken from Van der Meulen *et al.* [52] and assumed to scale linearly with the thickness of the deposited layer
[a] The consumption and emission of NF_3 has been scaled to a-Si layer thickness based on the gas consumption and emission values and layer thicknesses reported in [52]. Here, we did not correct for utilization rate of the reactor.

Table A.3 · Process parameters for exhaust gas abatement. MSE indicates the standard error of the mean.

Parameter	Unit	Value	MSE	Remarks/references
Electricity consumption	kWh/h	1.62	0.58	Average from [82]
Water consumption	L/min	30	n.a.[a]	Average from specifications listed in [82]
Propane consumption	L/min	37.5	n.a.[a]	Average from specifications listed in [82]

[a] Insufficient sample size.

Table A.4 · Process parameters for TCO sputtering. MSE indicates the standard error of the mean.

Parameter	Unit	Value	MSE	Remarks/references
Throughput	m^2/h	90.6	5.4	Average from [62]
Utilization rate	%	74	1.3	Average from [62]
Electricity consumption	kW	565	113	Average from [62]
Electricity consumption[a]	kWh/m^2	6.3	1.25	Calculated
Water consumption	L/min	817	147	Average from [62]
ITO target consumption[b]	$mg/(nm\ m^2)$	17.13		Calculated

[a] Electricity consumption is calculated as the average of electricity consumption / throughput for the selected devices.
[b] ITO consumption is calculated based on the average utilization rate found in [62], ITO density, and divided by the mass fraction of ITO in the ITO target

Table A.5 · Process parameters for screen printing. MSE indicates the standard error of the mean.

Parameter	Unit	Value	MSE	Remarks/references
Throughput	wafers/h	1699	202	Average from [63]
Electricity consumption(a)	kW	5.5	0.98	Average from [63]
Electricity consumption	kWh/m^2	0.133	0.02	Average from [63]
Compressed air flow(a)	L/min	189	33.7	Average from [63]
Breakage	%	0.13	0.03	Average from [63]
Silver paste consumption[c]	mg/wafer	720		Based on [33, 57]

[a] Electricity consumption and compressed airflow are expressed as normalized values, corrected for throughput, normalized at 1700 wafers/h
[b] Silver paste consumption for metallization on both sides of the wafer was assumed to be 4 times that of a standard crystalline silicon solar cell front side metallization

Table A.6 · Process parameters for copper electroplating. MSE indicates the standard error of the mean.

Parameter	Unit	Value	Remarks/references
Throughput[a]	wafers/h	3000	[64]
Electricity consumption[a]	kW	100	[64]
Electricity consumption[a,b]	kWh/m^2	1.37	[64]
Water consumption[a]	L/h	100	[64]
Ni electrolyte consumption[c]	mL/m^2	23.9	Calculation
Cu electrolyte consumption[c]	mL/m^2	3.66	Calculation
Ag electrolyte consumption[c]	mL/m^2	0.56	Calculation

[a] Average copper plating specifications were based on the Meco DPL tool.
[b] The survey in [64] reported only maximum power consumption. Electricity consumption per unit of cell area was calculated based on continuous maximum power consumption. We consider this a conservative estimate, as the tool might - on average - operate at a lower power level.
[c] We calculated electrolyte consumption based on 1) the assumption that the plated grid pattern is similar to that of screen printed contacts; 2) the width of the plated gridlines is 50 µm [83] and 3) the thickness of the plated metals is 1 µm, 7 µm and 0.1 µm, respectively for nickel, copper and silver [84].

Appendix B

Input data for Chapter 3

Table B.1 · Equipment Cost. Variability refers to the standard error of the mean.

Tool	Avg Price (kUSD)	Variability (kUSD)	Avg Throughput (wafers/hr)	Variability (wafers/hr)	at 3600 wafers/hr Price (kUSD)	at 3600 wafers/hr Variability (kUSD)	Source
Diffusion Furnace	1915	287	2812	493	2707	251	[244]
SiNx PECVD reactor	1496	95	1760	157	3174	240	[111]
a-Si:H PECVD reactor	7325	5317	1763	588	5362	79	[61]
Spatial ALD	1948	477	2517	332	2866	263	[245]
Sputtering tool	6060	825	4059	456	5662	851	[62]
Screen printer	353	49	1669	176	732	64	[246]
Plating tool	1617	383	3900	900	1128	323	[64]
Tabber/stringer	495	142	1044	236	1832	420	[119]
Cell tester	156	14	2300	313	302	38	[122]
Cell sorter	737	132	2401	209	1055	134	[122]
Layup machine	212	8	2211	78	397	15	[121]
Laminator	446	34	1592	91	1208	100	[120]

Table B.2 · Texturing/Cleaning - Main input parameters.

Input	Unit	Ref-cSi	Ref-SHJ	PVD-SHJ	NE-SHJ	ALD-SHJ	IBC-SHJ
Hydrogen Fluoride	g/wafer		0.918	0.918	0.918	0.918	0.918
Sodium Hydroxide	g/wafer	3.820					
Hydrogen Peroxide	g/wafer		0.870	0.870	0.870	0.870	0.870
Hydrochloric Acid	g/wafer	1.110	0.581	0.581	0.581	0.581	0.581
Ammonia	g/wafer	0.164	0.212	0.212	0.212	0.212	0.212
Ethanol	g/wafer	0.156					
Isopropanol	g/wafer	1.920	1.920	1.920	1.920	1.920	1.920
Solvents	g/wafer	0.034					
Acetic Acid	g/wafer	0.068					
Nitric Acid	g/wafer	0.649					
Calcium Chloride	g/wafer						
Sodium Silicate	g/wafer						
Potassium Hydroxide	g/wafer						
Electricity	kWh/wafer	0.031	0.066	0.066	0.066	0.066	0.066
Compressed Air	m3/wafer	0.012	0.018	0.018	0.018	0.018	0.018
DI-water	kg/wafer	0.497	0.745	0.745	0.745	0.745	0.745
Process Yield		0.999	0.998	0.998	0.998	0.998	0.998

Table B.3 · Emitter Formation / Diffusion - Main input parameters.

Input	Unit	Ref-cSi
Phosphoryl Chloride	g/wafer	0.038
Phosphoric Acid	g/wafer	0.183
Argon	g/wafer	0.614
Oxygen	g/wafer	2.436
Nitrogen	g/wafer	44.291
Propane	MJ/wafer	0.1139
Electricity	kWh/wafer	0.0310
Process Yield		0.999

Table B.4 · PECVD - Main input parameters.

Input	Unit	Ref-cSi	Ref-SHJ	PVD-SHJ	NE-SHJ	ALD-SHJ	IBC-SHJ
Silane	g/wafer	0.029	0.039	0.039	0.102	0.020	0.059
Hydrogen	g/wafer		0.059	0.059	0.153	0.029	0.088
Oxygen	g/wafer		0.006	0.006	0.017	0.003	0.009
Ammonia	kg/wafer	0.000					
Shadow-Mask	pc/wafer						0.001
Electricity	kWh/wafer	0.080	0.160	0.160	0.174	0.080	0.240
Cooling Water	L/wafer	4.79	9.59	9.59	10.93	4.79	14.38
Process Yield		0.999	0.999	0.999	0.999	0.999	0.972

Table B.5 · ALD - Main input parameters

Input	Unit	ALD-SHJ
TMA	g/wafer	0.0046
Oxygen	g/wafer	0.2090
Nitrogen	g/wafer	0.0027
Electricity	kWh/wafer	0.0069
Cooling Water	L/wafer	0.5523
Process Yield		0.9994

Table B.6 · TCO Sputtering - Main input parameters.

Input	Unit	Ref-SHJ	PVD-SHJ	NE-SHJ	ALD-SHJ	IBC-SHJ
ITO target	g/wafer	0.0317	0.0317	0.0158	0.0158	0.0158
ZnO target	g/wafer				0.0263	
Shadow-Mask	pc/wafer					0.0003
Electricity	kWh/wafer	0.1506	0.1506	0.1506	0.1506	0.1506
Cooling Water	L/wafer	12.232	12.232	12.232	12.232	12.232
Process Yield		0.999	0.999	0.999	0.999	0.974

Table B.7 · Metallization - Main input parameters.

Input	Unit	Ref-cSi	Ref-SHJ	PVD-SHJ	NE-SHJ	ALD-SHJ	IBC-SHJ
Silver paste	g/wafer	0.167					
Silver paste low temp	g/wafer		0.500	0.250	0.250	0.250	
Al paste	g/wafer	1.400					
Ag target	g/wafer			0.069	0.069	0.069	0.138
Electricity	kWh/wafer	0.013	0.013	0.088	0.088	0.088	0.075
Compressed Air	m3/wafer	0.027	0.027	0.027	0.027	0.027	
Process Yield		0.997	0.997	0.998	0.997	0.997	0.973

Table B.8 · Module Assembly - Main input parameters.

Input	Unit	Ref-cSi	Ref-SHJ	PVD-SHJ	NE-SHJ	ALD-SHJ	IBC-SHJ
Conductive Adhesive	g/module		3.60	3.60	3.60	3.60	1.80
Standard Backsheet	m^2/module	1.63					
HIT Backsheet	m^2/module		1.63	1.63	1.63	1.63	
IBC Backsheet	m^2/module						1.63
EVA	m^2/module	3.27	3.27	3.27	3.27	3.27	3.27
Glass	m^2/module	1.63	1.63	1.63	1.63	1.63	1.63
J-Box	pc/module	1.0	1.0	1.0	1.0	1.0	1.0
Stringing/Tabbing	pc/module	1.0	1.0	1.0	1.0	1.0	1.0
Frame	pc/module	1.0	1.0	1.0	1.0	1.0	1.0
Electricity	kWh/module	3.00	3.00	3.00	3.00	3.00	3.00
Process Yield		0.974	0.974	0.974	0.974	0.974	0.974

Table B.9 · Prices of input consumables.

Consumable	Price (USD)	Unit	Source
Acetic Acid	0.51	kg	[247]
Aluminium Frame	13.48	module	Market survey
Aluminium paste	0.052	g	[248]
Aluminium target	0.10	g	Own calculations
Ammonia	9.50	kg	Market survey
Argon	0.22	kg	[248]
Backsheet, HIT	7.00	m^2	Own estimate
Backsheet, standard	5.03	m^2	Market survey
Backsheet, structured IBC	10.00	m^2	[124]
Boron Trifluoride	4.42	g	[249]
Calcium Chloride	1.00	kg	Own estimate
Compressed Air	0.02	m^3	[248]
Conductive Adhesive	1.04	g	[124]
Cooling water	0.24	m^3	[248]
Cu paste	0.59	g	Own calculations
Cu paste HT	0.43	g	Own calculations
Cu plate solution	3.7	L	Own calculations
Cu target	0.05	g	Own calculations
DI-water	3.0	m^3	[248]
Electricity, general	0.10	kWh	Own estimate, for cell and module production
Electricity, hydro	0.025	kWh	Own estimate, for silicon production
Electricity, cogen	0.07	kWh	Own estimate, for silicon production
Ethanol	10.00	kg	Own estimate
EVA	1.85	m^2	Market survey
Fluid waste treatment	0.02	L	Own estimate
Hydrochloric Acid	6.2	kg	[248]
Hydrogen	1.4	kg	[248]
Hydrogen Fluoride	1.08	kg	[247]
Hydrogen Peroxide	1.48	kg	[247]
Isopropanol	10.65	kg	[250]
ITO target	0.85	g	Own calculations
J-Box	6.50	piece	[33]
Monocrystalline silicon wafer	1.03	piece	Own calculations
Nickel plate solution	0.05	mL	Own calculations
Nitric Acid	0.23	kg	[247]
Nitrogen	0.28	kg	[248]
Oxygen	0.65	kg	[248]
Phosphoryl Chloride	450	kg	[248]
Propane	0.011	MJ	[251]
Shadow-Mask	100	piece	Own estimate
Silane	0.070	g	[248]
Silver paste	0.82	g	Own calculations[a]
Silver paste low temp	1.06	g	Own calculations[b]
Silver plate solution	0.085	mL	Own calculations
Silver target	0.89	g	Own calculations
Sodium Hydroxide	1.94	kg	[247]
Sodium silicate	0.50	kg	Own estimate
Solar glass	5.5	m^2	Market survey
Solvents	10.00	kg	Own estimate
Stringing/tabbing and bussing ribbons	2.50	module	[33]
Titanium Dioxide	2.26	kg	[247]
Trimethyl aluminium (TMA)	2.3	g	[252]
ZnO target	0.05	g	[250]

[a] Based on silver content of 60%, silver price and paste price in [33].
[b] Based on silver content of 80%, silver price and paste price in [33].

Appendix C

Supporting information for Chapter 5

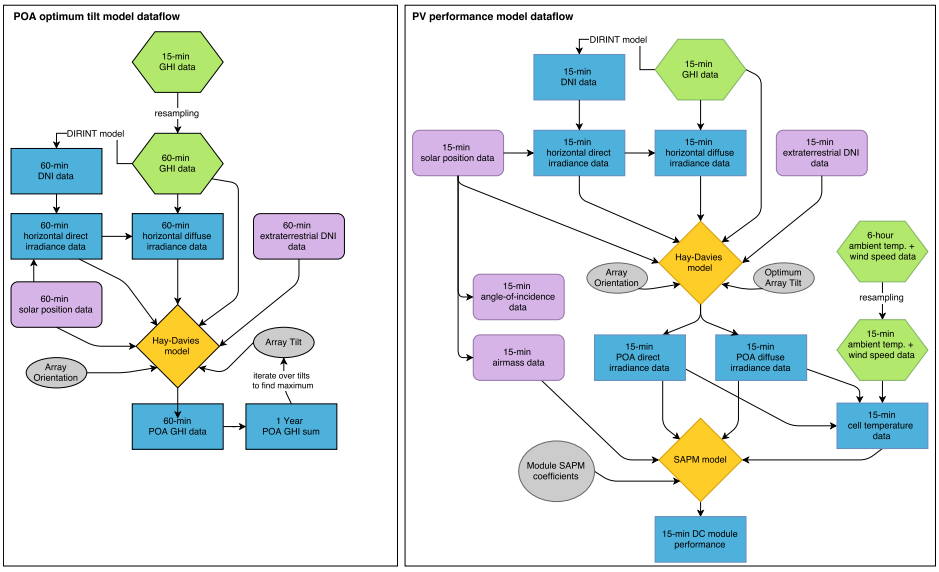

Figure C.1 · Dataflow for the determination of global irradiance optimum plane-of-array tilt.

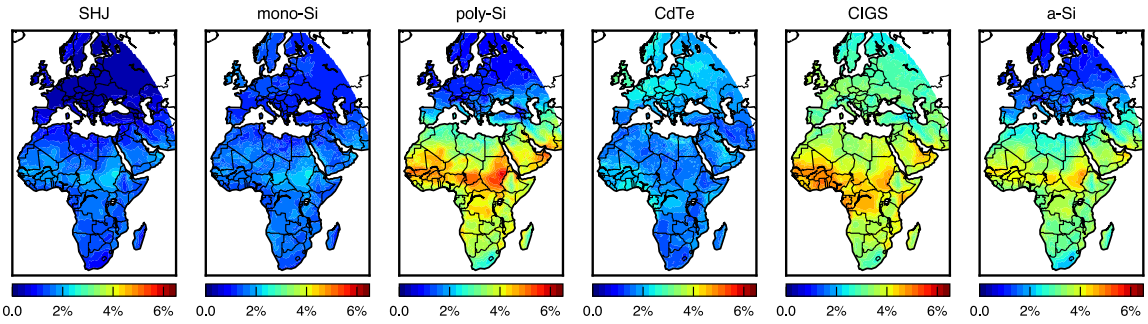

Figure C.2 · Overview of the variation of modelled annual yield between the eight modelled PV modules for each technology. The figures represent the standard deviation, relative to the mean at each location.

Appendix D

Supplementary Information for Chapter 6

Table D.1 · Data for the cumulative energy demand and energy payback time of multicrystalline silicon solar cells, modules and systems. Energy payback time was calculated from CED with a harmonised procedure, assuming an insolation of 1700 kWh $m^{-2}yr^{-1}$ and a performance ration of 0.75. Studies that did not present results for full systems, or that present results for worst or best case scenarios, as well as prospective studies, were excluded from our analysis.

Reference	Data Year	CED (MJ_P W_p^{-1})			EPBT (years)			Excluded	Prospective
		Cells	Modules	Systems	Cells	Modules	Systems		
[253]	1976	246			16.7			•	
[253]	1976	510			34.6			•	
[254]	1977	93.6	96.1		6.34	6.51		•	
[223]	1977		270	637		18.3	43.1	•	
[255]	1985	166			11.3			•	
[222]	1989		59.4	72.0		4.02	4.88		
[256]	1993	60.6	63.2	68.4	4.10	4.28	4.63		
[257]	1996	24.3	33.0		1.65	2.24		•	
[222]	1997		27.0	32.4		1.83	2.20	•	•
[258]	1997	23.9	30.5		1.62	2.06		•	
[258]	1997	22.5	28.9		1.52	1.96		•	
[258]	1997	10.7	14.4		0.73	0.98		•	•
[259]	1997	70.3	93.1		4.76	6.31		•	
[259]	1997	24.1	36.2		1.63	2.45		•	
[260]	1998		36.8			2.49		•	
[259]	1999	25.7	36.2		1.74	2.45		•	
[261]	1999	29.6	36.2	57.9	2.01	2.45	3.92		
[261]	1999	26.9	35.4	41.8	1.82	2.40	2.83		
[262]	2003		34.0			2.30		•	
[263]	2005	22.0	29.8	32.5	1.49	2.02	2.20		
[264]	2006			32.5			2.20		
[265]	2005		25.6	35.3		1.73	2.39		
[266]	1999	43.1	48.1	53.2	2.92	3.26	3.60		
[267]	2006		16.9	32.5		1.14	2.21		
[268]	1999			49.2			3.34		
[265]	2007		69.4	78.6		4.70	5.33	•	
[265]	2007		25.3	34.4		1.71	2.33		
[269]	2008			33.1			2.24		
[270]	2008		16.0	31.3		1.08	2.12		
[271]	2009			23.5			1.59		
[272]	2009		19.7	23.9		1.33	1.62		
[261]	2010		17.3	21.6		1.17	1.46	•	•
[35]	2011	6.25	14.8	15.8	0.42	1.00	1.07		
[35]	2011	6.17	17.9	18.9	0.42	1.21	1.28		
[36]	2013	3.71	7.82	13.7	0.25	0.530	0.930		
[261]	2020		12.9	16.7		0.877	1.13	•	•

Supplementary Methods

Data filtering

Data filtering was performed on the data gathered from the LCA studies cited in Supplementary Tables 1-5, to exclude studies that in our opinion do not reflect the state of PV production corresponding with the reported data ages. In order to maximise the available datapoints, we however only exclude those results that:

Table D.2 · Data for cumulative energy demand and energy payback time of mono-crystalline silicon solar cells, modules and systems. Energy payback time was calculated from CED with a harmonised procedure, assuming an insolation of 1700 kWh m^2yr^{-1} and a performance ratio of 0.75. Studies that did not present results for full systems, or that present results for worst case or best case scenarios, as well as prospective studies were excluded from our analysis.

Reference	Data Year	CED (MJ_P W_P^{-1})			EPBT (years)			Excluded	Prospective
		Cells	Modules	Systems	Cells	Modules	Systems		
[222]	1989		63.0	73.8		4.32	5.06		
[256]	1993	57.4	59.6	63.3	3.94	4.09	4.34		
[273]	1995		63.1			4.33		•	
[273]	1995		11.3			0.779		•	
[222]	1997		39.6	43.9		2.72	3.01	•	•
[274]	1997			63.2			4.34		
[258]	1997	123	127		8.45	8.73		•	
[258]	1997	91.5	95.7		6.28	6.57		•	
[258]	1997	29.9	34.1		2.05	2.34		•	•
[259]	1997	44.5	49.6	53.5	3.05	3.40		•	
[259]	1997	107	116	123	7.32	7.93		•	
[260]	1998		63.7			4.37		•	
[275]	1999	52.2	64.0		3.58	4.39		•	
[261]	1999		44.3	58.1		3.04	3.99		
[261]	1999		44.3	50.3		3.04	3.45		
[276]	2003		31.9	45.2		2.19	3.10		
[276]	2003		31.9	56.0		2.19	3.84		
[264]	2005			39.8			2.70		
[277]	2005	37.8	41.3		2.59	2.83		•	
[268]	1999			56.4			3.87		
[278]	2006		37.1	39.8		2.55	2.73		
[269]	2008			41.9			2.88		
[271]	2009			23.3			1.60		
[272]	2009		27.9	32.0		1.91	2.20		
[261]	2010		40.7	44.9		2.79	3.08	•	•
[261]	2010		38.0	42.2		2.61	2.90	•	•
[35]	2011	13.4	25.3	26.2	0.92	1.74	1.80		
[35]	2011	13.2	30.8	31.7	0.90	2.11	2.18		
[102]	2012	16.3	21.2	29.2	1.12	1.45	2.00		
[36]	2013	5.15	10.0	16.1	0.35	0.684	1.10		
[261]	2020		33.5	37.0		2.30	2.54	•	•
[261]	2020		33.5	37.0		2.30	2.54	•	•
[102]	2020	6.87	10.3	17.1	0.47	0.708	1.17	•	•
[70]	2020		9.23			0.633		•	•
[70]	2020		7.14			0.490		•	•
[70]	2020		7.00			0.480		•	•

- Are specifically mentioned to be valid for worst case or best case scenarios
- Are specifically mentioned to refer to prospective studies
- Are not for complete PV systems, but only for parts (e.g. only cells or modules).

Table D.3 · Data for life cycle greenhouse gas emissions of multi-crystalline silicon PV systems. Harmonised system GHG was calculated from the reported values assuming an insolation of 1700 kWh m^2yr^{-1}, a performance ratio of 0.75, a lifetime of 30 years and a degradation rate of 0.7% per year. Studies that did not present results for full systems, or that present results for worst case or best case scenarios, as well as prospective studies were excluded from our analysis.

Reference	Data Year	Reported GHG (gCO_2-eq/kWh)				Harmonised system GHG		Excluded	Prospective
		Cells	Modules	BOS	System	(gCO_2-eq/kWh)	($kgCO_2$-eq/Wp)		
[222]	1989				245	143	4.90		
[222]	1989				123	143	4.90		
[279]	1991				188	94.9	3.25		
[273]	1995				305	178	6.10	•	
[273]	1995				245	143	4.90	•	
[273]	1995				179	178	6.09	•	
[273]	1995				144	143	4.90	•	
[280]	1993	42.9	55.4	58.3	114	118	4.04		
[280]	1993	58.8	76.0	67.6	144	109	3.72		
[280]	1993	57.5	73.1	59.0	132	137	4.69		
[259]	1997				60.0	67.0	2.30		
[259]	1997				150	168	5.74		
[281]	1992				189	142	4.88		
[258]	1998				73.3	49.5	1.70	•	
[258]	1998				66.0	44.6	1.53	•	
[282]	1998				87.0	87.0	2.98		
[261]	1999				60.0	67.0	2.30		
[266]	1996					138.2	4.73	•	
[264]	2005				36.4	40.7	1.39		
[278]	2006				35.0	39.1	1.34		
[265]	2005		52.0	20.0	72.0	53.6	1.84		
[283]	2005				53.0	61.0	2.09		
[284]	2007				29.5	29.5	1.01		
[261]	2010				30.0	33.5	1.15	•	•
[35]	2011	14.0	21.7	5.5	27.2	27.7	0.95		
[35]	2011	35.5	43.6	5.5	49.1	50.0	1.71	•	
[36]	2013				28.0	19.0	0.65		
[36]	2013				26.0	18.5	0.63		
[36]	2013				21.0	20.4	0.70		
[36]	2013				18.0	18.7	0.64		
[261]	2020				20.0	22.3	0.77	•	•

Table D.4 · Data for life cycle greenhouse gas emission of mono-crystalline silicon PV systems. Harmonised system GHG was calculated from the reported values assuming an insolation of 1700 kWh m^2yr^{-1}, a performance ratio of 0.75, a lifetime of 30 years and a degradation rate of 0.7% per year. Studies that did not present results for full systems, or that present results for worst case or best case scenarios, as well as prospective studies were excluded from our analysis.

Reference	Data Year	Reported GHG (gCO_2-eq/kWh)				Harmonised system GHG		Excluded	Prospective
		Cells	Modules	BOS	System	gCO_2-eq/kWh	$kgCO_2$-eq/Wp		
[223]	1983		123		289	409	14.0		
[223]	1986				43	60	2.1	•	
[223]	1986				39	56	1.9	•	
[285]	1992				334	225	7.7		
[285]	1992				238	161	5.5		
[285]	1992				77	52	1.8	•	•
[281]	1992				189	142	4.9		
[258]	1998				304	206	7.0		
[258]	1998				224	151	5.2		
[264]	2005				45	50	1.7		
[278]	2006				45	50	1.7		
[270]	2008				44	61	2.1		
[270]	2008				34	48	1.6		
[284]	2008				30	30	1.0		
[35]	2011	26	33	5	38	41	1.4		
[35]	2011	69	76	5	81	88	3.0	•	
[102]	2012				38	42	1.5		
[36]	2013				36	24	0.8		
[36]	2013				33	23	0.8		
[36]	2013				26	25	0.9		
[36]	2013				24	24	0.8		
[102]	2020				25	28	1.0	•	•

Bibliography

[1] E. Zackrisson, P. Calissendorff, J. González, A. Benson, A. Johansen, and M. Janson, "Terrestrial planets across space and time", arXiv preprint arXiv:1602.00690 (2016).

[2] WWF International, *Living Planet Report 2014*, tech. rep. (Gland, Switzerland, 2014).

[3] R. K. Pachauri, L. Mayer, and Intergovernmental Panel on Climate Change, eds., *Climate change 2014: synthesis report*, OCLC: 914851124 (Intergovernmental Panel on Climate Change, Geneva, Switzerland, 2015).

[4] P. J. Webster, G. J. Holland, J. A. Curry, and H.-R. Chang, "Changes in Tropical Cyclone Number, Duration, and Intensity in a Warming Environment", Science **309**, 1844–1846 (2005).

[5] C. D. Allen, A. K. Macalady, H. Chenchouni, D. Bachelet, N. McDowell, M. Vennetier, T. Kitzberger, A. Rigling, D. D. Breshears, E. H. Hogg, P. Gonzalez, R. Fensham, Z. Zhang, J. Castro, N. Demidova, J.-H. Lim, G. Allard, S. W. Running, A. Semerci, and N. Cobb, "A global overview of drought and heat-induced tree mortality reveals emerging climate change risks for forests", Forest Ecology and Management, Adaptation of Forests and Forest Management to Changing ClimateSelected papers from the conference on "Adaptation of Forests and Forest Management to Changing Climate with Emphasis on Forest Health: A Review of Science, Policies and Practices", Umeå, Sweden, August 25-28, 2008. **259**, 660–684 (2010).

[6] C. D. Thomas, A. Cameron, R. E. Green, M. Bakkenes, L. J. Beaumont, Y. C. Collingham, B. F. N. Erasmus, M. F. de Siqueira, A. Grainger, L. Hannah, L. Hughes, B. Huntley, A. S. van Jaarsveld, G. F. Midgley, L. Miles, M. A. Ortega-Huerta, A. Townsend Peterson, O. L. Phillips, and S. E. Williams, "Extinction risk from climate change", Nature **427**, 145–148 (2004).

[7] P. H. Gleick, "Water, Drought, Climate Change, and Conflict in Syria", Weather, Climate, and Society **6**, 331–340 (2014).

[8] C. P. Kelley, S. Mohtadi, M. A. Cane, R. Seager, and Y. Kushnir, "Climate change in the Fertile Crescent and implications of the recent Syrian drought", Proceedings of the National Academy of Sciences **112**, 3241–3246 (2015).

[9] D. M. Chapin, C. S. Fuller, and G. L. Pearson, "A New Silicon p-n Junction Photocell for Converting Solar Radiation into Electrical Power", Journal of Applied Physics **25**, 676–677 (1954).

[10] R. S. Muller, T. I. Kamins, and M. Chan, *Device electronics for integrated circuits*, 3. ed, OCLC: 248909947 (Wiley, New York, NY, 2003).

[11] P. F. Baldasaro, J. E. Raynolds, G. W. Charache, D. M. DePoy, C. T. Ballinger, T. Donovan, and J. M. Borrego, "Thermodynamic analysis of thermophotovoltaic efficiency and power density tradeoffs", Journal of Applied Physics **89**, 3319–3327 (2001).

[12] NREL, *Research Cell Efficiency Records*, http://www.nrel.gov/Ncpv/Images/Efficiency_Chart.Jpg, 2016.

[13] M. A. Green, K. Emery, Y. Hishikawa, W. Warta, and E. D. Dunlop, "Solar cell efficiency tables (version 43)", Progress in Photovoltaics: Research and Applications **22**, 1–9 (2014).

[14] M. A. Green, K. Emery, Y. Hishikawa, W. Warta, and E. D. Dunlop, "Solar cell efficiency tables (version 48)", Progress in Photovoltaics: Research and Applications **24**, 905–913 (2016).

[15] A. H. M. E. Reinders, and W. G. J. H. M. van Sark, "1.34 - Product-Integrated Photovoltaics A2 - Sayigh, Ali", in *Comprehensive Renewable Energy* (Elsevier, Oxford, 2012), pp. 709–732.

[16]W. C. Turkenburg, D. J. Arent, R. Bertani, A. Faaij, M. Hand, W. Krewitt, E. D. Larson, J. Lund, M. Mehos, T. Merrigan, C. Mitchell, J. R. Moreira, W. Sinke, V. Sonntag-O'Brien, B. Thresher, W. van Sark, and E. Usher, "Chapter 11 - Renewable Energy", in *Global Energy Assessment - Toward a Sustainable Future* (Cambridge University Press, Cambridge, UK and New York, NY, USA and the International Institute for Applied Systems Analysis, Laxenburg, Austria, 2012), pp. 761–900.

[17] IEA PVPS, *A Snapshot of Global PV (1992-2015)*, tech. rep. (IEA Photovoltaic Power Systems Programme, 2016).

[18] IEA PVPS, *A Snapshot of Global PV 1992-2014*, tech. rep. EA PVPS T1-26:2015 (IEA Photovoltaic Power Systems Programme, 2015).

[19] IEA PVPS, *Trends 2015 in Photovoltaic Applications*, tech. rep. IEA-PVPS T1-27:2015 (International Energy Agency, 2015).

[20] IEA PVPS, *Trends 2014 in Photovoltaic Applications*, tech. rep. IEA-PVPS T1-25:2014 (IEA Photovoltaic Power Systems Programme, 2014).

[21] IEA PVPS, *Snapshot of Global PV 1992-2013*, tech. rep. IEA-PVPS T1-24:2014 (IEA Photovoltaic Power Systems Programme, 2014).

[22] IEA PVPS, *Trends 2013 in Photovoltaic Applications*, tech. rep. IEA-PVPS T1-23:2013 (IEA Photovoltaic Power Systems Programme, 2013).

[23] Energy Information Administration, *International Energy Statistics*, http://www.eia.gov/beta/international/data/browser/, 2016.

[24] Fraunhofer ISE, *Current and Future Cost of Photovoltaics - Long-term Scenarios for Market Development, System Prices and LCOE of Utility Scale PV Systems*, tech. rep. (Agora Energiewende, 2015).

[25]S. Lacey, *Jinko and Marubeni Bid 2.4 Cents to Supply Solar in Abu Dhabi. How Low Can Solar Prices Go?*, http://www.greentechmedia.com/articles/read/jinko-solar-and-marubeni-bid-2.4-cents-for-solar-power-plant-in-abu-dhabi, Sept. 2016.

[26] Schmela, Michael, Masson, Gaetan, and N. N. T. Mai, *Global Market Outlook For Solar Power / 2016-2020*, tech. rep. (SolarPower Europe, 2016).

[27] International Energy Agency, *Medium-Term Renewable Energy Market Report 2015*, OCLC: 927971013 (OECD Publishing, 2015).

[28] International Energy Agency, *World Energy Outlook 2015*, OCLC: 930994298 (OECD Publishing, 2015).

[29]W. van Sark, L. Korte, and F. Roca, *Physics and Technology of Amorphous-Crystalline Heterostructure Silicon Solar Cells*, edited by W. G. J. H. M. van Sark, L. Korte, and F. Roca, Engineering Materials (Springer Berlin Heidelberg, Berlin, Heidelberg, 2012).

[30]G. Niu, X. Guo, and L. Wang, "Review of recent progress in chemical stability of perovskite solar cells", J. Mater. Chem. A **3**, 8970–8980 (2015).

[31] NEDO New Energy Technology Department, and Kaneka Corporation, *World's Highest Conversion Efficiency of 26.33% Achieved in a Crystalline Silicon Solar Cell*, http://www.kaneka.co.jp/kaneka-e/images/topics/1473811995/1473811995_101.pdf, Sept. 2016.

[32]C. Battaglia, A. Cuevas, and S. De Wolf, "High-efficiency crystalline silicon solar cells: status and perspectives", Energy Environ. Sci. **9**, 1552–1576 (2016).

[33]A. Goodrich, P. Hacke, Q. Wang, B. Sopori, R. Margolis, T. L. James, and M. Woodhouse, "A wafer-based monocrystalline silicon photovoltaics road map: Utilizing known technology improvement opportunities for further reductions in manufacturing costs", Solar Energy Materials and Solar Cells **114**, 110–135 (2013).

[34]P.-J. Ribeyron, D. Muñoz, J.-P. Kleider, W. Favre, P. Roca i Cabarrocas, M. Labrune, B. Geerligs, A. Weeber, M. Späth, C. Olson, N. Dekker, W. van Sark, J. Schüttauf, J. Rath, R. Schropp, M. Tucci, S. De Iullis, I. Gordon, B. O'Sullivan, A. Descoeudres, S. De Wolf, C. Ballif, T. Schultze, L. Korte, F. Madon, N. Le Quang, M. Scherff, R. Doll, Y. Zemen, and G. Zietek, "European Record Efficiency Amorphous-Crystalline-Silicon Heterojunction Solar Cells: Final Results from the HETSI Project", in Proceedings of the 26th European Photovoltaic Solar Energy Conference and Exhibition, edited by H. Ossenbrink, A. Jäger-Waldau, and P. Helm, (2011), pp. 853–857.

[35]M. J. de Wild-Scholten, "Energy payback time and carbon footprint of commercial photovoltaic systems", Solar Energy Materials and Solar Cells **119**, 296–305 (2013).

[36]T. Wetzel, and S. Borchers, "Update of energy payback time and greenhouse gas emission data for crystalline silicon photovoltaic modules: Broader perspectives", Progress in Photovoltaics: Research and Applications, (In press) (2014).

[37]E. Leccisi, M. Raugei, and V. Fthenakis, "The Energy and Environmental Performance of Ground-Mounted Photovoltaic Systems—A Timely Update", Energies **9**, 622 (2016).

[38]S. L. Dolan, and G. A. Heath, "Life Cycle Greenhouse Gas Emissions of Utility-Scale Wind Power: Systematic Review and Harmonization", Journal of Industrial Ecology **16**, S136–S154 (2012).

[39] Bloomberg L.P., *New Record Set for World's Cheapest Solar, Now Undercutting Coal*, http://www.bloomberg.com/news/articles/2016-05-03/solar-developers-undercut-coal-with-another-record-set-in-dubai, 2016.

[40]C. Breyer, and A. Gerlach, "Global overview on grid-parity", Progress in Photovoltaics: Research and Applications **21**, 121–136 (2013).

[41] IEC 60904-3 (Ed 2.), *Photovoltaic devices - Part 3: Measurement principles for terrestrial photovoltaic (PV) solar devices with reference spectral irradiance data*, tech. rep. (2008).

[42] ISO, *ISO 14040:2006 - Environmental management – Life Cycle Assessment – Principles and Framework*, tech. rep. (International Organization for Standardization (ISO), Geneva, Switzerland, 2006).

[43] ISO, *ISO 14044:2006 - Life cycle assessment - Requirements and guidelines*, tech. rep. (International Organization for Standardization (ISO), Geneva, Switzerland, 2006).

[44]V. Fthenakis, R. Frischknecht, M. Raugei, H. Kim, E. Alsema, M. Held, and M. de Wild-Scholten, *Methodology Guidelines on Life Cycle Assessment of Photovoltaic Electricity, 2nd Edition*, tech. rep. IEA-PVPS T12-03:2011 (IEA Photovoltaic Power Systems Programme, Nov. 2011).

[45] European Photovoltaic Industry Association, *Global Market Outlook For Photovoltaics 2013-2017*, tech. rep. (European Photovoltaic Industry Association, Brussels, Belgium, 2013).

[46]E. Wesoff, "Germany's PV Generation Peaked at 23.4 Gigawatts on June 6", (2013).

[47] Renewables International, "Germany sets record for peak solar power production", (2012).

[48]H. C. Kim, V. Fthenakis, J.-K. Choi, and D. E. Turney, "Life Cycle Greenhouse Gas Emissions of Thin-film Photovoltaic Electricity Generation", Journal of Industrial Ecology **16**, S110–S121 (2012).

[49]A. Arvesen, and E. G. Hertwich, "Assessing the life cycle environmental impacts of wind power: A review of present knowledge and research needs", Renewable and Sustainable Energy Reviews **16**, 5994–6006 (2012).

[50]M. de Wild-Scholten, E. Alsema, V. Fthenakis, G. Agostinelli, H. Dekkers, K. Roth, and V. Kinzig, "Fluorinated greenhouse gases in photovoltaic module manufacturing: potential emissions and abatement strategies", in Proceedings of the 22nd European Photovoltaic Solar Energy Conference (2007), pp. 3–7.

[51]V. Fthenakis, D. O. Clark, M. Moalem, P. Chandler, R. G. Ridgeway, F. E. Hulbert, D. B. Cooper, and P. J. Maroulis, "Life-cycle nitrogen trifluoride emissions from photovoltaics.", Environmental science & technology **44**, 8750–7 (2010).

[52]R. van der Meulen, and E. Alsema, "Life-cycle greenhouse gas effects of introducing nano-crystalline materials in thin-film silicon solar cells", Progress in Photovoltaics: Research and Applications **19**, 453–463 (2011).

[53] Olson, C., de Wild-Scholten, M., Scherff, M., and Ribeyron, P.-J., "Life Cycle Assessment of Hetero-junction Solar Cells and Modules", in Proceedings of the 26th European Photovoltaic Solar Energy Conference and Exhibition (2011).

[54] Pré Consultants, "SimaPro v7.3.3",

[55] IPCC, *Climate Change 2007: The Physical Science Basis. Contribution of Working Group I to the Fourth Assessment Report of the Intergovernmental Panel on Climate Change*, edited by S. Solomon, D. Qin, M. Manning, Z. Chen, M. Marquis, K. Averyt, M. Tignor, and H. Miller, (Cambridge University Press, Cambridge, United Kingdom and New York, NY, USA, 996 pp., 2007).

[56]M. A. J. Huijbregts, S. Hellweg, R. Frischknecht, H. W. M. Hendriks, K. Hungerbühler, and A. J. Hendriks, "Cumulative Energy Demand As Predictor for the Environmental Burden of Commodity Production", Environmental Science & Technology **44**, 2189–2196 (2010).

[57]N. Jungbluth, M. Stucki, and R. Frischknecht, "Photovoltaics", in *Sachbilanzen von Energiesystemen: Grundlagen für den ökologischen Vergleich von Energiesystemen und den Einbezug von Energiesystemen in Ökobilanzen für die Schweiz. ecoinvent report No. 6-XII*, edited by R. Dones, 6 (Swiss Centre for Life Cycle Inventories, Dübendorf, Switzerland, 2009).

[58] Applied Materials, "Advanced Wire Sawing Technology for Solar Photovoltaic Cells", Santa Clara, CA, USA, 2011.

[59] PHOTON Europe GmbH, "Market survey on wet etching equipment", Photon International, 166–177 (2011).

[60]H.-J. Althaus, M. Chudacoff, R. Hischier, N. Jungbluth, M. Osses, and A. Primas, *Life Cycle Inventories of Chemicals. ecoinvent report No. 8, v2.0.* Tech. rep. (EMPA Dübendorf, Swiss Centre for Life Cycle Inventories, Dübendorf, Switzerland, 2007).

[61] PHOTON Europe GmbH, "Market survey on silicon thin-film absorber deposition equipment", Photon International, 166–181 (2011).

[62] PHOTON Europe GmbH, "Market survey on deposition equipment for transparent conductive oxide layers", Photon International, 160–175 (2011).

[63] PHOTON Europe GmbH, "Market survey on screen printers", Photon International, 112–137 (2012).

[64] PHOTON Europe GmbH, "Market survey on plating equipment", Photon International, 118–125 (2013).

[65]M. Späth, D. Veldman, N. Dekker, I. Bennett, W. Eerenstein, P. de Jong, P. Ribeyron, S. Harrison, and D. Muñoz, "Hetero-junction Module Technology", in Proceedings of the 26th European Photovoltaic Solar Energy Conference and Exhibition, edited by P. Helm, A. Jäger-Waldau, and H. Ossenbrink, (2011).

[66] Dunmore, "Every Backsheet Solution Under the Sun", (2013).

[67]H. Gatz, "Multifunctional Emitters for Heterojunction Solar Cells", (2011).

[68] A. Louwen, W. G. J. H. M. van Sark, W. C. Turkenburg, R. E. I. Schropp, and A. P. C. Faaij, "R&D Integrated Life Cycle Assessment: A Case Study On The R&D of Silicon Heterojunction (SHJ) Solar Cell Based PV Systems", in Proceedings of the 27th European Photovoltaic Solar Energy Conference and Exhibition, edited by S. Nowak, A. Jäger-Waldau, and P. Helm, (2012), pp. 4673–4678.

[69] M. Scherff, "Novel method for preparation of interdigitated back contacted a-Si:H/cSi heterojunction solar cells", in Proceedings of the 26th European Photovoltaic Solar Energy Conference and Exhibition, edited by H. Ossenbrink, A. Jäger-Waldau, and P. Helm, (2011), pp. 2125–2129.

[70] S. A. Mann, M. J. de Wild-Scholten, V. M. Fthenakis, W. G. van Sark, and W. C. Sinke, "The energy payback time of advanced crystalline silicon PV modules in 2020: a prospective study", Progress in Photovoltaics: Research and Applications **22**, 1180–1194 (2014).

[71] Panasonic Corporation, "Panasonic HIT Solar Cell Achieves World's Highest Conversion Efficiency of 25.6% at Research Level", (2014).

[72] Panasonic Corporation, "HIT Power Series", (2014).

[73] PHOTON Europe GmbH, "Module Survey", Photon International, 72–73, 162–339 (2013).

[74] M. Schottler, and M. de Wild-Scholten, "Carbon footprint of PECVD chamber cleaning", Photovoltaics International **November**, 212–213 (2008).

[75] M. A. Green, "Ag requirements for silicon wafer-based solar cells", Progress in Photovoltaics: Research and Applications **19**, 911–916 (2011).

[76] P. Verlinden, *Cost analysis of current PV production and strategy for future silicon PV modules.* Sydney, Australia, Jan. 2014.

[77] C. Clement, H. Bell, F. Vogg, L. Rebenklau, P. Gierth, and U. Partsch, "Inert Drying System for Copper Paste Application in PV", Energy Procedia **38**, 423–429 (2013).

[78] GeoModel Solar s.r.o., "SolarGIS Solar Map Europe", (2013).

[79] A. de Keizer, E. Ter Horst, E. Molenbroek, and W. van Sark, "Evaluating 5-years performance monitoring of 1 MW building integrated PV project in Nieuwland, Amersfoort, the Netherlands", in Proceedings of the 22nd European Photovoltaic Solar Energy Conference, edited by G. Willeke, H. Ossenbrink, and P. Helm, (2007), pp. 2960–2965.

[80] N. H. Reich, B. Mueller, A. Armbruster, W. G. J. H. M. van Sark, K. Kiefer, and C. Reise, "Performance ratio revisited: is PR $>$ 90% realistic?", Progress in Photovoltaics: Research and Applications **20**, 717–726 (2012).

[81] ecoinvent Centre, *Ecoinvent data v2.1. ecoinvent reports No. 1-25*, tech. rep. (Swiss Centre for Life Cycle Inventories, Dübendorf, Switzerland, 2007).

[82] PHOTON Europe GmbH, "Market survey on gas abatement systems for thin-film applications", Photon International, 136–141 (2010).

[83] L. Tous, R. Russell, J. Das, R. Labie, M. Ngamo, J. Horzel, H. Philipsen, J. Sniekers, K. Vandermissen, L. van den Brekel, T. Janssens, M. Aleman, D. van Dorp, J. Poortmans, and R. Mertens, "Large Area Copper Plated Silicon Solar Cell Exceeding 19.5% Efficiency", Energy Procedia **21**, 58–65 (2012).

[84] L. Tous, "Re: Copper electroplated solar cells", (2013).

[85] Rena GmbH, "Data Sheet - Solar BatchTex HT", (2012).

[86] M. A. Huijbregts, L. Rombouts, S. Hellweg, R. Frischknecht, A. J. Hendriks, D. van de Meent, A. Ragas, L. Reijnders, and J. Struijs, "Is cumulative fossil energy demand a useful indicator for the environmental performance of products?", Environmental science & technology **40**, 641–648 (2006).

[87] N. Reich, E. Alsema, W. van Sark, W. Turkenburg, and W. Sinke, "Greenhouse gas emissions associated with photovoltaic electricity from crystalline silicon modules under various energy supply options", Progress in Photovoltaics: Research and Applications **19**, 603–613 (2011).

[88] D. D. Hsu, P. O'Donoughue, V. M. Fthenakis, G. A. Heath, H. C. Kim, P. Sawyer, J.-K. Choi, and D. E. Turney, "Life Cycle Greenhouse Gas Emissions of Crystalline Silicon Photovoltaic Electricity Generation", Journal of Industrial Ecology **16**, S122–S135 (2012).

[89] B. A. Andersson, C. Azar, J. Holmberg, and S. Karlsson, "Material constraints for thin-film solar cells", Energy **23**, 407–411 (1998).

[90] M. Z. Jacobson, and M. a. Delucchi, "Providing all global energy with wind, water, and solar power, Part I: Technologies, energy resources, quantities and areas of infrastructure, and materials", Energy Policy **39**, 1154–1169 (2011).

[91] C. Candelise, J. F. Speirs, and R. J. Gross, "Materials availability for thin film (TF) PV technologies development: A real concern?", Renewable and Sustainable Energy Reviews **15**, 4972–4981 (2011).

[92] C. S. Tao, J. Jiang, and M. Tao, "Natural resource limitations to terawatt-scale solar cells", Solar Energy Materials and Solar Cells **95**, 3176–3180 (2011).

[93] M. Goedkoop, R. Heijungs, M. Huijbregts, A. De Schryver, J. Struijs, and R. van Zelm, "ReCiPe 2008", A life cycle impact assessment method which comprises harmonised category indicators at the midpoint and the endpoint level **1** (2009).

[94] W. van Sark, G. Rutten, and J. Cace, *Inventarisatie PV markt Nederland - Status april 2014*, tech. rep. (Stichting Monitoring Zonnestroom, Utrecht, the Netherlands, 2014).

[95] N. S. Lewis, "Toward cost-effective solar energy use.", Science (New York, N.Y.) **315**, 798–801 (2007).

[96] M. Bazilian, I. Onyeji, M. Liebreich, I. MacGill, J. Chase, J. Shah, D. Gielen, D. Arent, D. Landfear, and S. Zhengrong, "Re-considering the economics of photovoltaic power", Renewable Energy **53**, 329–338 (2013).

[97] C. Budischak, D. Sewell, H. Thomson, L. Mach, D. E. Veron, and W. Kempton, "Cost-minimized combinations of wind power, solar power and electrochemical storage, powering the grid up to 99.9% of the time", Journal of Power Sources **225**, 60–74 (2013).

[98] S. Reichelstein, and M. Yorston, "The prospects for cost competitive solar PV power", Energy Policy **55**, 117–127 (2013).

[99] K. D. Swift, "A comparison of the cost and financial returns for solar photovoltaic systems installed by businesses in different locations across the United States", Renewable Energy **57**, 137–143 (2013).

[100] PVinsights, *PVinsights: Solar Photovoltaic (Polysilicon wafer cell and panel) Prices and Research Reports*, http://pvinsights.com, 2015.

[101] V. M. Fthenakis, and H. Kim, "Photovoltaics: Life-cycle analyses", Solar Energy **85**, 1609–1628 (2011).

[102] A. Louwen, W. G. J. H. M. van Sark, R. E. I. Schropp, W. C. Turkenburg, and A. P. C. Faaij, "Life-cycle greenhouse gas emissions and energy payback time of current and prospective silicon heterojunction solar cell designs", Progress in Photovoltaics: Research and Applications **23**, 1406–1428 (2015).

[103] International Energy Agency, *World Energy Outlook 2014* (International Energy Agency, Paris, France, 2014).

[104] H. Wirth, *Recent Facts about Photovoltaics in Germany*, tech. rep. (Fraunhofer ISE, Freiburg, Germany, May 2015), pp. 19–20.

[105] K. Blok, *Introduction to Energy Analysis* (Techne Press, Amsterdam, the Netherlands, 2007).

[106] OpenEI, "Transparent Cost Database | Transparent Cost Database",

[107] S. De Wolf, A. Descoeudres, Z. C. Holman, and C. Ballif, "High-efficiency Silicon Heterojunction Solar Cells: A Review", green **2**, 7–24 (2012).

[108] A. L. Roes, E. Marsili, E. Nieuwlaar, and M. K. Patel, "Environmental and Cost Assessment of a Polypropylene Nanocomposite", Journal of Polymers and the Environment **15**, 212–226 (2007).

[109] G. Rebitzer, and S. Seuring, "Methodology and Application of Life Cycle Costing", The International Journal of Life Cycle Assessment **8**, 110–111 (2003).

[110] D. Hunkeler, and G. Rebitzer, "Life Cycle Costing - Paving the Road to Sustainable Development?", The International Journal of Life Cycle Assessment **8**, 109–110 (2003).

[111] PHOTON Europe GmbH, "SiNx deposition systems survey", Photon International, 50–61 (2014).

[112] USGS, *2010 Minerals Yearbook Silica*, tech. rep. (U.S. Geological Survey, 2012).

[113] M. Woodhouse, R. Fu, T. James, K. Horowitz, B. Gallagher, D. Feldman, D. Chung, and R. Margolis, "Current Results from NREL's Wafer-Based Monocrystalline Silicon PV Module Manufacturing Cost Models Current Results from NREL's Wafer-Based Monocrystalline Silicon PV Module Manufacturing Cost Models", in NREL crystalline silicon workshop, July 2014 (2014).

[114] ITRPV working group, *International Technology Roadmap for Photovoltaic (ITRPV) - 2013 Results*, tech. rep. March (2014), pp. 1–37.

[115] J. Tyler, "Manufacturers Will Slowly Switch To Diamond Wire", Solar Industry Magazine (2013).

[116] G. Roters, J. Krause, S. Leu, A. Richter, and B. Strahm, "Heterojunction Technology The Solar Cell of the Future", Gwatt (Thun), Switzerland, 2014.

[117] Z. C. Holman, A. Descoeudres, S. De Wolf, and C. Ballif, "Record Infrared Internal Quantum Efficiency in Silicon Heterojunction Solar Cells With Dielectric/Metal Rear Reflectors", IEEE Journal of Photovoltaics **3**, 1243–1249 (2013).

[118] Y. Zemen, S. Schulz, H. Trommler, S. Buschhorn, W. Bauhofer, and K. Schulte, "Comparison of new conductive adhesives based on silver and carbon nanotubes for solar cells interconnection", Solar Energy Materials and Solar Cells **109**, 155–159 (2013).

[119] PHOTON Europe GmbH, "Cell interconnection equipment survey", Photon International (2014).

[120] PHOTON Europe GmbH, "Survey laminators", Photon International, 100–103, 228–275 (2012).

[121] PHOTON Europe GmbH, "Survey lay up machines", Photon International, 102–117 (2012).

[122] PHOTON Europe GmbH, "Cell testers & sorters survey", Photon International, 66–80 (2014).

[123] IHS, *Solar Glass Price Plunge to Cease as Trade Sanctions Take Effect | IHS Online Newsroom*, http://press.ihs.com/press-release/design-supply-chain-media/solar-glass-price-plunge-cease-trade-sanctions-take-effect, 2014.

[124] C. J. J. Tool, E. J. Kossen, I. J. Bennett, M. J. H. Kloos, and W. Eerenstein, "Improved efficiency and cost of ownership for p-type MWT cell and module technology", (2012).

[125] ITRPV working group, *International Technology Roadmap for Photovoltaic (ITRPV) 2014 Results*, tech. rep. April (SEMI, 2015), pp. 1–38.

[126] D. Wood, N. Powell, A. Zambova, B. Chislea, P. Chevalier, C. Boulord, A. Beucher, N. Zeghers, G. Beaucarne, I. Kuzma-filipek, R. Russell, F. Duerinckx, J. Szlufcik, W. Deng, Z. Feng, and P. J. Verlinden, "Passivated Busbars from Screen-Printed Low Temperature Copper Paste", 2014.

[127] A. Kohn, and M. Eizenberg, "Diffusion Barriers for Ultra-Large-Scale Integrated Copper Metallization", in *Advanced Nanoscale ULSI Interconnects: Fundamentals and Applications* (Springer New York, New York, NY, 2009), pp. 93–120.

[128] M. Yoshida, H. Tokuhisa, U. Itoh, T. Kamata, I. Sumita, and S. Sekine, "Novel Low-Temperature-Sintering Type Cu-Alloy Pastes for Silicon Solar Cells", Energy Procedia **21**, 66–74 (2012).

[129] PHOTON Europe GmbH, "Plating Equipment Survey", Photon International, 118–125 (2013).

[130] B. Andersson, "Materials Availability for Large-scale Thin-film Photovoltaics", Progress in Photovoltaics: Research and Applications **8**, 61–76 (2000).

[131] L. Grandell, and A. Thorenz, "Silver supply risk analysis for the solar sector", Renewable Energy **69**, 157–165 (2014).

[132] A. Zuser, and H. Rechberger, "Considerations of resource availability in technology development strategies: The case study of photovoltaics", Resources, Conservation and Recycling **56**, 56–65 (2011).

[133] PV-Magazine, "Polysilicon industry to resume growth in 2013", (2013).

[134] London Bullion Market Association, "LBMA - Pricing and Statistics", (2015).

[135] F. Roca, G. Sinno, G. Di Francia, P. Prosini, G. Fameli, P. Grillo, a. Citarella, F. Pascarella, and D. della Sala, "Process development of amorphous silicon/crystalline silicon solar cells", Solar Energy Materials and Solar Cells **48**, 15–24 (1997).

[136] Meyer Burger, "SWCT | Meyer Burger Technology AG", (2015).

[137] Panasonic, *Panasonic HIT™*, http://panasonic.net/ecosolutions/solar/hit/, 2016.

[138] ASTM International, *ASTM E2848-13, Standard Test Method for Reporting Photovoltaic Non-Concentrator System Performance*, tech. rep. (ASTM International, West Conshohocken, PA, 2013).

[139] T. R. Betts, C. N. Jardine, R. Gottschalg, D. G. Infield, and K. Lane, "Impact of spectral effects on the electrical parameters of multijunction amorphous silicon cells", in Proceedings of 3rd World Conference on Photovoltaic Energy Conversion, 2003, Vol. 2 (May 2003), 1756–1759 Vol.2.

[140] van Sark, W G J H M, Louwen, A., de Waal, A C, and Schropp, R E I, "UPOT: The Utrecht Photovoltaic Outdoor Test Facility", in Proceedings of the 27th European Photovoltaic Solar Energy Conference and Exhibition (2012), pp. 3247–3249.

[141] EKO Instruments, *MP-160 I-V Tracer*, http://eko-eu.com/products/photovoltaic-evaluation-systems/i-v-tracers/mp-160-i-v-tracer, 2016.

[142] National Instruments, *LabVIEW*, 2010.

[143] The SciPy community, *Scipy.optimize.curve_fit*, http://docs.scipy.org/doc/scipy/reference/generated/scipy.optimize.curve_fit.html, 2016.

[144] D. Dirnberger, G. Blackburn, B. Müller, and C. Reise, "On the impact of solar spectral irradiance on the yield of different PV technologies", Solar Energy Materials and Solar Cells **132**, 431–442 (2015).

[145] L. Fanni, A. Virtuani, and D. Chianese, "A detailed analysis of gains and losses of a fully-integrated flat roof amorphous silicon photovoltaic plant", Solar Energy **85**, 2360–2373 (2011).

[146] A. Virtuani, and L. Fanni, "Seasonal power fluctuations of amorphous silicon thin-film solar modules: distinguishing between different contributions: Seasonal power fluctuations of a-Si thin-film solar modules", Progress in Photovoltaics: Research and Applications **22**, 208–217 (2014).

[147] A. Skoczek, A. Virtuani, T. Cebecauer, and D. Chianese, "Energy Yield Prediction of Amorphous Silicon PV Modules Using Full Time Data Series of Irradiance and Temperature for Different Geographical Locations", (2011) 10.4229/26thEUPVSEC2011-4DO.6.3.

[148] A. Virtuani, A. Skoczek, and D. Strepparava, "Modeling the Performance of Amorphous Silicon Photovoltaic Modules in Different Geographical Locations in Europe", (2014) 10.4229/EUPVSEC20142014-5CO.16.6.

[149] D. L. King, W. E. Boyson, and J. A. Kratochvill, *Photovoltaic Array Performance Model*, tech. rep. SAND2004-3535 (Sandia National Laboratories, Albuquerque, New Mexico, USA, 2004).

[150] T. Markvart, and L. Castañer, eds., *Practical handbook of photovoltaics: fundamentals and applications*, Repr, OCLC: 179994435 (Elsevier, Oxford, 2003).

[151] N. H. Reich, W. G. J. H. M. van Sark, E. A. Alsema, R. W. Lof, R. E. I. Schropp, W. C. Sinke, and W. C. Turkenburg, "Crystalline silicon cell performance at low light intensities", Solar Energy Materials and Solar Cells **93**, 1471–1481 (2009).

[152] N. H. Reich, W. G. J. H. M. van Sark, and W. C. Turkenburg, "Charge yield potential of indoor-operated solar cells incorporated into Product Integrated Photovoltaic (PIPV)", Renewable Energy **36**, 642–647 (2011).

[153] D. Dirnberger, B. Müller, and C. Reise, "PV module energy rating: opportunities and limitations", Progress in Photovoltaics: Research and Applications, n/a–n/a (2015).

[154] W. Heydenreich, B. Müller, and C. Reise, "Describing the world with three parameters: a new approach to PV module power modelling", in Proceedings of the 23rd European Photovoltaic Solar Energy Conference, Valencia, Spain (2008), pp. 2786–2789.

[155] J. John, V. Rajasekar, S. Boppana, S. Tatapudi, and G. Tamizhmani, "Angle of incidence effects on soiled PV modules", in, Vol. 9179 (2014), pp. 91790D–91790D–7.

[156] Schropp, R.E.I., *FW: IQE/EQE data HIT cellen*, Mar. 2014.

[157] O. M. ten Kate, M. de Jong, H. T. Hintzen, and E. van der Kolk, "Efficiency enhancement calculations of state-of-the-art solar cells by luminescent layers with spectral shifting, quantum cutting, and quantum tripling function", Journal of Applied Physics **114**, 084502 (2013).

[158] M. Alonso-Abella, F. Chenlo, G. Nofuentes, and M. Torres-Ramírez, "Analysis of spectral effects on the energy yield of different PV (photovoltaic) technologies: The case of four specific sites", Energy **67**, 435–443 (2014).

[159] G. Nofuentes, B. Garćıa-Domingo, J. V. Muñoz, and F. Chenlo, "Analysis of the dependence of the spectral factor of some PV technologies on the solar spectrum distribution", Applied Energy **113**, 302–309 (2014).

[160] Sutterlueti, J., Ransome, S., Kravets, R., and Schreier, L., "Characterising PV Modules Under Outdoor Conditions: What's Most Important for Energy Yield", in Proceedings of the 26th European Photovoltaic Solar Energy Conference and Exhibition (2011).

[161] T. Huld, and A. M. G. Amillo, "Estimating PV Module Performance over Large Geographical Regions: The Role of Irradiance, Air Temperature, Wind Speed and Solar Spectrum", Energies **8**, 5159–5181 (2015).

[162] Y. Hirata, and T. Tani, "Output variation of photovoltaic modules with environmental factors—I. The effect of spectral solar radiation on photovoltaic module output", Solar Energy **55**, 463–468 (1995).

[163] T. Ishii, K. Otani, T. Takashima, and Y. Xue, "Solar spectral influence on the performance of photovoltaic (PV) modules under fine weather and cloudy weather conditions", Progress in Photovoltaics: Research and Applications **21**, 481–489 (2013).

[164] S. Nann, and K. Emery, "Spectral effects on PV-device rating", Solar Energy Materials and Solar Cells **27**, 189–216 (1992).

[165]C. Cornaro, and A. Andreotti, "Influence of Average Photon Energy index on solar irradiance characteristics and outdoor performance of photovoltaic modules", Progress in Photovoltaics: Research and Applications **21**, 996–1003 (2013).

[166]R. Gottschalg, T. R. Betts, D. G. Infield, and M. J. Kearney, "On the importance of considering the incident spectrum when measuring the outdoor performance of amorphous silicon photovoltaic devices", Measurement Science and Technology **15**, 460 (2004).

[167]R. Rüther, G. Kleiss, and K. Reiche, "Spectral effects on amorphous silicon solar module fill factors", Solar Energy Materials and Solar Cells **71**, 375–385 (2002).

[168]T. Ishii, K. Otani, A. Itagaki, and K. Utsunomiya, "A simplified methodology for estimating solar spectral influence on photovoltaic energy yield using average photon energy", Energy Science & Engineering **1**, 18–26 (2013).

[169]T. Ishii, K. Otani, A. Itagaki, and K. Utsunomiya, "A Methodology for Estimating the Effect of Solar Spectrum on Photovoltaic Module Performance by Using Average Photon Energy and a Water Absorption Band", Japanese Journal of Applied Physics **51**, 10NF05 (2012).

[170]N. Kataoka, S. Yoshida, S. Ueno, and T. Minemoto, "Evaluation of solar spectral irradiance distribution using an index from a limited range of the solar spectrum", Current Applied Physics **14**, 731–737 (2014).

[171]J. Chantana, S. Ueno, Y. Ota, K. Nishioka, and T. Minemoto, "Uniqueness verification of direct solar spectral index for estimating outdoor performance of concentrator photovoltaic systems", Renewable Energy **75**, 762–766 (2015).

[172]T. Minemoto, Y. Nakada, H. Takahashi, and H. Takakura, "Uniqueness verification of solar spectrum index of average photon energy for evaluating outdoor performance of photovoltaic modules", Solar Energy **83**, 1294–1299 (2009).

[173]R. Moreno-Sáez, and L. Mora-López, "Modelling the distribution of solar spectral irradiance using data mining techniques", Environmental Modelling & Software **53**, 163–172 (2014).

[174]R. Moreno Sáez, M. Sidrach-de-Cardona, and L. Mora-López, "Data mining and statistical techniques for characterizing the performance of thin-film photovoltaic modules", Expert Systems with Applications **40**, 7141–7150 (2013).

[175]J. W. Twidell, and T. Weir, *Renewable energy resources*, 2. ed., reprinted (Taylor & Francis, London, 2010).

[176]B. King, D. Riley, C. Robinson, and L. Pratt, "Recent advancements in outdoor measurement techniques for angle of incidence effects", in Photovoltaic Specialist Conference (PVSC), 2015 IEEE 42nd (June 2015), pp. 1–6.

[177]M. Donovan, B. Bourne, and J. Roche, "Efficiency VS. irradiance characterization of PV modules requires angle-of-incidence and spectral corrections", in 2010 35th IEEE Photovoltaic Specialists Conference (PVSC) (June 2010), pp. 002301–002305.

[178]N. Martin, and J. M. Ruiz, "Calculation of the PV modules angular losses under field conditions by means of an analytical model", Solar Energy Materials and Solar Cells **70**, 25–38 (2001).

[179]D. King, J. Kratochvil, and W. Boyson, "Measuring solar spectral and angle-of-incidence effects on photovoltaic modules and solar irradiance sensors", in , Conference Record of the Twenty-Sixth IEEE Photovoltaic Specialists Conference, 1997 (Sept. 1997), pp. 1113–1116.

[180]J. L. Balenzategui, and F. Chenlo, "Measurement and analysis of angular response of bare and encapsulated silicon solar cells", Solar Energy Materials and Solar Cells **86**, 53–83 (2005).

[181] R. Beal, B. Potter, and J. Simmons, "Angle of Incidence Effects on External Quantum Efficiency in Multicrystalline Silicon Photovoltaics", IEEE Journal of Photovoltaics **4**, 1459–1464 (2014).

[182] A. Virtuani, E. Lotter, and M. Powalla, "Performance of Cu(In,Ga)Se2 solar cells under low irradiance", Thin Solid Films, Proceedings of Symposium B, Thin Film Chalcogenide Photovoltaic Materials, E-MRS Spring Meeting **431–432**, 443–447 (2003).

[183] G. Makrides, B. Zinsser, G. E. Georghiou, M. Schubert, and J. H. Werner, "Temperature behaviour of different photovoltaic systems installed in Cyprus and Germany", Solar Energy Materials and Solar Cells, 17th International Photovoltaic Science and Engineering Conference **93**, 1095–1099 (2009).

[184] A. Shah, J. Meier, E. Vallat-Sauvain, C. Droz, U. Kroll, N. Wyrsch, J. Guillet, and U. Graf, "Microcrystalline silicon and 'micromorph' tandem solar cells", Thin Solid Films, Proceedings of Symposium P on Thin Film Materials for Photovoltaics **403–404**, 179–187 (2002).

[185] Fraunhofer ISE, *Photovoltaics Report*, tech. rep. (Fraunhofer ISE, Freiburg, Germany, 2014).

[186] J. Jean, P. R. Brown, R. L. Jaffe, T. Buonassisi, and V. Bulović, "Pathways for solar photovoltaics", Energy & Environmental Science **8**, 1200–1219 (2015).

[187] Solar Frontier, *Performance*, http://www.solar-frontier.com/eng/technology/Performance/index.html, 2016.

[188] First Solar, *First Solar Series 5 Modules | First Solar*, http://www.firstsolar.com/Technologies-and-Capabilities/PV-Modules/First-Solar-Series-5-Modules, 2016.

[189] Panasonic Corporation, *State of the art technology | Solar | Eco solutions | Business | Panasonic Global*, http://panasonic.net/ecosolutions/solar/hit/, 2016.

[190] Stion, *Performance*, http://www.stion.com/products/performance/, 2016.

[191] KANEKA Solar Energy, *Why Thin-Film Silicon?|Technology|KANEKA Solar Energ*, http://www.kaneka-solar.com/, 2016.

[192] J. Zhao, H. Mehlich, J. Hausmann, M. Richter, B. Gruber, M. Weinke, M. Schorch, J. Kowalewski, J. Krause, P. Papet, W. Stein, M. Blanchet, T. Söderström, A. Richter, S. Beyer, and J. Ufheil, "Pilot Production of 6"-Heterojunction Cells and Modules at Meyer-Burger and Outdoor Performance", (2013) 10.4229/28thEUPVSEC2013-2DV.3.19.

[193] V. Sharma, A. Kumar, O. S. Sastry, and S. S. Chandel, "Performance assessment of different solar photovoltaic technologies under similar outdoor conditions", Energy **58**, 511–518 (2013).

[194] B. Zinsser, G. Makrides, M. Schubert, G. Georghiou, and J. Werner, "Temperature and Irradiance Effects on Outdoor Field Performance", (2009) 10.4229/24thEUPVSEC2009-5BV.2.19.

[195] G. Makrides, B. Zinsser, M. Schubert, and G. E. Georghiou, "Performance loss rate of twelve photovoltaic technologies under field conditions using statistical techniques", Solar Energy **103**, 28–42 (2014).

[196] SoDa, *SoDa - Free time-series of solar radiation data*, http://www.soda-is.com/eng/services/services_radiation_free_eng.php, 2016.

[197] European Centre for Medium-Range Weather Forecasts, *Public Datasets*, http://apps.ecmwf.int/datasets/, 2016.

[198] J. E. Hay, and J. A. Davies, "Calculation of the solar radiation incident on an inclined surface", in Proc. of First Canadian Solar Radiation Data Workshop (Eds: JE Hay and TK Won), Ministry of Supply and Services Canada, Vol. 59 (1980).

[199] P. Ineichen, R. R. Perez, R. D. Seal, E. L. Maxwell, and A. Zalenka, "Dynamic global-to-direct irradiance conversion models", ASHRAE Transactions **98**, 354–369 (1992).

[200] G. W. Paltridge, and C. M. R. Platt, *Radiative processes in meteorology and climatology*, Developments in atmospheric science 5, OCLC: 2430889 (Elsevier, Amsterdam, 1976).

[201] J. A. Duffie, and W. A. Beckman, *Solar engineering of thermal processes*, 4. ed, OCLC: 934630622 (Wiley, New York, 2013).

[202] W. F. Holmgren, R. W. Andrews, A. T. Lorenzo, and J. S. Stein, "PVLIB Python 2015", in Photovoltaic Specialist Conference (PVSC), 2015 IEEE 42nd (2015), pp. 1–5.

[203] D. Picault, B. Raison, S. Bacha, J. de la Casa, and J. Aguilera, "Forecasting photovoltaic array power production subject to mismatch losses", Solar Energy **84**, 1301–1309 (2010).

[204] R. Frischknecht, G. Heath, M. Raugei, P. Sinha, and M. de Wild-Scholten, *Methodology Guidelines on Life Cycle Assessment of Photovoltaic Electricity*, tech. rep. IEA-PVPS T12-08:2016 (International Energy Agency Photovoltaic Power Systems Programme, Jan. 2016).

[205] World Resources Institute, *Climate Analysis Indicators Tool: WRI's Climate Data Explorer*, http://cait.wri.org, 2015.

[206] United Nations Statistics Division, *Energy Statistics Database*, http://data.un.org/, 2015.

[207] E. A. Alsema, D. Fraile, R. Frischknecht, V. Fthenakis, M. Held, H. C. Kim, W. Pölz, M. Raugei, and M. de Wild-Scholten, *Methodology guidelines on life cycle assessment of photovoltaic electricity, Subtask 20 'LCA', IEA PVPS Task 12* (by: Publication date: ECN Solar Energy 5-10-2009, 2009).

[208] D. C. Jordan, S. R. Kurtz, K. VanSant, and J. Newmiller, "Compendium of photovoltaic degradation rates: Photovoltaic degradation rates", Progress in Photovoltaics: Research and Applications **24**, 978–989 (2016).

[209] M. Rekinger, F. Thies, G. Masson, and S. Orlandi, *Global Market Outlook for Photovoltaics 2015-2019*, tech. rep. ISBN 9-789082-228410 (SolarPower Europe, Brussels, Belgium, 2015).

[210] British Petroleum, *BP Statistical Review of World Energy 2015*, tech. rep. (British Petroleum, June 2015).

[211] IHS, *Top Solar Power Industry Trends for 2015*, tech. rep. (IHS, 2015).

[212] W. G. J. H. M. van Sark, E. A. Alsema, H. M. Junginger, H. H. C. de Moor, and G. J. Schaeffer, "Accuracy of progress ratios determined from experience curves: the case of crystalline silicon photovoltaic module technology development", Progress in Photovoltaics: Research and Applications **16**, 441–453 (2008).

[213] D. P. Grimmer, "Solar energy breeders", Solar Energy **26**, 49–53 (1981).

[214] E. H. Lysen, and C. Daey Ouwens, "Energy effects of the rapid growth of PV capacity and the urgent need to reduce the energy payback time", in Proceedings of 17th European Photovoltaic Solar Energy Conference, München (2002).

[215] C. J. M. Emmott, N. J. Ekins-Daukes, and J. Nelson, "Dynamic carbon mitigation analysis: the role of thin-film photovoltaics", Energy & Environmental Science **7**, 1810 (2014).

[216] J. Mathur, N. K. Bansal, and H.-J. Wagner, "Dynamic energy analysis to assess maximum growth rates in developing power generation capacity: case study of India", Energy Policy **32**, 281–287 (2004).

[217] D. Ravikumar, T. P. Seager, M. V. Chester, and M. P. Fraser, "Intertemporal Cumulative Radiative Forcing Effects of Photovoltaic Deployments", Environmental Science & Technology **48**, 10010–10018 (2014).

[218] M. Junginger, W. van Sark, and A. Faaij, *Technological Learning in the Energy Sector: Lessons for Policy, Industry and Science* (2010).

[219]M. Dale, and S. M. Benson, "Energy Balance of the Global Photovoltaic (PV) Industry - Is the PV Industry a Net Electricity Producer?", Environmental Science & Technology **47**, 3482–3489 (2013).

[220] PHOTON Publishing GmbH, "A slight increase overall", PHOTON International **June**, 44–49 (2014).

[221] PHOTON Publishing GmbH, "Minor but interesting differences", PHOTON International **April**, 54–58 (2015).

[222]H. Schaefer, and G. Hagedorn, "Hidden energy and correlated environmental characteristics of PV power generation", Renewable Energy **2**, 159–166 (1992).

[223]F. Kreith, P. Norton, and D. Brown, "A comparison of CO 2 emissions from fossil and solar power plants in the United States", Energy **15**, 1181–1198 (1990).

[224]K. P. Bhandari, J. M. Collier, R. J. Ellingson, and D. S. Apul, "Energy payback time (EPBT) and energy return on energy invested (EROI) of solar photovoltaic systems: A systematic review and meta-analysis", Renewable and Sustainable Energy Reviews **47**, 133–141 (2015).

[225]F. Ferroni, and R. J. Hopkirk, "Energy Return on Energy Invested (ERoEI) for photovoltaic solar systems in regions of moderate insolation", Energy Policy **94**, 336–344 (2016).

[226] Marco Raugei, Sgouris Sgouridis, David Murphy, Vasilis Fthenakis, Rolf Frischknecht, Christian Breyer, Ugo Bardi, Charles Barnhart, Adam Brandt, Alastair Buckley, Michael Carbajales-Dale, Denes Csala, Mariska de Wild-Scholten, Garvin Heath, Arnuf Jaeger-Waldau, Christopher Jones, Arthur Keller, Enrica Leccisi, Pierluigi Mancarella, Nicola Pearsall, Adam Siegel, Wim Sinke, and Philippe Stolz, "Energy Return on Energy Invested (ERoEI) for photovoltaic solar systems in regions of moderate insolation: A comprehensive response", Energy Policy **(under review)** (2016).

[227]D. Nugent, and B. K. Sovacool, "Assessing the lifecycle greenhouse gas emissions from solar PV and wind energy: A critical meta-survey", Energy Policy **65**, 229–244 (2014).

[228]M. Görig, and C. Breyer, "Energy learning curves of PV systems", Environmental Progress & Sustainable Energy, n/a–n/a (2016).

[229] IEA, *World Energy Outlook 2014* (Organisation for Economic Co-operation and Development, Paris, Nov. 2014).

[230] PHOTON Publishing GmbH, "Solar module price development until Oct. 16", PHOTON International **November**, 54–58 (2015).

[231] IEA PVPS, *A Snapshot of Global PV 1992-2012*, tech. rep. EA PVPS T1-22:2013 (IEA Photovoltaic Power Systems Programme, 2013).

[232]G. Masson, S. Orlandi, and M. Rekinger, *Global Market Outlook for Photovoltaics 2014-2018*, tech. rep. (European Photovoltaic Industry Association, Brussels, Belgium, 2014).

[233] United States Department of Labor Bureau of Labor Statistics, *Consumer Price Index (CPI)*, http://www.bls.gov/cpi/, Dec. 2015.

[234] Boston Consulting Group, *Perspectives on experience* (Boston Consulting Group Inc., Boston, MA, 1968).

[235]S. Weisberg, *Applied linear regression*, Vol. 528 (John Wiley & Sons, 2005).

[236]D. Yue, F. You, and S. B. Darling, "Domestic and overseas manufacturing scenarios of silicon-based photovoltaics: Life cycle energy and environmental comparative analysis", Solar Energy **105**, 669–678 (2014).

[237]D. Yue, F. You, and S. B. Darling, "Corrigendum to "Domestic and overseas manufacturing scenarios of silicon-based photovoltaics: Life cycle energy and environmental comparative analysis" [Solar Energy 105 (2014) 669–678]", Solar Energy **107**, 380 (2014).

[238]R. Frischknecht, M. Tuchschmid, M. Faist Emmeneger, C. Bauer, and R. Dones, "Strommix und Stromnetz", in *Sachbilanzen von Energiesystemen: Grundlagen für den ökologischen Vergleich von Energiesystemen und den Einbezug von Energiesystemen in Ökobilanzen für die Schweiz*, edited by R. Dones, v2.0, ecoinvent report 6 (Paul Scherrer Institut Villigen, Swiss Centre for Life Cycle Inventories, Duebendorf, CH, 2007).

[239]N. Jungbluth, "Life cycle assessment of crystalline photovoltaics in the Swiss ecoinvent database", Progress in Photovoltaics: Research and Applications **13**, 429–446 (2005).

[240]T. Nordmann, L. Clavadetscher, W. van Sark, and M. Green, *Analysis of Long-Term Performance of PV Systems*, tech. rep. IEA-PVPS T13-05:2014 (IEA Photovoltaic Power Systems Programme, 2015).

[241]P. Moraitis, and W. G. J. H. M. van Sark, "Operational performance of grid-connected PV systems", in Proceedings of the 40th IEEE Photovoltaic Specialists Conference (PVSC) (June 2014), pp. 1953–1956.

[242] Jordan, D.C., and Kurtz, S.R., "Reliability and Geographic Trends of 50,000 Photovoltaic Systems in the USA", in Proceedings of the 29th European Photovoltaic Solar Energy Conference and Exhibition (2014), pp. 2208–2215.

[243]C. Breyer, and J. Schmid, "Population Density and Area weighted Solar Irradiation: global Overview on Solar Resource Conditions for fixed tilted, 1-axis and 2-axes PV Systems", Proceedings of the 25th European Photovoltaic Solar Energy Conference and Exhibition (2010).

[244] PHOTON Europe GmbH, "Diffusion furnaces survey", Photon International, 68–78 (2013).

[245] PHOTON Europe GmbH, "Aluminum oxide deposition systems survey", Photon International, 62–81 (2014).

[246] PHOTON Europe GmbH, "Screen printers and printing lines survey", Photon International, 68–79, 102–111 (2014).

[247] SunSirs, "SunSirs, China Commodity Data Group, provides Bulk Commodity Prices & Commodity Markets & Commodity Information & Commodity News", (2014).

[248] N.N.; Tempress, "Private communications", (2013).

[249] Sigma-Aldrich, "Boron trifluoride $\geq$ 99.5% | Sigma-Aldrich", (2014).

[250] Sigma-Aldrich, "United States | Sigma-Aldrich", (2014).

[251] U.S. Energy Information Administration, "U.S. Weekly Heating Oil and Propane Prices (October - March)", (2014).

[252] Sigma-Aldrich, "Trimethylaluminum 97% | Sigma-Aldrich", (2014).

[253]L. P. Hunt, "Total energy use in the production of silicon solar cells from raw materials to finished product", in 12th Photovoltaic Specialists Conference (1976), pp. 347–352.

[254]J. Lindmayer, *Solar breeder: energy payback time for silicon photovoltaic systems*, tech. rep. (Solarex Corp, Rockville, MD, USA, 1977).

[255]H. A. Aulich, F. W. Schulze, and B. Strake, "Energy pay-back time for crystaline silicon photovoltaic modules using new technologies", in IEEE photovoltaic specialists conference. 18 (1985), pp. 1213–1218.

[256]T. Wetzel, E. Baake, and A. Mühlbauer, "Energy requirements and ways of saving energy in the production process of photovoltaic modules", International Journal of Solar Energy **20**, 185–196 (2000).

[257]E. A. Alsema, *Environmental aspects of solar cell modules: summary report* (Dept. of Science, Technology and Society, University Utrecht, Utrecht, 1996).

[258]K. Kato, A. Murata, and K. Sakuta, "Energy pay-back time and life-cycle CO2 emission of residential PV power system with silicon PV module", Progress in Photovoltaics: Research and Applications **6**, 105–115 (1998).

[259]E. A. Alsema, P. Frankl, and K. Kato, "Energy pay-back time of photovoltaic energy systems: present status and prospects", in 2nd World Conference on photovoltaic solar energy conversion, Vienna (1998), pp. 6–10.

[260]S. Krauter, and R. Rüther, "Considerations for the calculation of greenhouse gas reduction by photovoltaic solar energy", Renewable Energy **29**, 345–355 (2004).

[261]E. A. Alsema, "Energy pay-back time and CO2 emissions of PV systems", Progress in photovoltaics: research and applications **8**, 17–25 (2000).

[262]A. Meijer, M. A. J. Huijbregts, J. J. Schermer, and L. Reijnders, "Life-cycle assessment of photovoltaic modules: Comparison of mc-Si, InGaP and InGaP/mc-Si solar modules", Progress in Photovoltaics: Research and Applications **11**, 275–287 (2003).

[263]E. Alsema, and M. J. de Wild, "Environmental impact of crystalline silicon photovoltaic module production", in MRS Proceedings, Vol. 895 (2005), 0895–G03.

[264]V. Fthenakis, and E. Alsema, "Photovoltaics energy payback times, greenhouse gas emissions and external costs: 2004–early 2005 status", Progress in Photovoltaics: Research and Applications **14**, 275–280 (2006).

[265]M. Raugei, S. Bargigli, and S. Ulgiati, "Life cycle assessment and energy pay-back time of advanced photovoltaic modules: CdTe and CIS compared to poly-Si", Energy **32**, 1310–1318 (2007).

[266]R. Battisti, and A. Corrado, "Evaluation of technical improvements of photovoltaic systems through life cycle assessment methodology", Energy **30**, 952–967 (2005).

[267]C. Koroneos, N. Stylos, and N. Moussiopoulos, "LCA of Multicrystalline Silicon Photovoltaic Systems - Part 1: Present Situation and Future Perspectives (8 pp)", The International Journal of Life Cycle Assessment **11**, 129–136 (2006).

[268]C. Bankier, and S. Gale, *Energy payback of roof mounted photovoltaic cells* (2006).

[269]M. Ito, K. Komoto, and K. Kurokawa, "Life-cycle analyses of very-large scale PV systems using six types of PV modules", Current Applied Physics **10**, S271–S273 (2010).

[270]M. Ito, K. Kato, K. Komoto, T. Kichimi, and K. Kurokawa, "A comparative study on cost and life-cycle analysis for 100 MW very large-scale PV (VLS-PV) systems in deserts using m-Si, a-Si, CdTe, and CIS modules", Progress in Photovoltaics: Research and Applications **16**, 17–30 (2008).

[271]M. Raugei, P. Fullana-i-Palmer, and V. M. Fthenakis, "The energy return on energy investment (EROI) of photovoltaics: Methodology and comparisons with fossil fuel life cycles", Energy Policy **45**, 576–582 (2012).

[272]M. Ito, M. Kudo, M. Nagura, and K. Kurokawa, "A comparative study on life cycle analysis of 20 different PV modules installed at the Hokuto mega-solar plant", Progress in Photovoltaics: Research and Applications **19**, 878–886 (2011).

[273]J. Bates, P. Watkiss, and T. Thorpe, "Life cycle emissions from renewable energy technologies", (1997).

[274]D. Gürzenich, J. Mathur, N. K. Bansal, and H.-J. Wagner, "Cumulative energy demand for selected renewable energy technologies", The International Journal of Life Cycle Assessment **4**, 143–149 (1999).

[275]K. Knapp, and T. Jester, "An empirical perspective on the energy payback time for photovoltaic modules", in Proceedings of the Solar 2000 Conference (2000), pp. 641–648.

[276]I. Nawaz, and G. Tiwari, "Embodied energy analysis of photovoltaic (PV) system based on macro- and micro-level", Energy Policy **34**, 3144–3152 (2006).

[277]S. Boyd, and D. A. Dornfeld, "Technology choices for the PV Industry: A comparative life cycle assessment", Laboratory for Manufacturing and Sustainability (2005).

[278]E. A. Alsema, M. J. de Wild-Scholten, and V. M. Fthenakis, "Environmental impacts of PV electricity generation-a critical comparison of energy supply options", in 21st European photovoltaic solar energy conference, Dresden, Germany, Vol. 3201 (2006).

[279]K. Yamada, H. Komiyama, K. Kato, and A. Inaba, "Evaluation of photovoltaic energy systems in terms of economics, energy and CO 2 emissions", Energy conversion and management **36**, 819–822 (1995).

[280]H. Komiyama, K. Yamada, A. Inaba, and K. Kato, "Life cycle analysis of solar cell systems as a means to reduce atomospheric carbon dioxide emissions", Energy conversion and management **37**, 1247–1252 (1996).

[281]R. Dones, and R. Frischknecht, "Life-cycle assessment of photovoltaic systems: results of Swiss studies on energy chains", Progress in Photovoltaics Research and Applications **6**, 117–125 (1998).

[282]E. A. Alsema, and E. Nieuwlaar, "Energy viability of photovoltaic systems", Energy policy **28**, 999–1010 (2000).

[283]H. Hondo, "Life cycle GHG emission analysis of power generation systems: Japanese case", Energy **30**, 2042–2056 (2005).

[284]V. M. Fthenakis, H. C. Kim, M. Held, M. Raugei, and J. Krones, "Update of PV energy payback times and life-cycle greenhouse gas emissions", in 24th European Photovoltaic Solar Energy Conference and Exhibition (2009), pp. 21–25.

[285]K. Kato, A. Murata, and K. Sakuta, "An evaluation on the life cycle of photovoltaic energy system considering production energy of off-grade silicon", Solar Energy Materials and Solar Cells **47**, 95–100 (1997).

List of Abbreviations

a-Si	amorphous silicon
a-Si:H	hydrogenated amorphous silicon
Ag	silver
ALD	atomic layer deposition
AM	airmass
AOI	angle of incidence
APE	average photon energy
AR	anti-reflective, anti-reflection
ARC	anti-reflective coating
BOM	back of module
BOS	balance of system
BSF	back surface field
c-Si	crystalline silicon
CA	conductive adhesive
CdTe	cadmium telluride
CED	cumulative energy demand
CH_4	methane
CIGS	copper indium gallium (di)selenide
CIPC	cumulative installed PV capacity
CIS	copper indium (di)selenide
CO_2	carbon dioxide
CO_2-eq	carbon dioxide equivalent
CSI	clear sky index
Cu	copper
Cz	czochralski
DNI	direct normal irradiance
EPBT	energy payback time
EVA	ethyl-vinyl-acetate
FBR	fluidised bed reactor
GHG	greenhouse gas
GHGPBT	greenhouse gas emissions payback time
GHI	global horizontal irradiance
GIS	geographic information system
GWP	global warming potential
I_{mpp}	maximum power point current
I_{sc}	short-circuit current
IBC	interdigitated back contacted
IQE	internal quantum efficiency
ITO	indium tin oxide

IV-curve	current-voltage curve
LCA	lifecycle assessment
LCC	lifecycle costing
LCI	lifecycle inventory
LCOE	levelised cost of electricity
MG-Si	metallurgical grade silicon
MMF	(spectral) mismatch factor
NOCT	nominal operating cell temperature
P_{mpp}	maximum power point power
PBT	payback time
PECVD	plasma-enhanced chemical vapour deposition
POA	plane of array
PR	performance ratio
PV	photovoltaics
PVD	physical vapour deposition
RD	research and development
RMSE	root mean square error
SF	spectral factor
SHJ	silicon heterojunction
Si	silicon
SR	spectral response
STC	Standard testing conditions: 1000 W/m^2 irradiance, 25°C cell temperature, airmass 1.5 spectrum
TCO	transparent conductive oxide
UF	useful fraction
UPOT	Utrecht Photovoltaic Outdoor Test facility
V_{mpp}	maximum power point voltage
V_{oc}	open-circuit voltage
W_{p}	watt-peak, photovoltaic module power output at standard testing conditions
ZnO	zinc oxide

List of Figures

List of Tables

List of publications

Publications related to this thesis

- A. Louwen, W.G.J.H.M. van Sark, W.C. Turkenburg, R.E.I. Schropp and A.P.C. Faaij., 2012. *R&D Integrated Life Cycle Assessment: A Case Study on the R&D of Silicon Heterojunction Solar Cell Based PV Systems.* Proceedings of the 27th European Photovoltaic Solar Energy Conference and Exhibition, 24-28 September 2012, Frankfurt, Germany.
- A. Louwen, W.G.J.H.M. van Sark, R.E.I. Schropp, W.C. Turkenburg and A.P.C. Faaij, 2013. *Cost analysis of two silicon heterojunction solar cell designs.* Proceedings of the 39th IEEE Photovoltaic Specialists Conference, 16-21 June 2013, Tampa, Florida, USA.
- A. Louwen, W.G.J.H.M. van Sark, W.C. Turkenburg, R.E.I. Schropp and A.P.C. Faaij, 2015. *Life-cycle greenhouse gas emissions and energy payback time of current and prospective silicon heterojunction solar cell designs.* Progress in Photovoltaics: Research and Applications, vol. 23, issue 10, pp 1406-1428.
- Atse Louwen, Wilfried van Sark, Ruud Schropp and André Faaij, 2016. *A cost roadmap for silicon heterojunction solar cells*. Solar Energy Materials and Solar Cells, vol. 147, pp 295-314.
- A. Louwen, W.G.J.H.M. van Sark, A.P.C. Faaij and R.E.I. Schropp, 2016. *Re-assessment of net energy production and greenhouse gas emissions avoidance after 40 years of photovoltaics development.* Nature Communications 7:13728.
- A. Louwen, R.E.I. Schropp, A.P.C. Faaij and W.G.J.H.M. van Sark, 2016. *Comprehensive characterisation and analysis of PV module performance under real operating conditions*. Progress in Photovoltaics: Research and Applications (Early View; doi: 10.1002/pip.2848)
- A. Louwen, W.G.J.H.M. van Sark, R.E.I. Schropp and A.P.C. Faaij, 2016. *Geospatial analysis of the energy yield and environmental footprint of different types of PV module technologies*. (submitted)
- A. Louwen, A.C. de Waal, W.G.J.H.M. van Sark, 2016. *Evaluation of different indicators for representing solar spectra*, Proc. 43rd IEEE PV specialist conference, June 2016 (in press) (oral)

Publications unrelated to this thesis

- Momir Tabakovic, Hubert Fechner, Wilfried van Sark, Atse Louwen, George Georghiou, George Makrides, Eliza Loucaidou, Monica Ioannidou, Ingrid Weiss, Sofia Arancon, Stephanie Betz, 2016. *Status and outlook for building integrated photovoltaics (BIPV) in relation to educational needs in the BIPV sector*, 8th International Conference on

Sustainability in Energy and Buildings, SEB-16, 11-13 September 2016, Turin, Italy, Energy Procedia (in press)

- W.G.J.H.M. van Sark, A. Louwen, O. Tsafarakis, P. Moraitis, *PV system monitoring and characterization*, Chapter 11.4 in *Photovoltaics from Fundamentals to Applications* (Eds. A. Reinders, P. Verlinden, W. van Sark, A. Freundlich), Wiley, 2017 (in press), pp. 547-556.
- Wilfried van Sark, Atse Louwen, Arjen de Waal, *Zonsverduistering van geringe invloed op elektriciteitsvoorziening*, Nederlands Tijdschrift voor Natuurkunde 81 (2015) 186-187. (in Dutch).
- T.J. Silverman, U. Jahn, G. Friesen, M. Pravettoni, M. Apolloni, A. Louwen, W.G.J.H.M. van Sark, M. Schweiger, G. Belluardo, J. Wagner, A. Tetzlaff, P. Ingenhoven, D. Moser, *Characterization of Performance of Thin-film Photovoltaic Technologies*, report number IEA-PVPS T13-02:2014 (2014), pp. 69.
- Atse Louwen, Arjen de Waal, Wilfried van Sark, *Onderzoek aan zonne-energie in Nederland: de Utrecht Photovoltaic Outdoor Test facility*, Nederlands Tijdschrift voor Natuurkunde 80 (2014) 52-55. (in Dutch)
- W.G.J.H.M. van Sark, A. Louwen, A.C. de Waal, R.E.I. Schropp, *UPOT: the Utrecht Photovoltaic Outdoor Test facility*, Proceedings of the 27th European Photovoltaic Solar Energy Conference, WIP-Renewable Energies, Munich, Germany, 2012 (poster, 4BV.2.11), pp. 3247-3249.

Dankwoord

Het doen van een promotieonderzoek was wel het laatste waar ik aan dacht in de afrondende fase van mijn masteropleiding Energy Science. Ik studeerde al ruim 7 jaar aan de Universiteit Utrecht, en zag het wel zitten om het bedrijfsleven in te gaan en 'geld te verdienen'. Ongeveer een maand voor het einde, misschien iets eerder kwam er echter een vacature voorbij voor een PhD plek binnen de vakgroep die toen nog *Natuurwetenschap en Samenleving* heette. De luxe van een baan direct na het afronden van de opleiding was echter aanlokkelijk, en als ik er over nadacht leek het me toch wel wat om voor een carrière als wetenschapper te gaan.

Mijn dank is dus ook groot voor ten eerste Wilfried, mijn co-promotor en begeleider, die mij heeft aangenomen op dit project, voor Ruud Schropp, die mijn promotor en programmaleider van het project was, en Evert Nieuwlaar, die me tijdens mijn sollicitatiegesprek heeft weten te overtuigen om te kiezen voor een promotietraject.

Wilfried, Ruud, en ook promotor André Faaij wil ik bedanken voor de begeleiding van begin tot eind van dit promotieonderzoek. Jullie hebben mij grote vrijheid en vertrouwen gegeven, en jullie commentaar op mijn stukken was altijd zeer complementair. Het was jammer dat eerst Ruud, en daarna André de Universiteit Utrecht hebben verlaten. Het kleine eenzame eilandje waar de PhD-er regelmatig op zit, leek daardoor soms nog wat verder uit de kust te drijven. Maar jullie enthousiasme, hoewel soms van afstand, was zeer motiverend. Wilfried, bedankt dat je van mij een echte 'Zon PV-er' hebt gemaakt, hoezeer we ook gruwelen van dat woord. Je hebt mij klaargestoomd voor een academische carrière en alles wat daarbij komt kijken.

Verder wil ik natuurlijk mijn collega's bedanken. Allereerst mijn kamergenoot van het eerste uur, Boudewijn E., ik heb de politiek-incorrecte *safe-space* die ons kantoor was altijd een fijne plek gevonden om me terug te trekken en al mijn cynisme te kunnen uiten, naast de meer gezellige discussies over al wat ons leven wél leuk maakt. Ik hoop je Russische pan nog een keer in actie te zien. Arjen, bedankt voor het opzetten en runnen van UPOT, en je *zero f#cks given* houding ten opzichte van alles! Boudewijn P. bedankt voor je enthousiasme over Elon Musk en alles wat hij doet, de goede gesprekken voor en na werk, en voor het feit dat je tegelijk met mij ging verbouwen en de uitwisseling van ergernissen én het plezier wat daarbij komt kijken. Geert, bedankt voor je oneindige optimisme en energie, die zelfs immuun bleken te zijn voor het eerder genoemde cynische klimaat in onze kamer.

I would also like to thank the rest of *Team PV*: Panos, Odysseas, Bhavya, Kostas, Ioannis, Mart, Wouter and Tarek, for interesting presentations and discussions during out meetings and for contributing to this growing group of PV(-related) researchers at our group. Big thanks also to all the other colleagues of the E&R department, I have enjoyed and still do really enjoy working at this diverse and gezellige group.

Daarnaast ook grote dank voor het 'ondersteunend personeel': Aisha, ik weet nog steeds niet wat er wel en niet binnen je takenpakket hoort, ik heb ook de indruk dat veel mensen er daarom vanuit gaan dat ze alles op je bureau kunnen gooien. Ik kon in ieder geval altijd met

de meest wisselende kwesties bij je terecht, waarvoor mijn dank! Petra, Siham en Fiona, bedankt dat jullie de groep in goede banen weten te leiden en alle steun tijdens de lange periode die mijn onderzoek duurde.

Ook wil ik mijn familie bedanken: mijn ouders Alex en Trudy, voor alle steun, financieel en emotioneel, tijdens mijn studie en daarvoor en daarna, voor het helpen klussen en verhuizen ongeveer drie keer binnen mijn promotieonderzoek, voor de interesse in mijn onderzoek en jullie trots. Jullie liefde voor natuur heeft mij er toe bewogen om me in te zetten voor een duurzame samenleving. Mijn zussen Wietske en Margriet, die me bewust en onbewust veel hebben geleerd over het leven. De kinderen van Wietske, Melle en Pepijn die zo'n prachtig voorbeeld zijn van de belangrijkste reden waarom we vechten voor duurzaamheid.

Mijn vriendin Marieke, je gezelschap en de leuke tijden die we hadden en hebben zijn een enorme steun geweest om het lange traject vol te houden. Onze reizen samen waren de beste ontsnapping die ik kon wensen. We hebben zulke verschillende banen maar juist daarbuiten zoveel gemeen. Jouw werkhouding en de relativering die dit me geeft hebben me erg geholpen om de motivatie te blijven vinden om het promotietraject tot een goed einde te brengen. Ook je ouders Ed en Anne-Marie wil ik bedanken voor de gezelligheid, steun en interesse in mijn werk.

About the author

Atse Louwen was born in Bodegraven, the Netherlands, on April 16, 1986. In 2004 he started his bachelor's study in Biology at Utrecht University, and quickly developed an interest in subjects related to climate change and, being on of the major causes of it, the energy supply system. After his graduation in 2009 he started with the Energy Science master at Utrecht University. His master's thesis analysed the application of shale gas for heat and electricity in the Netherlands, by means of Lifecycle Assessment.

In November 2011, directly after graduating, Atse started with his PhD project at the Copernicus Institute of Sustainable Development. The project was part of the FLASH programme, which aimed to develop low-cost, highly efficient silicon heterojunction solar cells. During four and a half years, Atse researched the economics, energy performance and environmental footprint of silicon heterojunction technology. He published five peer-reviewed papers, and contributed to conferences in the Netherlands, the United States, and Germany with oral and poster presentations. Furthermore, Atse supervised a number of master and bachelor students with writing their theses, and has assisted in teaching both bachelor and master-level courses within the Science and Innovation bachelor's programme and the Energy Science master's programme. After his PhD, Atse will continue to work at Utrecht University, researching performance of novel silicon based PV modules, studying technological progress in the energy sector, and contributing to education in the Energy Science master.